...H Tc (>110K) Bi, Tl and Y-BASED MATERIALS
...UCTING CIRCUIT ELEMENTS

FINAL REPORT

to

...Aeronautics and Space Administration
Langley Research Center
Hampton, VA 23665-5225

...eriod: March, 1990 - July, 1994

Gene Haertling

...:

Gregory Grabert
Phillip Gilmour

...108

The Gilbert C. Robins...
Department of Ceram...

College of Engineering

DEVELOPMENT OF HIGH Tc (>110K) Bi, Tl and Y-BASED MATERIALS AS SUPERCONDUCTING CIRCUIT ELEMENTS

FINAL REPORT

to

National Aeronautics and Space Administration
Langley Research Center
Hampton, VA 23665-5225

Period: March, 1990 - July, 1994

Principal Investigator:

Gene Haertling

Supporting Investigators:

Gregory Grabert
Phillip Gilmour

Contract No. NAG-1-1108   July 15, 1994

The Gilbert C. Robinson
Department of Ceramic Engineering

CLEMSON
UNIVERSITY

College of Engineering

Summary

Experimental work on this project over the last four years has resulted in establishing processing and characterization techniques for producing both the Bi-based and Tl-based superconductors in their high temperature (2223) forms. In the bulk, dry pressed form, maximum critical temperatures (Tc) of 108.2K and 117.8K, respectively, were measured. Results have further shown that the Bi and Tl-based superconducting materials in bulk form are noticeably different from the Y-based 123 material in that superconductivity is considerably harder to achieve, maintain and reproduce. This is due primarily to the difficulty in obtaining the higher Tc phase in pure form since it commonly co-exists with other undesirable, lower Tc phases. In particular, it has been found that long processing times for calcining and firing (20 - 200 hrs.) and close control of temperatures which are very near the melting point are required in order to obtain higher proportions of the desirable, high Tc (2223) phase.

Thus far, the BSCCO bulk materials has been prepared in uniaxially pressed, hot pressed and tapecast form. The uniaxially pressed material has been synthesized by the mixed oxide, coprecipitation and melt quenching processes. The tapecast and hot pressed materials have been prepared via the mixed oxide process. In addition, thick films of BSCCO (2223 phase) have been prepared by screen printing on to yttria and magnesia stabilized zirconia with only moderate success; i.e., superconductivity was achieved in these thick films, but the highest Tc obtained in these films was 89.0K. The Tc's of the bulk hot pressed, tapecast and screen printed thick film materials were found to be 108.2, 102.4 and 89.0K, respectively.

When synthesizing both the mixed oxide and coprecipitated thick film materials, which includes tapecasting, the best results occurred when the materials were sintered under low oxygen atmosphere because the films could be sintered longer and became more dense. This allowed a larger percentage of the 2223 phase to form. The BSCCO thick films printed on MgO substrates and fired at 845°C for 1 hour had the highest Tc of 89.0K. The Jc's for all films were very low. This could be increased by making denser, single phase films. A MgO buffer layer improved the electrical properties of the BSCCO thick films, and the MSZ substrate was found to be the best material for this work. The coprecipitated powder was preferred over the mixed oxide powder because a larger percentage of the 2223 phase could be formed in a much smaller amount of time.

Compositional and processing investigations were carried out on the Tl-based superconductors. Manganese and lithium additions and sintering temperature and time were examined to determine their influence on superconducting properties. It was found that lithium substitutions for copper enhance the transition temperatures while manganese additions produced deleterious effects on the superconducting properties.

Research on thin film Tl and Bi-containing superconductors included preliminary investigations into thick films produced via the acetate dip coat process and dielectrophoretic deposition of bismuth containing superconducting films on silver

substrates. Of these two coating techniques, it appears dielectrophoretic deposition is a novel technique that has the potential of developing superconductor coatings with preferred orientation.

Acetate dip coating produced 2223 TBCCO superconductor thick films when fired at 600°C for 30 minutes. Using this low temperature firing method, encapsulation is not needed to contain the volatile thallium. It appears thicker films produce a greater proportion of the 2223 phase.

Dielectrophoretic depositions were produced on silver wires. In this technique, high voltage is applied between two electrodes which are immersed in a suspension of superconducting powders and an insulating fluid. A non-uniform field is set up when a voltage is applied to a wire electrode that is surrounded by a cylindrical counter electrode. If the particle possesses a relatively high permittivity compared to the suspending fluid, a dipole is created in the particle. The particle is then drawn to the wire electrode due to the attraction of the dipole to the greater field intensity. Results of dielectrophoresis depositions suggest that superconductor films may be produced with particle orientation.

Both the Bi and Tl-based superconductors prepared by tapecasting were fabricated into SAFIRE-type grounding links. These links were similar in configuration to the Y-based 123 superconductor grounding straps produced in previous work for NASA.

I. Introduction

This report details work that was carried out over the period from February, 1990 thru February, 1994, in the Ceramic Engineering Department of Clemson University under NASA contract No. NAG-1-1108. The work described in this report covers the four-year program involving the development of high Tc superconducting circuit elements in the Bi-Sr-Ca-Cu-O and Tl-Ba-Ca-Cu-O compositional systems. This effort is intended to build on the results of the previous contract (NAG-1-820) which involved the development of the $YBa_2Cu_3O_{7-x}$ (123) material in circuit elements; and more specifically, a superconducting grounding link for the SAFIRE (Spectroscopy of the Atmosphere using Far Infra-Red Emission) program.

The technology developed for the SAFIRE grounding link involves a rigid-structure approach to superconducting elements rather than the flexible-wire idea promoted by most other institutions. In principle, the rigid-structure concept is quite simple and is tailor-made to take advantage of the inherent desirable properties of the superconducting ceramics while at the same time recognizing the low strength and basic brittleness of these materials. This is accomplished by pre-forming, sintering and testing the ceramic superconductor prior to bonding it to a rigid supporting substrate which is then totally encapsulated for further support and environmental protection. This approach has the advantages of (1) pre-testing of the superconducting material separate from the substrate, (2) optimization of the development of superconductivity in the ceramic without temperature limitations imposed by the substrate, (3) wider selection of substrate materials since the high temperature processing step precedes mounting of the superconductor to the printed circuit board, (4) freedom from firing shrinkage and other material compatibility problems and (5) high anticipated reliability because of its simplicity, rigid design and total encapsulation from the environment.

The report is presented in two parts; i.e., Part I dealing with the Bi-based materials and Part II covering work on the Tl-based materials.

DEVELOPMENT OF HIGH Tc (>110K) Bi, Tl and Y-BASED MATERIALS AS SUPERCONDUCTING CIRCUIT ELEMENTS

Final Report

Part I

Materials Synthesis and Characterization of Bi and Y-Based Materials

to

National Aeronautics and Space Administration
Langley Research Center
Hampton, VA 23665-5225

Principal Investigator:

Gene Haertling

Supporting Investigator:

Gregory Grabert

Contract No. NAG-1-1108   July, 1994

I. Objectives

The objectives of this work were to (1) develop and demonstrate the feasibility of producing superconducting powders in the Y and Bi-based systems and fabricate these materials into rigidly supported, environmentally protected superconducting circuit elements such as conductors, coils, connectors and crossovers on dielectric substrates for microelectronic applications, (2) develop a reliable and reproducible mixed oxide or chemical coprecipitation process for producing Y and Bi-based superconductors, (3) Investigate various techniques such as melt quenching, zone refining, molten salt processing, extrusion, hot pressing, freeze drying, etc. for producing maximum density and grain orientation in an effort to maximize the J_c, (4) investigate the sol-gel or metallo-organic decomposition chemical processes for the development of superconducting thin films in the Y and Bi-based systems, (5) adapt previously developed techniques for superconducting grounding straps to the bismuth-based materials, including tapecasting, tape cutting, sintering, electroding, mounting tapes on PC boards and encapsulating, (6) evaluate new compositions in the YBCO system that were reported to have T_c's in the 235 K to 265 K range and (7) characterize and evaluate the superconducting materials and devices in regard to their various properties of interest; i.e., bulk density, crystalline structure, microstructure, thermal conductivity, thermal expansion, T_c, J_c, contact resistivity, and oxygen sensitivity.

II. Introduction

Since the discovery of a High T_c superconducting phase in the Bi-Sr-Ca-Cu-O (BSCCO) system by Maeda and his coworkers in January 1988[1], extensive research has gone into the areas of processing, characterization, phase equilibria, physical property measurement, and device fabrication of these materials. Ceramic superconducting devices in the Y-Ba-Cu-O, Bi-Pb-Sr-Ca-Cu-O and Tl-Ba-Ca-Cu-O systems have been fabricated at Clemson University using the rigid conductor process (RCP)[2,3] for the SAFIRE (Spectroscopy of the Atmosphere using Far Infra-Red Emission) program.

Of the material systems that superconduct above liquid nitrogen temperature (77.3 K), processing in the bismuth-based system seems to be the most attractive because of the following reasons:

1) The high critical temperature (T_c) BSCCO 2223 phase has a T_c 17 °K higher than that of the YBCO system.

2) The bismuth-based materials are less oxygen stoichiometry sensitive than the yttrium-based materials.

3) The bismuth-based materials are much more resistant to moisture degradation than the yttrium or thallium-based materials because the bismuth-based materials do not contain barium, which in a moist environment results in the rapid formation of alkaline conditions on the sample surface and accelerated degradation. This is basically due to the formation of $BaCO_3$.

4) The bismuth-based material has a higher intrinsic critical current density (J_c) than the yttrium-based material and with better grain alignment could possibly have higher extrinsic J_c.

5) The bismuth-based materials are easier to prepare than the thallium-based materials due to the extreme volatility of the Tl^{+3} which makes the results nonreproducible and unreliable.

6) The bismuth-based materials are less dangerous than the thallium or mercury-based materials due to the poisonous nature of the Tl/Hg vapors.

The BSCCO compound consists of an oxygen deficient perovskite layer containing copper oxide planes sandwiched between bismuth oxide layers. The number of copper oxide planes corresponds to the n in the chemical formula $Bi_2Sr_2Ca_{(n-1)}Cu_nO_x$ where n = 1, 2, or 3. As the number of copper oxide planes increases, so does the critical temperature. The three main compounds are,

$$Bi_2Sr_2Cu_1O_x \qquad T_c \sim 7\,K$$
$$Bi_2Sr_2Ca_1Cu_2O_x \qquad T_c \sim 80\,K$$
$$Bi_2Sr_2Ca_2Cu_3O_x \qquad T_c \sim 110\,K$$

and are shown in Figure 1. The compounds we are most concerned with are the $Bi_2Sr_2Ca_1Cu_2O_x$ (2212 phase) and primarily the $Bi_2Sr_2Ca_2Cu_3O_x$ (2223 phase). The highest T_c material is very difficult to synthesize in phase-pure form because separation of the 2223 phase from the 2212 phase is near impossible in bulk form. The 2223 phase has a very small sintering temperature range and long sintering times are required to obtain bulk material which is almost phase-pure. Many investigators found it necessary to dope the BSCCO material with lead to achieve significant quantities of the 2223 phase. They showed that the lead (although it is not known why) increased the percentage of the 2223 phase formed and acted as a flux by decreasing the sintering temperature and time required to form the 2223 phase[4-10]. The lead was also shown to promote crystallization. Another reason for doping the BSCCO material with lead is to increase the apparent valence of copper. As with the lanthanum-based system, the copper valence should be greater than 2+. By replacing some of the Bi^{3+} with Pb^{2+}, the apparent valence of copper is increased. Other phases that were present in other investigators' work were the 2201 and 2212 phases, Ca_2PbO_4, $(Ca, Sr)_2CuO_3$, a semiconducting phase, $(Sr, Ca)_xCu_yO_z$, Cu_2O, $(Ca, Sr)_{14}Cu_{21}O_{41}$ and excess CuO. Some of these investigators believe that the Ca_2PbO_4 phase, the CuO and the 2212 phase interact with one another by liquid phase sintering, precipitation, dissolution or in some other way to form the 2223 phase[10-21]. Besides lead, a number of other dopants have been studied to determine if the superconducting properties could be improved. Of the many dopants investigated, antimony was one of the additives which actually improved the

electrical properties. Several investigators showed that the critical temperature of the BSCCO superconductor was increased with the addition of small amounts of antimony[22-25]. Again, as with the lead, the antimony appears to enhance the conversion of mixed phases and impurities to the 2223 phase, but the mechanism behind this is not yet understood.

The amount of strontium in these superconductors has also been investigated. It was shown that as the amount of strontium in the superconductor was increased, the 2212 phase tends to form instead of the 2223 phase[26-29]. The reason for this is that the 2212 phase is strontium-rich and leaves the leftover calcium in the Ca_2PbO_4 form. The optimum amount of strontium was found to be somewhere between 1.6 and 1.95 moles. As a result of these ideas the composition decided upon for this investigation was $Bi_{1.6}Pb_{0.4}Sr_{1.9}Ca_{2.05}Cu_{3.05}O_x$ or $Bi_{1.6}Pb_{0.4}Sb_{0.1}Sr_{1.9}Ca_{2.05}Cu_{3.05}O_x$ when the effect of antimony additions was investigated.

In trying to understand the 2223 phase formation of the bismuth-based material, there are many variables which must be considered. First, the lead doped BSCCO system is a five component system and understanding the bulk system requires an understanding of the binary and tertiary systems which make up the bulk system. Some of the phases formed from the smaller systems become impurity phases of the bulk system or the phases actually intergrow within each other. In either case, they are difficult to remove. Secondly, the literature is contradictory and more over, confusing. Many investigators have published data on the optimum composition for formation of phase-pure 2223 based on powder X-ray diffraction studies (XRD) and electrical property data. The investigators all had different starting compositions, firing schedules and atmospheric controls. Such disagreement implies that (1) cationic substitutions can occur readily or (2) impurity phases are present and either dissolved to form a glassy phase or their XRD peaks overlap with those of the 2223 phase[28]. The same happens with temperatures, ranging from 827 °C to 890 °C, and atmospheres, which go from reducing to air to oxidizing. In all cases, it appears that no one is really sure exactly what is going on. One thing is certain, there is still a lot of work to be done on the BSCCO system to fully understand the mechanisms of formation for the different phases. The most important parameters which influence the formation of the 2223 phase are chemical composition, atmosphere, powder preparation, sintering time and sintering

temperature. Also important, but rarely mentioned in literature, is the particle size and distribution of the processed powders. These affect the reactivity and density of the bulk superconductor, which has been shown to not only be related to the phase formation but to the final physical properties as well.

The bismuth-based material has been synthesized by several techniques, including glass preparation, melt quenching, mixed oxides and chemical coprecipitation routes[30-39]. Chemical coprecipitation via an oxalate route was chosen for this investigation because of the ability to make very homogeneous and uniform powders. Powder prepared by the mixed oxide process must be ground and calcined several times in order to obtain a powder which gives reliable and reproducible results. However, each time the material is ground or ball milled, impurities are introduced, thus lowering the quality of the powder produced. Coprecipitated powder, on the other hand, because of fine particle size (less than 1 μm) and high purity, is more reactive and may not need to be calcined at all[38]. Although, some investigators have obtain good results using melt quenched or glass prepared powders, we believe that the coprecipitation route is the most reliable technique for this study. The BSCCO material had been coprecipitated at Clemson University using the oxalate route with both the acetates and nitrates. The nitrates were chosen over the acetates for the bismuth-based material because copper acetate is soluble only in a basic solution and bismuth acetate only in an acidic solution. The only problem with the nitrates is the solubility of bismuth nitrate[38-40]. Actually, the bismuth nitrate powder was found to dissolve in a dilute nitric acid solution quite easily.

Among all of the possible applications of high T_c superconductors, electric wiring, high density data transmission lines, magnetic shielding and hybrid technology are the areas in which the first high T_c components could be used. At this time, thick film technology appears to be the best avenue for making these components. Table 1 shows different phases of BSCCO thick films on a variety of substrate materials[41-56]. The key substrate materials shown are $SrTiO_3$, MgO, Ag and the zirconia based substrates. The major phases researched are 1112, 2212, 2223 and 4334. The properties range from non-superconducting, due to film-substrate reaction or a yellow-green insulating phase, to transition temperatures in excess of 100 K on MgO. Cold rolling of the BSCCO thick film on silver also produced T_c's greater

than 100 K. The highest T_c obtained on a YSZ substrate was 72 K. Al_2O_3 and quartz were shown to be poor substrate materials. Overall, the best superconducting properties were obtained on the MgO substrates. However, the stabilized zirconia substrates are preferred because of their lower thermal conductivity. Some of the problems with thick film technology are low density films and reactions between the substrate and the film. To obtain BSCCO thick films with good properties, very dense, single phase films are required. Long sintering times are necessary to obtain these dense, single phase films. Reactions occurring between the films and the substrate materials are intensified as the sintering times increase. These reactions have been reported by other investigators and are not altogether understood. What is known is that the reactions occurring at the interface between the film and the substrate are the main barrier inhibiting practical device design and understanding them could be the key to avoiding them. Screen printing appears to be the easiest and most economical way of depositing films onto the substrate. Other methods which have been used are tapecasting, spray pyrolysis, molten oxide and rapid quench methods. Due to the different phase transformations occurring in the BSCCO system, fabrication of thick films is much more complex than for other systems. Thick films in both the yttrium and bismuth-based systems have been successfully fabricated at Clemson University by tapecasting and screen printing.

The $Y_5Ba_6Cu_{11}O_y$ compound possessed critical temperatures in the 235 K to 265 K range, although, there was a problem with reproducibility. The investigators believed that oxidation at low temperatures, 150 °C to 70 °C, helped to stabilize this high-T_c phase, so the samples were annealed in oxygen for 96 hours at 150 °C. They also used high pressures on the order of 130 atmospheres of oxygen to synthesize this material. Although they could no longer reach 77.3 K, the investigators chose an acetone bath with dry ice, rather than liquid nitrogen, to confirm the T_c's because of the ease of temperature control. This material did not show a Meissner effect but the investigators speculated that this was due to the microstructure or to the fact that the superconducting path could be more filamentary which would imply that "the observed phenomena is not bulk-like."[57]

To date, the results in the BSCCO system include synthesis of the BSCCO material by mixed oxide, melt quenching and chemical coprecipitation techniques in bulk, thin and thick film, and hot pressed forms. Studies have been performed on the effect antimony additions,

the number of calcinations, pressing pressure, fast firing, quenching and atmosphere have on the final superconducting properties as well as the influence of resistance changes during sintering on phase formation. Table 2 summarizes these results.

This report contains the sample preparation procedure for the bismuth-based materials synthesized in bulk, thin and thick film, and hot pressed form by the nitrate and acetate based chemical coprecipitation, mixed oxide and melt quench processes. It also contains data on the bismuth-based superconducting grounding link.

III. Experimental Procedure

As previously stated, the composition decided upon for this investigation was $Bi_{1.6}Pb_{0.4}Sr_{1.9}Ca_{2.05}Cu_{3.05}O_x$ or $Bi_{1.6}Pb_{0.4}Sb_{0.1}Sr_{1.9}Ca_{2.05}Cu_{3.05}O_x$ when the effect of antimony additions was investigated. All of the materials were first tested for the Meissner effect. The critical temperature and critical current density were evaluated using a standard four point method. The resistance was measured with a Keithley micro-ohmmeter (Model 580, Keithley Instruments Inc., Cleveland, Oh.) with a sensitivity of 10^{-6} Ω. The critical currents were measured using a 1 μV per mm standard with a Keithley Autoranging MicroVolt DMM (Model 197, Keithley Instruments Inc., Cleveland, Oh.). In addition, the structures of the samples were examined by powder X-ray diffraction (XRD) using Cu K_α radiation (Model XDS 2000, Scintag Inc., Sunnyvale, Ca.). Scanning electron microscopy (SEM) (Model JSM-IC848, Jeol, Peabody, Ma.) equipped with an Energy Dispersive X-ray Analysis (EDAX) unit (Model TN 5500, Tracor Northern Inc., Middleton, Wi.) and Optical microscopy (OM) (Model ICM 405, Zeiss, Oberkochen, West Germany) were used to observe the homogeneity and surface morphology of the materials. A BET Surface Area Analyzer (Model Gemini 2360, Micromeritics Instrument Corp., Norcross, Ga.) and a Sedigraph (Model 5100, Micromeritics Instrument Corp., Norcross, Ga.) were used to determine the particle size and distribution of the BSCCO materials. Differential Thermal Analysis (DTA) (Model DTA 1700, Perkin-Elmer, Norwalk, Co.) was used to determine the thermal effects of the BSCCO materials. The electrodes for all materials were applied using a

commercial silver paste (Model C8710, Heraeus Inc., Cermalloy Division, West
Conshohocken, Pa.) and fired at 845 °C for eighteen minutes.

1. BSCCO Mixed Oxide Process

Figure 2 shows the preparation process for the uniaxial and hot pressed bulk
bismuth-based material. Figure 3 shows the preparation process for the tapecast
bismuth-based material. In all cases, the starting materials were Bi_2O_3, PbO, $SrCO_3$, $CaCO_3$
and CuO. The powders were weighed out according to the batch information sheet shown in
Table 3 and ball milled with distilled water for one hour and dried at 100 °C for eighteen
hours. The dried powder was then pressed into pellets and calcined at 810 °C for twelve
hours and one or three times at 830 °C for twenty-four hours depending on the process. The
calcined powder was then ground with a mortar and pestle for processing into the bulk and
tapecast material. For the uniaxially pressed material, the calcined powder was pressed into
one square inch pellets and sintered at 845 °C for twenty to two hundred hours in air. For the
hot pressed material, the calcined powder was hot pressed at 5000 psi for six hours at 845 °C
in oxygen. This material was then tested or subjected to an additional heat treatment of
twenty-four hours at 845 °C in air. The furnace schedule for the bulk material can be seen in
Figure 4. For the tapecast material, the calcined powder was ball milled with trichloroethylene
for one hour and dried at 100 °C for eighteen hours. The dried powder was then mixed with a
commercial binder (Model B73305, Palomar-Metoramic Sciences, Inc., San Marcos, Ca.) in
the ratio of 150 grams of powder to 80 grams of binder and ball milled for one hour. The
mixture was deaired for ten minutes and tapecast by a conventional tapecasting processes[57].
The tape was cut into strips with the dimensions 25.4 mm x 2.0 mm x 0.5 mm. The strips
were sintered by a single and double ramp process. In the single ramp process the tapes were
sintered at 845 °C for twenty-eight to forty-eight hours in air using the furnace schedule seen
in Figure 4. In the double ramp process, the tapes were covered and sintered at 500°C to
800°C for two hours, cooled down to room temperature, uncovered and sintered at 845 °C
for thirty hours in air. Tapes were also sintered covered at 845 °C for thirty hours using the

double ramp process. The furnace schedule for the double ramp process can be seen in Figure 5.

A study on fast heating and quenching was performed to determine the effects on the bulk material and electrical properties. In fast heating, the square inch pellets were put directly into the furnace at 845 °C rather than being ramp heated at 100 °C/hour. In quenching, the pellets were removed from the furnace at 845 °C and cooled by the atmosphere to room temperature in a few minutes.

2. YBCO Mixed Oxide Process

The YBCO "superconductors" were synthesized in both bulk and tapecast form. The starting materials were Y_2O_3, $BaCO_3$ and CuO. . The materials were weighed out according to the batch information sheet shown in Table 4. The procedure used to synthesize the bulk and tapecast materials was the same as that of the bismuth-based superconductors except the dried powder was calcined three times at 900 °C for twelve hours and annealed at 450 °C for twelve hours. The calcined powder was sintered at 910 °C for twelve hours and annealed at 450 °C for twelve hours in both air and oxygen. The electrodes were applied using the same silver paste and double firing method as was used in the bismuth-based superconductors except the firing temperature was 910 °C. A flow chart for the process can be seen in Figure 6 and the furnace schedule and operation can be seen in Figure 7.

3. BSCCO Coprecipitation Process - Nitrate

Figure 8 shows the preparation process for the coprecipitated bulk bismuth-based material and Figure 9 shows the process for the tapecast bismuth-based material. In both cases the starting materials were $Bi(NO_3)_3$, in a dilute nitric acid solution, $Pb(NO_3)_2$, $Sr(NO_3)_2$, $Ca(NO_3)_2 \cdot 4H_2O$ and $Cu(NO_3)_2 \cdot 2.5H_2O$. The materials were weighed out according to the batch information sheet shown in Table 5. In the case where small additions of antimony were added, Sb_2O_3 (As = 0.035%) from Metal and Thermit Corporation was used since a nitrate form of antimony was not available. The bismuth nitrate solution was

poured into a beaker and the other constituents were added one at a time, until each dissolved in the dilute nitric acid solution. Distilled water was added periodically to aid in this process. The solution was constantly stirred by a magnetic stirrer. Once all the constituents were dissolved, a twenty percent excess aqueous solution of oxalic acid was added and stirred for twenty minutes. During this time, the pH was adjusted to approximately 3.5 with ammonium hydroxide. The solution was then dried in a vacuum oven for twelve hours. After drying, the powder was heated to 600 °C for two hours in an alumina crucible to burn off all of the organic radicals. This precalcined powder was then ground and pressed into pellets and sintered at 845 °C for thirty hours in air or calcined at 830 °C for twelve hours in air. The calcined powder was then ground with a mortar and pestle for processing into bulk and tapecast material or calcined again at 830 °C for twelve hours in air. For the bulk material, the calcined and precalcined powder was sintered at 845 °C for twenty-four to thirty hours in air. These materials were then electroded and tested. For the tapecast material, only calcined material was used to cast tape. The calcined powder was ball milled with trichloroethylene for one hour and dried at 100 °C for eighteen hours. The dried powder was then mixed with the same commercial binder used for the mixed oxide materials in the ratio of 100 grams of powder to 45 grams of binder and ball milled for one hour. The mixture was deaired for ten minutes and tapecast. The tape was cut into strips with the dimensions 25.4 mm x 2.0 mm x 0.5 mm. The strips were sintered covered at 845 °C for twenty-four to fifty hours in air and sintered covered at 845 °C for twenty-four to fifty hours in a low oxygen atmosphere. Both process used the furnace schedule seen in Figure 4.

4. BSCCO Coprecipitation Process - Acetate

Figure 10 shows the preparation process for the coprecipitated bulk bismuth-based materials. The starting materials were $Bi(O_2C_2H_3)_3$, $Sb(O_2C_2H_3)_3$, Pb Subacetate in methanol and acetic acid, $Sr(O_2C_2H_3)_2$ in water, $Ca(O_2C_2H_3)_2 \cdot H_2O$ in water and $Cu(O_2C_2H_3)_2 \cdot H_2O$. The materials were weighed out according to the batch information sheet shown in Table 6. The bismuth acetate and antimony acetate were put in a beaker and dissolved with acetic acid. Then, the solutions of strontium, calcium and lead were poured

into the beaker as well as some methanol. When everything had dissolved, the solution was made basic with ammonium hydroxide and the copper acetate was added. The solution was constantly stirred by a magnetic stirrer. Once the copper acetate dissolved, the solution was changed to acidic with acetic acid and the excess solution of oxalic acid and methanol was added and stirred for twenty minutes. The solution was then dried in a vacuum oven for twelve hours. After drying, the powder was heated to 600 °C for two hours in an alumina crucible to burn off all of the organic radicals. This precalcined powder was then ground and pressed into pellets and calcined at 830 °C for twelve hours in air. The calcined powder was then ground with a mortar and pestle for processing. The calcined and precalcined powder was sintered at 845 °C for twenty-four hours in air using the furnace schedule seen in Figure 4. These materials were then electroded and tested.

5. BSCCO Melt Quench Process

Figure 11 shows the preparation process for the melt quenched bulk bismuth-based material. The starting materials were Bi_2O_3, PbO, Sb_2O_3, $SrCO_3$, $CaCO_3$ and CuO. The powders were weighed out and ball milled with distilled water for one hour and dried at 100 °C for eighteen hours. The dried powder was then calcined once in an alumina crucible at 820 °C for twelve hours. The calcined powder was then ground with a mortar and pestle for melt processing. The powder was then melted in an alumina crucible at 1200 °C for twenty minutes in air and rapidly cooled to 1100 °C for two hours in air. The crucible was removed from the furnace and the BSCCO melt was quenched in a stainless steel pan. When the material cooled to room temperature, it was cut and subjected to an additional heat treatment at temperatures ranging from 845 °C to 865 °C for twenty-four hours in air. The samples were then electroded and tested.

6. BSCCO Thick Film

The MgO, YSZ (Yttria Stabilized Zirconia), and MSZ (Magnesia Stabilized Zirconia) substrates for this work were made using standard tapecasting processes. The

9.5/65/35 PLZT (Lanthanum doped Lead Zirconate Titanate) substrates were cut from a hot pressed slug. The different substrate tapes were cut into strips with the approximate dimensions 45 mm x 13 mm. The 9.5/65/35 PLZT substrates were cut into 1 cm^2 squares. The silver substrates were cut from 0.127 mm silver foil with the same dimensions as the tapecast substrates. The yttria content in the YSZ substrates varied from 6% to 12% and the magnesia content in the MSZ substrates varied from 8% to 12%. The tapecast substrates were fired between 1500 °C and 1600 °C for four hours in air. Some of these substrates were coated with different buffer layer materials to determine if the reactions between the films and the substrates could be reduced. An MgO buffer layer was used because of the good superconducting properties observed from the films on the MgO substrates. Several BSCCO compounds were also tried as buffer layer materials. The buffer layers were applied by the dip coating process, which can be seen in Figure 12, at 600 °C for 3 minutes per layer. The number of layers applied to the substrates varied from five to twenty layers. After coating, the substrates were annealed at temperatures ranging from 1400 °C to 1600 °C for one hour. All of the thick films were screen printed onto the various substrates. The screen print dimensions were 1.50 in. x 0.25 in. The paste for screen printing was made from nearly single phase coprecipitated BSCCO powders mixed with alpha terpineol, binder, toluene and ethanol in the ratio of 25:7:1:1:1. A flowchart for this process can be seen in Figure 13. After the films were printed onto the substrates, they were dried at room temperature for twelve hours and sintered at temperatures ranging from 830 °C to 890 °C for times ranging from one to twenty-four hours.

7. In-Situ Resistivity Development

In electronic materials, the resistance of the material has a major effect on its physical properties. In superconductivity, it is used to define the material. The resistance of a material must be zero for that material to be classified as a superconductor. Because of this, an in-situ resistivity development study was undertaken to determine if a correlation between the resistance of the material during sintering and the formation of the 2223 phase existed. If so, this could aid in determining the optimum firing conditions for the BSCCO materials.

The powder for this study was made by the coprecipitation process described in section III.3. Precalcined, once and twice calcined powder was used for this study. The electrode materials were silver wires of 0.25 mm and 1 mm diameter. The wires were cleaned using a commercial jewelry cleaner and distilled water prior to use. Each of the test samples consisted of twenty-five grams of powder and the silver wires were pressed into the BSCCO pellets using a pressing force of 20,000 psi. Once the electrodes were embedded into the sample, it was sintered at 845 °C for twenty-four to seventy-two hours or until one of the silver wires broke. A low oxygen (6% O_2 / 94% N_2) atmosphere was used to reduce the oxidation or degradation of the silver wires. The embedded silver wires were connected to the Keithley micro-ohmmeter (Model 580, Keithley Instruments Inc., Cleveland, Oh.) and data points were taken every fifteen minutes using a 100 mA DC testing current. An IBM 386 SX-20 computer acquired the data from the micro-ohmmeter via HPIB (IEEE-488 Bus) interface.

IV. Results and Discussion

1. BSCCO Mixed Oxide Bulk Material

Figure 14 shows the resistance versus temperature curves for compacts which were prepared at 845 °C for twenty and two hundred hours in air. The curve of the two hundred hour compact showed that the material had a sharp transition to the superconducting state at 108.1 K, where as the curve of the twenty hour compact had a wide transition from 120 K (onset) to 98.9 K (zero). This wide transition is due to a second phase of $(Bi,Pb)_2Sr_2Ca_1Cu_2O_x$ (2212). All of the compacts had a certain percentage of the 2212 phase but this phase decreased and the $(Bi,Pb)_2Sr_2Ca_2Cu_3O_x$ (2223) phase increased as the sintering time increased. This can be seen from the Xray diffraction data shown in Figure 15. The four patterns are from compacts which were prepared at 845 °C for twenty, twenty-eight, thirty-three and one hundred hours. Looking at the double peak at approximately thirty-five degrees, one can see that as the sintering time increased the amount of the 2212 phase decreased as the 2223 phase increased. The room temperature resistivities, between 10 and

15 mΩ, and the onset of superconductivity, 120 K, was about the same for both compacts. The only measured difference was the transition width which was influenced by the amount of each phase present. The amount of each phase present, which is due to the sintering time, also influenced the critical temperature of the compacts. The sintering time versus critical temperature curve shown in Figure 16 shows that as the sintering time increased the critical temperature increased. From twenty to fifty hours the critical temperature increased linearly by 6 K but only by 3 K over the next one hundred fifty hours. This is basically due to the conversion of the 2212 phase to the 2223 phase. At first, the material is almost all 2212 phase, so it is easier to convert it to the 2223 phase, but as more and more 2223 phase is formed, the driving force for conversion of the 2212 phase to the 2223 phase is decreased dramatically. As the material was converted to the 2223 phase the grain size increased and the grains exhibited a more flaky behavior as shown in the SEM micrographs in Figure 17. The grain size ranged from five to ten microns in the twenty hour compact to twenty to thirty microns in the two hundred hour compact.

The results on the fast heating and quenching showed that the heating and cooling rates were important factors in the processing of the BSCCO materials. Four pellets were sintered at 845 °C for fifty-four hours. The slow heat/slow cool compact had the highest T_c of 104.7 K. The slow heat/quench compact's T_c dropped to 102.9 K. The two compacts that were fast heated had T_c's in the 101.2 to 101.4 range. The resistance versus temperature curves for these materials can be seen in Figure 18. This study showed that while the cooling rate was important to the T_c of the compact, it was not as influential as the heating rate.

A study of the effect the number of calcinations had on the superconducting properties of the uniaxially and hot pressed material was performed. In the uniaxially pressed material sintered for thirty hours at 845 °C in air, shown in Figure 19, the two times calcined material had a T_c of 99.1 K, whereas the three times calcined material had a T_c that was 3 K higher at 102.0 K. In the hot pressed material with no additional heat treatment, shown in Figure 20, the two times calcined material did not superconduct, while the three times calcined material had a T_c of 83.3 K. The same two compacts with an additional heat treatment of twenty-four hours at 845 °C in air, shown in Figure 21, the two times calcined material had a T_c of 104.4 K, and the three times calcined material had a T_c that was 4 K higher at 108.2 K. When

four times calcined powder was used to produce the uniaxially pressed bulk material, which was sintered for thirty hours at 845 °C in air, the material did not show a significant change in either critical temperature, critical current density or bulk density. Four times calcined powder has not yet been used to produce the hot pressed material.

2. BSCCO Coprecipitated Bulk Material

The coprecipitated powder was much easier to process and the time required to obtain a workable material was much less. Figure 22 shows the resistance versus temperature curve for the coprecipitated material which was sintered, uncalcined, at 845 °C for thirty hours in air. The curve showed that the material had a transition to the superconducting state at 99.1 K. Figure 23 shows the resistance versus temperature curve for the coprecipitated material which was calcined at 830 °C for twelve hours and sintered at 845 °C for thirty hours in air. The curve showed that the material had a transition to the superconducting state at 104.8 K. The T_c increased about five degrees with the addition of the twelve hour calcine. Calcining the material for twenty-four hours, instead of twelve, did not seem to affect the results. Again from the microstructure, shown in Figure 24, one can see that the grains of the coprecipitated compact exhibit the same plate like morphology as those of the uniaxial and hot pressed mixed oxide compacts. Comparing the SEM micrograph shown in Figure 25 (a), which has been pressed at a higher pressing pressure, to that of Figure 24, one can see that the compact is more dense. In fact, a closer look, Figure 25 (b), at the same micrograph at a higher magnification shows that there is actually some partial melting which contributes to the increase in density and T_c. This again reinforces the idea that liquid phase sintering contributes to the formation of the high T_c phase. Since partial melting has occurred more and more in the higher T_c/J_c samples, a Differential Thermal Analysis (DTA) curve was run for the coprecipitated powder to determine the melting point of the high T_c phase. Figure 26 shows the DTA curve, and the melting point was determined to be about 865 °C. From this information, work done by other investigators[59-61], and work currently going on at Clemson University in the area of thick films, a compact was sintered at 845 °C for thirty hours after the powder had been calcined at 860 °C for twelve hours in air. Figure 27 shows

the resistance versus temperature curve for the two compacts which were calcined at 830 °C and 860 °C for twelve hours and sintered at 845 °C for thirty hours in air. As one can see, the T_c curves are very similar and the other properties tested were also very close to identical, so it appears that this change in calcination temperature did not have an effect on the final properties.

Again, as with the mixed oxide materials, the number of calcinations had a major effect on the superconducting properties of the bulk material. In the hot pressed material with no additional heat treatment, shown in Figure 28, the one time calcined material did not superconduct, while the two times calcined material had a T_c of 84.0 K. The same two compacts with an additional heat treatment of twenty-four hours at 845 °C in air, shown in Figure 29, showed that the one time calcined material had a T_c of 106.4 K, and the two times calcined material had a higher T_c of 108.2 K. Three times calcined coprecipitated powder has not yet been used to produce the hot pressed material. Conversely, in the uniaxially pressed materials, the critical temperature decreased as the number of calcinations increased. Figures 30 through 32 show the resistance versus temperature curves for the uniaxially pressed BSCCO coprecipitated compacts which were calcined once, twice and three times at 830 °C for twelve hours. These materials were then sintered at 845 °C for twenty-four hours in air. The pressing pressure used to press these materials was 15000 psi. The decrease in critical temperature was most probably due to the increased amount of the 2212 phase being formed during the calcination period. This, in turn, slowed down the conversion to the 2223 phase during sintering.

Due to the results obtained from other investigators, the mixed oxide and chemically coprecipitated powders, both acetate and nitrate based, were doped with antimony. Figure 33 shows the resistance versus temperature curve for the BSCCO nitrate based coprecipitated compact doped with lead and antimony. The T_c of 106.5 K was not as high as was seen in literature but it was slightly higher than the T_c of the lead doped BSCCO compact which was 104.8 K. Similarly, the acetate based coprecipitated compact doped with lead and antimony had a T_c of 105.3 K which was higher than lead doped BSCCO acetate based compact's T_c of 104.1 K. The resistance versus temperature curve for the BSCCO acetate based coprecipitated compact doped with lead and antimony can be seen in Figure 34. These

materials were calcined once at 830 °C for twelve hours and sintered at 845 °C for twenty-four hours in air. Low pressing pressures were used to press these materials.

3. Pressure Effects

The samples prepared by the mixed oxide route required sintering times in excess of two hundred hours to obtain materials which were nearly pure 2223 phase. The X-ray powder diffraction analysis confirmed the existence of the 2223 phase with small impurities of Ca_2PbO_4 and Ca_2CuO_3 after two hundred hours sintering. The T_c of this material was 108.1 K. The average particle size of the calcined mixed oxide powder was 15 μm and the green density of the pellet pressed from the powder at 34.5 MPa (5000 psi) was 4.23 g/cc. When the pressing pressure was increased to 138.7 MPa (20120 psi), the green density increased to 4.95 g/cc. Figure 35 shows the resistance versus temperature curves for the mixed oxide pellets uniaxially cold pressed both at the high and low pressures and sintered at 845 °C for 125 hours in air. The high pressure compact had a T_c of 107.3 K while the low pressure compact's T_c was 0.5 °K lower at 106.8 K. This may have, at first, seemed to be a trivial difference in T_c until the approximate sintering time required for the low pressure compact to reach the T_c of 107.3 K was determined. Figure 36 shows the sintering time versus critical temperature plot for the mixed oxide compacts uniaxially cold pressed at 34.5 MPa (5000 psi) and sintered at 845 °C in air for times ranging from twenty to two hundred hours. Also shown in Figure 36 is a point from the 138.7 MPa (20120 psi) high pressure compact sintered at 845 °C for 125 hours in air. The other point on the plot is the approximate sintering time required to achieve the 107.3 K using the lower starting pressure. This approximate value is 155 hours, which means the low pressure compact would require an additional thirty hours sintering to achieve the higher T_c. This increase in T_c with increased pressing pressure was believed to be due primarily to the increase in density, which increased the number of particle to particle contacts, thus making the material more reactive. This increase in the particle to particle contacts enhanced the formation of the high T_c 2223 phase and allowed the sintering times to be reduced. Referring again to Figure 35, another interesting aspect of the difference in pressing pressure was a reduction in room temperature

resistivity by approximately half from the low pressure compact to the high pressure one. This effect was also believed to be due to the increase in density and reactivity. The other aspects of the two curves were basically similar. The transition widths were approximately the same for both curves, and they showed a decrease in resistivity with a sharp drop to zero starting around 120 K. The microstructure of both pellets can be seen from scanning electron micrographs shown in Figure 37. The high pressure compact was much more dense and appeared to have a higher degree of grain alignment when compared to that of the low pressure compact.

The chemically coprecipitated powders were much more homogeneous and reactive than those of the mixed oxide powders. In addition, the average particle size for the chemically coprecipitated powders was 3 μm. The green densities were approximately the same as those for the mixed oxide powders, however, the fired densities were higher. The relative fired density for the chemically coprecipitated compact was approximately 84 % (5.3 g/cc) while the mixed oxide compact's was only around 75 % (4.8 g/cc). Figure 38 shows the resistance versus temperature curves for the chemically coprecipitated pellets uniaxially cold pressed both at the high and low pressures and sintered at 845 °C for thirty hours in air. As was the case for the mixed oxide samples, the room temperature resistivities of the high pressing pressure compacts was lower than that of the low pressing pressure compacts. Overall, the resistivities for the chemically coprecipitated pellets were found to be much lower than those of the mixed oxide pellets. Both of the curves in Figure 38 decreased in resistance with decreasing temperature, but the onset of superconductivity was 123 K which was slightly higher for these materials as compared with the mixed oxide pellets. The biggest difference between the two methods was the sintering time required to form the nearly pure 2223 phase. The mixed oxide route required sintering times six to seven times longer than the chemically coprecipitated materials. The increased pressing pressure also increased the T_c of the materials but this time by 3.6 °K. The microstructure of the chemically coprecipitated material, as shown from the SEM micrographs in Figure 25, had the same flaky behavior as the mixed oxide materials but the grain size is now much smaller and the compact much more dense. Similarly, the high pressure compact was much more dense and had a much higher degree of orientation when compared with the low pressure compact. A closer

look at the high pressure compact shows that there was actually some partial melting taking place, and this definitely contributed to the higher densities and increased T_c's. This also shows that sintering was aided by the presence of the liquid phase and this increased the rate of formation of the high T_c 2223 phase.

Since initial pressing pressure has shown to be effective in increasing the density and developing grain oriented microstructures, the effectiveness of pressure throughout sintering was investigated via hot pressing. It was believed that hot pressing would intensify the effects seen from the increased pressing pressure. Figure 39 shows the resistance versus temperature curves for uniaxial hot pressed mixed oxide compacts which were prepared at 845 °C for six hours in oxygen at 34.5 MPa (5000 psi), with and without a post anneal at 845 °C for twenty-four hours in air. The as hot pressed sample showed that the material had a sharp transition to the superconducting state at 83.3 K. The X-ray powder diffraction analysis showed this material to be primarily composed of the 2212 phase. When the material was post annealed the T_c increased by approximately 25 °K to a T_c of 108.2 K. The phase was almost entirely converted to the 2223 phase. In addition, the resistivity dropped by an order of magnitude from the hot press to the post anneal. Although the chemically coprecipitated powder was much more reactive, homogeneous and had a finer particle size, the results of the chemically coprecipitated material were the same as those for the mixed oxide samples. The microstructure of the as hot pressed sample and the post annealed both can be seen in Figure 40. The as hot pressed sample appears to be a very dense melt with partial orientation, but when the material was post annealed, the density dropped from about 97 % to about 92 % relative density. The grains actually appeared to grow right out of the melt to give the appearance of a very open structure. This could be a little deceiving but this material was still much more dense than any of those produced by the increase in initial pressing pressure. The high T_c 2223 phase of the mixed oxide samples was shown to be formed in a much smaller amount of time when hot pressed and post annealed as opposed to the material just being sintered. In contrast, the chemically coprecipitated materials could be used to form the high T_c phase in the same amount of time by either method. The pressure throughout sintering had a similar effect to that of the processing pressure, in that, the density of these materials increased and the grains became more oriented. The increased density caused an increase in

the number of particle to particle contacts which increased the reactivity and this together decreased the amount of time required to form the high T_c 2223 phase.

4. BSCCO Melt Quenched Material

Figure 41 shows the resistance versus temperature curve for the melt quenched compact with no additional heat treatment. The curve showed that the material, originally in the semiconducting state, did show superconducting behavior with an onset temperature of approximately 100 K. However, the material did not superconduct at 77.3 K. Figure 42 shows the resistance versus temperature curves for the melt quenched compacts with additional heat treatment. Curve (a) shows a compact with thirty hours of additional heat treatment at 845 °C and curve (b) shows a compact with sixty hours of additional heat treatment at 845 °C. Both curves showed metallic behavior, the thirty hour compact had an onset temperature of about 110 K and the sixty hour compact had an onset temperature of about 120 K. Neither of the compacts superconducted at 77.3 K and both curves showed double hump transitions, indicating the presence of a large amount of low T_c second phase material. The room temperature resistance of the sixty hour compact was about half that of the thirty hour compact. The microstructure of the melt quenched material looks very inhomogeneous, there are areas of solid melt and areas of very porous material. Figure 43 shows the microstructure of the two different areas of a melt quenched sample with sixty hours of additional heat treatment. If these micrographs are compared with those of the hot pressed material in Figure 40, similarities can be detected. One possible conclusion would be that these are regions of high T_c phase, the porous grain growth region, and low T_c phase, the solid melt region.

The melt quenched powders were also doped with antimony to see if this could increase the amount of high T_c superconducting material formed. The powders doped with lead and antimony did not show superconducting behavior at liquid nitrogen temperature. Figure 44 shows the resistance versus temperature curve for the BSCCO melt quenched compact doped with lead and antimony. The sections were sintered at 855 °C for twenty-four hours in air.

5. BSCCO Tapecast Material

The tapecast material required a longer processing time than the bulk material to achieve superconductivity above 77 K. All of the powder used to make the mixed oxide tapecast material was calcined three times. Figure 45 shows a resistance versus temperature curve for a mixed oxide tape sintered at 845 °C for twenty hours. The tape still had 0.94 mΩ resistance at 77.3 K but just like the bulk material, the lower sintering time specimens had a higher percentage of 2212 phase. This is clearly shown by the extremely large transition width of the T_c curve. The onset was still 120 K but the transition width was in excess of 43 K. The smallest sintering time required to achieve superconductivity was twenty-eight hours and the T_c was 98.2 K. The resistance versus temperature curves for the twenty-eight hour tapecast and bulk materials can be seen in Figure 46. Again, both curves had an onset of 120 K, but the transition width of the tape was wider that that of the compact. The T_c of the bulk material, 99.7 K, was higher than that of the tape, 98.2 K. Also, the room temperature resistivities of the tapecast materials were four times higher than that of the bulk materials. From the Xray diffraction data, shown in Figure 47, one can see that the tape is much less defined than the bulk material. The tape has several overlapping and low intensity peaks which are undefined. Looking again at the double peak at thirty-five degrees, the tape was primarily 2212 while the bulk was half 2212 and half 2223. Looking at the surface morphology of a tape and a compact that were prepared at 845 °C for thirty-three hours, shown in the SEM micrographs in Figure 48, the tapecast material has a much smaller grain size than the bulk material. Referring to the twenty hour compact in Figure 17 and comparing it to the thirty-three hour tape, one can immediately see the similarities. The grain size and density are about the same but the tape appears to have better orientation than the twenty hour compact.

There was a problem with the tapecast material, after thirty hours sintering, a percentage of the tapes started to curl and fracture. As the sintering time increased so did the percentage of unacceptable tapes. To alleviate the curling problem, the tapes were covered and sintered at 845 °C for thirty hours using the single ramp furnace schedule shown in Figure 4. These tapes did not curl but they did partially react with the setter plate. From

information about the binder burnout rate and the Y-Ba-Cu-O system, it was decided that the tapes were to be covered and sintered at 500 to 800 °C for two hours using the double ramp furnace schedule shown in Figure 5, then uncovered and sintered for thirty hours at 845 °C. These results are shown in Table 7. The best results came from the tapes which were covered and sintered at 845 °C, but these tapes partially reacted with the setter plate. A sintering time versus critical temperature curve in the twenty-eight to forty-eight hour single ramp sintering time range with a dot for the double ramp process of 700 °C is shown in Figure 49. The curve shows just how much higher the T_c of the double ramp process is over the single ramp process. The J_c's of the double ramp process are twice that of the single ramp process.

The coprecipitated tapecast material, like the bulk material, was much easier to process. Figure 50 shows the resistance versus temperature curve for coprecipitated tapecast material which was sintered for thirty hours. For all the tapecasting, the powder used was calcined at 830 °C for twelve hours. The curve, like those for the bulk material, showed that the material had a sharp transition to the superconducting state and the T_c was 102.4 K. Comparing the microstructure of the coprecipitated tapecast material to that of the mixed oxide tapecast material, one can see, from Figure 51, that the coprecipitated tape is much more uniform and seems to have a better alignment than the mixed oxide tape. Also, the curling problem experienced with the mixed oxide tape, has not seemed to be a problem with the coprecipitated tape. Although, curling was not a problem with the coprecipitated tape, low strength was.

Both the mixed oxide curling problem and the coprecipitated low strength problem were solved by firing the tapes in a low oxygen atmosphere. The T_c's remained virtually the same, 101.5 K versus 101.7 K for the mixed oxide tapecast material and 102.4 K versus 102.1 K for the coprecipitated tapecast material. The mixed oxide tapecast material no longer needed to be covered and all of the tapes appeared to be stronger. A resistance versus temperature curve for the coprecipitated tapecast material, which was sintered for thirty hours in the low oxygen atmosphere, can be seen in Figure 52.

6. BSCCO Grounding Links

Superconducting grounding links were made from the coprecipitated tapecast material and can be seen, along with the resistance versus temperature curve, in Figure 53. The critical temperature of the links were approximately 101 K. The resistance at liquid nitrogen temperature due to the solder and the gold pins was 0.9 mΩ. The thermal expansion of the material was determined to see if the links could be made from the same materials as the YBCO links were made from. The thermal expansion was determined to be approximately 12×10^{-6} in/in °C from the thermal expansion curve shown in Figure 54. The thermal expansion of the printed circuit board was determined to be 16×10^{-6} in/in °C and for the epoxy resin was 50×10^{-6} in/in °C [2]. From this information, the materials used for the YBCO links should work fine for the BSCCO material.

7. BSCCO Thick Films

MgO was the first substrate material chosen for the BSCCO thick film material based on the data in Table 1. Figure 55 shows a resistance versus temperature curve for a coprecipitated screen printed thick film which was sintered for one hour at 845 °C in air and had a T_c of 89.0 K. Figure 56 shows an SEM micrograph of the BSCCO thick film on the MgO substrate. It is evident from the microstructure that the film is not very dense, this is due primarily to the short sintering time. As previously stated, longer sintering times are required for denser films and denser films are required for improved properties. The results obtained from the films on the MgO substrates are not bad considering that the substrates were made in house and not purchased for better quality. Once good results were obtained on the MgO substrates, the focus was directed toward the stabilized zirconia substrates because the zirconia based substrates are preferred in the SAFIRE project due to their low thermal conductivities. The BSCCO thick films on PLZT substrates showed similar results to the MgO substrates.

Figure 57 shows the progression of the YSZ substrate from the zirconia powder through the annealing of the substrate to the application and annealing of the buffer layer from

the Xray diffraction data. Comparing the YSZ substrate to that of the JCPDS (Joint Committee on Powder Diffraction Studies) card # 30-1468 for YSZ in Figure 58, one can see that the substrate without a buffer layer was not pure YSZ. This could have been a major factor contributing to the reactions between the film and the substrate. When the substrate was coated with the an MgO buffer layer and annealed at 1500 °C, the XRD pattern matched that of YSZ with the additional MgO peak due to the buffer layer. Figure 59 shows the resistance versus temperature curves for the BSCCO thick films printed on the 10 % YSZ substrates and sintered for three hours at 845 °C in air, with and without the MgO buffer layer. The curves show that the buffer layer definitely improves the electrical properties of the thick film printed on YSZ, although both films were non-superconducting at liquid nitrogen temperature. The amount of reaction with the substrate was reduced with the addition of the buffer layer but the reactions still occurred. Since the MgO buffer layer changed the phase of the YSZ substrate, the structural integrity of the buffer layer was in question. However, from the Xray data of the top and bottom of the YSZ substrate, shown in Figure 60, it is clear that the MgO peak only occurs on the top of the substrate indicating that this was, in fact, a buffer layer and not a reaction between the MgO layer and the YSZ substrate. An SEM micrograph, shown in Figure 61, of the MgO buffer layer showed microcracks in the buffer layer which explains why the reactions, although reduced, were still occurring. The next step was to consider the amount of yttria used to stabilized the zirconia substrate. Figure 62 shows the resistance versus temperature curves for the BSCCO thick films printed on the 8 % YSZ substrates and Figure 63 shows the resistance versus temperature curves for the BSCCO thick films printed on the 6 % YSZ substrates. All were sintered for three hours at 845 °C in air, with and without the MgO buffer layer. In each case, the buffer layered substrate provided better electrical properties than the substrate without a buffer layer. In addition, as the amount of yttria used to stabilize the zirconia decreased, the electrical properties improved. However, none of the samples superconducted at liquid nitrogen temperature.

Several BSCCO buffer layers were also tried with the YSZ substrates. Figure 64 shows a resistance versus temperature curve for a BSCCO thick film printed on the BSCCO / YSZ substrate and sintered for one hour at 845 °C in air. The T_c was 88.4 K which was comparable to the results observed on the MgO substrates. The only drawback was that the

BSCCO buffer layer itself showed metallic behavior after being sintered at 880 °C in air for ten minutes. The resistance versus temperature curve for the BSCCO / YSZ substrate can be seen in Figure 65. The other BSCCO buffer layers tried did not adhere to the substrate. Silver was also used as a substrate material for the BSCCO thick films. No reactions were observed from the BSCCO thick film sintered in air at 845 °C for twenty-four hours but an apparatus sensitive enough to measure the properties was not available.

Due, again, to the results obtained by other investigators on MgO and the fact that the MgO buffer layer would be more compatible with a magnesia based substrate, MSZ was used as a substrate material. Figure 66 shows the Xray diffraction pattern obtained from the MSZ substrates with and without a buffer layer. These patterns show that this substrate is a pure stabilized zirconia substrate as opposed to the YSZ ones. In addition, the pattern shows the MgO peaks after the buffer layer had been applied. There were some problems applying the buffer layers to the MSZ substrates. After approximately seven layers the substrates started to break apart. When the bottom side of the substrate was Xrayed, shown in Figure 67, the MgO peaks appeared on both sides which confirmed the suspicion that the substrate was breaking apart due to the MgO solution reacting with the MSZ substrate. Figure 68 shows a resistance versus temperature curve for a BSCCO thick film printed on a 12 % MSZ substrate without a buffer layer. Due to the metallic behavior of the sample without the buffer layer, which was the best electrical property observed from the stabilized zirconia substrates, it was believed that the MSZ substrate was the best possible substrate for further study. A differential thermal expansion curve, shown in Figure 69, was performed to see which substrate was better in terms of thermal expansion mismatch. The thermal expansion of the BSCCO material was determined to be approximately 12×10^{-6} in/in °C, which is very close to that of the MSZ substrate.

Based on the results obtained from the tapecast materials, the BSCCO thick films were fired on 12 % MSZ substrates at 845 °C for two hours under a low oxygen atmosphere. Figure 70 shows the resistance versus temperature curve for the BSCCO thick films printed on the 12 % MSZ substrate with a five coat buffer layer and without a buffer layer. The buffer layer improved the properties again, this time by 7 K. Both thick films superconducted at transitions of 82 K and 89 K respectively. Figure 71 shows the microstructure of two

BSCCO thick films. The dense thick film superconducted at 87 K and the porous thick film did not superconduct at liquid nitrogen temperature. These results reinforce the theory that the film must be dense to have the best superconducting properties.

8. In-Situ Resistivity Development

Figure 72 shows the resistivity data taken using the 0.25 mm silver wires and one time calcined powder. The top graph is the entire run from the initial dwell at 845 °C until a silver wire broke after sixty-four hours. The bottom graph is a close up view of the specific areas of interest. Area 1 starts at the beginning of the 2223 phase formation and continues on through area 2. The break in between the two areas was due to the degradation of the silver wire. In area 3, the temperature was raised to 855 °C to see the effect on the material through the resistance. As one would expect from a material which shows metallic behavior, an increase in the temperature causes an increase in the resistance. The opposite was the case in area 4. The temperature was reduced to 835 °C and the resistance dropped along with it. Figure 73 shows the same run using new powder and silver wire. This time when the silver wire degraded it broke immediately after forty-two hours. These two curves show the influence of the silver wire on the resistance and the nonreproducible nature of this particular setup. Because of the difficulty and problems of using the 0.25 mm silver wires, the 1 mm wire was used in the next run and the powder used was calcined twice. Figure 74 shows the 2 cycle graph where each cycle lasted twenty-four hours. The purpose of this was to determine whether or not a single sample's resistance curve would be reproducible. By using the two times calcined powder the curves appeared much more regular and controlled. A very interesting point of this run was that the second cycle had a higher dwell resistance than the first cycle. This seemed exactly opposite of what one would expect. The most interesting aspect of the resistivity data is shown in Figure 75. This was the heating curve shown in Figure 74. If the curve would have been run against temperature instead of time, then a resistance versus temperature curve could have been graphed from 77.3 K to 1118 K (845 °C). Even so, it is easy to see from the time data that the metallic behavior continues all the way to the sintering temperature of 845 °C.

9. YBCO Material

The synthesis of the near room temperature superconductor, $Y_5Ba_6Cu_{11}O_y$ was not successful. None of the materials prepared ever showed even a small hint of the Meissner effect. The resistance versus temperature curves for the tapecast samples annealed in air and oxygen are shown in Figure 76. Both curves showed insulator behavior although the tape annealed in oxygen does show a drop in resistance around the 123 onset temperature. The resistivities however are very different, the oxygen annealed tape's resistivities are 10^{-3} lower than that of the air annealed tape's. The tapes were not subjected to the extreme pressures that the previous investigators used.[57]

IV. Conclusions

In conclusion, we have developed and demonstrated the feasibility of producing superconducting powders in the Y and Bi-based systems and fabricated these materials into rigidly supported, environmentally protected superconducting circuit elements such as conductors, coils, and connectors. We have also developed reliable and reproducible mixed oxides and chemical coprecipitation process for producing Bi-based superconductors. Processing and forming techniques, such as melt quenching, hot pressing, pressing pressure, tapecasting, screen printing, sol-gel, and freeze drying have been investigated for producing maximum density and grain orientation in an effort to maximize the J_c. The Bi-based materials have been characterized and evaluated in regard to their various properties of interest; i.e., bulk density, crystalline structure, microstructure, thermal conductivity, thermal expansion, T_c, J_c, and contact resistivity.

To produce coprecipitated hot pressed material with the best properties the starting material should be calcined at least two times, but for uniaxially pressed materials the starting material should be calcined only once. The mixed oxide materials, however, should be calcined three times to obtain materials with the best properties. Higher pressing pressures have shown to produce materials which have better electrical properties than those produced

from the lower pressing pressures. The mixed oxide samples showed a 0.5 °K increase in T_c as the pressure was increased, and the chemically coprecipitated samples showed a 3.6 °K increase in T_c with the same increase in pressure. The chemically coprecipitated powder is preferred over the mixed oxide powder because a larger percentage of the high T_c 2223 phase can be formed in a much smaller amount of time. The hot pressed samples, both mixed oxide and chemically coprecipitated, showed an increase in T_c of approximately 25 °K from the as hot pressed condition to the post annealed condition. The hot press with post anneal enhanced the formation of the 2223 phase for the mixed oxide materials by reducing the sintering time required to form a nearly phase pure material. This shows the influence that pressure has on the conversion of the lower T_c phase to the higher T_c phase. The higher pressure causes conversion in a substantially shorter amount of time due to the compact being much more dense and uniform. The initial pressing pressure and the pressure throughout sintering had similar effects on the BSCCO materials, in that, the increased pressure increased the density of these materials and the grains became more oriented. The increased density caused an increase in the number of particle to particle contacts which increased the reactivity of the materials. This could be due to the sliding and/or breaking up of particles for increased particle packing. Altogether, the higher pressures decreased the amount of time required to form the high T_c 2223 phase and increased the critical transition temperature.

Doping the BSCCO material with antimony increases the critical temperature but not to the extent that other investigators have seen. The acetate and nitrate based coprecipitated powders have approximately the same electrical properties. When synthesizing both the mixed oxide and coprecipitated thick film materials, which includes tapecasting, the best results occur when the materials are sintered under a low oxygen atmosphere because the films can be sintered longer and become more dense. This allows a larger percentage of the 2223 phase to form. The BSCCO thick films printed on MgO and PLZT substrates, and fired at 845°C for 1 hour had the highest T_c of 89.0 K. The J_c for all films is very low due to the poor interconnections. This could be increased by making denser, single phase films. The MgO buffer layer improved the electrical properties of the BSCCO thick films and the MSZ substrate is considered to be the best substrate for this work.

Superconducting grounding links have been made with better properties than the YBCO grounding links using tapes made from coprecipitated powder. The critical temperature for these links was approximately 101 K. We were unable to reproduce the near room temperature superconductors in the YBCO system.

V. References

1. Maeda, H., Y. Tanaka, M. Fukutomi and T. Asano, (1988). "A New high-T_c Oxide Superconductor Without a Rare Earth Element," *Jap. J. Appl. Phys.*, vol. 27, No. 2, February, pp. L209-L210.

2. Haertling, G. H., (1990). "Development and Evaluation of Superconducting Circuit Elements," NASA Final Report, Contract No. NAG-1-820, October.

3. Haertling, G. H., (1991). "Ceramic Superconducting Components," *Ceramic Transaction*, Vol. 18

4. Tripathi, R. B., and D. W. Johnson Jr., (1991). "Influence of Lead in the Processing of High Temperature 2223 Bi-Sr-Ca-Cu-O Superconductor," *J. Am. Ceram. Soc.*, vol. 74, No. 1, January, pp. 247-249.

5. Takano M., J. Takada, K. Oda, H. Kitaguchi, Y. Miura, Y. Ikeda, Y. Tomii and H. Mazaki, (1988). "High-T_c Phase Promoted and Stabilized in the Bi, Pb-Sr-Ca-Cu-O System," *Jap. J. Appl. Phys.*, vol. 27, No. 2, February, pg. L1041.

6. Yamada Y., and S. Murase, (1988). "Pb Introduction to the High-T_c Superconductor Bi-Sr-Ca-Cu-O System," *Jap. J. Appl. Phys.*, vol. 27, No. 6, June, pp. L996-L998.

7. Mizuno, M., H. Endo, J. Tsuchiya, N. Kijima, A. Sumiyama and Y. Oguri, (1988). "Superconductivity of $Bi_2Sr_2Ca_2Cu_3Pb_xO_y$ (x = 0.2, 0.4, 0.6)," *Jap. J. Appl. Phys.*, vol. 27, No. 7, July, pp. L1225-L1227.

8. Togano, K., H. Kumakura, H. Maeda, E. Yanagisawa and K. Takahashi, (1988). "Properties of the Pb-doped Bi-Sr-Ca-Cu-O Superconductor," *Appl. Phys. Lett.*, 53 (14), 3 October, pp. 1329-1331.

9. Narumi, S., H. Ohtsu, I. Iguchi and R. Yoshizaki, (1989). "Synthesis of 110 K Bi(Pb)-Sr-Ca-Cu-O Oxide Superconductors," *Jap. J. Appl. Phys.*, vol. 28, No. 1, January, pp. L27-L30.

10. Kim, C. J., C. K. Rhee, H. G. Lee, S. J-L. Kang and D. Y. Won, (1989). "The Formation of the High-T_c Phase in the Pb-Doped Bi-Sr-Ca-Cu-O System," *Jap. J. Appl. Phys.*, vol. 28, No. 1, January, pp. L45-L48.

11. Chen, Y. L., and R. Stevens, (1992). "2223 Phase Formation in Bi(Pb)-Sr-Ca-Cu-O: II, The Role of Temperature - Reaction Mechanism," *J. Am. Ceram. Soc.*, vol. 75, No. 5, May, pp. 1150-1159.

12. Wong-Ng, W., C. K. Chiang, S. W. Freiman, L. P. Cook and M. D. Hill, (1992). "Phase Formation of the High T_c Superconducting Oxides in the Bi-Pb-Sr-Ca-Cu-O Glass," *Am. Ceram. Soc. Bull.*, vol. 78, No. 8, August, pp. 1261-1267.

13. Oota A., K. Ohba, A. Ishida, A. Kirihigashi, K. Iwasaki and H. Kuwajima, (1989). "Growth Process of the (2223) Phase in Pb-Added Bi-Sr-Ca-Cu-O," *Jap. J. Appl. Phys.*, vol. 28, No. 7, July, pp. L1171-L1174.

14. Oka, Y., N. Yamamoto, H. Kitaguchi, K. Oda and J. Takada, (1989). "Crystallization Behavior and Partially Melted States in Bi-Sr-Ca-Cu-O," *Jap. J. Appl. Phys.*, vol. 28, No. 2, February, pp. L213-L216.

15. Sasakura, H., S. Minamigawa, K. Nakahigashi, M. Kogachi, S. Nakanishi, N. Fukuoka, M. Yoshikowa, S. Noguchi, K. Okuda and A. Yanase, (1989). "Single High-T_c Region of the Bi-Pb-Sr-Ca-Cu-O," *Jap. J. Appl. Phys.*, vol. 28, No. 7, July, pp. L1163-L1166.

16. Huang, Y. T., W. N. Wang, S. F. Wu, C. Y. Shei, W. M. Hurng, W. H. Lee and P. T. Wu, (1990). "Formation of the Liquid Phase in the System Bi-Pb-Sr-Ca-Cu-O," *J. Am. Ceram. Soc.*, vol. 73, No. 11, pp. 3507-3510.

17. Chen, F. H., H. S. Koo and T. Y. Tseng, (1991). "Effect of Ca_2PbO_4 Additions on the Formation of the 110 K Phase in Bi-Pb-Sr-Ca-Cu-O Superconducting Ceramics," *Appl. Phys. Lett.*, 58 (6), 11 February, pp. 637-639.

18. Kijima, N., H. Endo, J. Tsuchiya, A. Sumiyama, M. Mizuno and Y. Oguri, (1988). "Reaction Mechanism of Forming the High-T_c Superconductor in the Bi-Pb-Sr-Ca-Cu-O System," *Jap. J. Appl. Phys.*, vol. 27, No. 10, October, pp. L1852-L1855.

19. Huang, Y. T., R. G. Liu, S. W. Lu, P. T. Wu and W. N. Wang, (1990). "Accelerated Formation of 110 K High T_c Phase in the Ca- and Cu-rich Bi-Pb-Sr-Ca-Cu-O System," *Appl. Phys. Lett.*, 56 (8), 19 February, pp. 779-781.

20. Yoon, K. H., and H. B. Lee, (1991). "Formation of the High-T_c Phase in Lead-Doped Bi-Sr-Ca-Cu-O Superconductors," *J. Mat. Sci.*, vol. 26, pp. 5101-5106.

21. Hatano T., K. Aota, S. Ikeda, K. Nakamura and K. Ogawa, (1988). "Growth of the 2223 Phase in Leaded Bi-Sr-Ca-Cu-O System," *Jap. J. Appl. Phys.*, vol. 27, No. 11, November, pp. L2055-L2058.

22. Rojek, A., G. Wasilewska, A. Bohdziewicz, B. Cendlewska and E. Trojnar, (1991). "115 K Superconductivity of Bi(Pb/Sb)-Sr-Ca-Cu-O Thick Films," *Physica C*, vol. 183, pp. 130-134.

23. Spencer, N. D., S. D. Murphy, G. Shaw, A. Gould, E. M. Jackson and S. M. Bhagat, (1989). "Solution-Phase Preparation and Characterization of $Bi_{1.6}Pb_{0.3}Sb_{0.1}Ca_2Sr_2Cu_3O_{10}$," *Jap. J. Appl. Phys.*, vol. 28, No. 9, September, pp. L1564-L1567.

24. Komatsu, T., R. Sato, K. Matusita and T. Yamashita, (1989). "Effect of Sb Addition on the Formation of High-T_c Phase in the Bi-Pb-Sr-Ca-Cu-O Ceramics," *Jap. J. Appl. Phys.*, vol. 28, No. 7, July, pp. L1159-L1162.

25. Maeda, T., K. Sakuyama, H. Yamauchi and S. Tanaka, (1989). "Effects of Sb-Doping on the Formation of Superconducting Phases in Bi-Pb-Sr-Ca-Cu Oxides," *Physica C*, vol. 159, pp. 784-788.

26. Endo, U., S. Koyama and T. Kawai, (1989). "Composition Dependence on the Superconducting Properties of Bi-Sr-Ca-Cu-O," *Jap. J. Appl. Phys.*, vol. 28, No. 2, February, pp. L190-L192.

27. Zorn, G., B. Seebacher, B. Jobst and H. Gobel, (1991). "Investigation of Formation Reactions in the System Bi-Pb-Sr-Ca-Cu-Oxide Starting from Oxides and Carbonates," *Physica C*, vol. 177, pp. 494-508.

28. Chen, Y. L., and R. Stevens, (1992). "2223 Phase Formation in Bi(Pb)-Sr-Ca-Cu-O: I, The Role of Chemical Composition," *Jap. J. Appl. Phys.*, vol. 75, No. 5, May, pp. 1142-1149.

29. Seshu Bai, V., S. Ravi, T. Rajasekharan and R. Gopalan, (1991). "On the Composition of 110 K Superconductor in a (Bi, Pb)-Sr-Ca-Cu-O System," *J. Appl. Phys.*, vol. 70, No. 8, October, pp. 4378-4382.

30. Endo, U., S. Koyama and T. Kawai, (1988). "Preparation of the High-T_c Phase of Bi-Sr-Ca-Cu-O Superconductor," *Jap. J. Appl. Phys.*, vol. 27, No. 8, August, pp. L1476-L1479.

31. Koyama, S., U. Endo and T. Kawai, (1988). "Preparation of Single 110 K Phase Bi-Pb-Sr-Ca-Cu-O Superconductor," *Jap. J. Appl. Phys.*, vol. 27, No. 10, October, pp. L1861-L1863.

32. Garzon, F. H., J. G. Beery and I. D. Raistrick, (1988). "Amorphous-to-Crystalline Transformations in the Bismuth-Oxide-Based High T_c Superconductors," *Appl. Phys. Lett.*, 53 (9), 29 August, pp. 805-807.

33. Komatsu, T., R. Sato, K. Matusita and T. Yamashita, (1989). "Superconducting Glass Ceramics With T_c = 100 K Based on the Bi-Pb-Sr-Ca-Cu-O System," *Jap. J. Appl. Phys.*, 54 (12), 20 March, pp. 1169-1171.

34. Nakajima, M., S. Kawarabuki, T. Sasaki, N. Nojiri, Y. Watanabe, H. Ikeda and R. Yoshizaki, (1989). "Synthesis of a 107 K Superconducting Phase in the Bi-Sr-Ca-Cu-O System," *Jap. J. Appl. Phys.*, vol. 28, No. 6, June, pp. L943-L945.

35. Tarascon, J. M., W. R. McKinnon, P. Barbour, D. M. Hwang, B. G. Bagley, L.H. Green, G. Hull, Y. LePage, N. Stoffel and M. Groud, (1988). "Preparation, Structure and Properties of the Superconducting Compound Series $Bi_2Sr_2Ca_{n-1}Cu_nO_y$ with n=1, 2 and 3." *Phys. Rev. B*, vol. 38, No. 13, November, pp. 8885-8892

36. Ono, A.,(1988). "Synthesis of the 107 K Superconducting Phase in the Bi-Sr-Ca-Cu-O System," *Jap. J. Appl. Phys.*, vol. 27, No. 7, July, pp. L1213-L1215.

37. Ibara, Y., H. Nasu, T. Imura and Y. Osaka, (1988). "Preparation and Crystallization Process of the High-T_c Superconducting Phase ($T_{c(end)}$>100 K) in Bi, Pb-Sr-Ca-Cu-O Glass-Ceramics," *Jap. J. Appl. Phys.*, vol. 28, No. 1, January, pp. L37-L40.

38. Hagberg, J., A. Uusimaki, J. Levoska and S. Leppavuori, (1989). "Preparation of Bi-Pb-Sr-Ca-Cu-O High-T_c Superconducting Material via oxalate route at Various pH Values," *Physica C*, vol. 160, pp. 369-374.

39. Shei, C. Y., R. S. Liu, C. T. Chang and P. T. Wu, (1990). "Preparation and Characterization of Superconducting $(Bi, Pb)_2Sr_2Ca_2Cu_3$ Oxides with T_c above 110 K by Coprecipitation in Triethylamine Media," *Inorg. Chem.*, vol. 29, pp. 3117-3119.

40. Weast, R. C., (1987). *CRC Handbook of Chemistry and Physics*, CRC Press Inc., Boca Raton, Florida

41. Hashimoto, T., T. Kosaka, Y. Yoshida, K. Fueki and H. Koinuma, (1988).
"Superconductivity and Substrate Interaction of Screen-Printed Bi-Sr-Ca-Cu-O Films,"
Jap. J. Appl. Phys., vol. 27, No. 3, March, pp. L384-L386.

42. Przybylski, K., J. Koprowski, J. Oblakowski and M. Wierzbicka, (1990). "Deposition
Thick Film Patterns of the High T_c Superconducting Y-Ba-Cu-O and Bi-Sr-Ca-Cu-O
Systems on Ceramic Substrate," *J. of Less Common Metals*, 164 & 165, pp. 470-477.

43. Tabuchi, J., Y. Shimakawa, A. Ochi and K. Utsumi, (1989). "Fabrication of
Screen-Printed High-T_c Superconducting Thick Films on Several Substrates," *High Tc
Superconductor I*, pp. 464-473.

44. Lee, K., and G. Park, (1991). "Patterned Bi-Sr-Ca-Cu-O Films on $Sr_2Ca_2Cu_4O_y$
Substrates by Surface Diffusion of Metallic Bismuth," *Jap. J. Appl. Phys.*, vol. 30,
No. 10, October, pp. 2468-2470.

45. Barboux, P., J. M. Tarascon, F. Shokoohi, B. J. Wikens and C. L. Schwartz, (1988).
"Thick Films of Bi-Sr-Ca-Cu-O and Tl-Ba-Ca-Cu-O by Solution Process," *J. Appl. Phys.*,
64 (11), 1 December, pp. 6382-6387.

46. Ho, J. C., C. Y. Wu, X. W. Cao and F. J. Schmidt, (1991). "Melt Textured Thick Films
of $Bi_{1.7}Pb_{0.3}Sr_2CaCu_2O_y$ Prepared by Electrophoretic deposition," *Supercond. Sci.
Technol. (UK)*, Vol. 4, no. 10, October,pg. 507-508.

47. Bohn, C. L., J. R. Delayen, U. Balachandran and M. T. Lanagan, (1989). "Radio
Frequency Surface Resistance of large-Area Bi-Sr-Ca-Cu-O Thick Films on Ag Plates,"
Appl. Phys. Lett., 55 (3), 17 July, pp. 304-306.

48. Kumakura, H., K. Togano, J. Kase, T. Morimoto and H. Maeda, (1990).
"Superconducting Properties of Textured Bi-Sr-Ca-Cu-O Tapes Prepared by Applying
Doctor Blade Casting," *Cryogenics*, 30, November, pp. 919-923.

49. Hoshino,K., and T.Takahara, (1989). "Fabrication of High-T_c Bi-Pb-Sr-Ca-Cu-O Superconducting Printed Films on Ag Tape," *Jap. J. Appl. Phys.*, vol. 28, No. 7, July, pp. L1214-L1216.

50. Hoshino, K., H. Takahara and M. Fukutomi, (1988). "Preparation of Superconducting Bi-Sr-Ca-Cu-O Printed Thick Films on MgO Substrate and Ag Metal Tape," *Jap. J. Appl. Phys.*, vol. 27, No. 7, July, pp. L1297-L1299.

51. Muthe, K. P., S. K. Sinha, S. C. Gadkari, S. C. Sabharwal and M. K. Gupta, (1990). "Phase Formation and Crystallization in Bi-Sr-Ca-Cu-O Thick Films," *Appl. Phys. A*, 51, pp. 65-67.

52. Kobayashi, T., K. Nomura, F. Uchikawa, T. Masumi and Y. Uehara, (1988). "Superconducting Bi-Sr-Ca-Cu-O Thick Films by the Sol-Gel Method," *Jap. J. Appl. Phys.*, vol. 27, No. 10, October, pp. L1880-L1882.

53. Tohge, N., Y. Akamatsu, S. Tsuboi, M. Tatsumisago and T. Minami, (1989). "Substitution effects of Pb for Bi on the Formation of High-T_c Superconducting Thick Films in the Bi-Pb-Sr-Ca-Cu-O System by the Melt-Solidification Method," *Jap. J. Appl. Phys.*, vol. 28, No. 8, August, pp. L1408-L1410.

54. Brousse, T., R. Retoux, G. Poulain, J. Provost, H. Murray, D. Bloyet and B. Raveau, (1989). "Superconducting Screen-Printed Thick Films of $YBa_2Cu_3O_7$ and $Bi_{1.6}Pb_{0.4}Sr_{1.6}Ca_{2.4}Cu_{3.6}O_{10}$ on Polycrystalline Substrates," *Appl. Phys. A*, 49, pp. 217-220.

55. Uusimaki, A., I. Kirschner, J. Levoska, J. Hagberg, G. Zsolt, G. Kovacs, T. Porjesz, I. Dodony, S. Leppavuori, E. Lahderanta and R. Laiho, (1990). "Relationship Between Microstructure and Critical Parameters in High-T_c Superconducting Bi-Pb-Sr-Ca-Cu-O Thick Films ," *Cryogenics*, 30, July, pp. 593-598.

56. Kim, D. H., W. S. Um, K. No and H. G. Kim, (1991). "Preparation of Superconducting Bi(Pb)-Sr-Ca-Cu-O Thick Films on Magnesia Substrate," *J. Am. Ceram. Soc.*, vol. 74, No. 9, September, pp. 2102-2106.

57. Chen, J. T., L. X. Qian, L. Q. Wang and L. E. Wenger, (1989). Zero Resistance States Above 200 K Found in $Y_5Ba_6Cu_{11}O_y$," *Superconductor Week*, Vol. 3, No. 38, October 2, pp. 1-2.

58. Reed, J. S., (1988). *Introduction to the Principles of Ceramic Processing*, John Wiley & Sons, New York.

59. Seshu Bai, V., S. Ravi, T. Rajasekharan and R. Gopalan, (1991). "On the composition of 110 K superconductor in a (Bi, Pb)-Sr-Ca-Cu-O system," *J. Appl. Phys.*, vol. 70, No. 8, October, pp. 4378-4382.

60. Strobel, P., and T. Fournier, (1990). Phase Diagram in the Bi (Pb)-Sr-Ca-Cu-O system," *J. of Less Common Metals*, 164 & 165, pp. 519-525.

61. Briggs, A., B. A. Bellamy, I. E. Denton and J. M. Perks, (1990). Preparation of Single Phase Bismuth-Based 2212 and 2223 Superconducting Oxides, and Quantitative X-Ray Diffraction Analysis of 2212 and 2223 Mixtures," *J. of Less Common Metals*, 164 & 165, pp. 559-567.

62. Sax, N. I., and R. J. Lewis Sr., (1988). *Hawley's Condensed Chemical Dictionary*, 11 th ed., Van Nostrand Reinhold Co., New York.

Table 1 Review of BSCCO Thick Films.

Substrate	Phase	Firing Condition	T_c (K)	Reference
Quartz	1112	830°C - 1hr.	NS	37
Alumina	1112	830°C - 1hr. 850°C - 1hr.	NS NS	37
Alumina	2223	890°C - 10 min.	M	38
Sapphire	1112 2223	890°C - 900°C 890°C - 900°C	I I	39
$Sr_2Ca_2Cu_4O_y$	2212	830°C - 1min.	79	40
SrTiO3	1112	840°C - 1hr. 850°C - 1hr.	11 NS	37
SrTiO3	4334	875°C - 2 min.	76	41
Ag	2212	900°C - 3 min. 860°C - 5-10 min.	75	42
Ag	2212	910°C - 10 min. 825°C - 4 hr.	81 - 83	43
Ag	2212	870°C (slow cooled) 870°C (quenched)	>77 89	44
Ag	2223	830°C - 845°C -- 48 hr. - 72 hr. 830°C - 845°C -- 12 hr. - 48 hr.	CR 100 - 105	45
Ag	2223	880°C - 10 min.	76	46
YSZ	1112	890°C - 1 hr. 890°C - 4 hr. 890°C - 5 min.	40 I 45	39
YSZ	1112	840°C - 1hr. 850°C - 1hr. 900°C - 1hr. 850°C - 1hr.	22 65 NS 11	37
YSZ	2212	840°C - 1hr. 850°C - 1hr.	35 68	37

NS -- Non Superconducting   D -- Two Phase   I — Insulating
CR -- Cold Rolling   S – Semiconducting   M – Metallic

Table 1 Cont.

Substrate	Phase	Firing Condition	T_c (K)	Reference
YSZ	2223	890°C - 4 hr.	I	39
		900°C - 5 min.	66	
		900°C - 1 hr.	72	
MgO	1112	890°C - 1 hr.	60	39
		890°C - 4 hr.	S	
		890°C - 5 min.	62	
MgO	2212	890°C (quenched)	84	47
MgO (100)	2112	860°C - 2 hr.	18 S	48
		870°C - 2 hr.	84 D	
		880°C - 2 hr.	76	
		890°C - 2 hr.	77	
		900°C - 2 hr.	78	
MgO	4334	860°C - 10 min.	NS	41
MgO (100)	2223	860°C - 30 min.	40	46
		880°C - 30 min.	80	
		885°C - 1 hr.--	107	
		872°C - 72 hr.		
MgO	$Bi_{1.8}Pb_{0.2}Sr_2Ca_2Cu_3O_{10}$	1000°C - 5 min. --		49
		840°C - 30 min.	82	
		850°C - 30 min.	90	
		850°C - 15 hr.	102	
		850°C - 38 hr.	92	
		860°C - 30 min.	M	
MgO	2223	890°C - 4 hr.	S	39
		900°C - 5 min.	55	
		900°C - 1 hr.	NS	
MgO	$Bi_{1.6}Pb_{0.4}Sr_{1.6}Ca_{2.4}Cu_3O_{10}$	865°C - 1 hr.	92	50
		865°C - 3 hr.	95	
		865°C - 5 hr.	101	
		865°C - 7 hr.	85	
		865°C - 10 hr.	99	
		865°C - 15 hr.	86	
		865°C - 250 hr.	104	
MgO	$Bi_{1.9}Pb_{0.4}Sr_{1.9}Ca_{2.1}Cu_{3.2}O_{10}$	895°C - 3 min.--		51
		852°C - 80 hr.	57	
		865°C - 80 hr.	105	

NS -- Non Superconducting   D -- Two Phase   I -- Insulating

CR -- Cold Rolling   S -- Semiconducting   M -- Metallic

Table 1 Cont.

Substrate	Phase	Firing Condition	T_c (K)	Reference
MgO	2223	890°C - 10 min.	M	38
MgO (100)	2223	500°C - 4 hr. --		52
		840°C - 4 hr.	50	
		+830°C - 30 hr.	80	
		+830°C - 60 hr.	89	
		+830°C - 90 hr.	45	
MgO (100)	$Bi_{1.6}Pb_{0.3}Sr_2Ca_2Cu_3O_{10}$	840°C - 60 hr.	85	53
	$Bi_{1.9}Pb_{0.6}Sr_2Ca_2Cu_3O_{10}$	920°C - 6 min.--		
		840°C - 65 hr.	102	
	$Bi_{1.9}Pb_{0.6}Sb_{0.1}Sr_2Ca_2Cu_3O_{10}$	920°C - 6 min.--		
		845°C - 65 hr.	115	

NS -- Non Superconducting   D -- Two Phase   I --- Insulating

CR -- Cold Rolling   S -- Semiconducting   M -- Metallic

Table 2 The results of the bismuth base material to date. The table contains information on the material, the process used, the T_c, the J_c, the bulk density and any special procedures used in synthesizing the material.

Material	Process	Special	T_c (K)	J_c (A/cm^2)	Bulk Density (gms/cc)
Mixed oxide	Bulk	200 hr Sintering	108.1	80	4.5
		High pressure (125 hr)	107.3	78	4.8
		Low pressure (125 hr)	106.8	75	4.4
		20 hr Sintering	98.9	50	4.1
		2 Calcines (30 hr)	99.1	50	4.1
		3 Calcines (30 hr)	102.0	50	4.2
		4 Calcines (30 hr)	102.0		
	Hot pressed	2 Calcines NAHT	M	M	M
		3 Calcines NAHT	83.3		6.2
		2 Calcines (24 hr)	104.4	100	5.7
		3 Calcines (24 hr)	108.2	140	6.0
	Tapecast	Single ramp	99.5	20	3.3
		Single ramp (covered)	101.5	81	3.5
		Double ramp (covered)	99.0	47	3.3
		Low O$_2$ Atmosphere	101.7	48	
Melt Quenched	Bulk	As quenched	T	T	T
		30 hr Sintering	M	M	M
		60 hr Sintering	M	M	M
		90 hr Sintering	102.3	72	4.9
		24 hr (Antimony)	M	M	M
Coprecipitated	Acetate Bulk	1 Calcine	104.1		
		1 Cal (Antimony)	105.3		
	Nitrate bulk	No Calcine	99.1		4.0
		1 Calcine	104.8		4.4
		1 Cal (Antimony)	106.5	100	
		High pressure (860 °C Calcine)	108.8		5.2

NAHT - No Additional Heat Treatment   NBL - No Buffer Layer   BL - Buffer Layer

IS - Insulating/Semiconducting   MS - More Sensitivity   M - Metal   T - Transition

Table 2 Cont.

Material	Process	Special	T_c (K)	J_c (A/cm^2)	Bulk Density (gms/cc)
Coprecipitated	Bulk (Cont.)	High pressure (830 °C Calcine)	108.4		5.1
		2 Calcine (high)	104.3		
		3 Calcine (high)	102.9		
	Hot pressed	1 Calcines NAHT	M	M	M
		2 Calcines NAHT	84.0		6.2
		1 Calcines (24 hr)	106.4	144	6.0
		2 Calcines (24 hr)	108.2	193	6.1
	Tapecast	Single ramp	102.4		
		Low O$_2$ Atmosphere	102.1	120	3.9
		Link	100.5		
	Thick Film				
	MgO	NBL	89.0		
	MSZ (12%)	NBL	M	M	M
		MgO 10 BL	M	M	M
		Low O$_2$, NBL	82.0		
		Low O$_2$, MgO 5 BL	89.0		
	YSZ	10 %, NBL	IS	IS	IS
		10 %, 10 BL	T	T	T
		8 %, NBL	IS	IS	IS
		8 %, 10 BL	T	T	T
		6 %, NBL	T	T	T
		6 %, 10 BL	M	M	M
		6% BSCCO 10 BL	88.4		
	Ag	NBL	MS	MS	MS

NAHT - No Additional Heat Treatment   NBL - No Buffer Layer   BL - Buffer Layer

IS - Insulating/Semiconducting   MS - More Sensitivity   M - Metal   T - Transition

Table 3 The batch information sheet for the Bismuth-based mixed oxide materials showing the raw materials used, their source, and the amount of each needed to achieve the required batch size.

Batch Information Sheet

Composition # 4   **Batch # 11**

Formula: $Bi_{1.6}Pb_{0.4}Sr_{1.9}Ca_{2.05}Cu_{3.05}O_x$

Batch Size: 400 gms.   **Date:** October 29, 1990

Raw Materials and Source

Bi_2O_3	Fisher	$CaCO_3$	Mallinckrodt	CaO	N/A
CuO	Mallinckrodt	$SrCO_3$	Mallinckrodt	PbO	Fisher

Batching

Oxide	Mole Wt	Moles	Formula Wt	Wt %	% Oxide	Batch Wt
Bi_2O_3	465.96	0.80	372.768	36.672	100.000	146.689
SrO	103.62	1.90	196.878	19.369	70.189	110.379
CaO	56.08	2.05	114.964	11.310	56.030	80.743
CuO	79.54	3.05	242.597	23.866	100.000	95.465
PbO	223.19	0.40	89.272	8.783	100.000	35.131
			1016.483	100.000		468.408

Table 4 The batch information sheet for the materials in the YBCO system showing the raw materials used, their source, and the amount of each needed to achieve the required batch size.

Batch Information Sheet

Composition # 1   **Batch #** 5

Formula: $Y_5Ba_6Cu_{11}O_x$

Batch Size: 400 gms.   **Date:** August 12, 1990

Raw Materials and Source

Y_2O_3   Molycorp   **$BaCO_3$**   Fisher   **BaO**   N/A

CuO   Fisher

Batching

Oxide	Mole Wt	Moles	Formula Wt	Wt %	% Oxide	Batch Wt
Y_2O_3	225.81	2.50	564.525	23.925	100.000	95.702
BaO	153.34	6.00	920.040	38.993	77.700	200.737
CuO	79.54	11.00	874.940	37.082	100.000	148.326
			2359.505	100.000		444.765

Table 5 The batch information for the materials in the BSCCO nitrate coprecipitation process, showing the raw materials used, their source, and the amounts of each needed to achieve the required batch size.

Batch Information Sheet

Composition # 1   **Batch #** 31

Formula: $Bi_{1.6}Pb_{0.4}Sr_{1.9}Ca_{2.05}Cu_{3.05}O_x$

Batch Size: 100 gms.   **Date:** November 13, 1992

Raw Materials and Source

$Bi(NO_3)_3$ Mallinckrodt $Pb(NO_3)_2$ Fisher $Sr(NO_3)_2$ Mallinckrodt

$Ca(NO_3)_2 \cdot 4H_2O$ Mallinckrodt NH_4OH Fisher HNO_3 Mallinckrodt

$Cu(NO_3)_2 \cdot 2.5H_2O$ Mallinckrodt Sb_2O_3 Metal and Thermit Corp.

Batching

Oxide	Mole Wt	Moles	Formula Wt	Wt %	% Oxide	Batch Wt
Bi_2O_3	465.96	0.80	372.768	36.672	11.030	332.478
SrO	103.62	1.90	196.878	19.369	48.963	39.558
CaO	56.08	2.05	114.964	11.310	23.748	47.626
CuO	79.54	3.05	242.597	23.866	34.198	69.790
PbO	223.19	0.40	89.272	8.783	67.388	13.033
			1016.483	100.000		502.484

Table 6 The batch information for the materials in the BSCCO acetate coprecipitation process, showing the raw materials used, their source, and the amounts of each needed to achieve the required batch size.

Batch Information Sheet

Composition # 3

Batch # 12

Formula: $Bi_{1.6}Pb_{0.4}Sr_{1.9}Ca_{2.05}Cu_{3.05}O_x$

Batch Size: 100 gms.

Date: October 2, 1992

Raw Materials and Source

$Bi(O_2C_2H_3)_3$	Johnson Matthey	$Sr(O_2C_2H_3)_2$	Johnson Matthey
$Ca(O_2C_2H_3)_2 \cdot H_2O$	Johnson Matthey	$Sb(O_2C_2H_3)_3$	Johnson Matthey
Pb Subacetate	Fisher	$Cu(O_2C_2H_3)_2 \cdot H_2O$	Fisher
Acetic Acid	Fisher	Methanol	Fisher	NH_4OH	Fisher

Batching

Oxide	Mole Wt	Moles	Formula Wt	Wt %	% Oxide	Batch Wt
Bi_2O_3	465.96	0.80	372.768	36.672	60.339	60.777
SrO	103.62	1.90	196.878	19.369	15.410	125.688
CaO	56.08	2.05	114.964	11.310	8.440	134.004
CuO	79.54	3.05	242.597	23.866	39.760	60.026
PbO	223.19	0.40	89.272	8.783	44.800	19.605
			1016.483	100.000		400.100

Table 7 The firing schedule, process, the Tc, and the Jc of the tapecast material using the two stage ramp firing process. All of the tapes were firing at 845 °C for thirty hours.

Sintering Temp. (°C)	Firing Process	T_c (K)	J_c (A/cm^2)
845	Single	101.5	80.8
800	Double	99.0	46.6
700	Double	101.3	50.9
650	Double	90.8	20.1
500	Double	NS	NS

NS - Non Superconducting

Bi2Sr2Cu1O6 Tc=7-20K : Bi2Ca1Sr2Cu2O8 Tc=80K   Bi2Ca2Sr2Cu3O10 Tc=110K
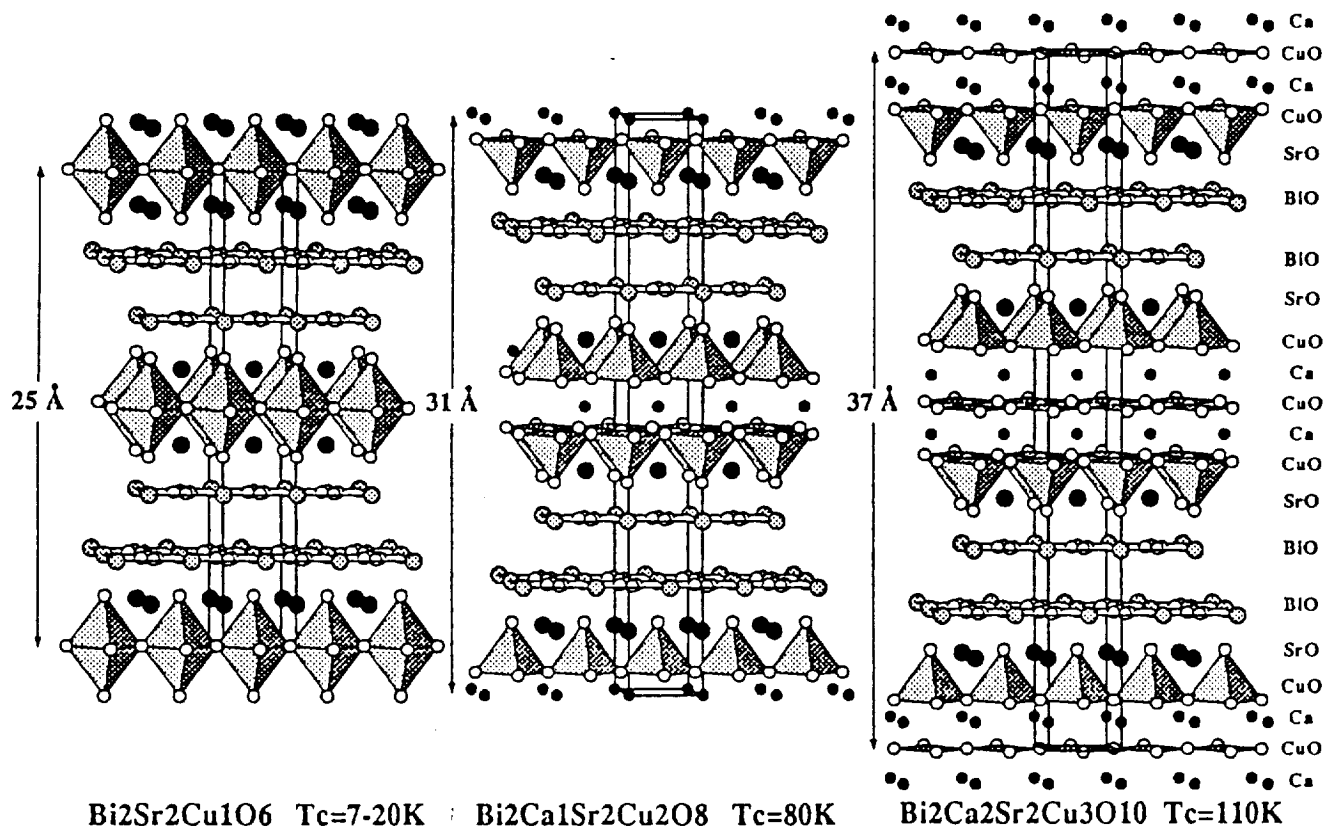
Figure 1 The structures of the three bismuth-based superconductors
$Bi_2Sr_2Ca_{n-1}Cu_nO_{2n+4}$, where n equals 1, 2, or 3 and is the number of CuO
planes sandwiched between double layers of BiO.
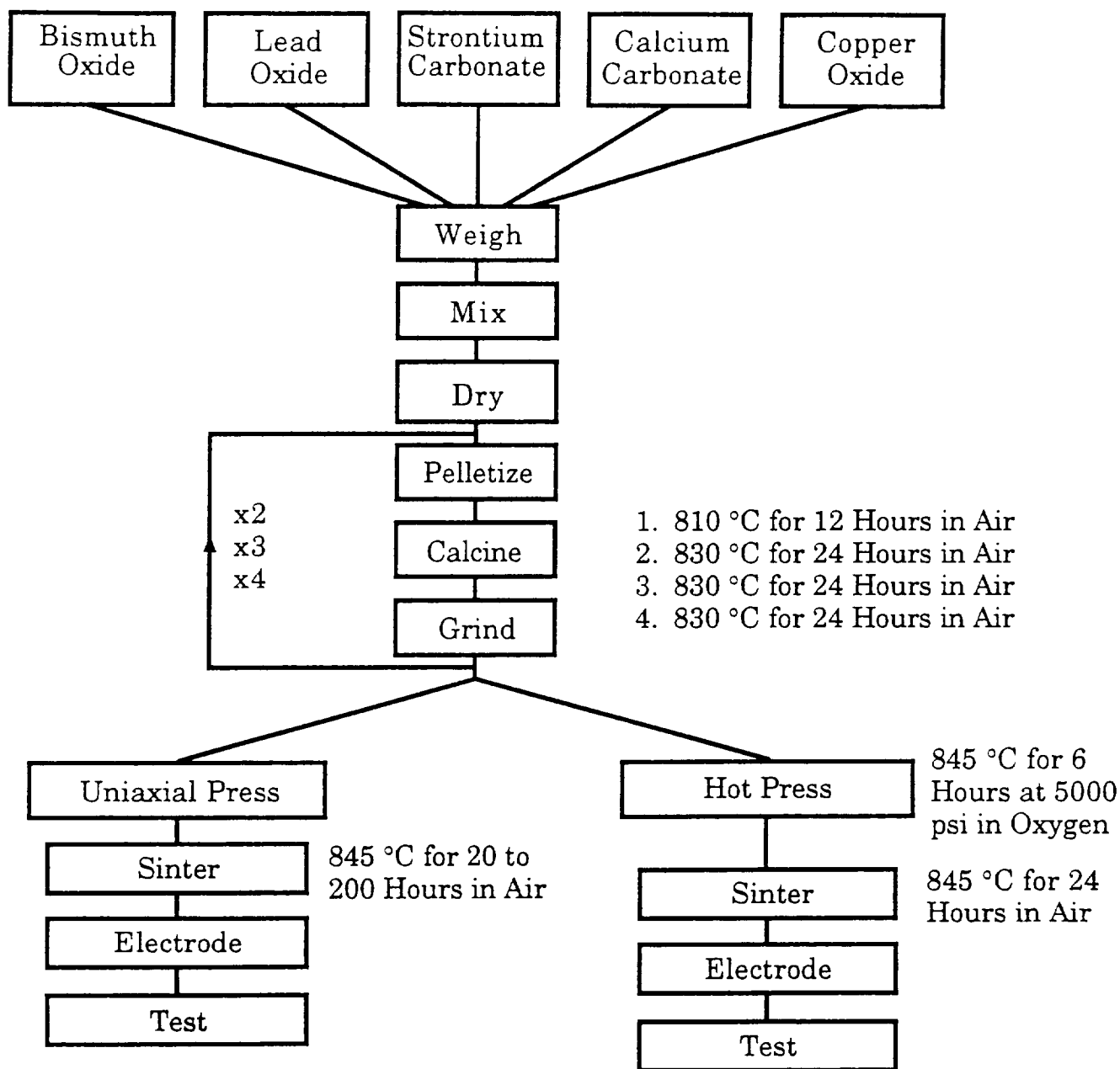
Figure 2 Flow chart for the uniaxially and hot pressed bismuth-based materials showing the procedures used to synthesize these materials. These materials were synthesized using both two, three, and four times calcined powder.
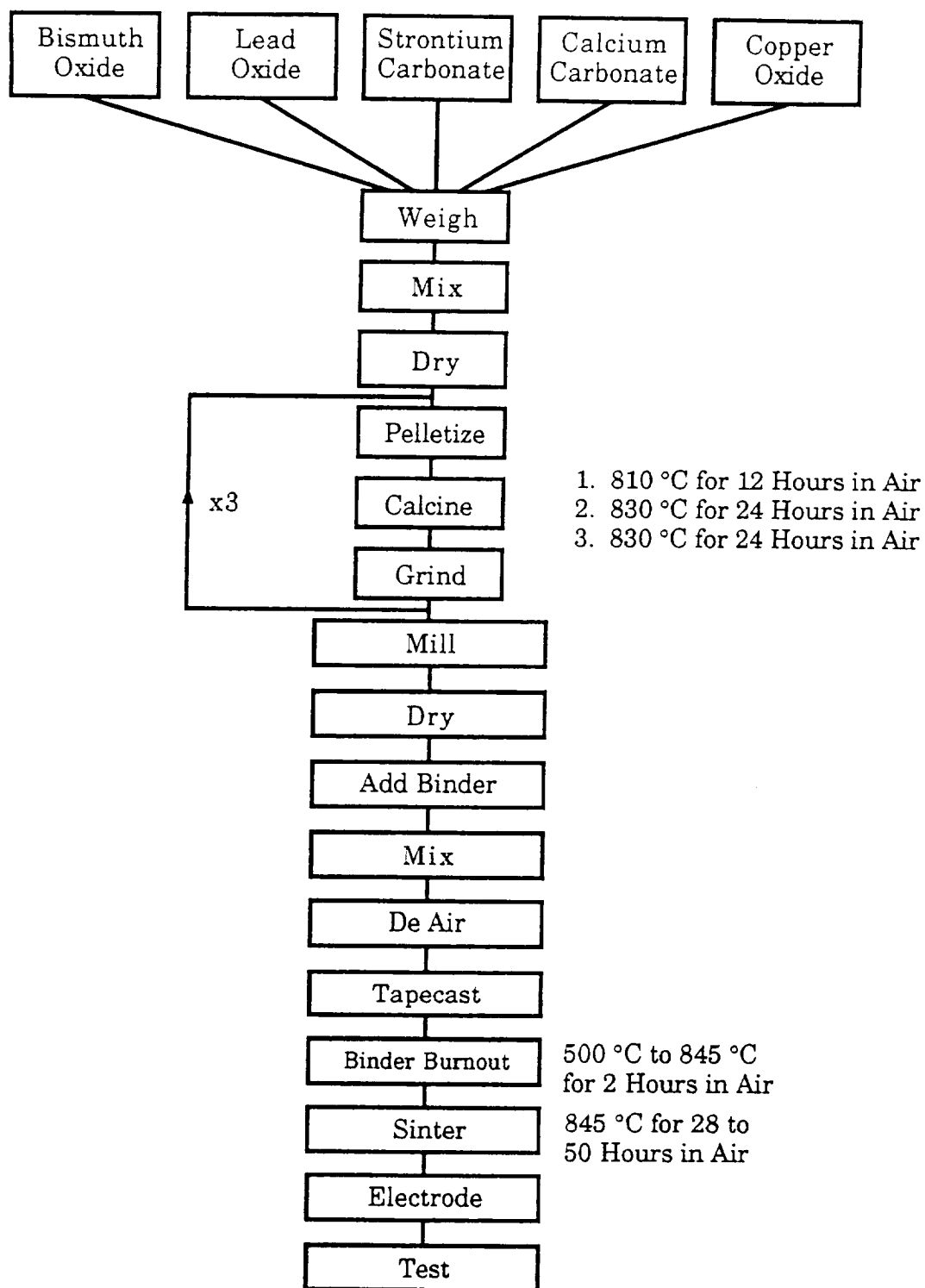
Figure 3 Flow chart for the tapecast bismuth-based materials showing the procedures used to synthesize these materials. These materials were synthesized using three times calcined powder.
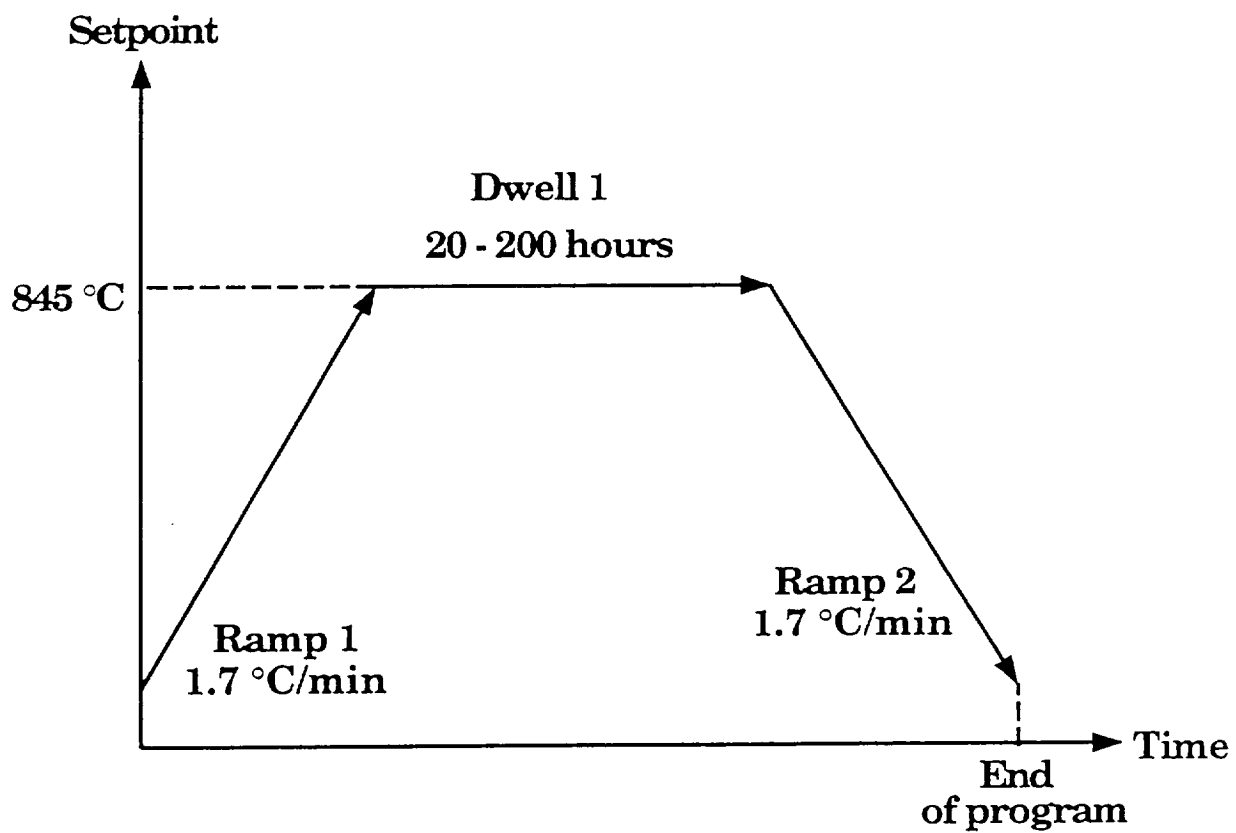
Figure 4 The furnace schedule and operation for the bulk, melt quench, and single ramp tapecast bismuth-based materials.
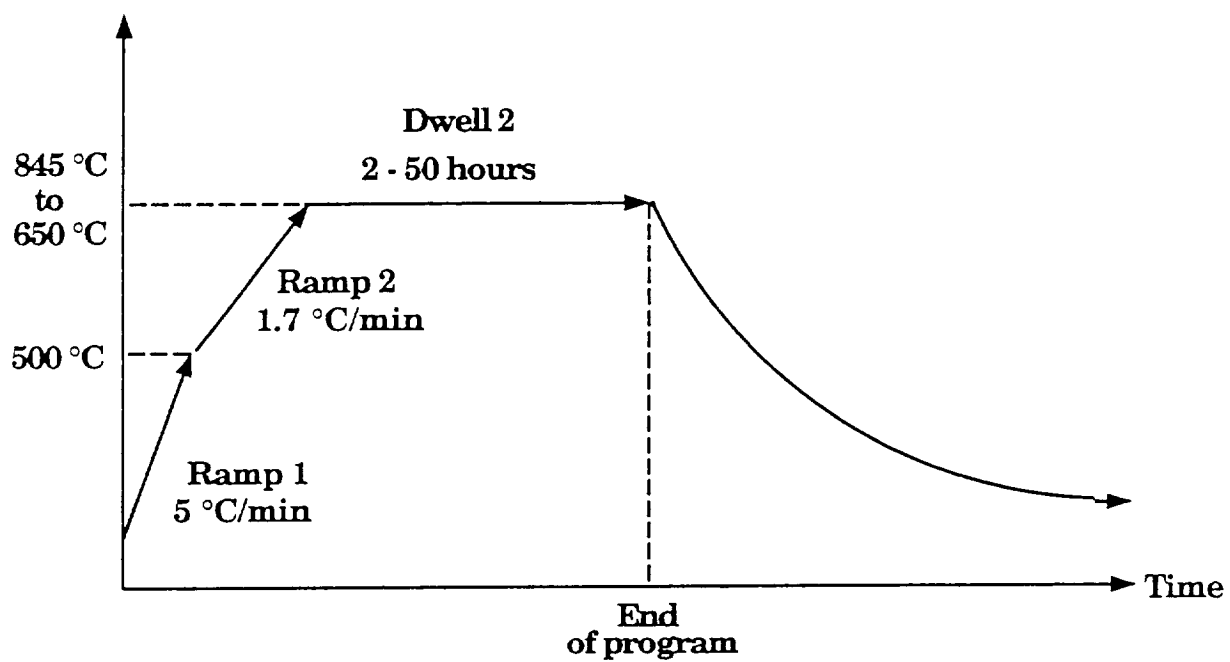
Figure 5 The furnace schedule and operation for the double ramp tapecast bismuth-based materials.
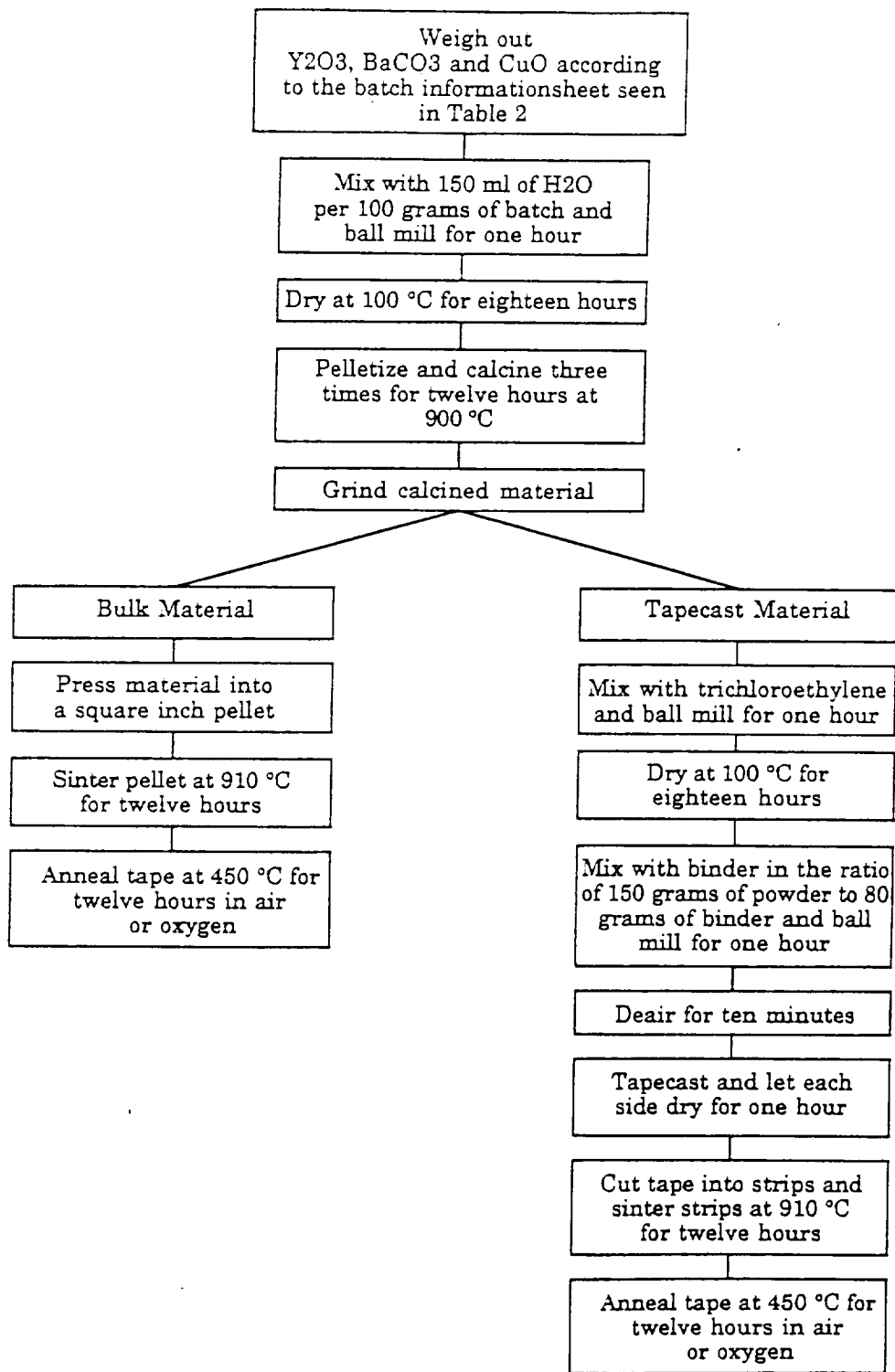
Figure 6 Flow chart for the bulk and tapecast materials in the YBCO system showing the procedures used to synthesize these materials.
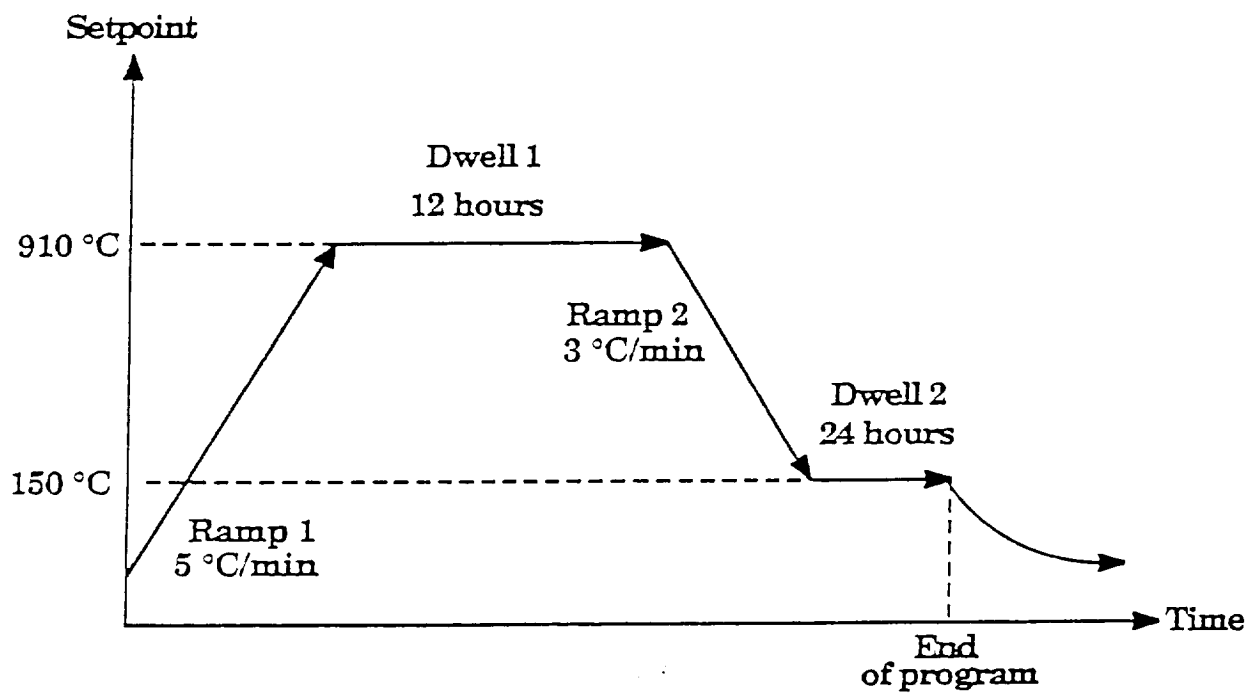
Figure 7 The furnace schedule and operation for the bulk and tapecast materials in the YBCO system.
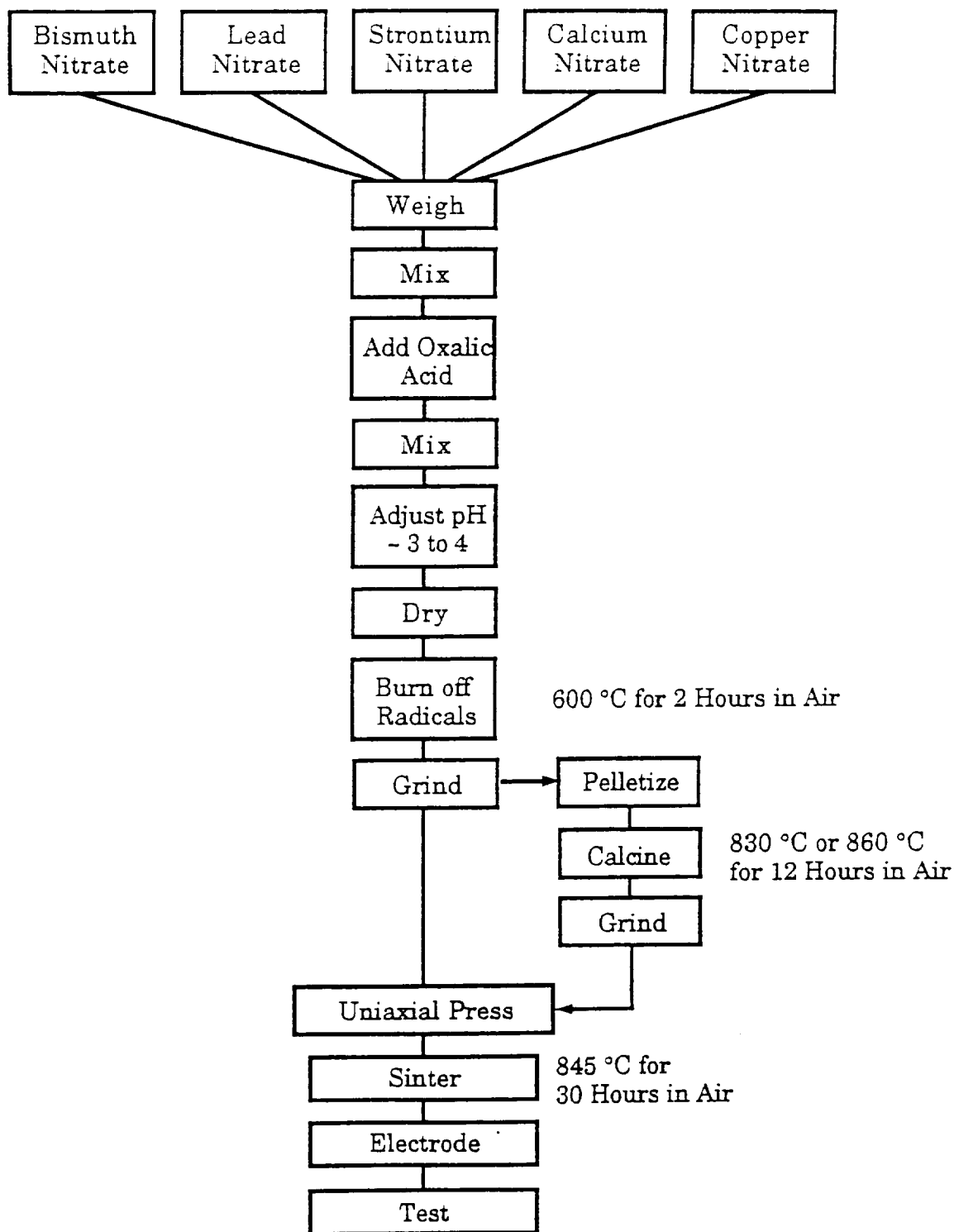
Figure 8 Flow chart for the coprecipitated bismuth-based materials showing the procedures used to synthesize these materials. These materials were synthesized using both calcined and uncalcined powder.
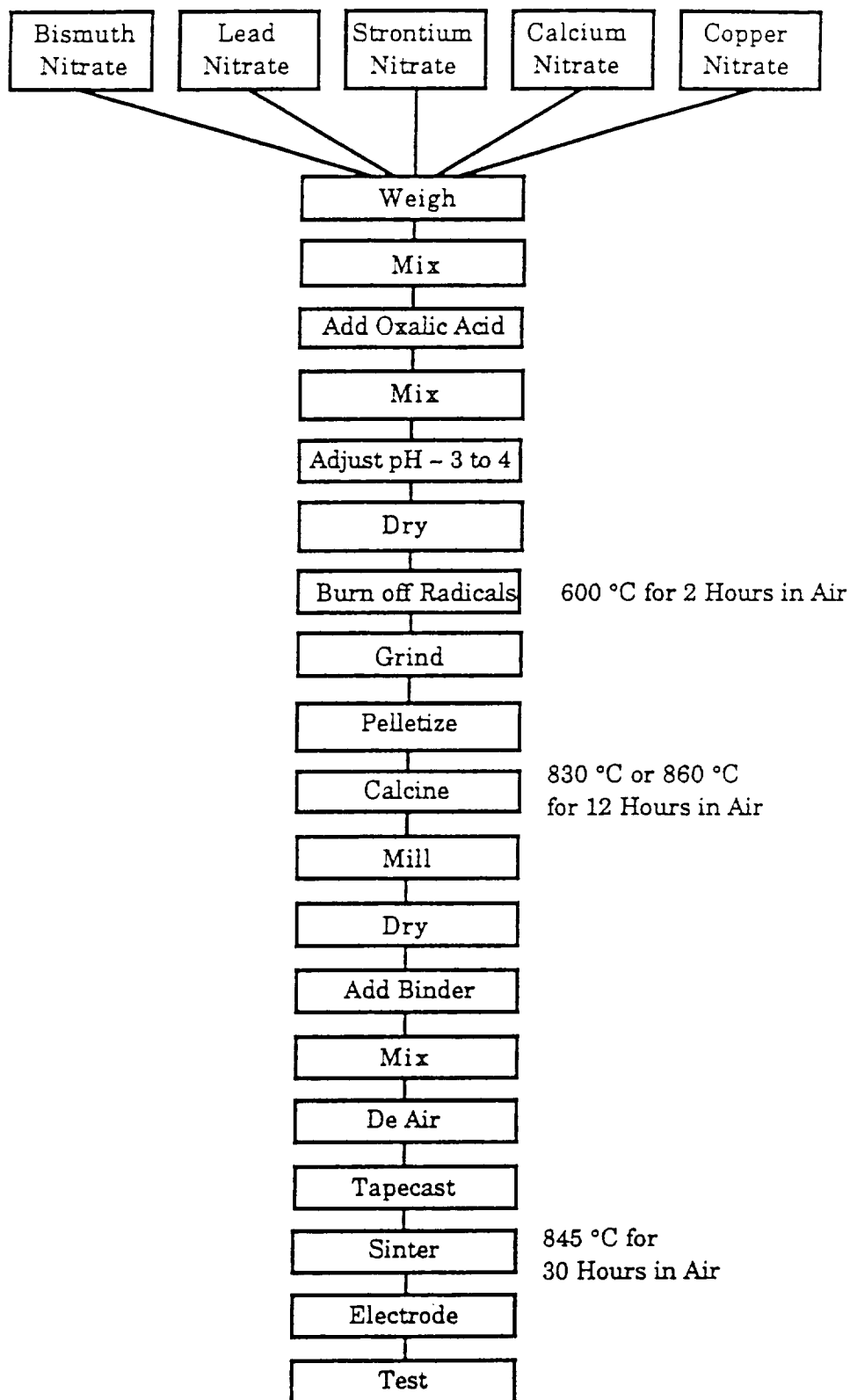
Figure 9 Flow chart for the tapecast bismuth-based materials, made by the coprecipitation process, showing the procedures used to synthesize these materials. These materials were synthesized using one time calcined powder.

```
┌──────────┐ ┌──────────┐ ┌──────────┐ ┌──────────┐ ┌──────────┐
│ Bismuth  │ │  Lead    │ │Strontium │ │ Calcium  │ │ Antimony │
│ Acetate  │ │SubAcetate│ │ Acetate  │ │ Acetate  │ │ Acetate  │
└──────────┘ └──────────┘ └──────────┘ └──────────┘ └──────────┘
                            │
                      ┌───────────┐
                      │   Weigh   │
                      └───────────┘
                      ┌───────────┐
                      │    Mix    │
                      └───────────┘
                      ┌─────────────┐        ┌──────────┐
                      │Adjust pH ~ 11│───────│  Copper  │
                      └─────────────┘        │ Acetate  │
                      ┌───────────┐          └──────────┘
                      │    Mix    │
                      └───────────┘
                      ┌────────────────┐
                      │Adjust pH ~ 3 to 4│
                      └────────────────┘
                      ┌────────────────┐
                      │ Add Oxalic Acid │
                      └────────────────┘
                      ┌───────────┐
                      │    Mix    │
                      └───────────┘
                      ┌───────────┐
                      │    Dry    │
                      └───────────┘
                      ┌────────────────┐
                      │ Burn off Radicals│   600 °C for 2 Hours in Air
                      └────────────────┘
                      ┌───────────┐
                      │   Grind   │
                      └───────────┘
                      ┌───────────┐
                      │ Pelletize │
                      └───────────┘
                      ┌───────────┐
                      │  Calcine  │   830 °C for 12 Hours in Air
                      └───────────┘
                      ┌───────────┐
                      │   Grind   │
                      └───────────┘
                      ┌───────────┐
                      │ Pelletize │
                      └───────────┘
                      ┌───────────┐
                      │  Sinter   │   845 °C for 24 Hours in Air
                      └───────────┘
                      ┌───────────┐
                      │ Electrode │
                      └───────────┘
                      ┌───────────┐
                      │   Test    │
                      └───────────┘
```
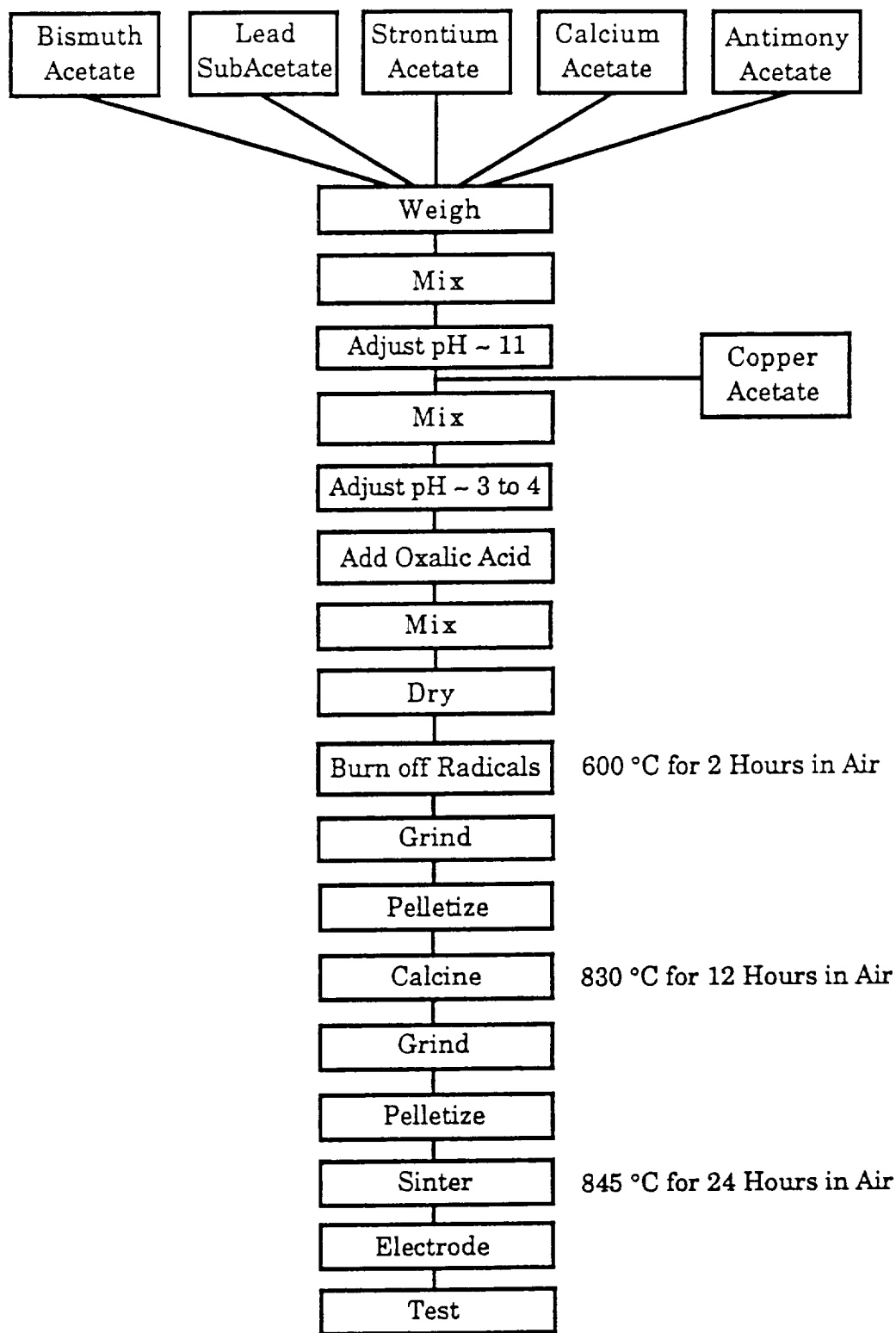
Figure 10 Flow chart for the acetate coprecipitated bismuth-based materials showing the procedures used to synthesize these materials. These materials were synthesized using both calcined and uncalcined powder.

```
┌──────────┐ ┌──────────┐ ┌──────────┐ ┌──────────┐ ┌──────────┐ ┌──────────┐
│ Bismuth  │ │  Lead    │ │ Antimony │ │Strontium │ │ Calcium  │ │ Copper   │
│  Oxide   │ │  Oxide   │ │  Oxide   │ │Carbonate │ │Carbonate │ │  Oxide   │
└──────────┘ └──────────┘ └──────────┘ └──────────┘ └──────────┘ └──────────┘
```

```
                    ┌──────────────┐
                    │    Weigh     │
                    └──────────────┘
                    ┌──────────────┐
                    │     Mix      │
                    └──────────────┘
                    ┌──────────────┐
                    │     Dry      │
                    └──────────────┘
                    ┌──────────────┐
                    │   Calcine    │      820 °C for 12 Hours in Air
                    └──────────────┘
                    ┌──────────────┐
                    │    Grind     │
                    └──────────────┘
                    ┌──────────────┐
                    │     Melt     │      1200 °C for 20 Minutes in Air
                    └──────────────┘      1100 °C for 2 Hours in Air
                    ┌──────────────┐
                    │    Quench    │
                    └──────────────┘
                    ┌──────────────┐      845 °C to 865 °C for
                    │    Sinter    │      24 Hours in Air
                    └──────────────┘
                    ┌──────────────┐
                    │  Electrode   │
                    └──────────────┘
                    ┌──────────────┐
                    │     Test     │
                    └──────────────┘
```
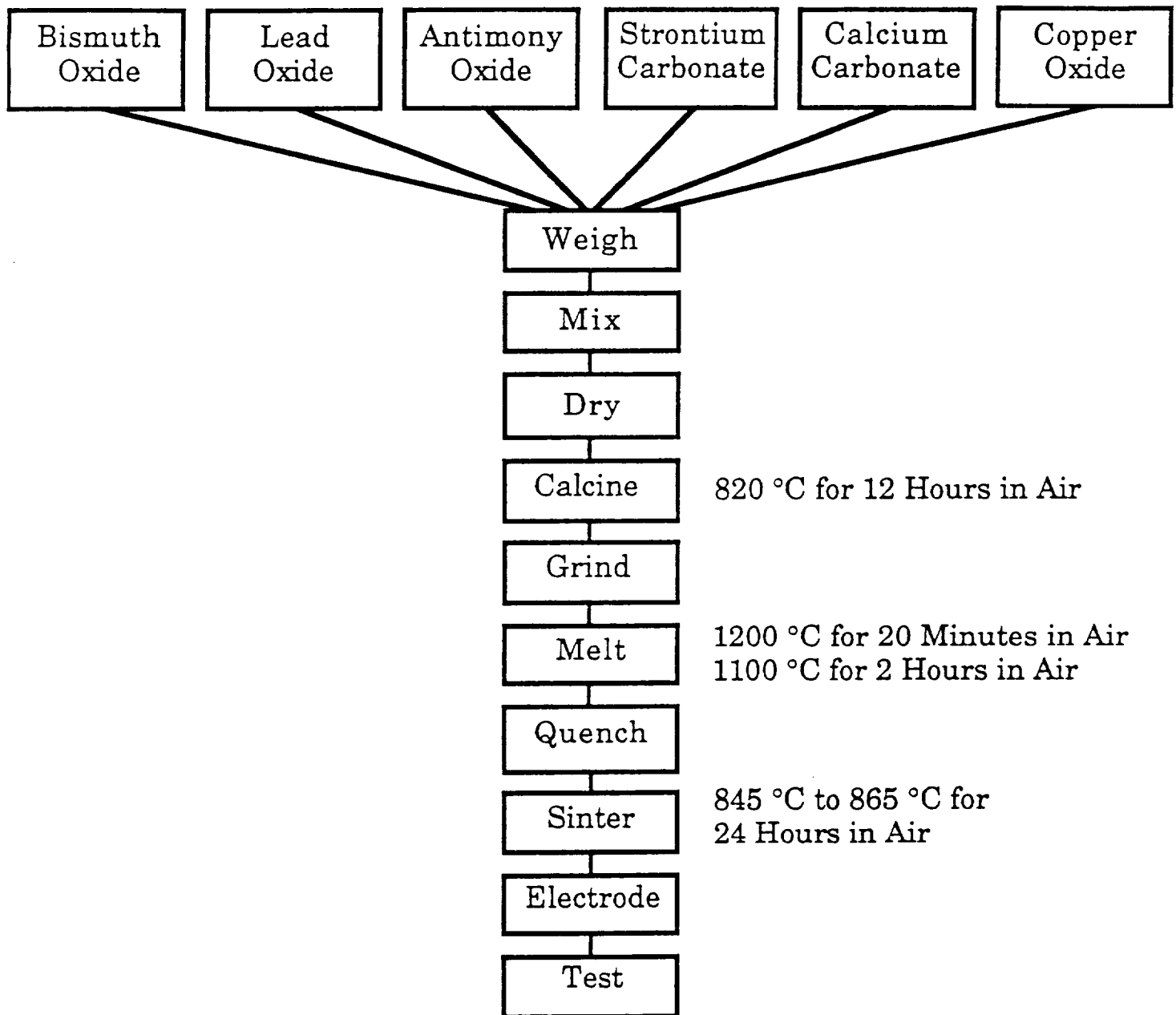
Figure 11 Flow chart for the melt quench process using powder prepared by the mixed oxide process for the bismuth-based materials showing the procedures used to synthesize these materials.

```
        ┌─────────────────┐              ┌─────────────────┐
        │  Buffer Layer   │              │   Substrate     │
        │   Solution      │              │                 │
        └─────────────────┘              └─────────────────┘
                    \                    /
                     \                  /
                      \                /
                   ┌──────────────────────┐
              ┌───▶│         Dip          │
              │    └──────────────────────┘
              │    ┌──────────────────────┐      Room Temperature
              │    │         Dry          │      for 2 minutes
              │    └──────────────────────┘
Repeat for number   ┌──────────────────────┐
of layers required  │         Fire         │      600 °C for 2 minutes in Air
              │    └──────────────────────┘
              │    ┌──────────────────────┐
              └────│         Cool         │      For 2 minutes in Air
                   └──────────────────────┘
                             │
                   ┌──────────────────────┐
                   │        Anneal        │      1500 °C for 4 Hours in Air
                   └──────────────────────┘
                             │
                   ┌──────────────────────┐
                   │   To Screen Printer  │
                   └──────────────────────┘
```
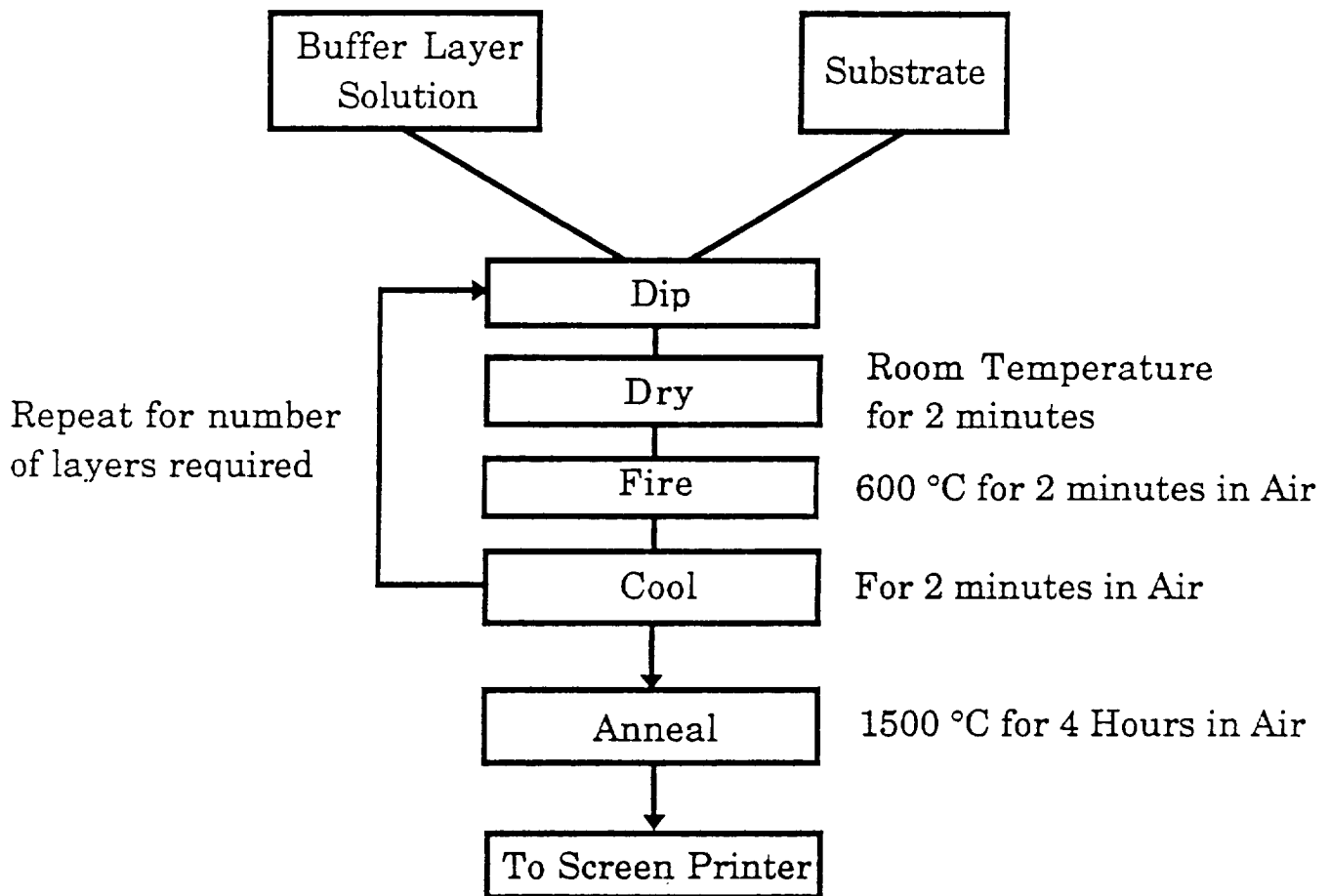
Figure 12 Flowchart of the dip coating process used to apply the buffer layers to the various substrates used for the BSCCO thick films.
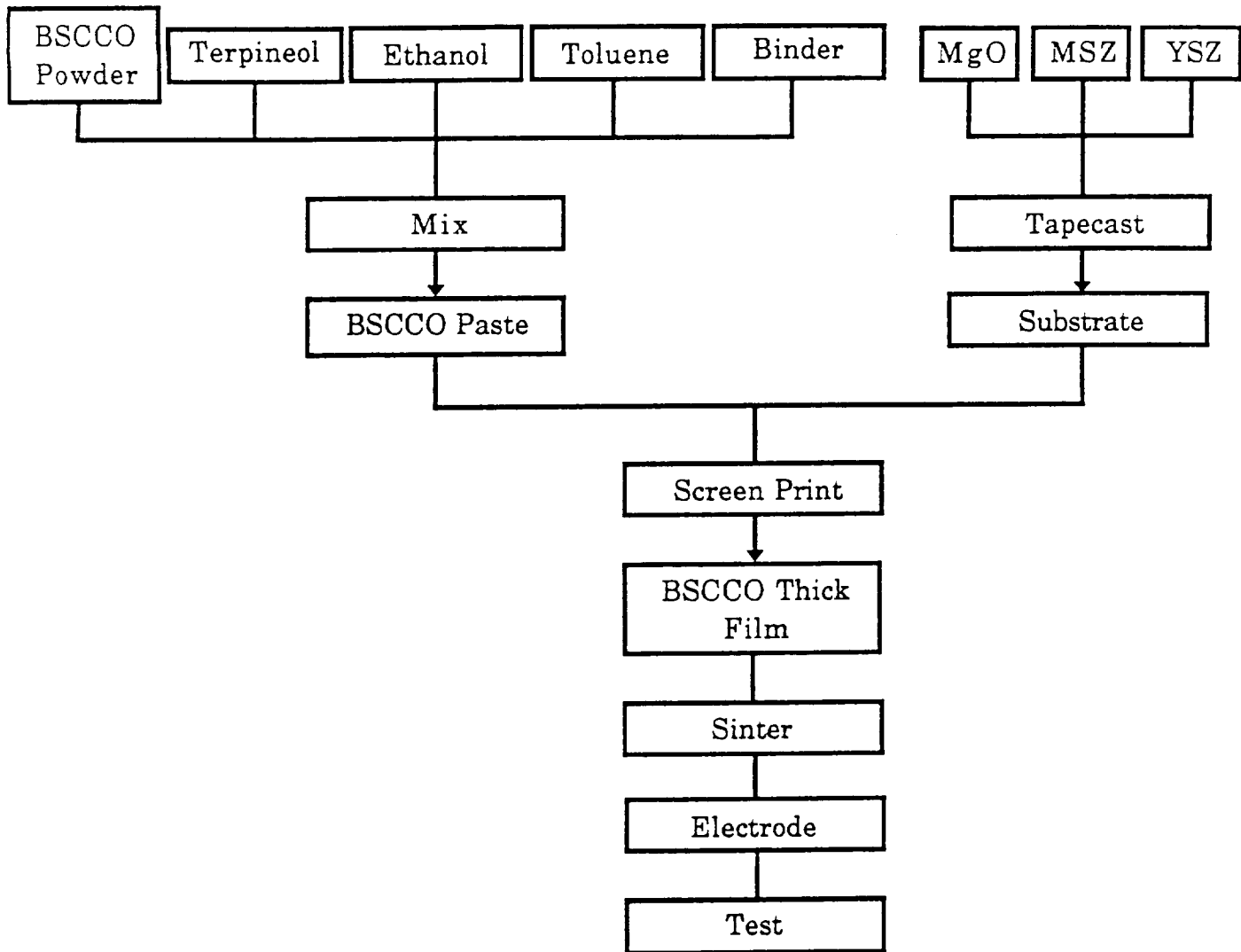
Figure 13 Fabrication process of the BSCCO superconducting thick films.
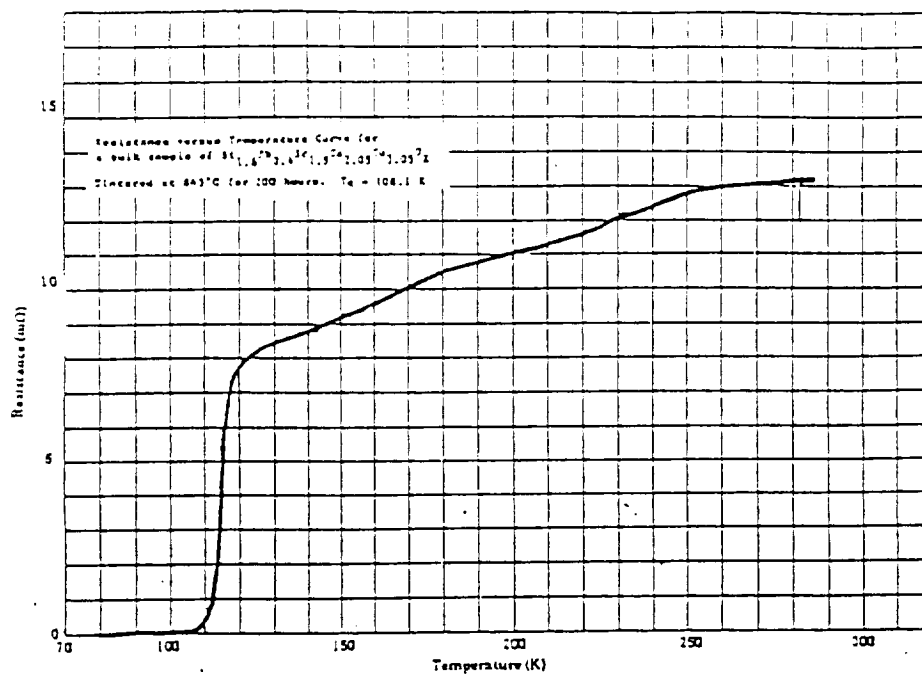
a) BSCCO pellet sintered for two hundred hours. The T_c was 108.1 K.
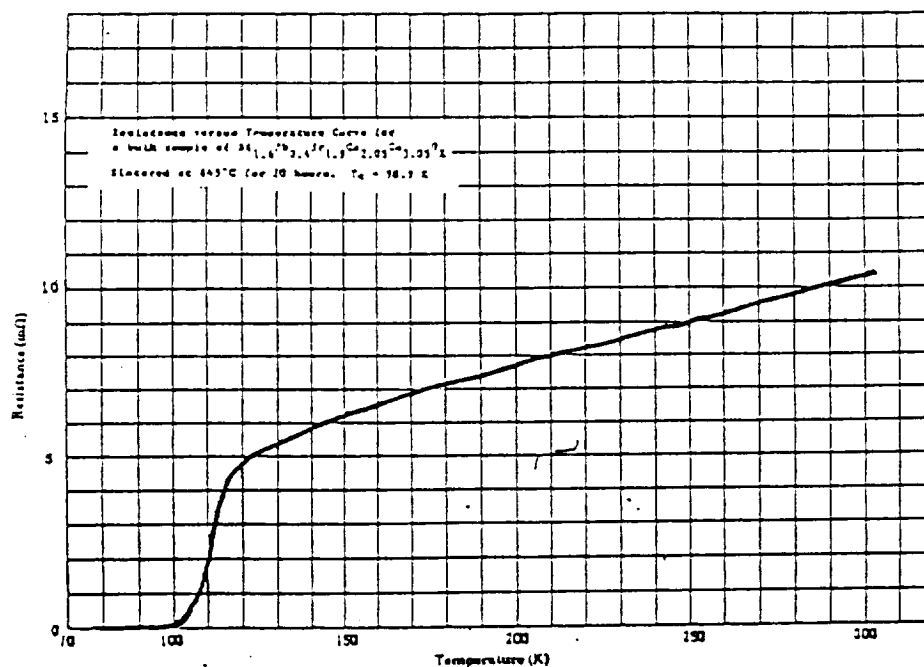
b) BSCCO pellet sintered for twenty hours. The T_c was 98.9 K.

Figure 14 Resistance versus temperature curves of bulk samples of $Bi_{1.6}Pb_{0.4}Sr_{1.9}Ca_{2.05}Cu_{3.05}O_x$ sintered at 845 °C for different times in air.
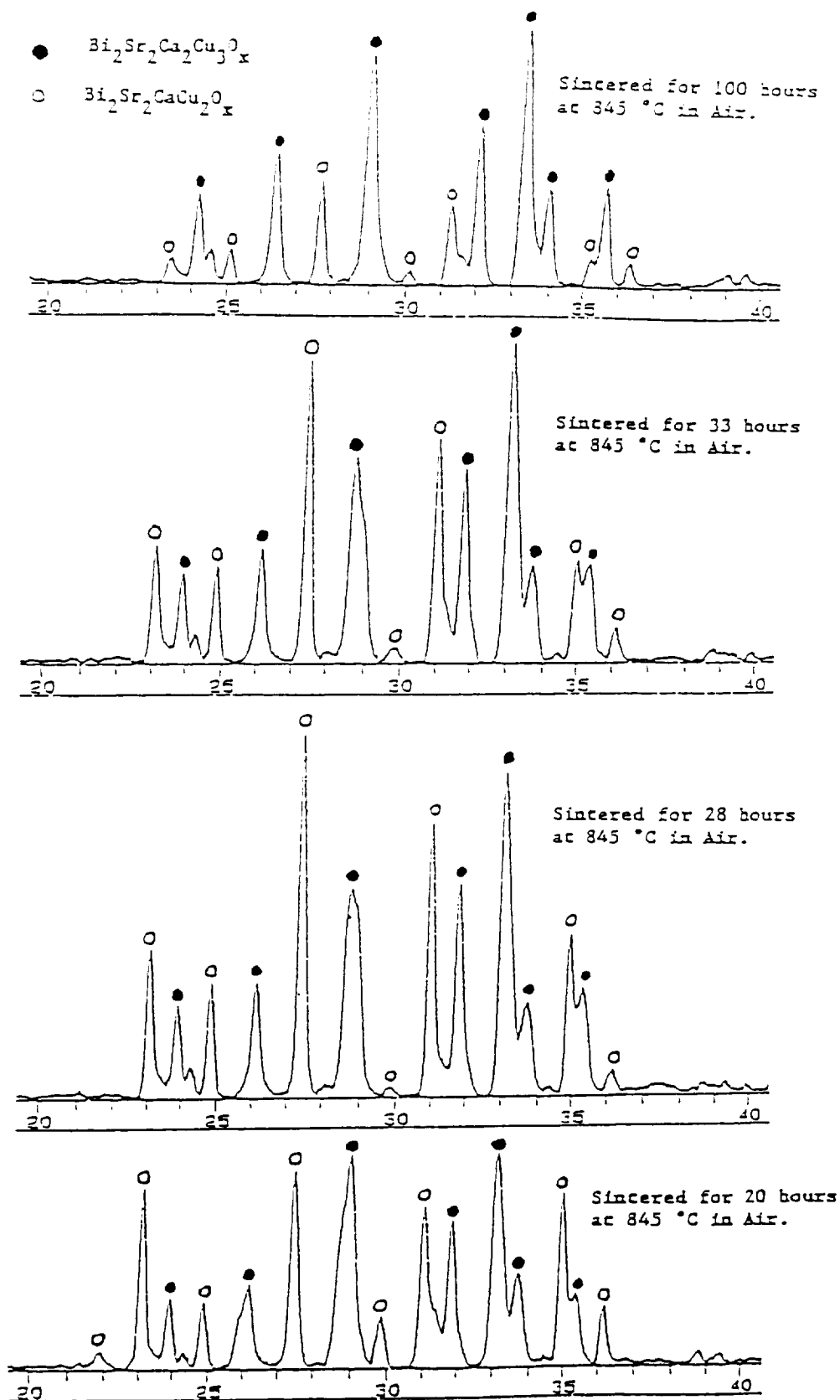
Figure 15 Xray diffraction data of four bulk compacts sintered at 845 °C for times ranging from twenty to one hundred hours in air.
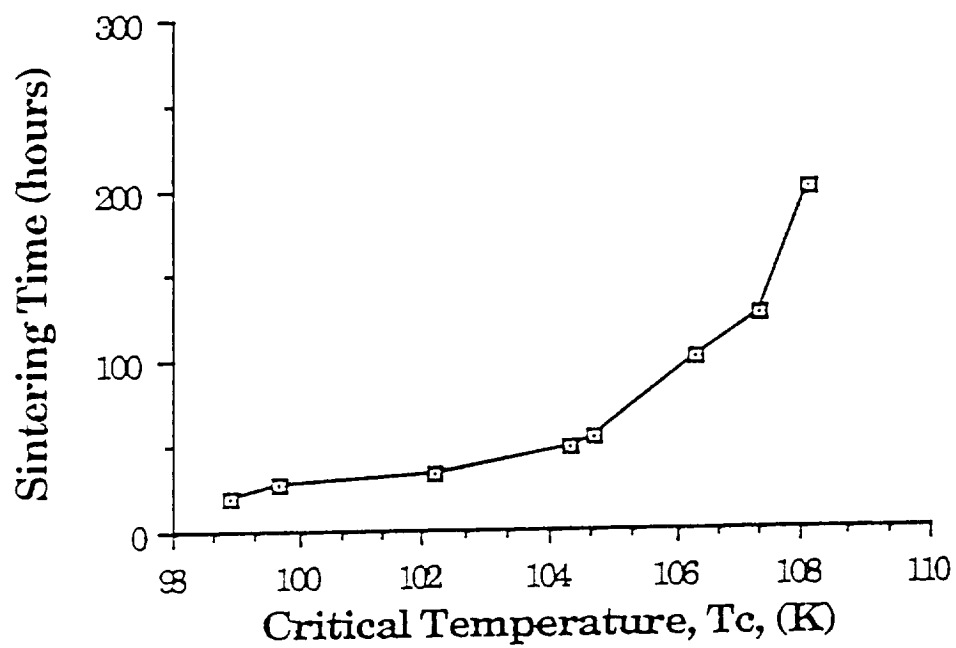
Figure 16 Sintering time versus critical temperature curve of bulk $Bi_{1.6}Pb_{0.4}Sr_{1.9}Ca_{2.05}Cu_{3.05}O_x$ showing an increase in T_c as sintering time increases.
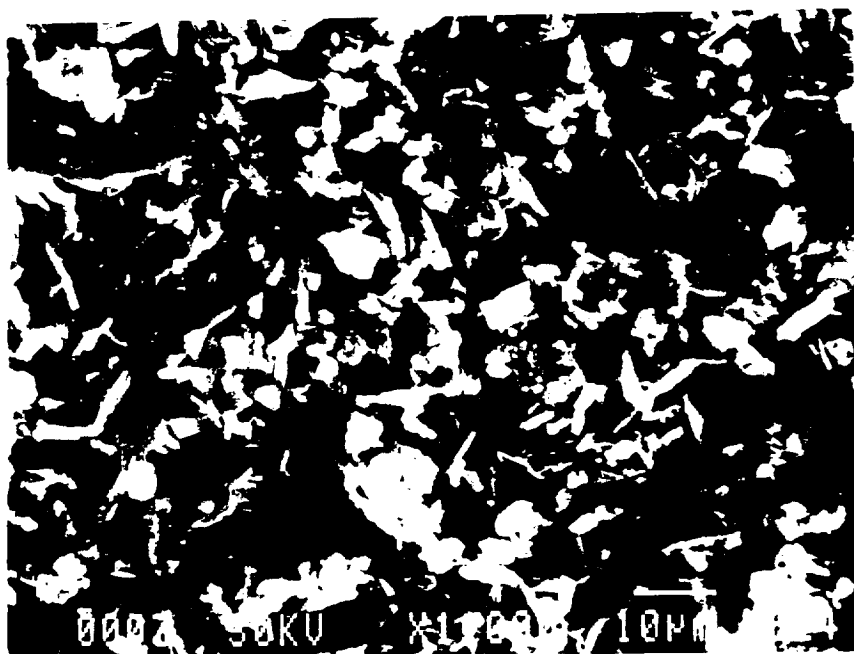
a) Pellet sintered for twenty hours.
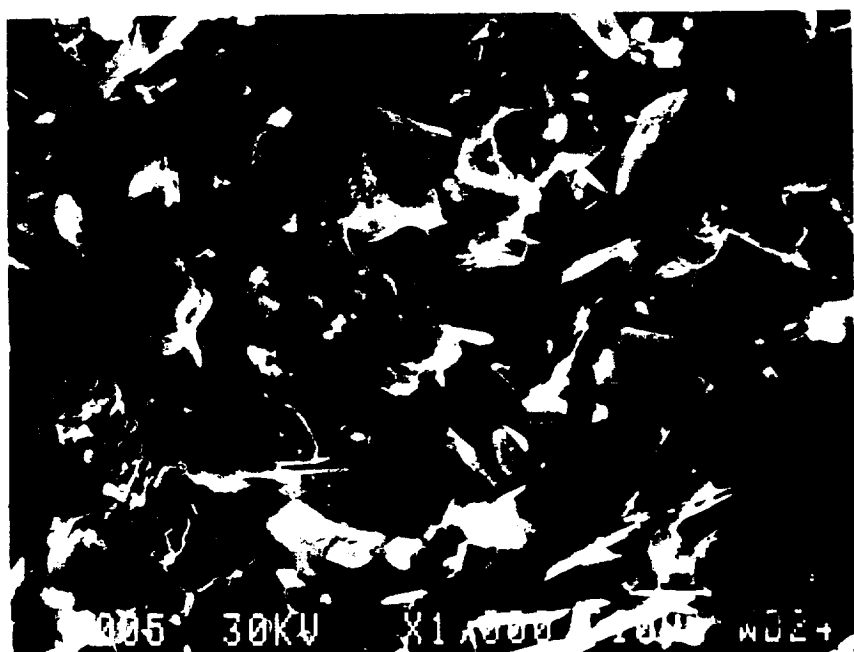
b) Pellet sintered for 33 hours.

Figure 17 SEM micrographs of $Bi_{1.6}Pb_{0.4}Sr_{1.9}Ca_{2.05}Cu_{3.05}O_x$ pellets sintered at 845 °C for different amounts of time in air.
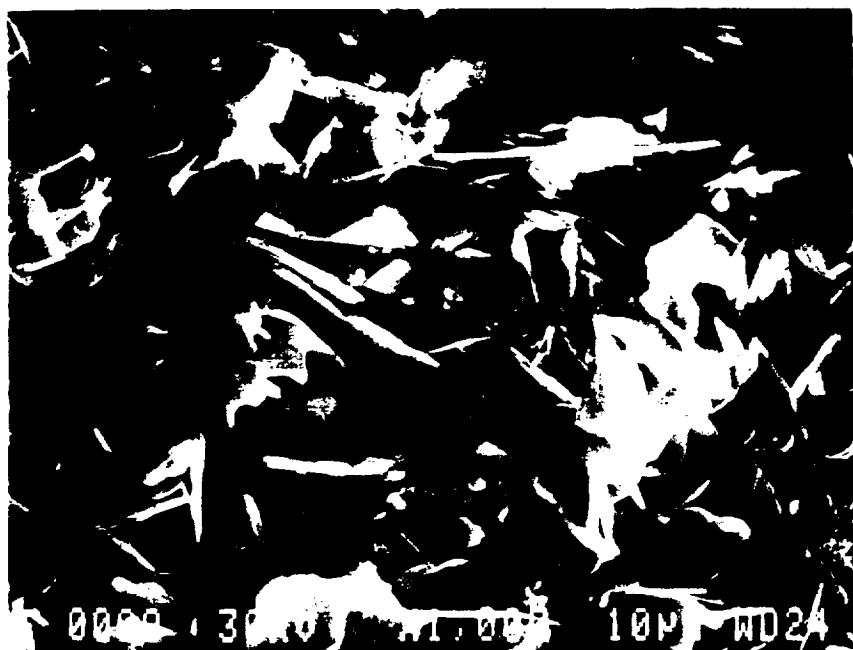
c) Pellet sintered for 125 hours.
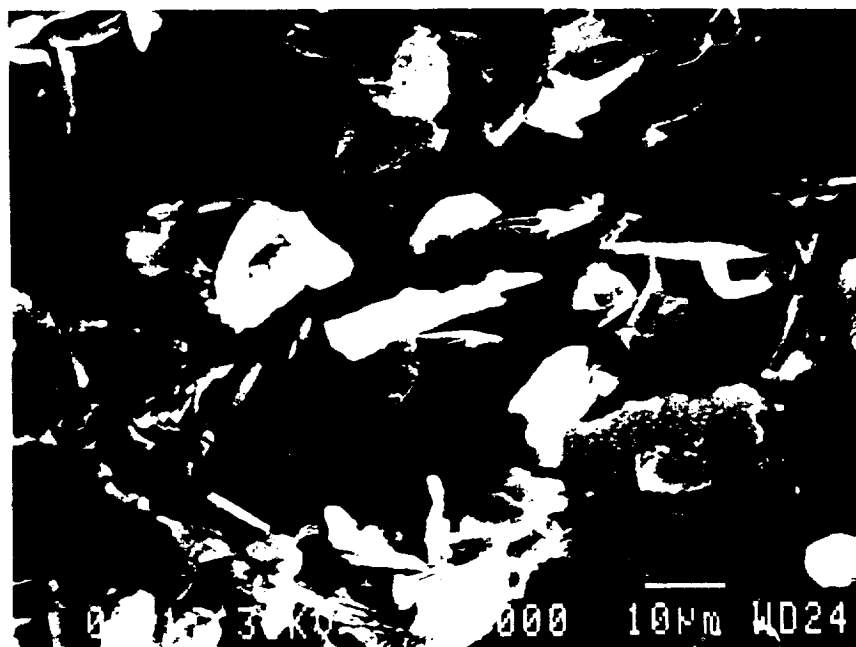
d) Pellet sintered for 200 hours.

Figure 17 (Continued)
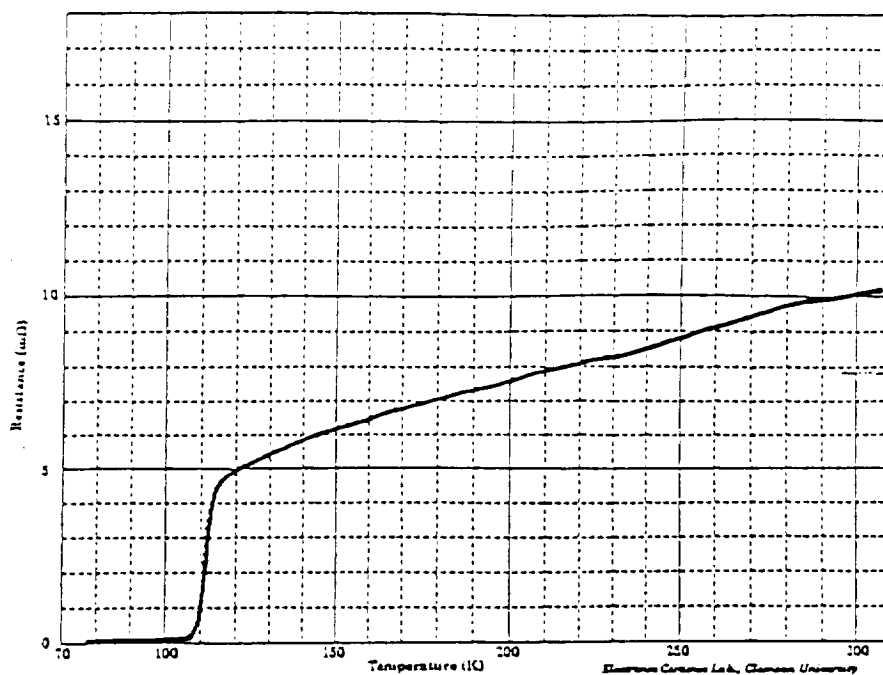
a) Pellet with a slow heating and cooling rate. The T_c was 104.7 K.
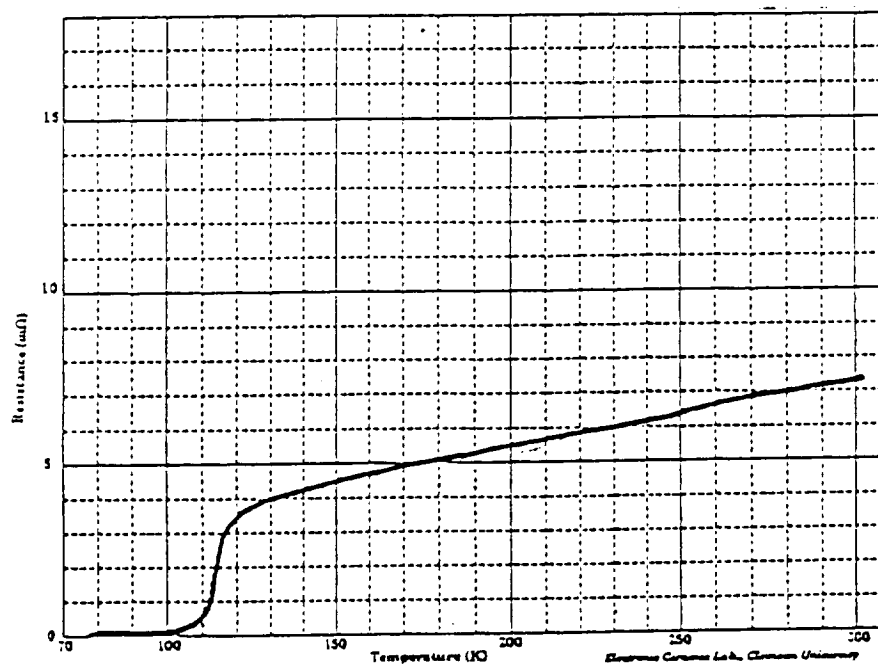
b) Pellet with a slow heating rate and quenched. The T_c was 102.9 K.

Figure 18 Resistance versus temperature curves of bulk samples of

$Bi_{1.6}Pb_{0.4}Sr_{1.9}Ca_{2.05}Cu_{3.05}O_x$ sintered at 845 °C for fifty-four hours in air. The curves show the influence of heating and cooling rates.
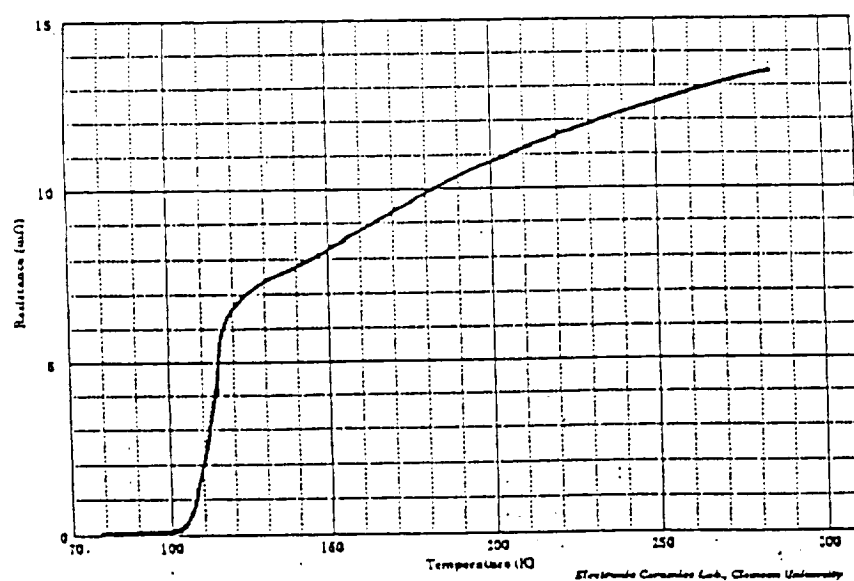
c) Pellet with a fast heating rate and slow cooling rate. The T_c was 101.4 K.
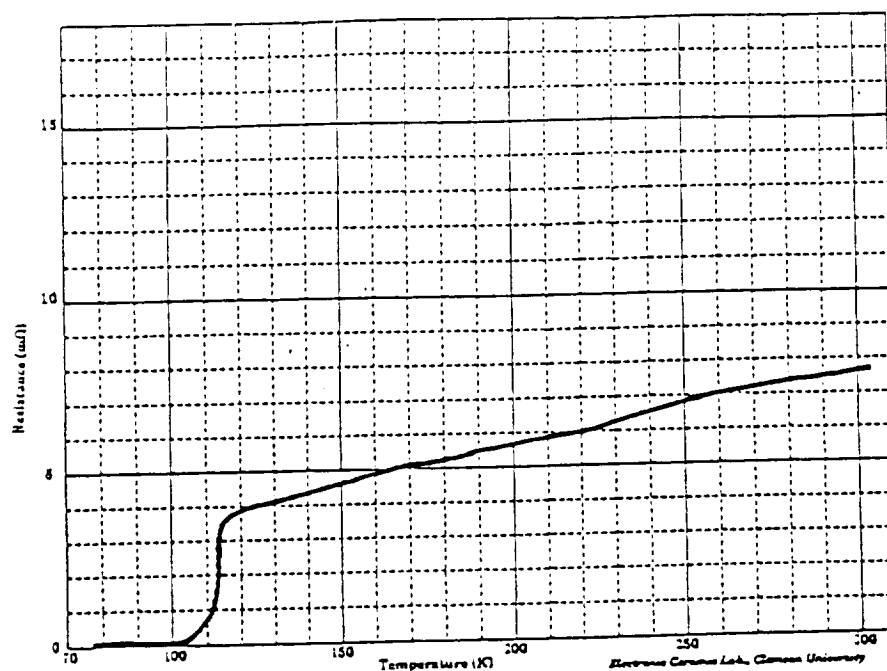
d) Pellet with a fast heating rate and quenched. The T_c was 101.2 K.

Figure 18 (Continued)

$Bi_{1.6}Pb_{0.4}Sr_{1.9}Ca_{2.06}Cu_{3.06}O_x$ material calcined
twice and sintered for 30 Hours. $T_c = 99.1$ K
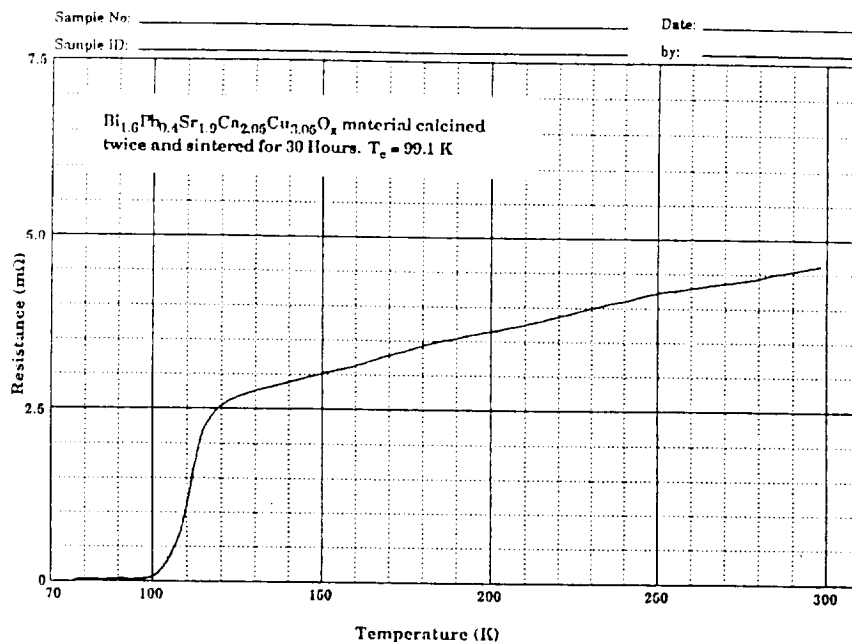
a) Uniaxially pressed pellet calcined twice. The T_c was 99.1 K.

$Bi_{1.6}Pb_{0.4}Sr_{1.9}Ca_{2.06}Cu_{3.06}O_x$ material calcined
three times and sintered for 30 Hours. $T_c = 102.0$ K
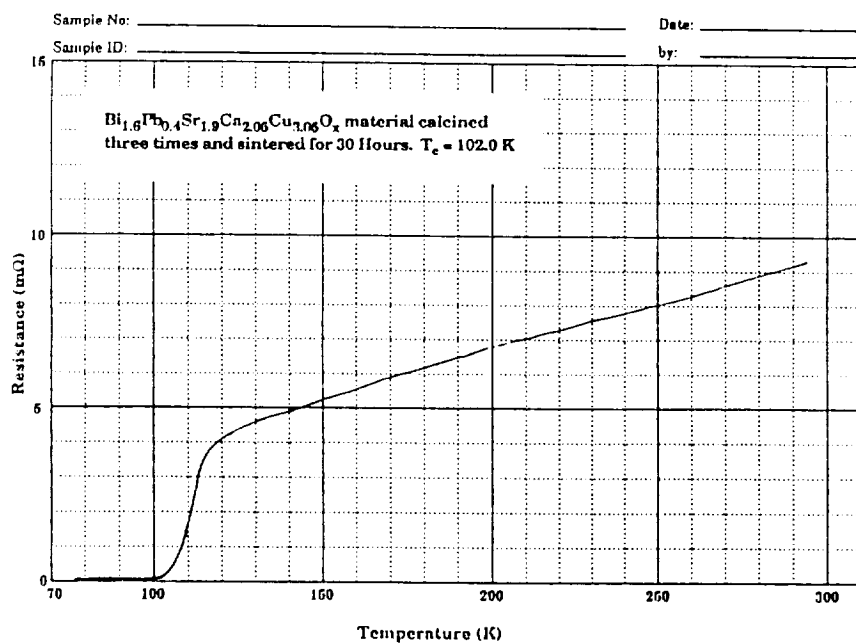
b) Uniaxially pressed pellet calcined three times. The T_c was 102.0 K.

Figure 19 Resistance versus temperature curves of bulk samples sintered for thirty hours in air at 845 °C. They varied in number of times the material was calcined.

$Bi_{1.6}Pb_{0.4}Sr_{1.9}Ca_{2.05}Cu_{3.05}O_x$ material calcined twice, hot pressed for 6 Hours at 815°C. The material did not superconduct at liquid nitrogen temperature.
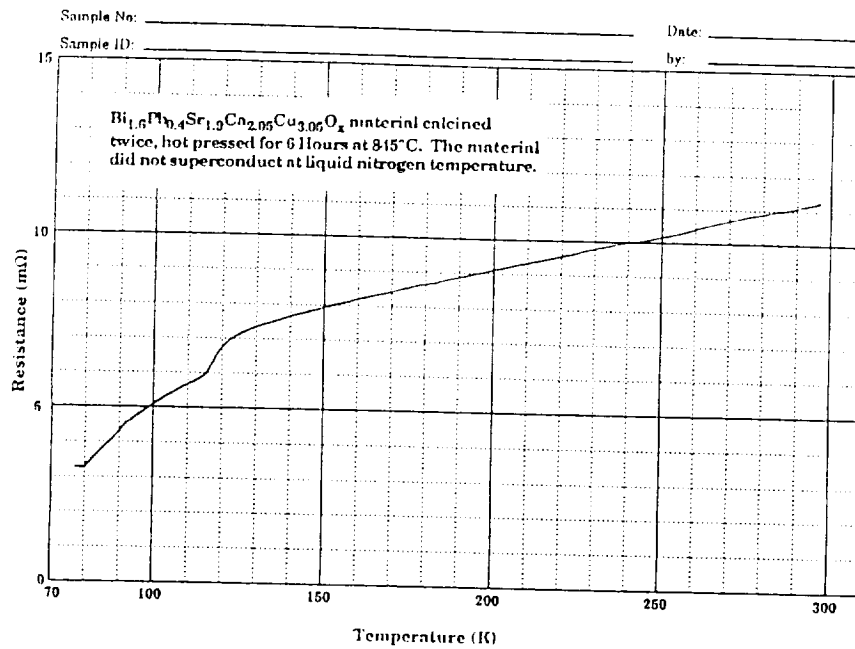
a) Hot pressed pellet with no additional heat treatment calcined twice. The material did not superconduct.

$Bi_{1.6}Pb_{0.4}Sr_{1.9}Ca_{2.05}Cu_{3.05}O_x$ material calcined three times, hot pressed for 6 Hours at 815°C. $T_c = 83.3$ K
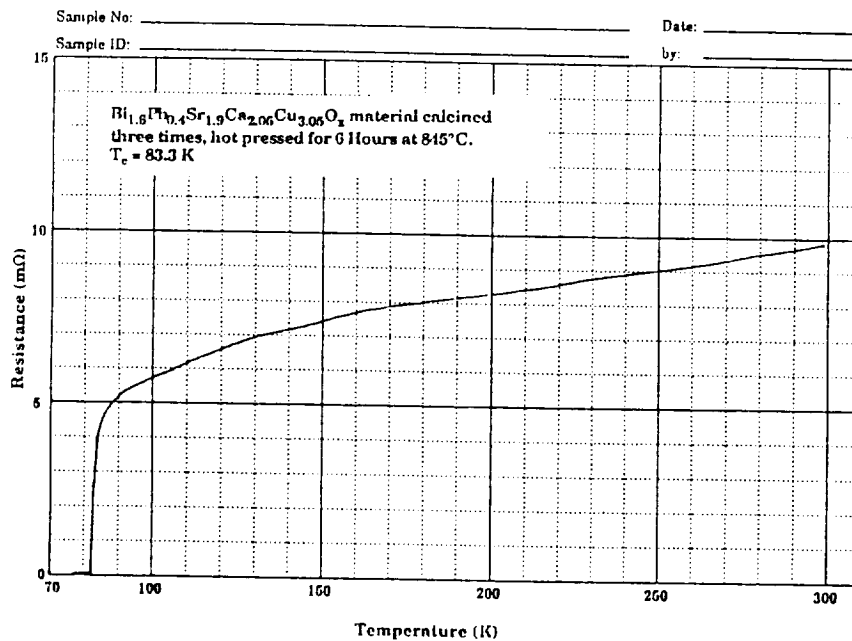
b) Hot pressed pellet with no additional heat treatment calcined three times. The T_c was 83.3 K.

Figure 20 Resistance versus temperature curves of bulk hot pressed samples with no additional heat treatment. They varied in number of times the material was calcined.

$Bi_{1.6}Pb_{0.4}Sr_{1.9}Ca_{2.05}Cu_{3.06}O_x$ material calcined
twice, hot pressed for 6 Hours at 845°C, and sintered
for 24 Hours at 845°C. $T_c = 104.4$ K

a) Hot pressed pellet with additional heat treatment calcined twice. The T_c was 104.4 K.

$Bi_{1.6}Pb_{0.4}Sr_{1.9}Ca_{2.05}Cu_{3.06}O_x$ material calcined
three times, hot pressed for 6 Hours at 845°C, and
sintered for 24 Hours at 845°C. $T_c = 108.2$ K
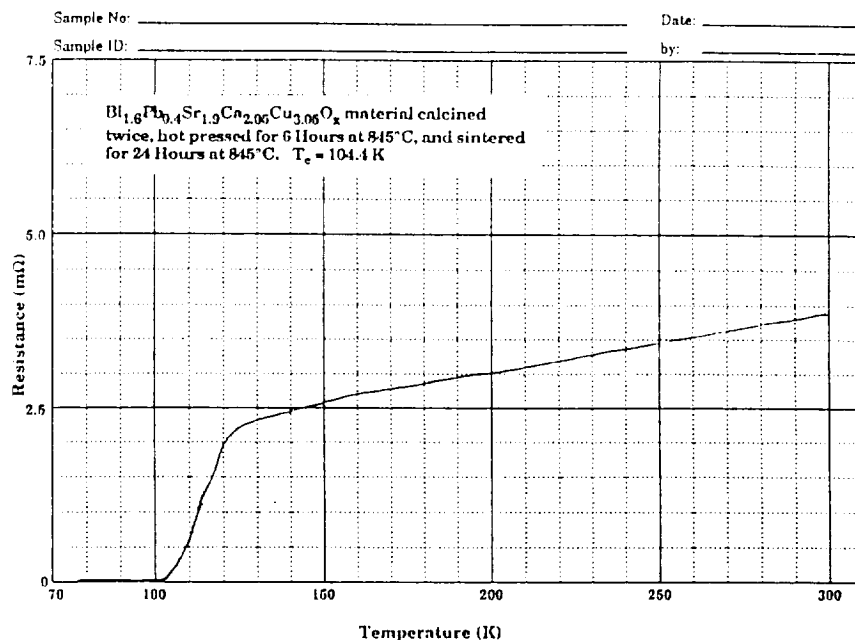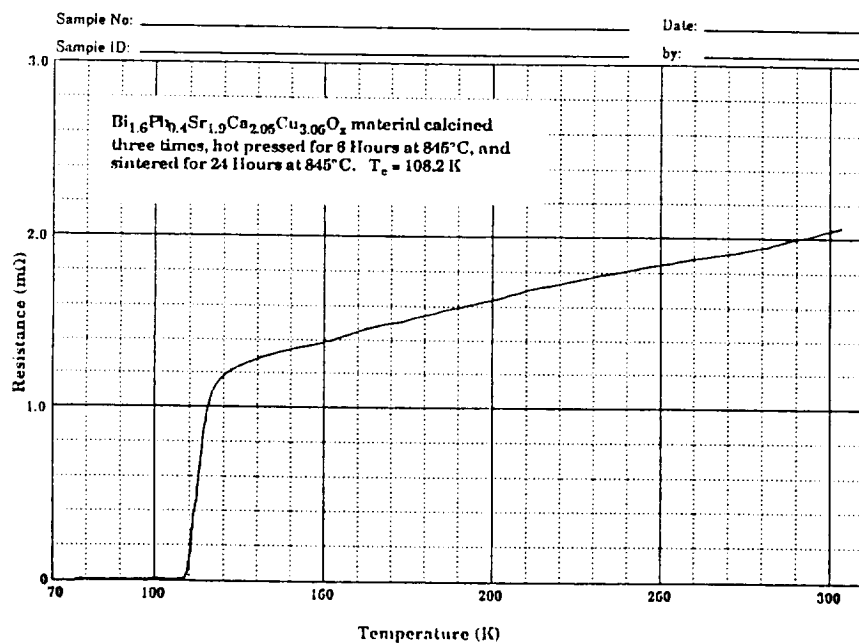
b) Hot pressed pellet with additional heat treatment calcined three times. The T_c was
108.2 K.

Figure 21 Resistance versus temperature curves of bulk hot pressed samples with
twenty-four hours additional heat treatment at 845 °C. They varied in number of
times the material was calcined.

$Bi_{1.6}Pb_{0.4}Sr_{1.9}Ca_{2.05}Cu_{3.05}O_x$ coprecipitated bulk material sintered at 845 °C for 30 hours, without a calcination. Tc = 99.1 K.
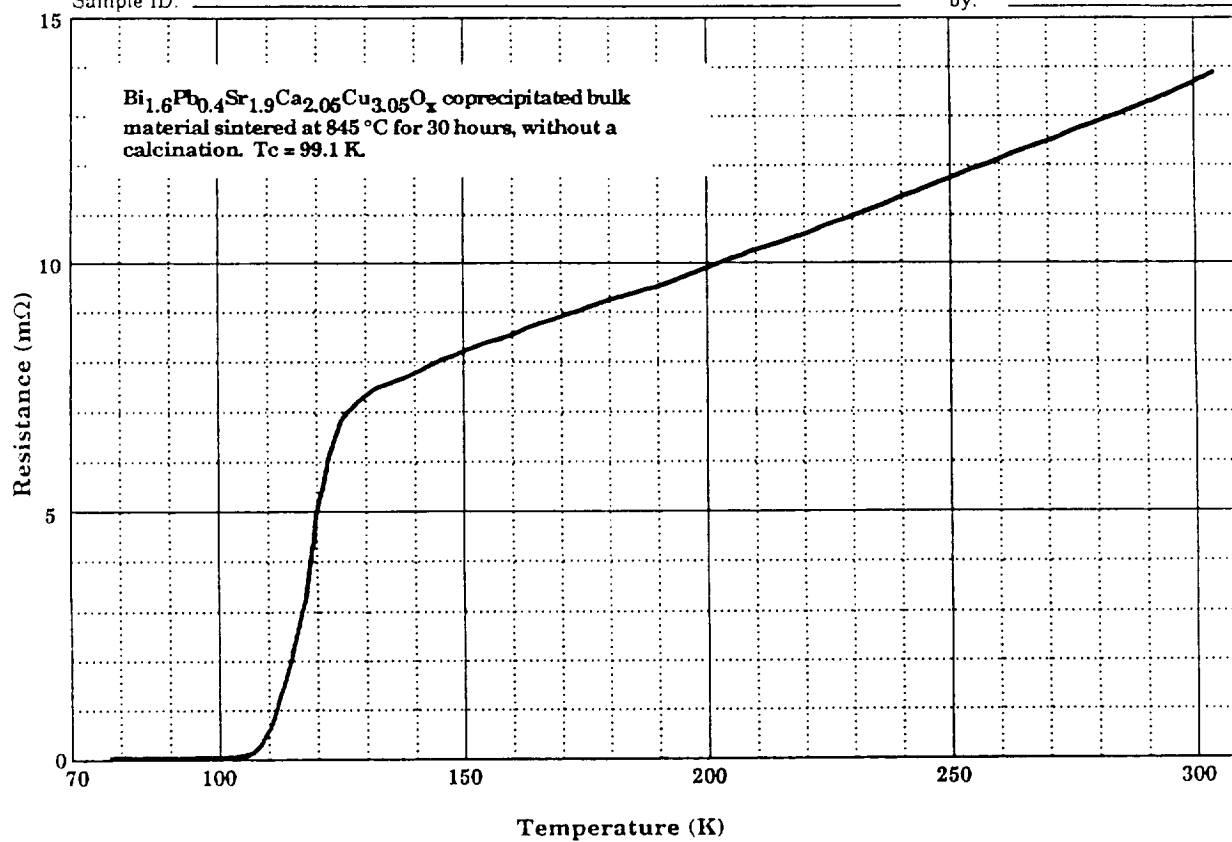
Figure 22 Resistance versus temperature curve of a bulk coprecipitated sample which was sintered, uncalcined, at 845 °C for thirty hours. The T_c was 99.1 K.

$Bi_{1.6}Pb_{0.4}Sr_{1.9}Ca_{2.05}Cu_{3.05}O_x$ coprecipitated bulk material sintered at 845 °C for 30 hours, calcined at 830 °C for 12 hours. Tc = 104.8 K.
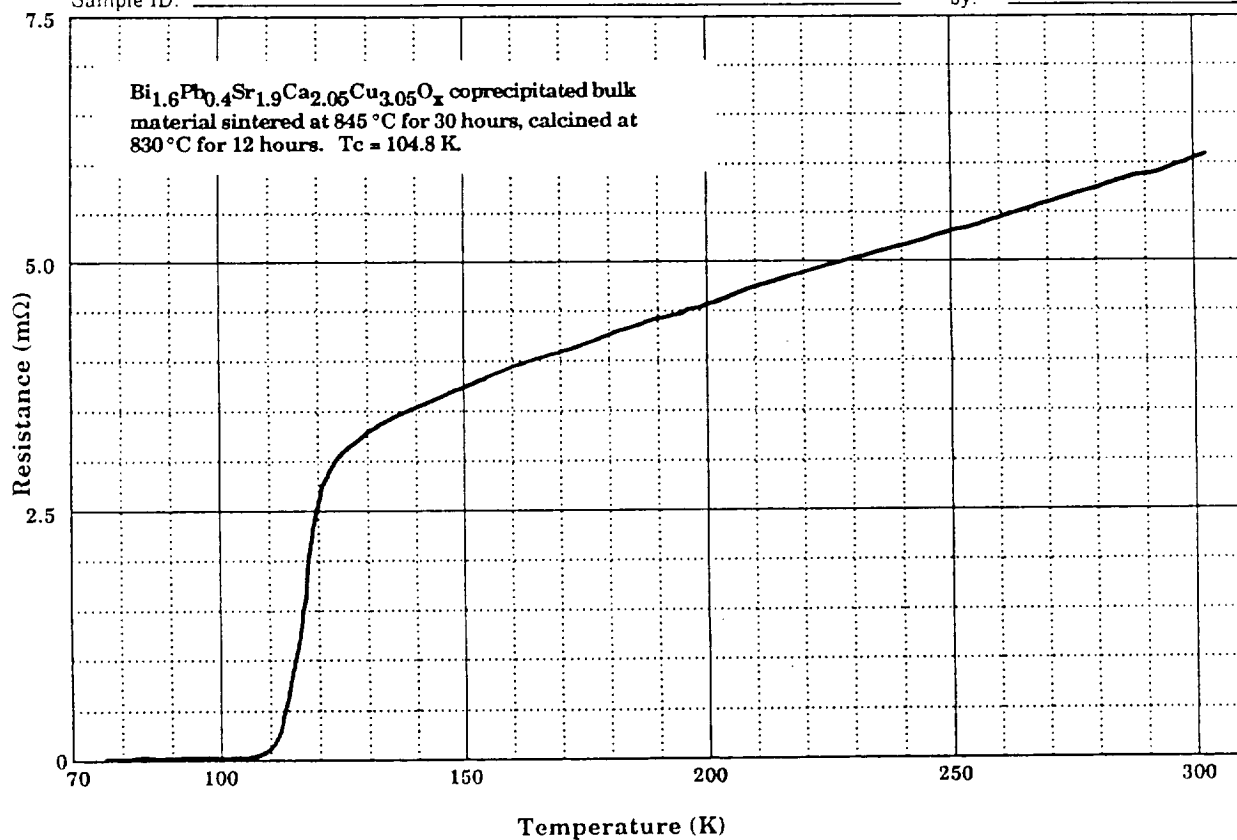
Figure 23 Resistance versus temperature curve of a bulk coprecipitated sample which was calcined at 830 °C for twelve hours and sintered at 845 °C for thirty hours. The T_c was 104.8 K.
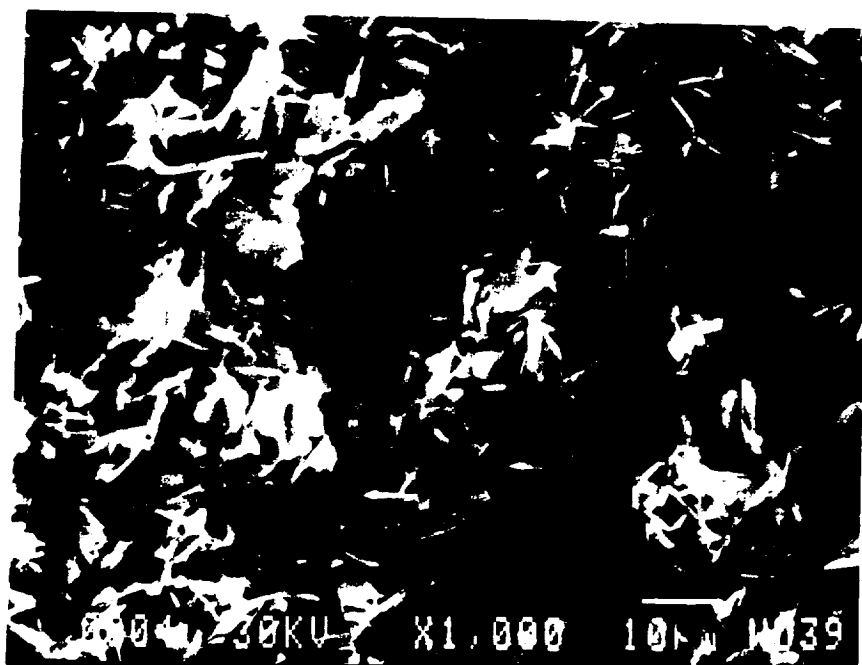
Figure 24 SEM micrograph of a bulk coprecipitated sample which was calcined at 830 °C for twelve hours and sintered at 845 °C for thirty hours.

a) High pressure compact at 1000 magnification.

b) High pressure compact at 4000 magnification.

Figure 25 SEM micrographs of coprecipitated samples which were calcined at 830 °C for twelve hours and sintered at 845 °C for thirty hours.
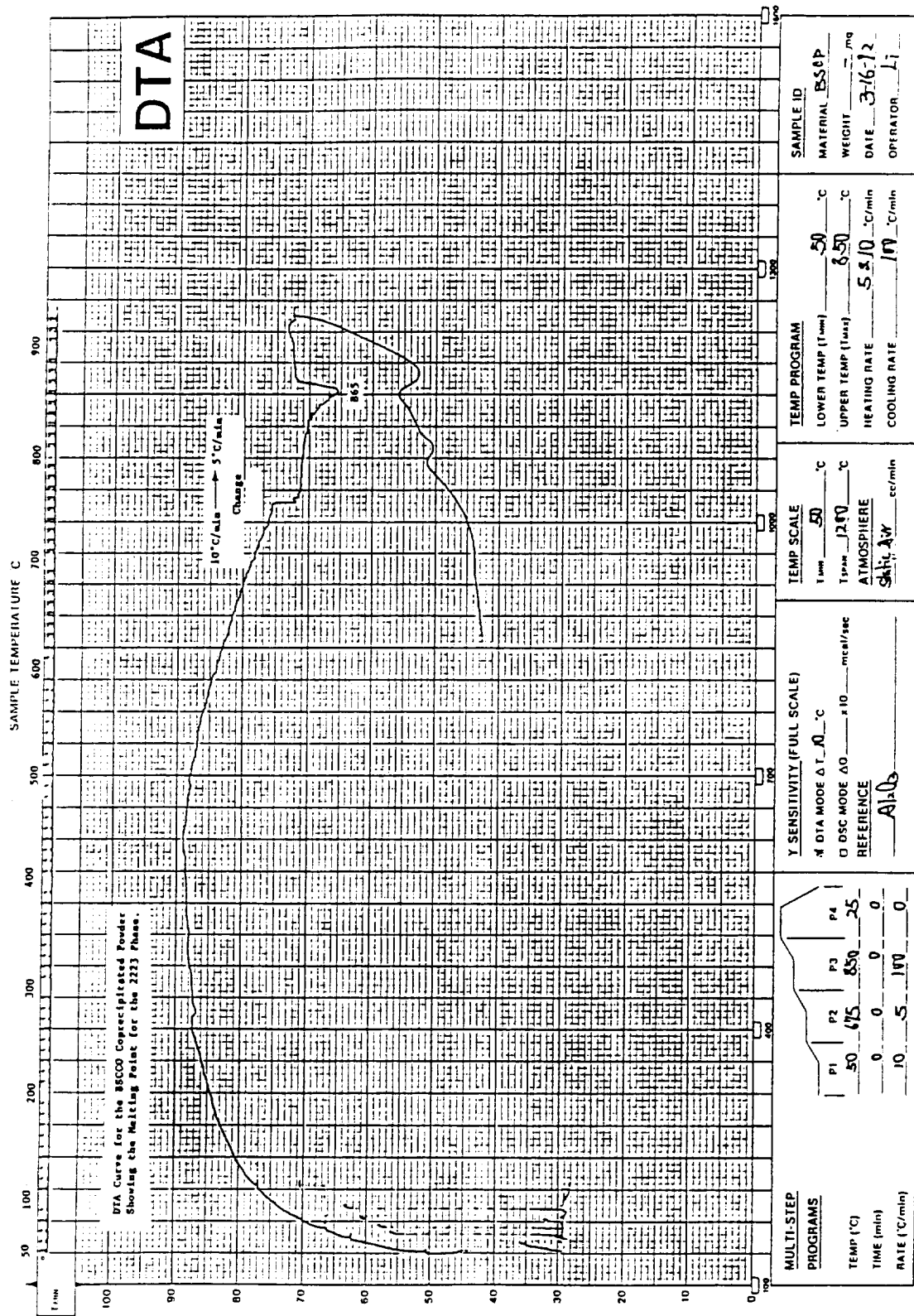
Figure 26 Differential thermal analysis curve of the BSCCO coprecipitated material showing the melting point of the 2223 phase at 865 °C.
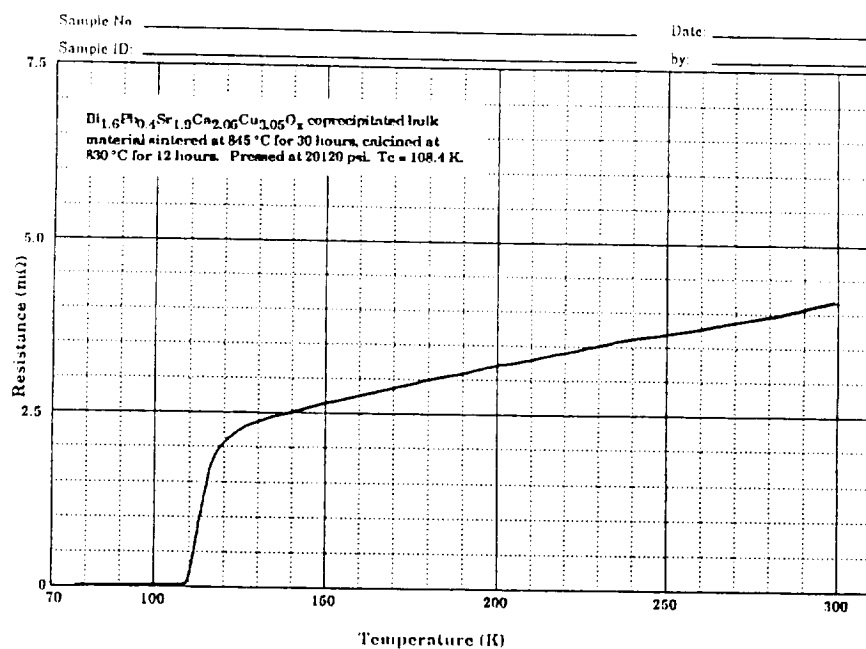
a) Coprecipitated compact which was calcined at 830 °C. The T_c was 108.4 K.
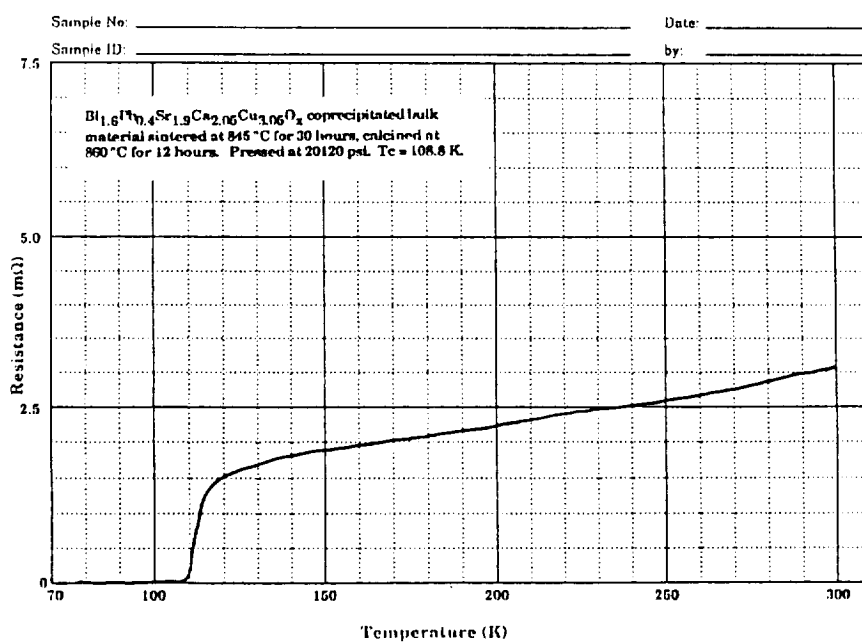
b) Coprecipitated compact which was calcined at 860 °C. The T_c was 108.8 K.

Figure 27 Resistance versus temperature curves of bulk coprecipitated samples which were calcined at different temperatures for twelve hours and sintered at 845 °C for thirty hours.

Bi$_{1.6}$Pb$_{0.4}$Sr$_{1.9}$Ca$_{2.05}$Cu$_{3.05}$O$_x$ coprecipitated material calcined once and hot pressed for 6 hours at 845 °C. The material did not superconduct at liquid nitrogen temperature.
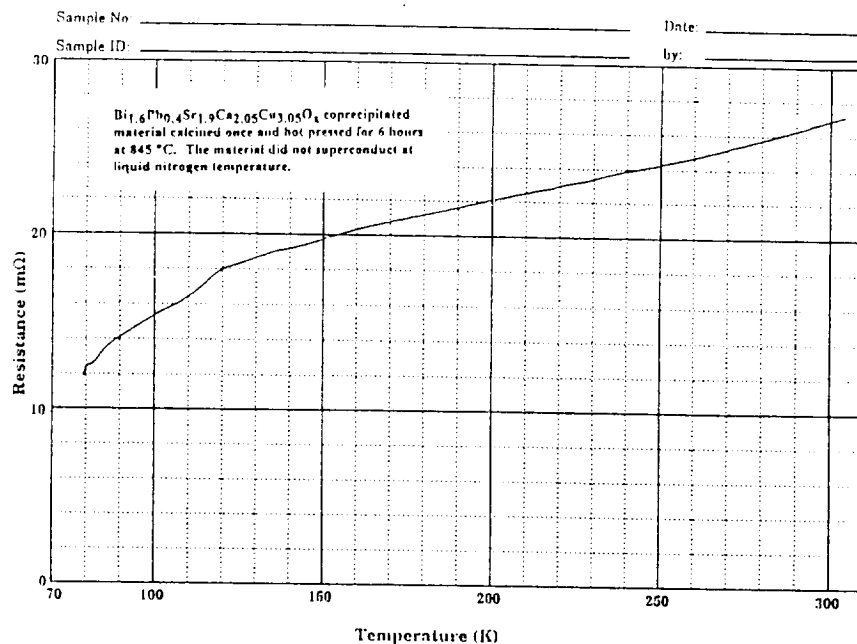
a) Hot pressed pellet with no additional heat treatment calcined once. The material did not superconduct at liquid nitrogen temperature.

Bi$_{1.6}$Pb$_{0.4}$Sr$_{1.9}$Ca$_{2.05}$Cu$_{3.05}$O$_x$ coprecipitated material calcined twice and hot pressed for 6 hours at 845 °C. The T$_c$ was 84.0 K.
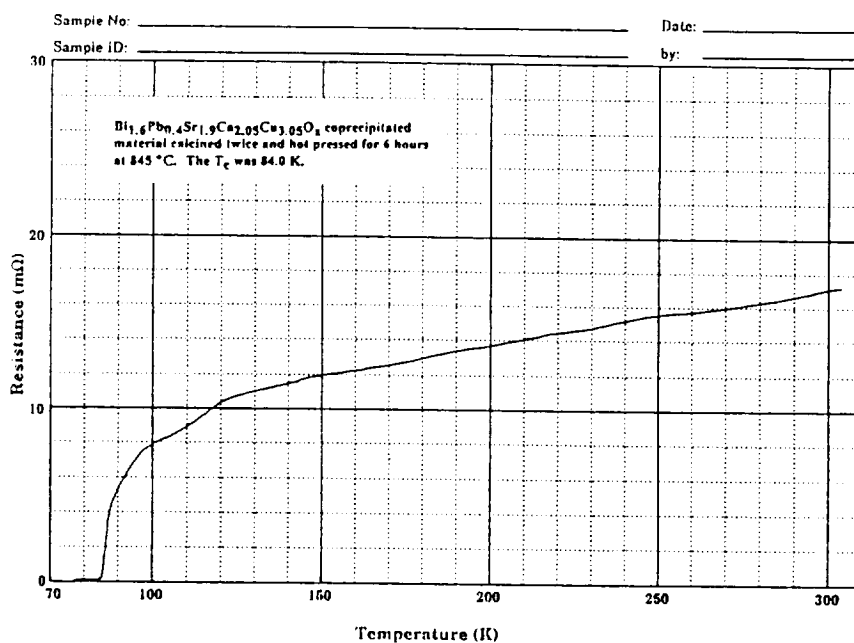
b) Hot pressed pellet with no additional heat treatment calcined twice. The Tc was 84.0 K.

Figure 28 Resistance versus temperature curves of coprecipitated hot pressed samples with no additional heat treatment. They varied in number of times the material was calcined.

$Bi_{1.6}Pb_{0.4}Sr_{1.9}Ca_{2.05}Cu_{3.05}O_x$ coprecipitated material calcined once, hot pressed for 6 hours at 845 °C and sintered for 24 hours at 845 °C. The T_c was 106.4 K.
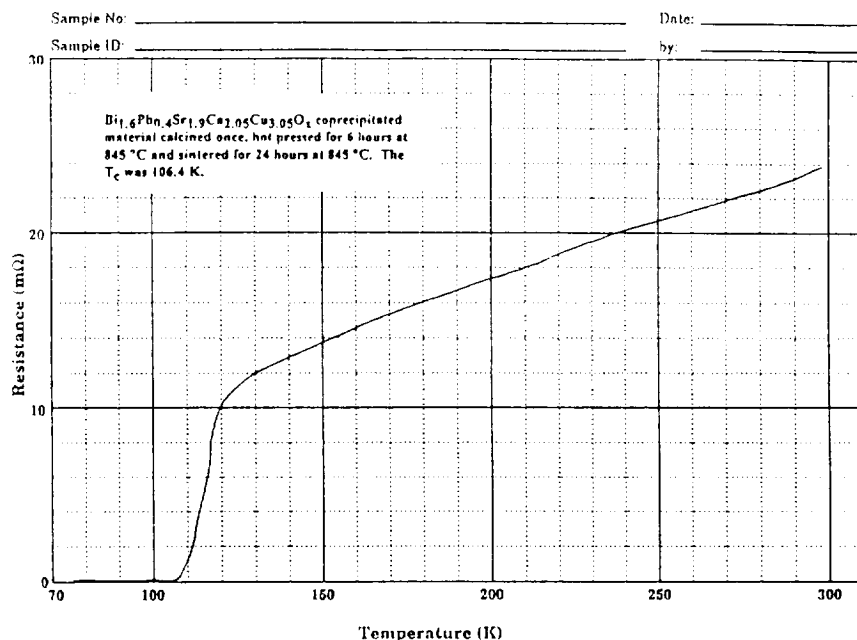
a) Hot pressed pellet with additional heat treatment calcined once. The Tc was 106.4 K.

$Bi_{1.6}Pb_{0.4}Sr_{1.9}Ca_{2.05}Cu_{3.05}O_x$ coprecipitated material calcined twice, hot pressed for 6 hours at 845 °C and sintered for 24 hours at 845 °C. The T_c was 108.1 K.
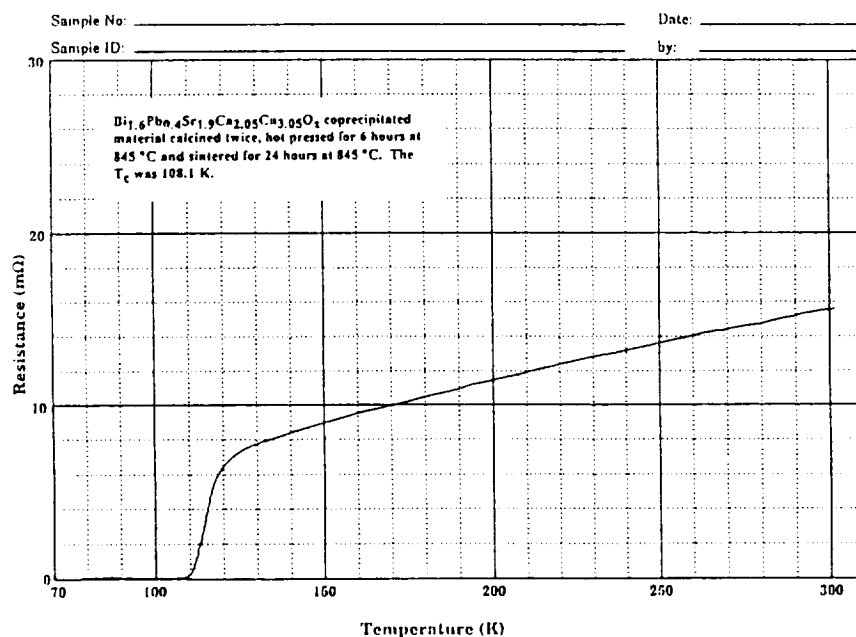
b) Hot pressed pellet with additional heat treatment calcined twice. The Tc was 108.1 K

Figure 29 Resistance versus temperature curves of coprecipitated hot pressed samples with twenty-four hours additional heat treatment at 845 °C. They varied in number of times the material was calcined.
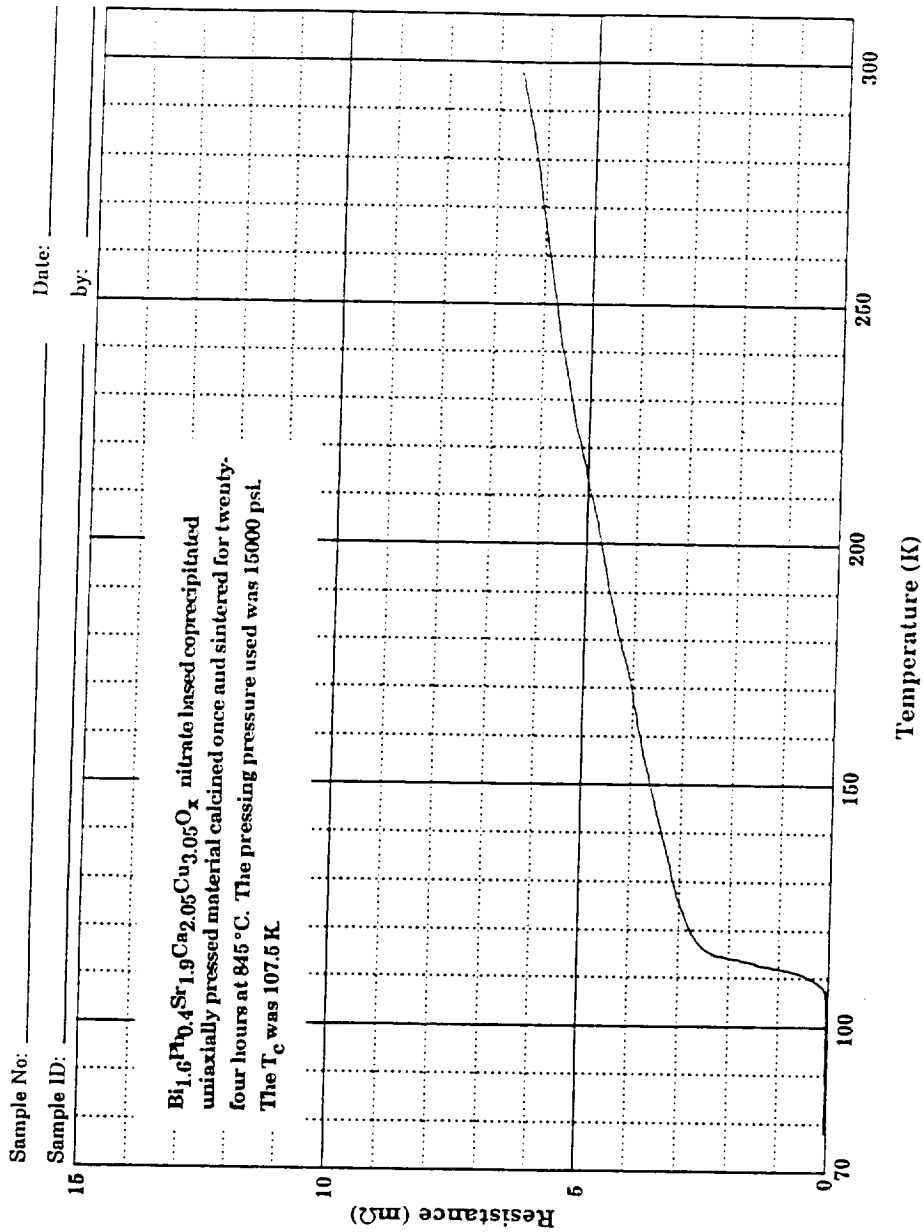
Figure 30 Resistance versus temperature curve of a nitrate based coprecipitated uniaxially pressed sample calcined once and sintered for twenty-four hours at 845 °C. The pressing pressure used was 15000 psi. The T_c was 107.5 K.
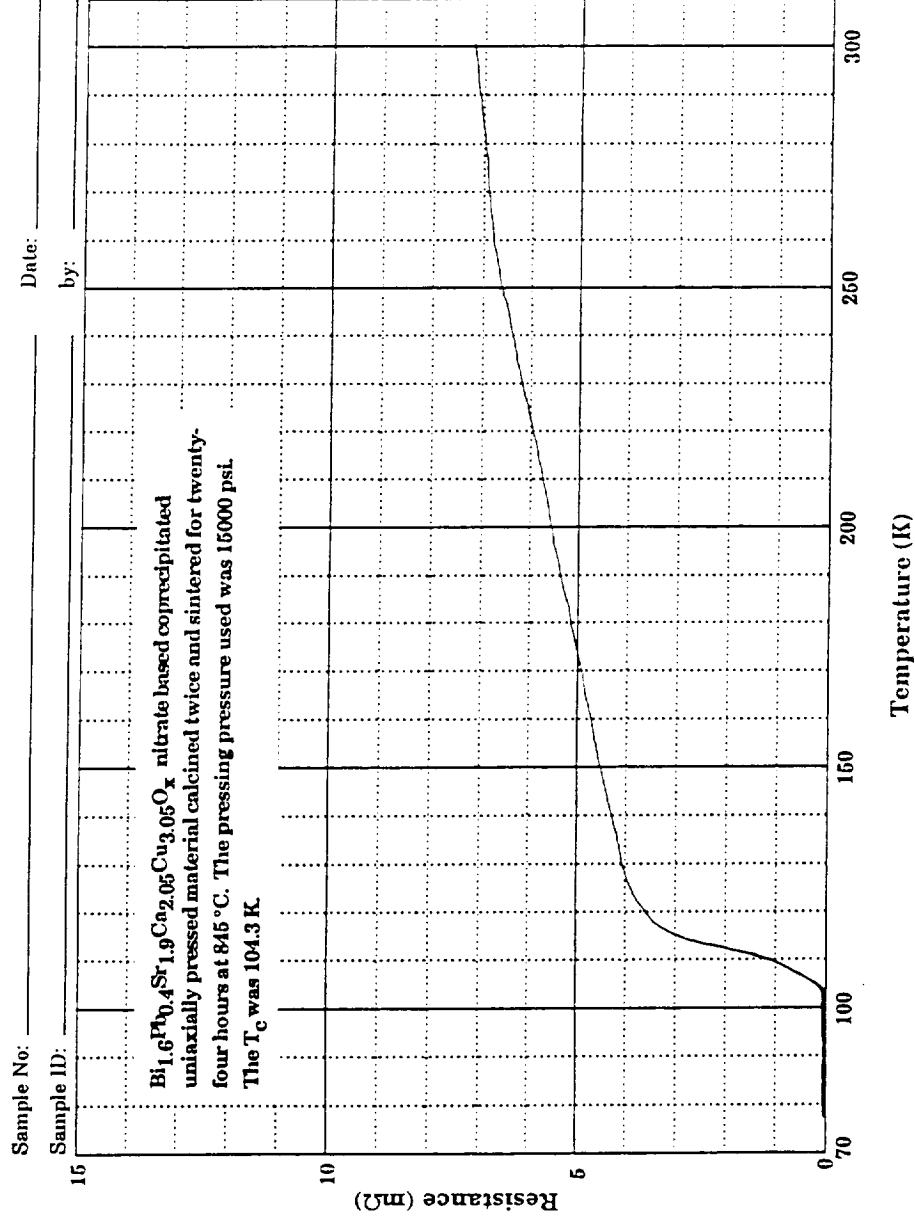
Figure 31 Resistance versus temperature curve of a nitrate based coprecipitated uniaxially pressed sample calcined twice and sintered for twenty-four hours at 845 °C. The pressing pressure used was 15000 psi. The T_c was 104.3 K.
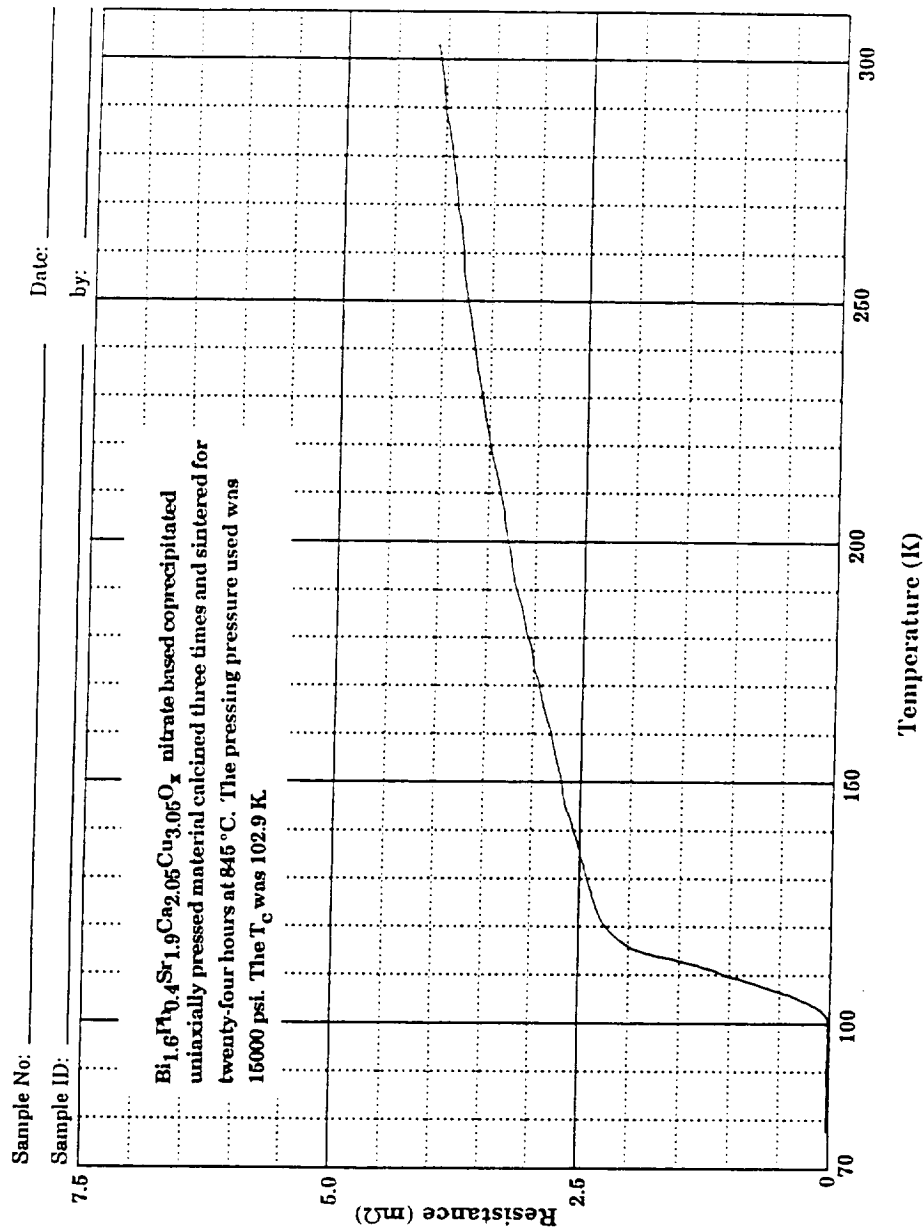
Figure 32 Resistance versus temperature curve of a nitrate based coprecipitated uniaxially pressed sample calcined three times and sintered for twenty-four hours at 845 °C. The pressing pressure used was 15000 psi. The T_c was 102.9 K.
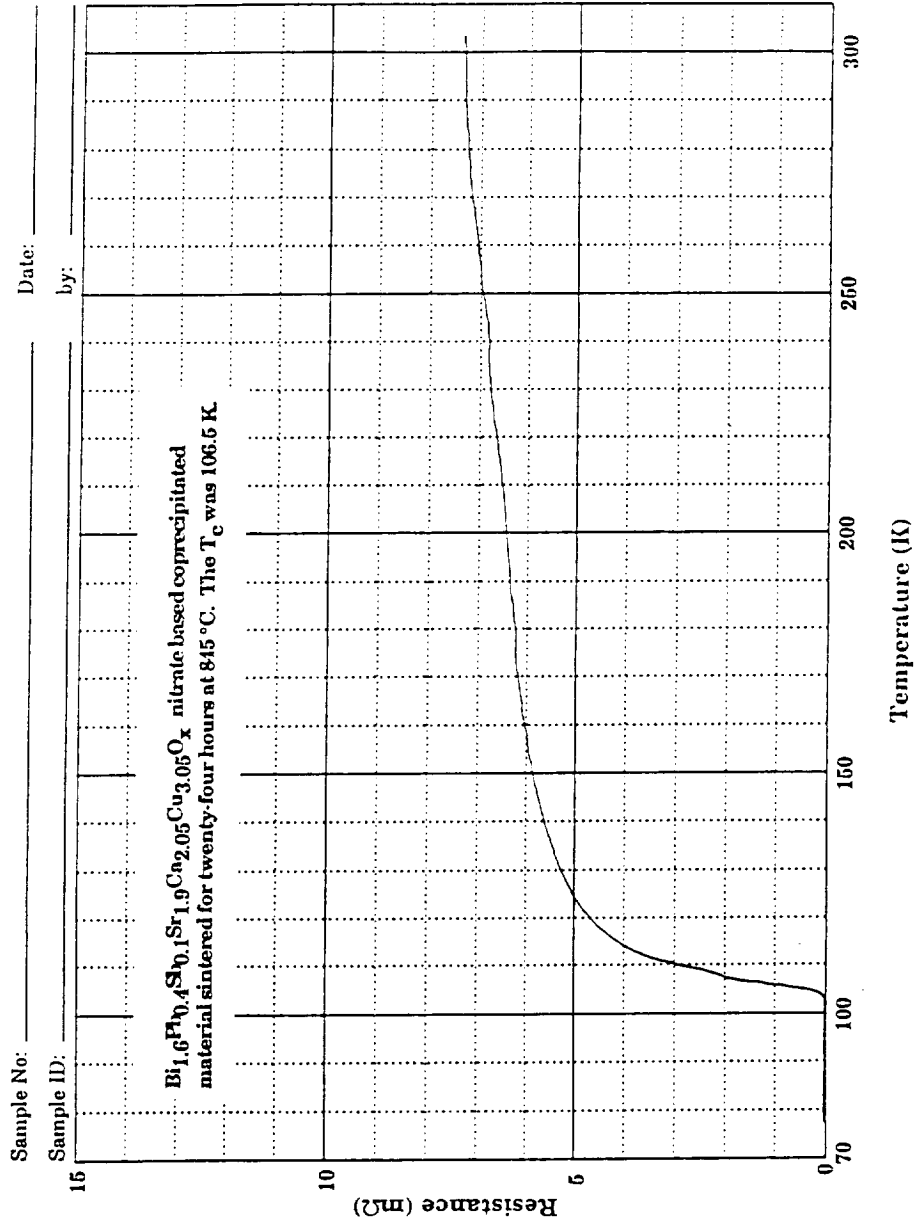
Figure 33 Resistance versus temperature curve of an antimony doped nitrate based coprecipitated sample sintered for twenty-four hours at 845 °C. The T_c was 106.5 K.

$Bi_{1.6}Pb_{0.4}Sb_{0.1}Sr_{1.9}Ca_{2.05}Cu_{3.05}O_x$ acetate based coprecipitated material sintered for twenty-four hours at 845 °C. The T_c was 105.3 K

Resistance (mΩ)
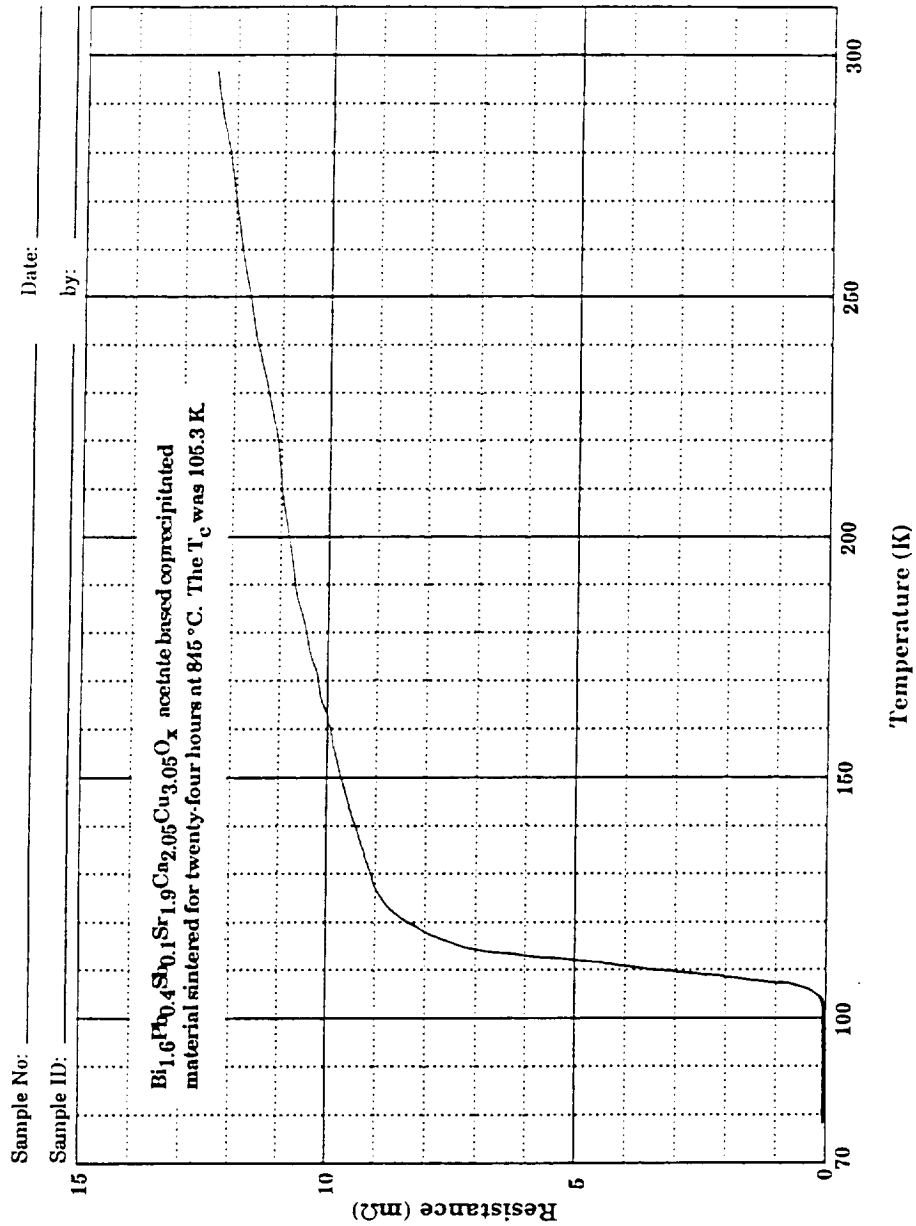
Temperature (K)

Figure 34 Resistance versus temperature curve of an antimony doped acetate based coprecipitated sample sintered for twenty-four hours at 845 °C. The T_c was 105.3 K.
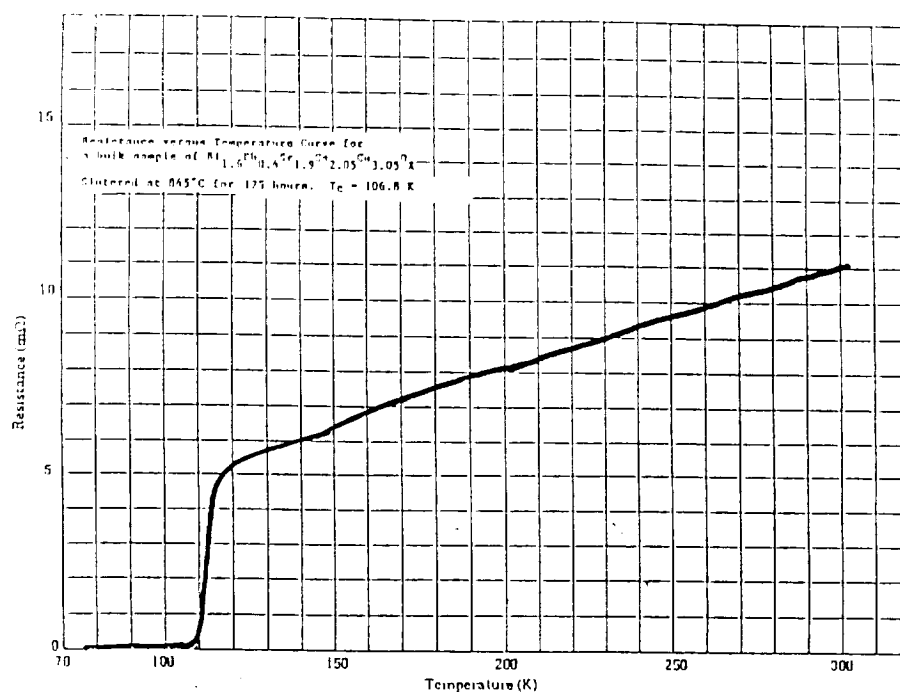
a) Pellet pressed at 5000 psi. The T_c was 106.8 K.
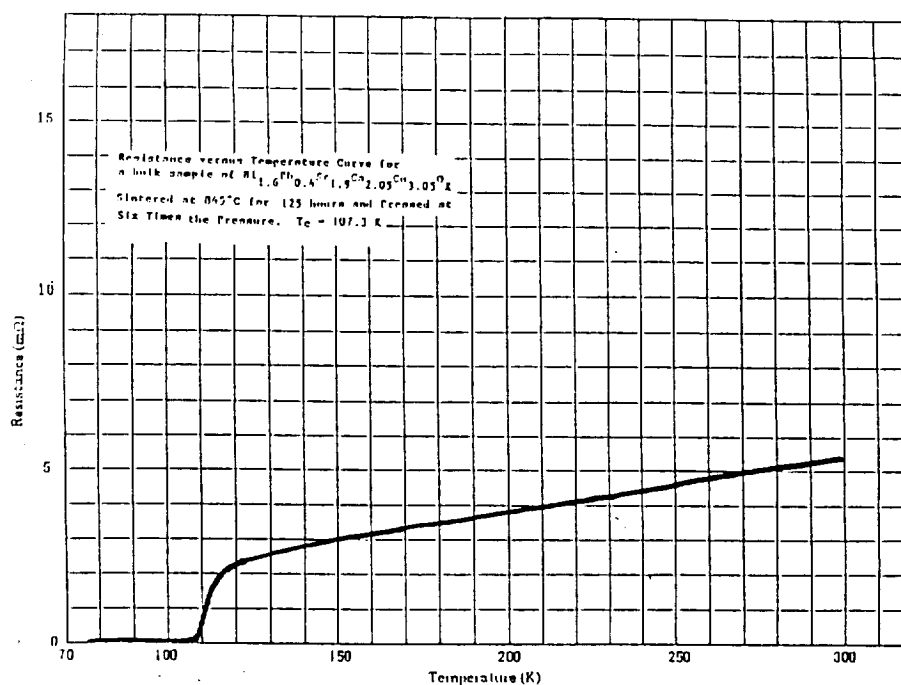
b) Pellet pressed at 20120 psi. The T_c was 107.3 K.

Figure 35 Resistance versus temperature curves of bulk samples of $Bi_{1.6}Pb_{0.4}Sr_{1.9}Ca_{2.05}Cu_{3.05}O_x$ pressed at different pressures and sintered at 845 °C for 125 hours in air.
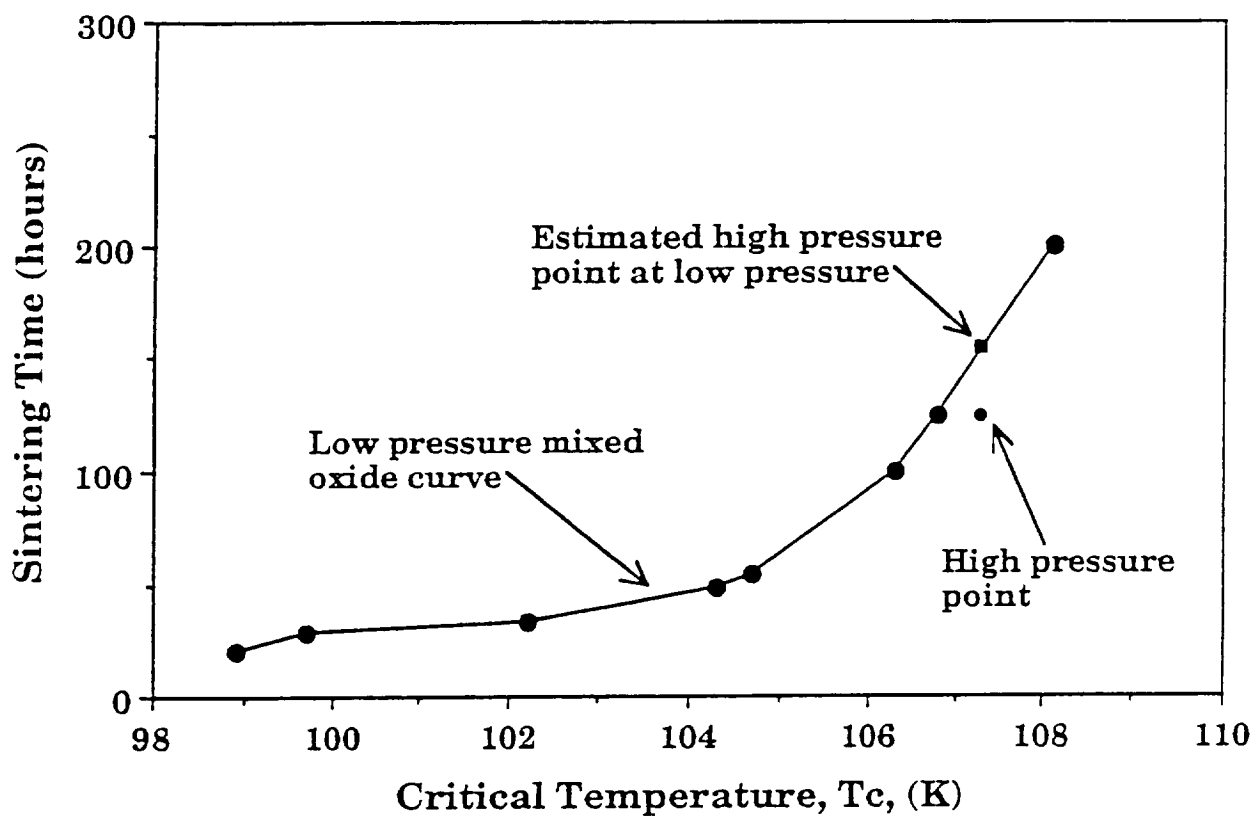
Figure 36 Sintering time versus critical temperature plot showing the effect of initial pressing pressure on the T_c.
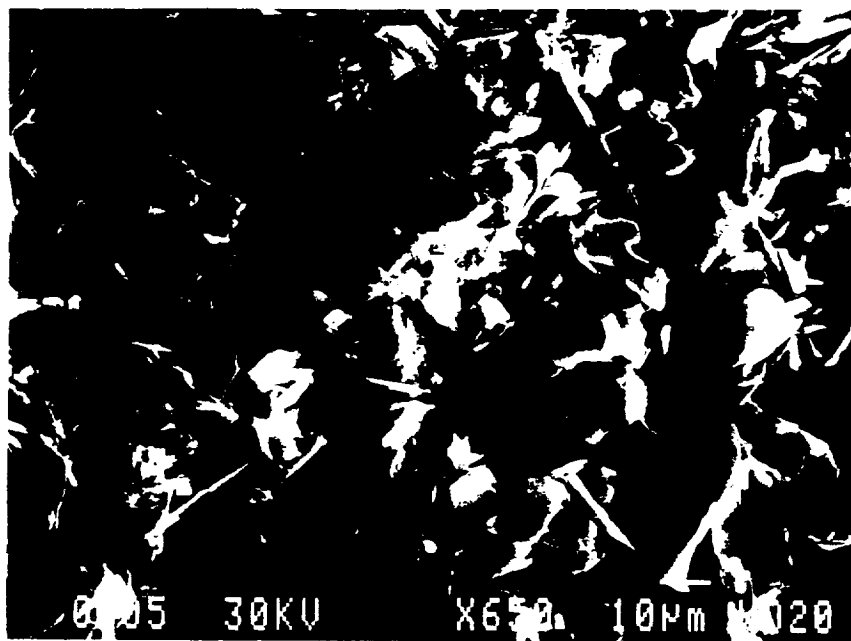
a) Pellet pressed at 5000 psi.

b) Pellet pressed at 20120 psi.

Figure 37 SEM micrographs of $Bi_{1.6}Pb_{0.4}Sr_{1.9}Ca_{2.05}Cu_{3.05}O_x$ pellets pressed at different pressures and sintered at 845 °C for 125 hours in air.
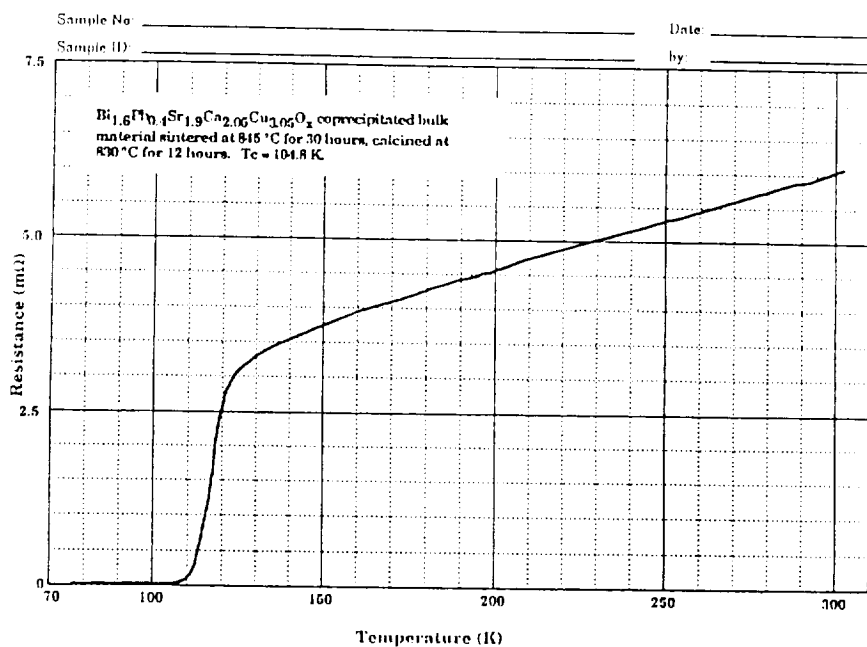
a) Coprecipitated compact which was pressed at 5000 psi. The T_c was 104.8 K.
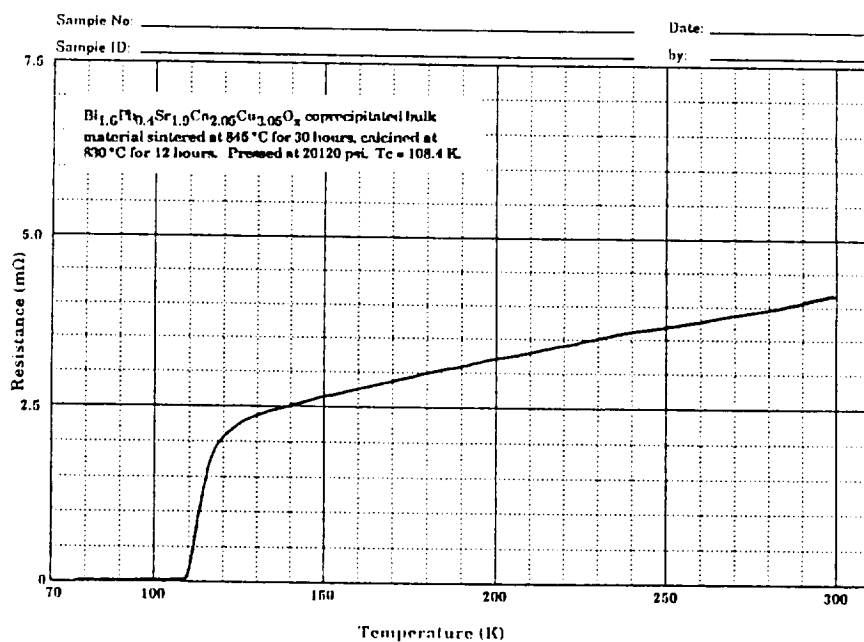
b) Coprecipitated compact which was pressed at 20120 psi. The T_c was 108.4 K.

Figure 38 Resistance versus temperature curves of bulk coprecipitated samples which were calcined at 830 °C for twelve hours and sintered at 845 °C for thirty hours.

15

$Bi_{1.6}Pb_{0.4}Sr_{1.9}Ca_{2.05}Cu_{3.05}O_x$ material calcined
three times, hot pressed for 6 Hours at 845°C.
$T_c = 83.3$ K

Resistance (mΩ)

10

5

0

70   100   160   200   260   300
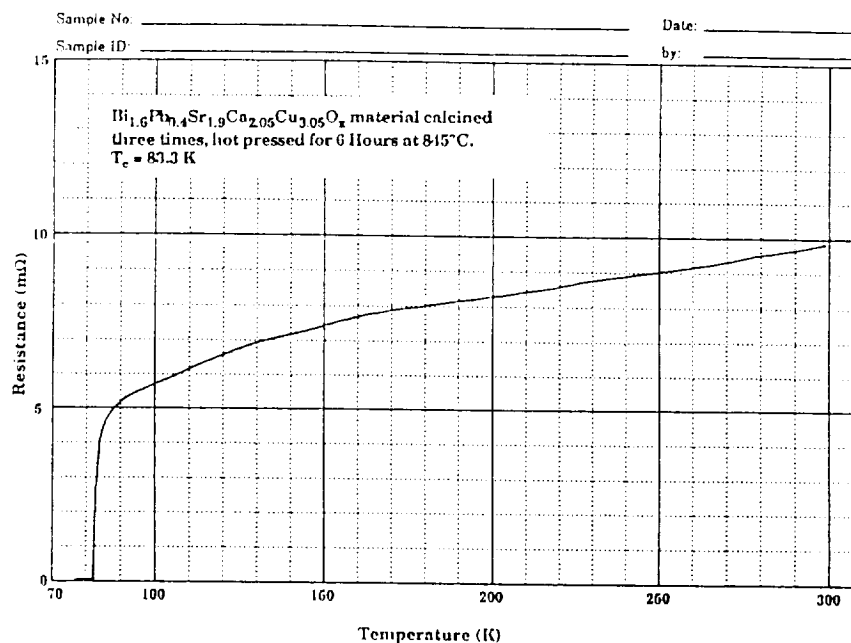
Temperature (K)

a) Hot pressed sample with no additional heat treatment.

3.0

$Bi_{1.6}Pb_{0.4}Sr_{1.9}Ca_{2.05}Cu_{3.05}O_x$ material calcined
three times, hot pressed for 6 Hours at 845°C, and
sintered for 24 Hours at 845°C. $T_c = 108.2$ K

Resistance (mΩ)

2.0

1.0

0

70   100   160   200   260   300
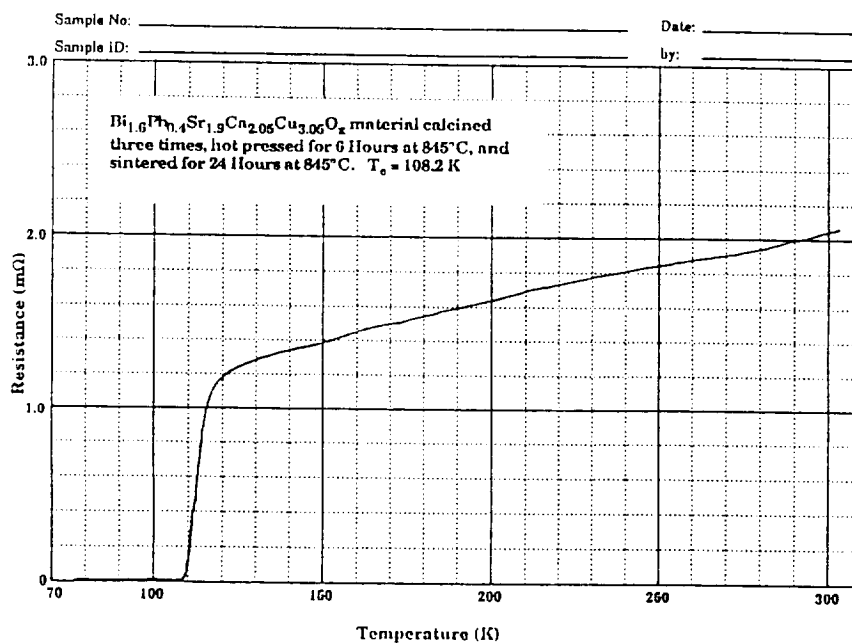
Temperature (K)

b) Hot pressed sample sintered for an additional twenty-four hours in air.

Figure 39 Resistance versus temperature curves of mixed oxide compacts hot pressed at
5000 psi in oxygen at 845 °C for six hours.
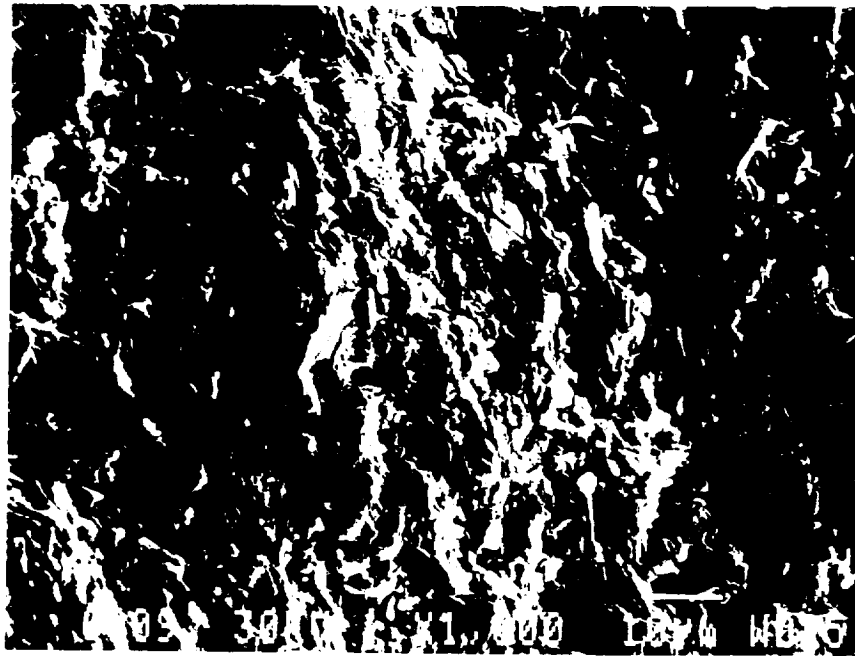
a) Hot pressed pellet with no additional heat treatment.
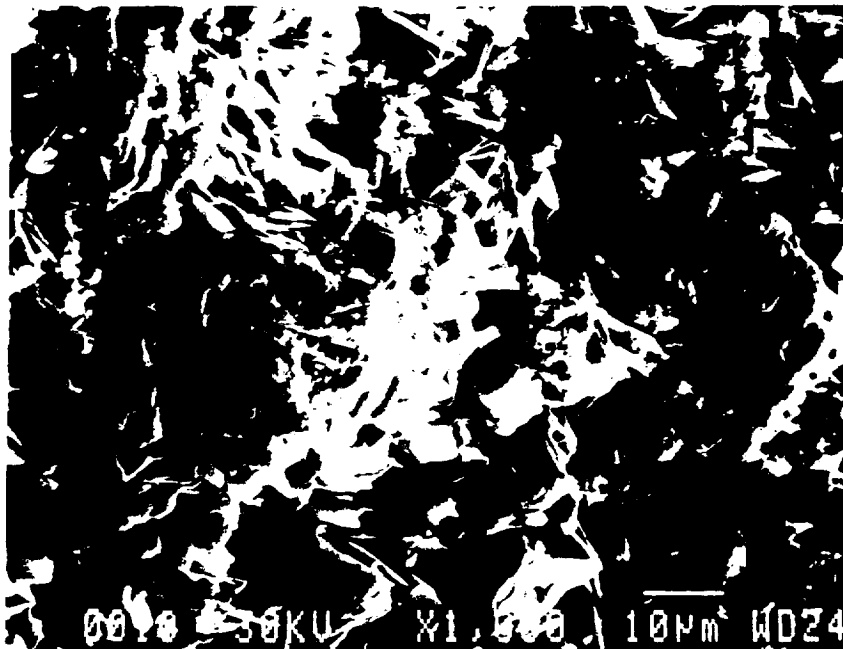
b) Hot pressed pellet sintered for an additional twenty-four hours in air.

Figure 40 SEM micrographs of bulk hot pressed pellets pressed at 5000 psi for six hours at 845 °C in oxygen.
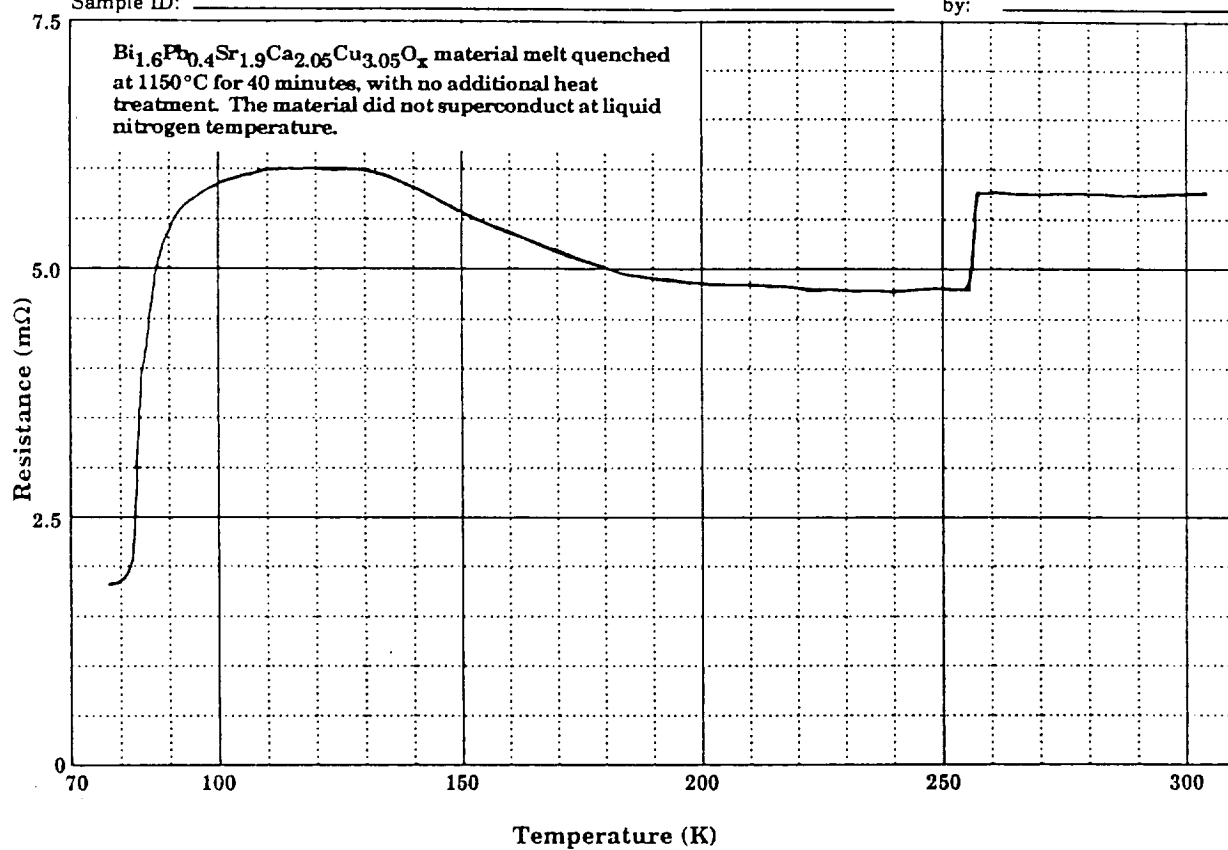
Figure 41 Resistance versus temperature curve of a melt quenched sample with no additional heat treatment. This material did not superconduct at 77.3 K.
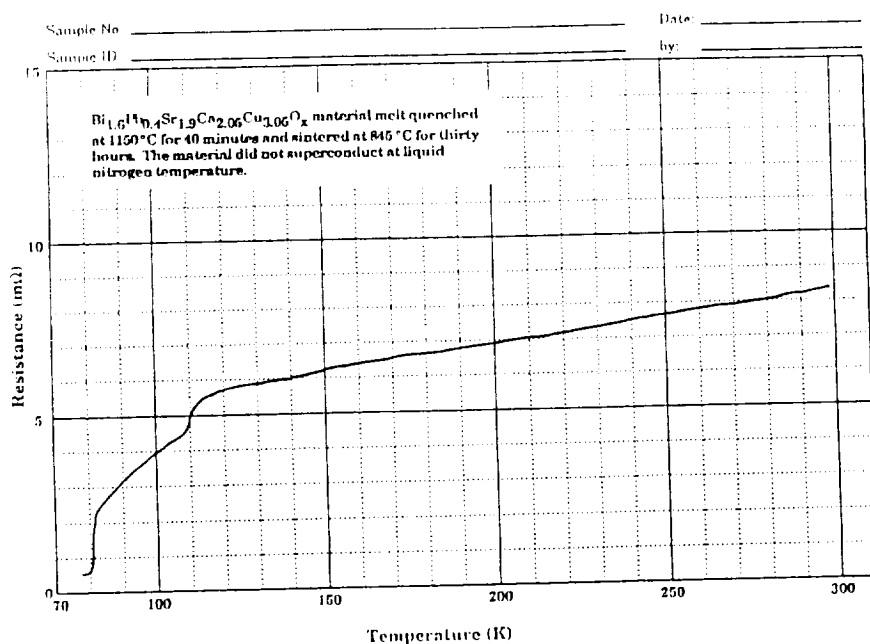
a) Melt quenched sample with thirty hours of additional heat treatment. The material did not superconduct at 77.3 K.
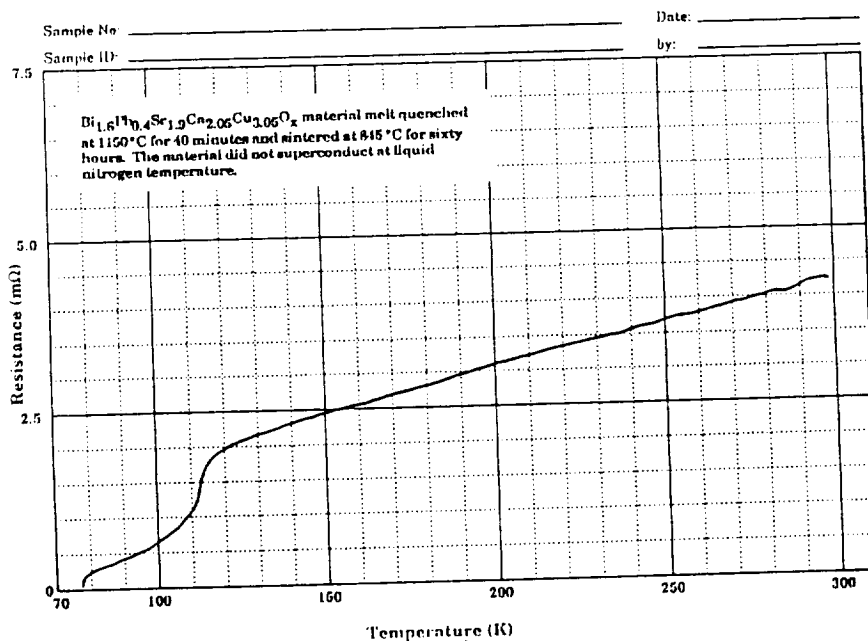
b) Melt quenched sample with sixty hours of additional heat treatment. The material did not superconduct at 77.3 K.

Figure 42 Resistance versus Temperature curves of melt quenched samples with additional heat treatment. They varied in the amount of additional heat treatment time at 845 °C.

C-2.

a) An area of a melt quenched sample which shows the solid melt behavior of the sample.

b) An area of a melt quenched sample which shows the porous behavior of the sample. This region appears to be exhibiting grain growth.

Figure 43 SEM micrographs of melt quenched samples with sixty hours of additional heat treatment at 845 °C in air. These micrographs show the inhomogeneities in the melt quenched materials.

$Bi_{1.6}Pb_{0.4}Sb_{0.1}Sr_{1.9}Ca_{2.05}Cu_{3.05}O_x$ melt quenched material sintered for twenty-four hours at 845 °C. The material did not superconduct at liquid nitrogen temperature.

Resistance (mΩ)
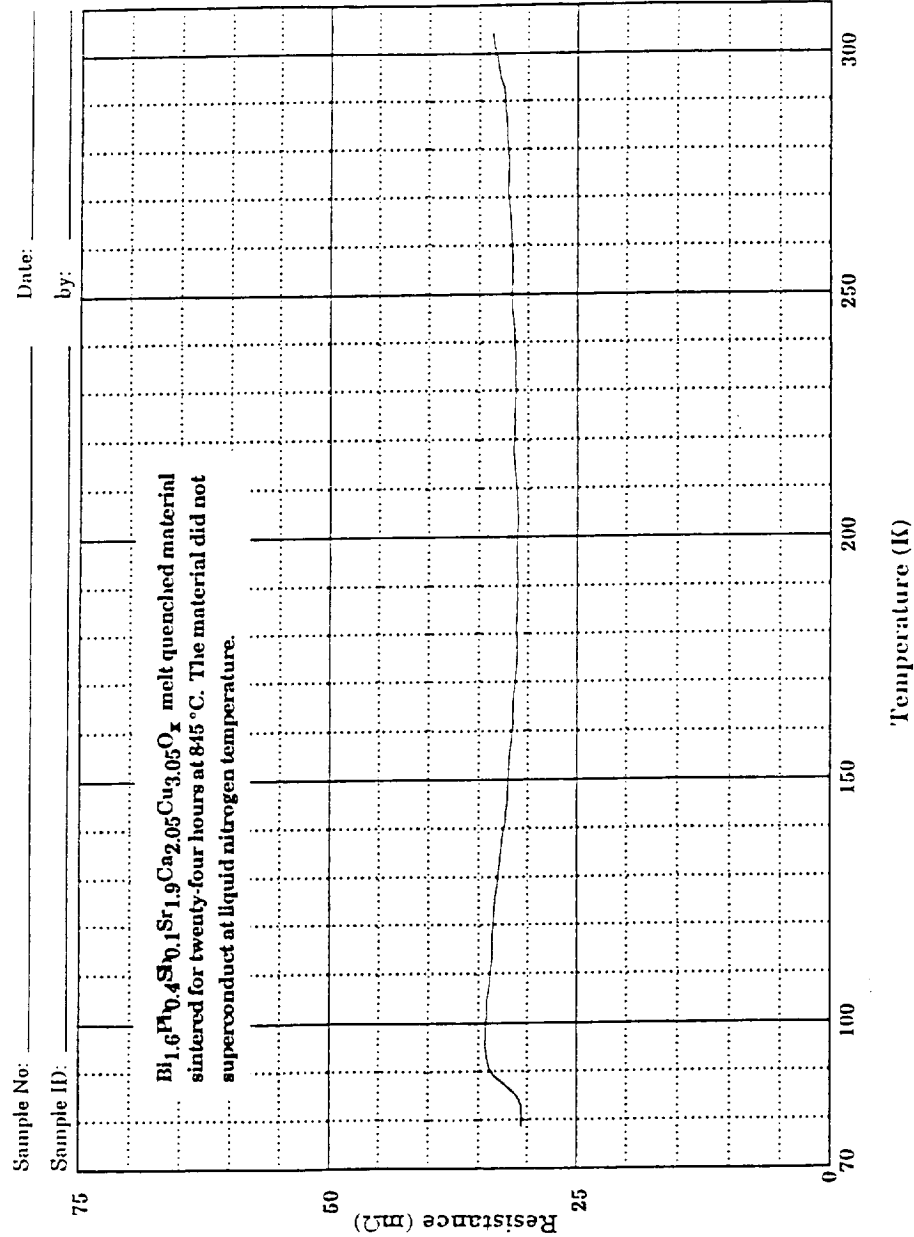
Temperature (K)

Figure 44 Resistance versus temperature curve of an antimony doped melt quenched sample sintered for twenty-four hours at 855 °C. The material did not superconduct at liquid nitrogen temperature.
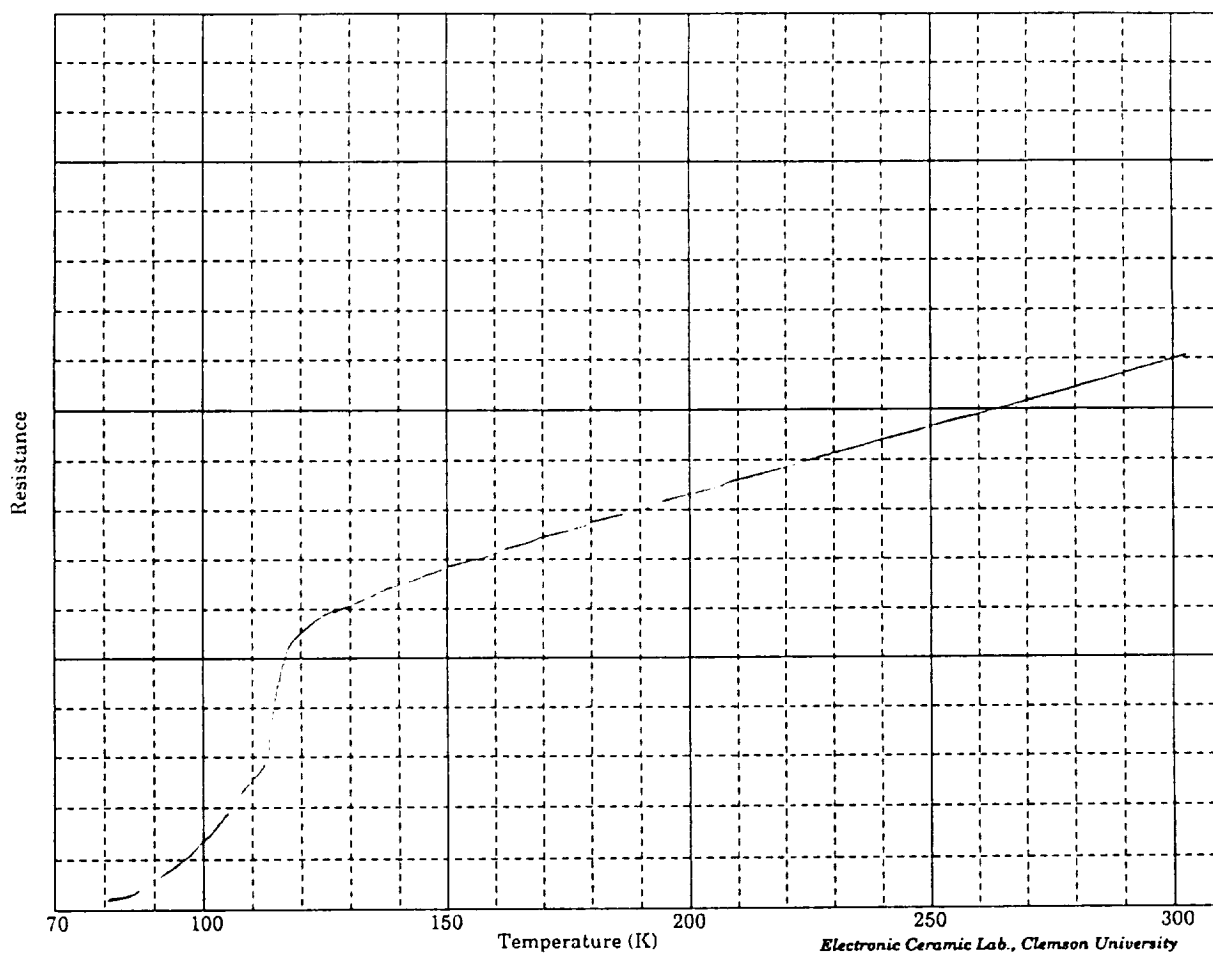
Figure 45 Resistance versus temperature curve of a tapecast sample of
$Bi_{1.6}Pb_{0.4}Sr_{1.9}Ca_{2.05}Cu_{3.05}O_x$ sintered at 845 °C for twenty hours in air. The
tape did not superconduct and had a resistance of 0.94 mΩ at 77.3 K.
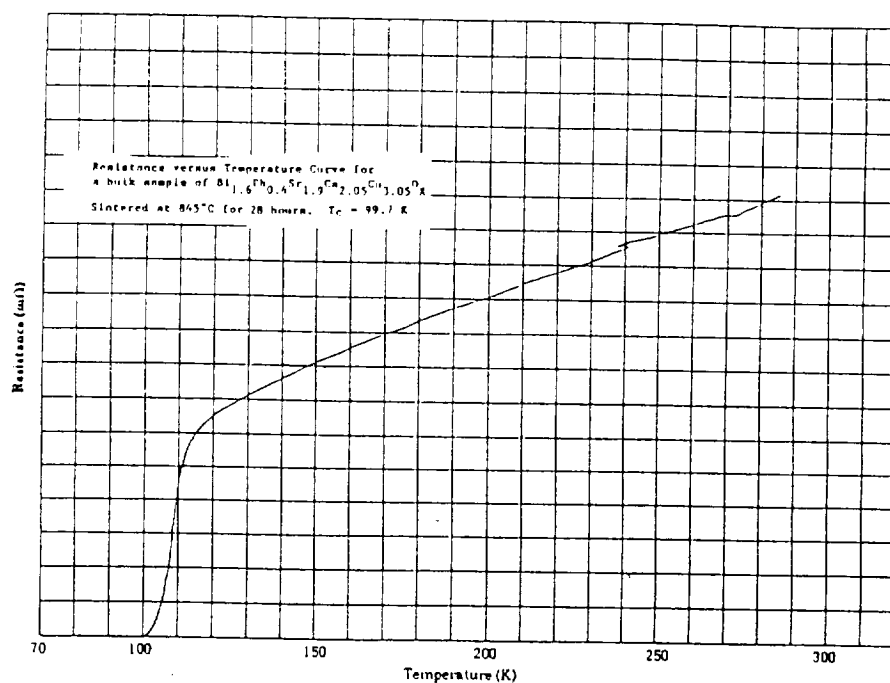
a) BSCCO bulk material. The T_c was 99.7 K.
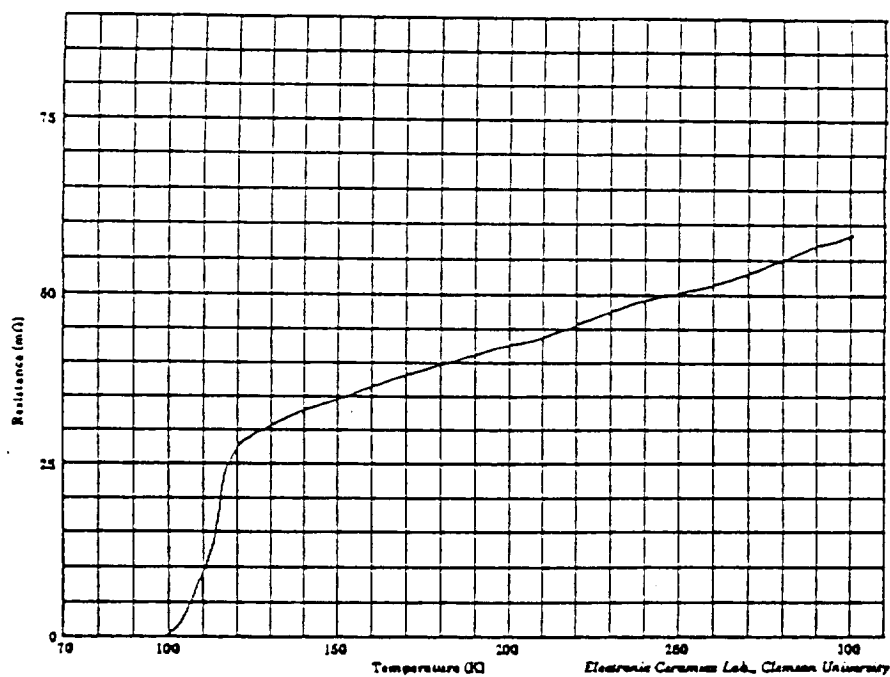
b) BSCCO tapecast material. The T_c was 98.2 K.

Figure 46 Resistance versus temperature curves of a bulk and a tapecast sample of $Bi_{1.6}Pb_{0.4}Sr_{1.9}Ca_{2.05}Cu_{3.05}O_x$ sintered at 845 °C for twenty-eight hours in air.
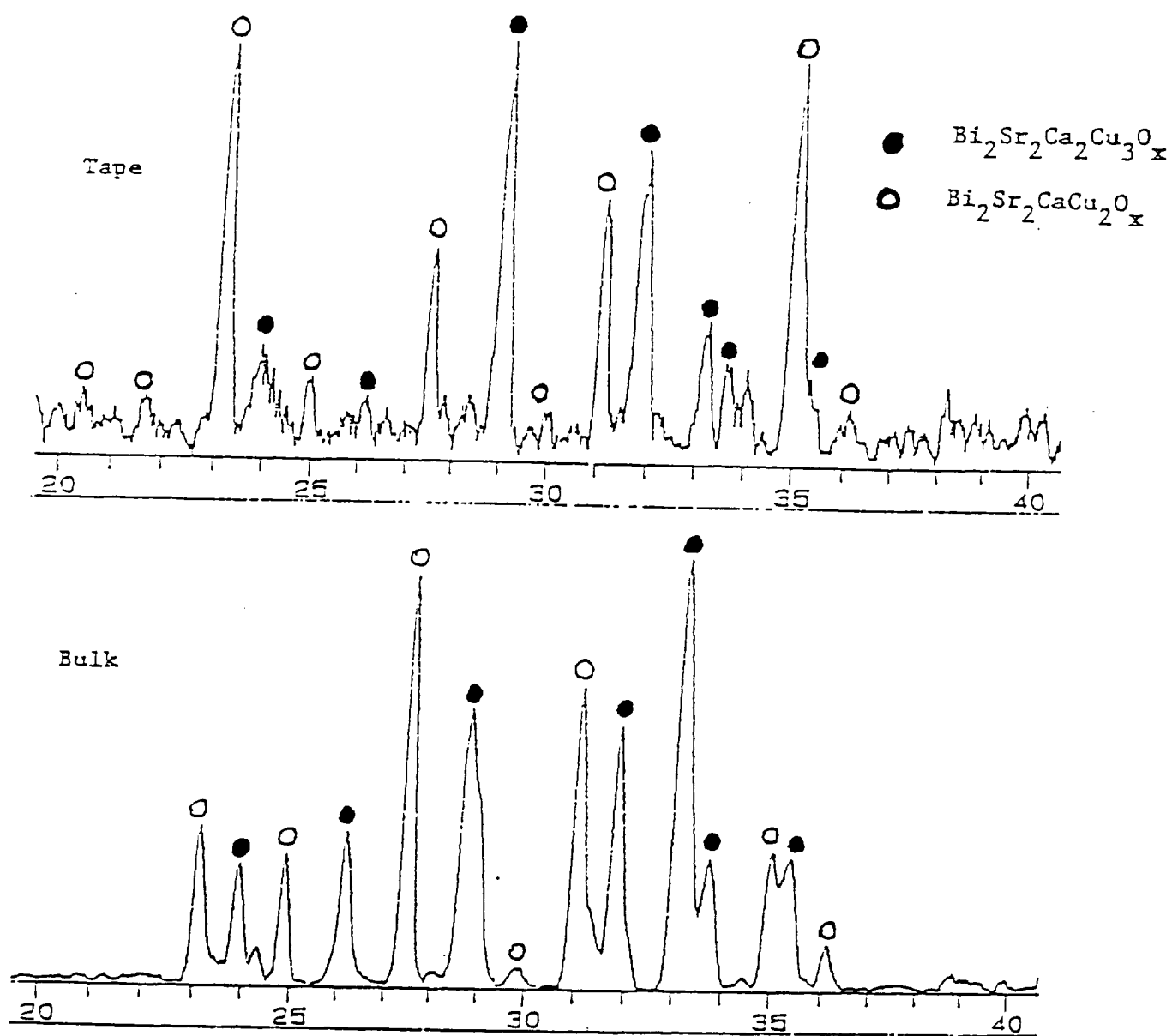
Figure 47 Xray diffraction data of a bulk compact and a tape sintered at 845 °C for twenty-eight hours in air.
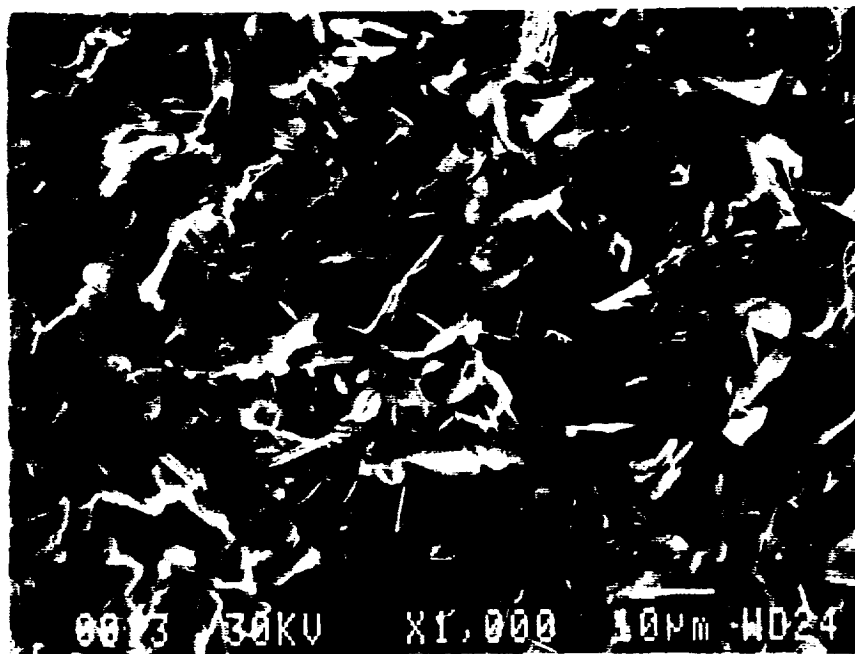
Figure 48 SEM micrograph of a $Bi_{1.6}Pb_{0.4}Sr_{1.9}Ca_{2.05}Cu_{3.05}O_x$ tape sintered at 845 °C for thirty-three hours in air.
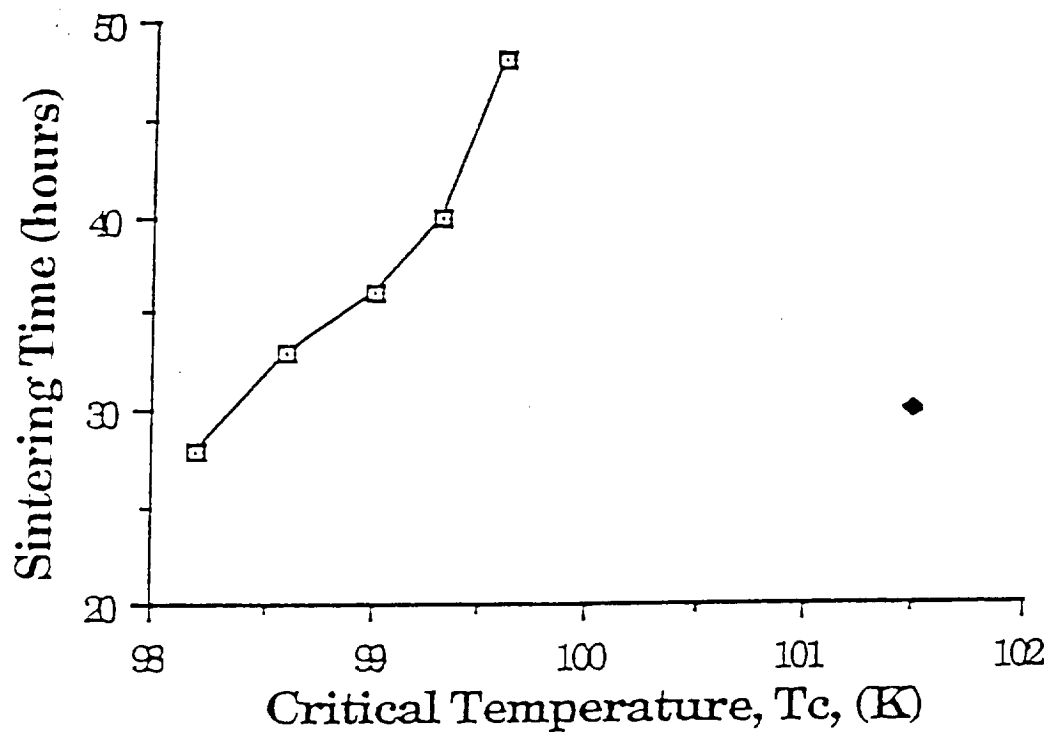
Figure 49 Sintering time versus critical temperature curve of the single ramp tapecast material with a dot for the double ramp tapecast material, showing why the double ramp process is preferred.
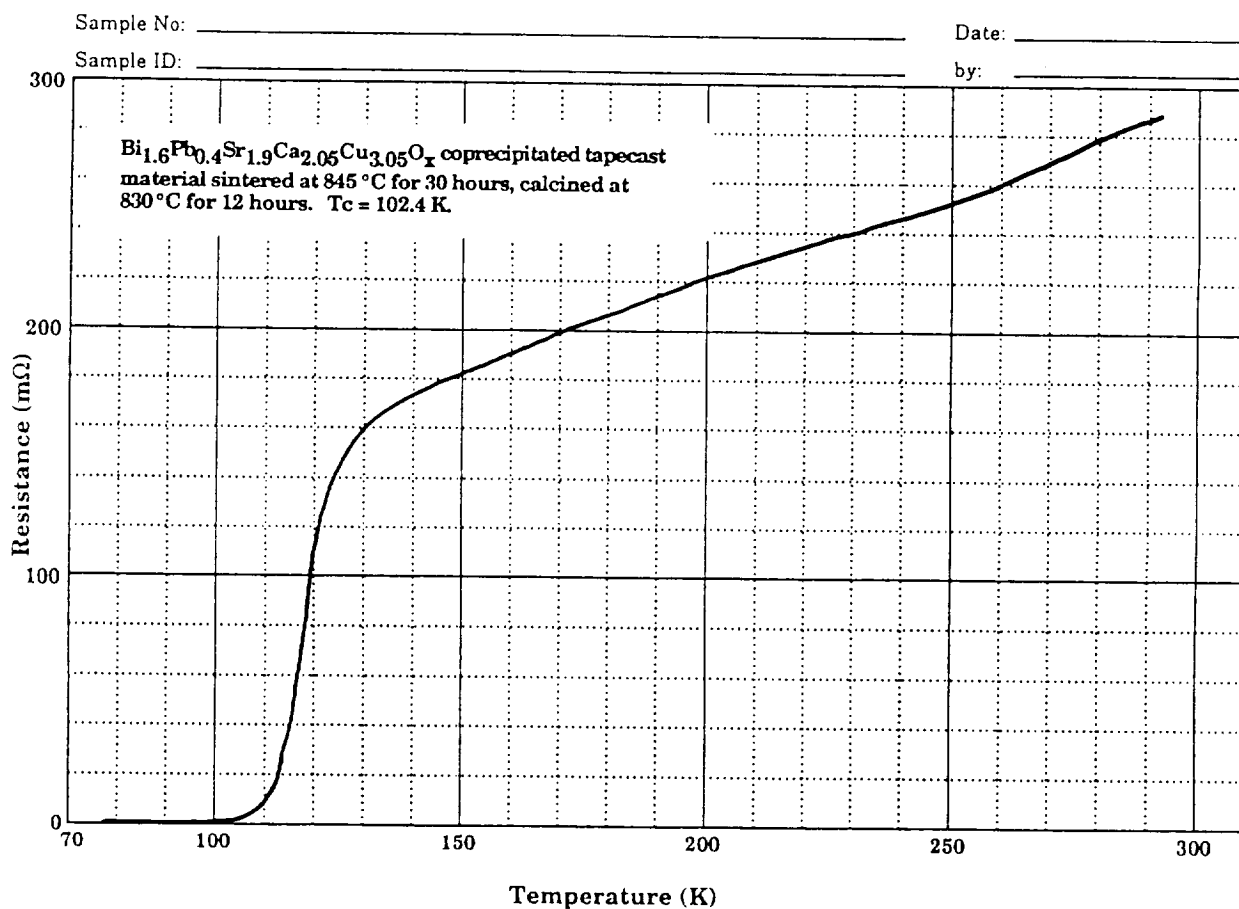
Figure 50 Resistance versus temperature curve of a coprecipitated tapecast sample which was sintered at 845 °C for thirty hours. The T_c was 102.4 K.
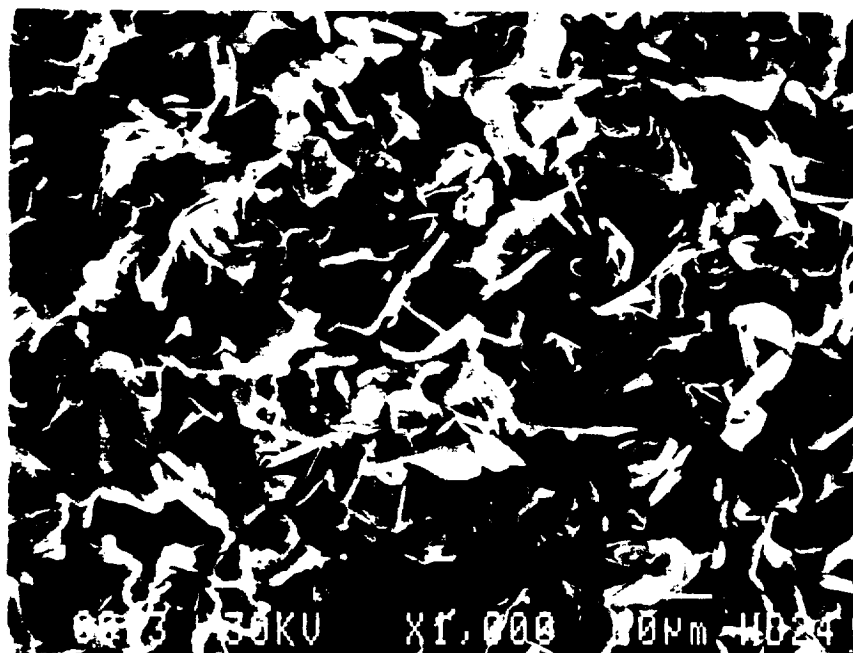
a) Tape that was prepared by the mixed oxide process.
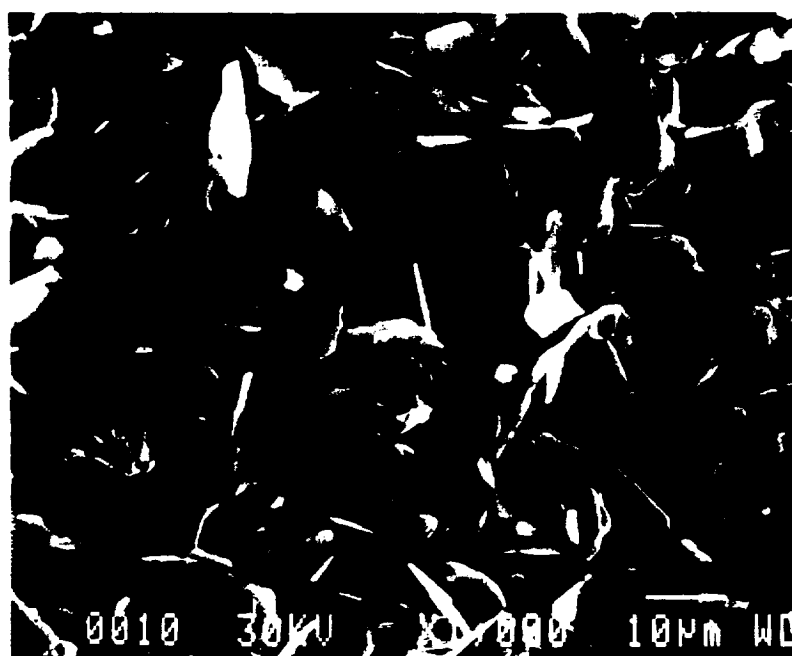
b) Tape that was prepared by the coprecipitation process.

Figure 51 SEM micrographs of tapecast samples which were sintered at 845 °C for thirty hours.
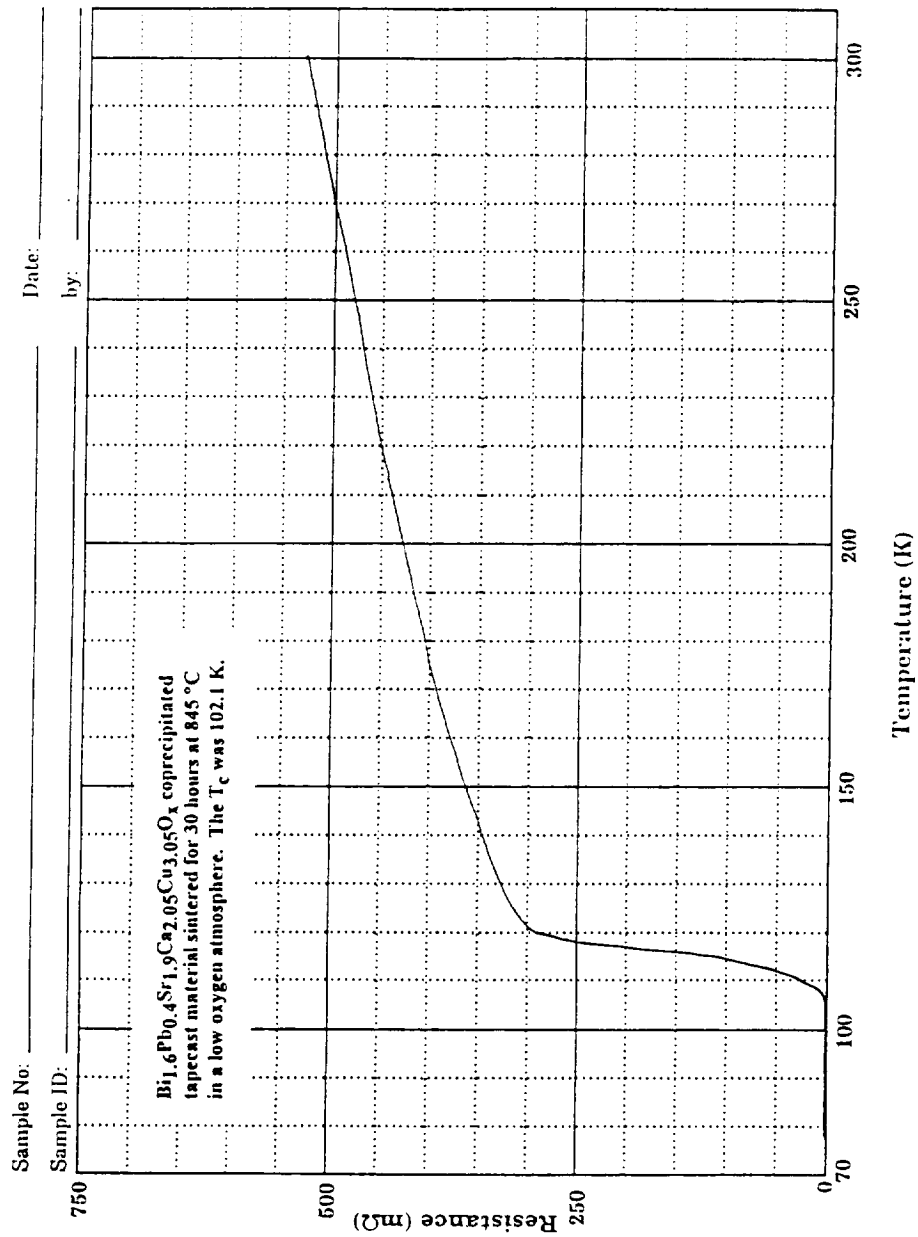
Figure 52 Resistance versus temperature curve of coprecipitated tapecast sample which was sintered for thirty hours in a low oxygen atmosphere at 845 °C. The T_c was 102.1 K.
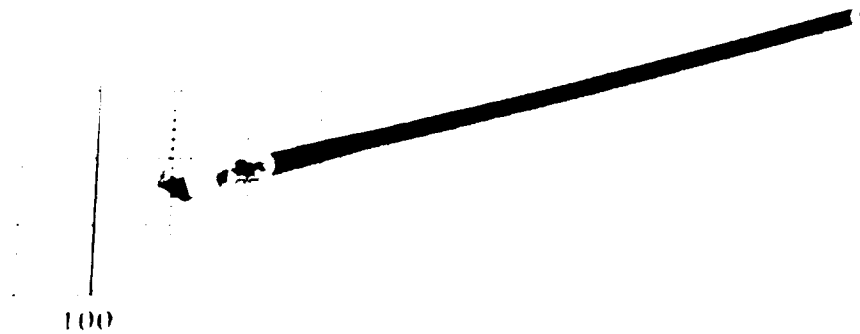
a) Superconducting grounding links produced with bismuth-based coprecipitated tapecast material. The T_c was 100.5 K.
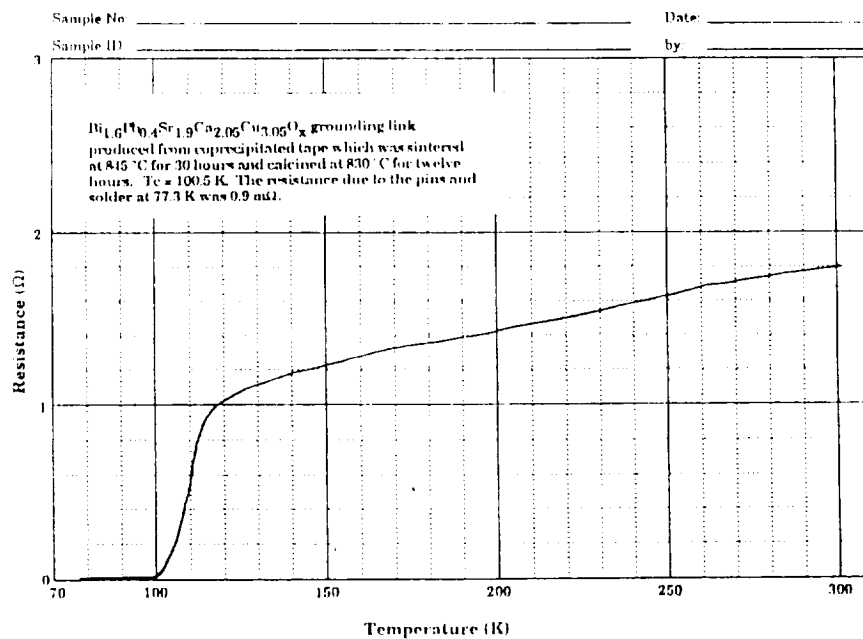
b) Resistance versus temperature curve of grounding links produced from coprecipitated tapecast material.

Figure 53 Superconducting grounding link property data.

ORION DILATOMETER MODEL 1600D

Differential Coefficient of Expansion
(10E-6 in./in.)

28   24   20   16   12   8   4   0

Temperature (°C)

0   100   200   300   400   500   600   700   800

Percent Linear Change

0.7000   0.6000   0.5000   0.4000   0.3000   0.2000   0.1000   0.0000

Legend
PLC
DCE
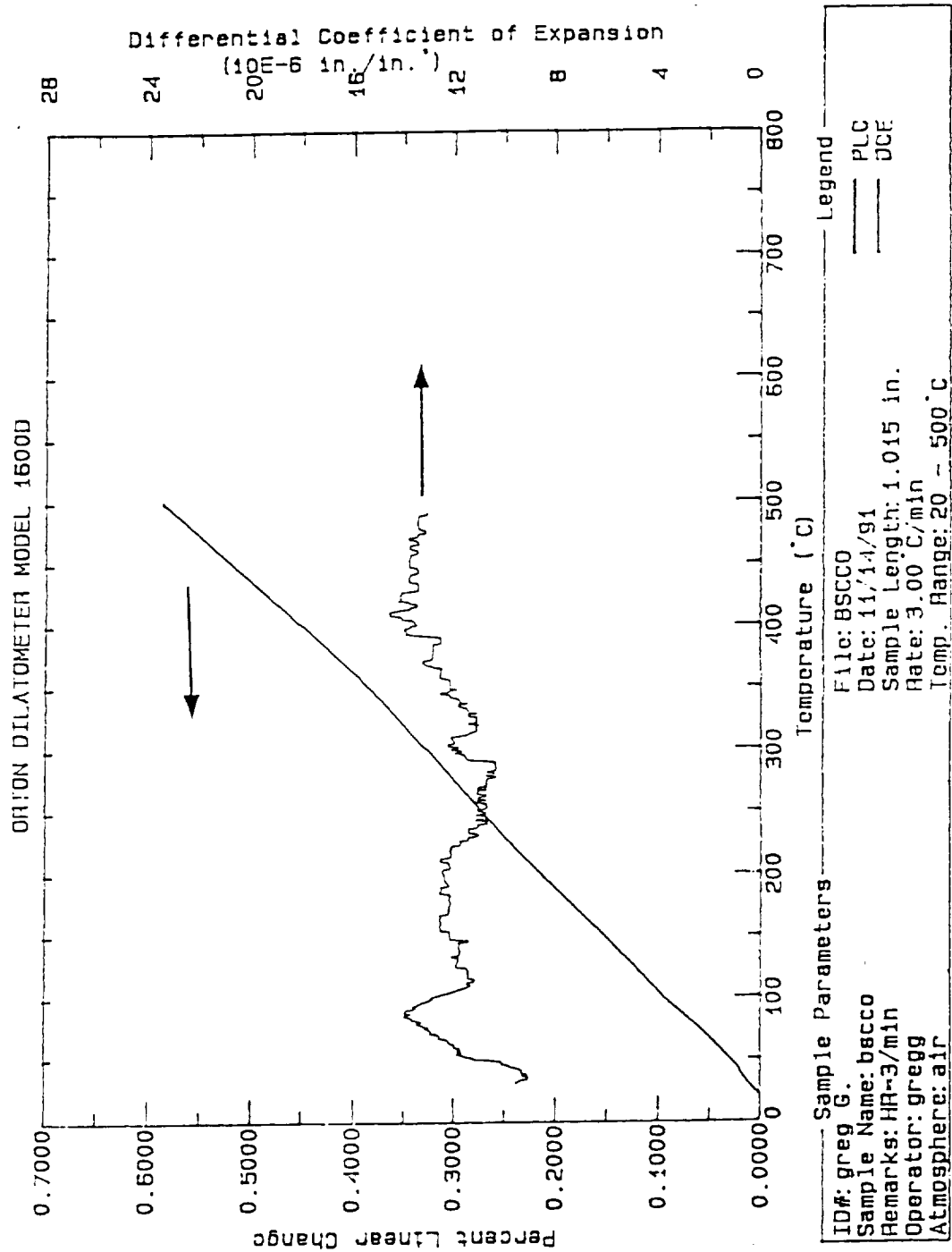
Figure 54 The thermal expansion curve of the coprecipitated bismuth-based material. The TE was 12×10^{-6} in/in °C.
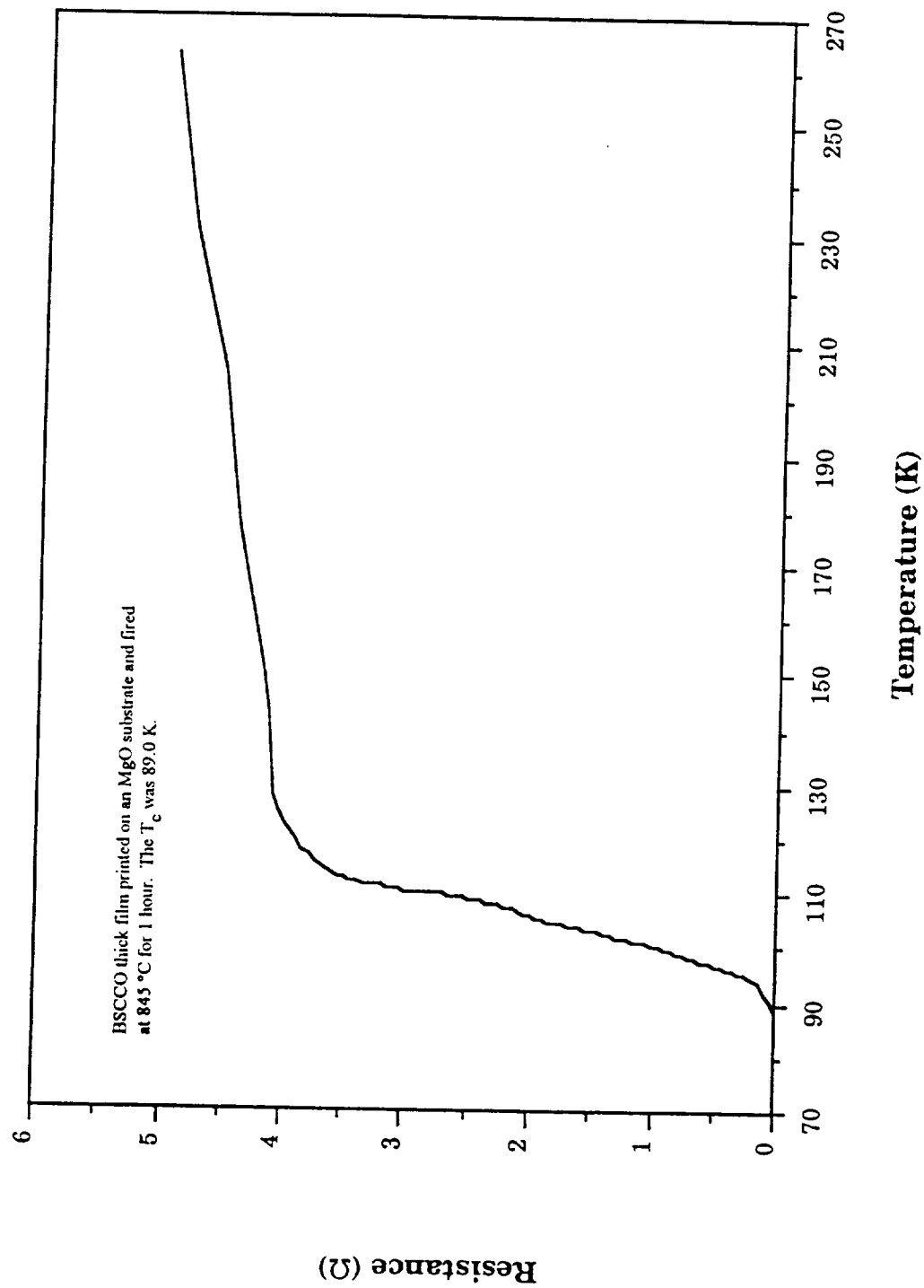
Figure 55 Resistance versus temperature curve of a BSCCO coprecipitated screen printed thick film which was sintered for one hour at 845 °C in air. The T_c was 89.0 K.
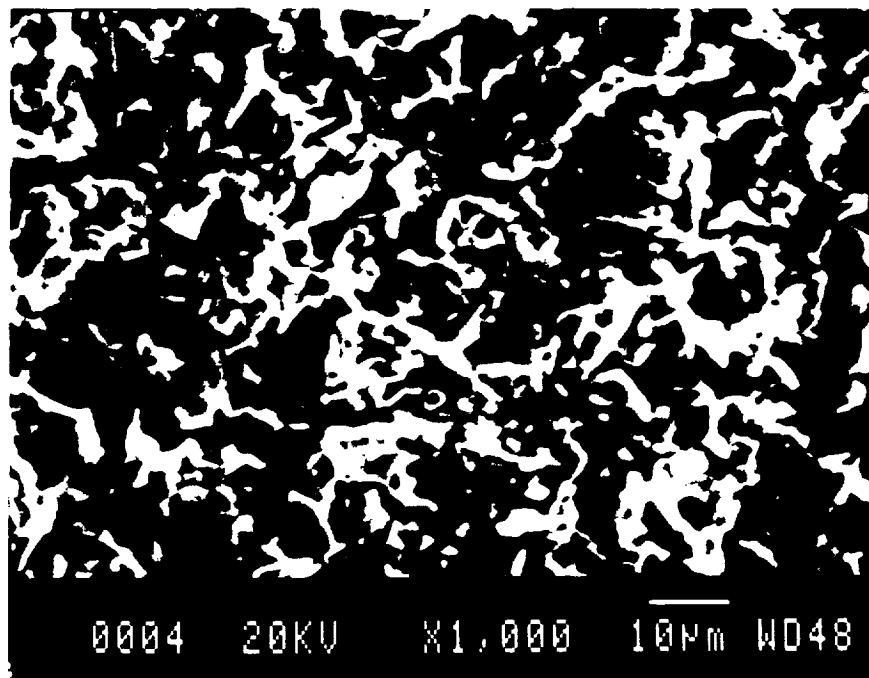
Figure 56 SEM micrograph of a BSCCO coprecipitated thick film printed on an MgO substrate. The film was sintered at 845 °C for one hour in air.
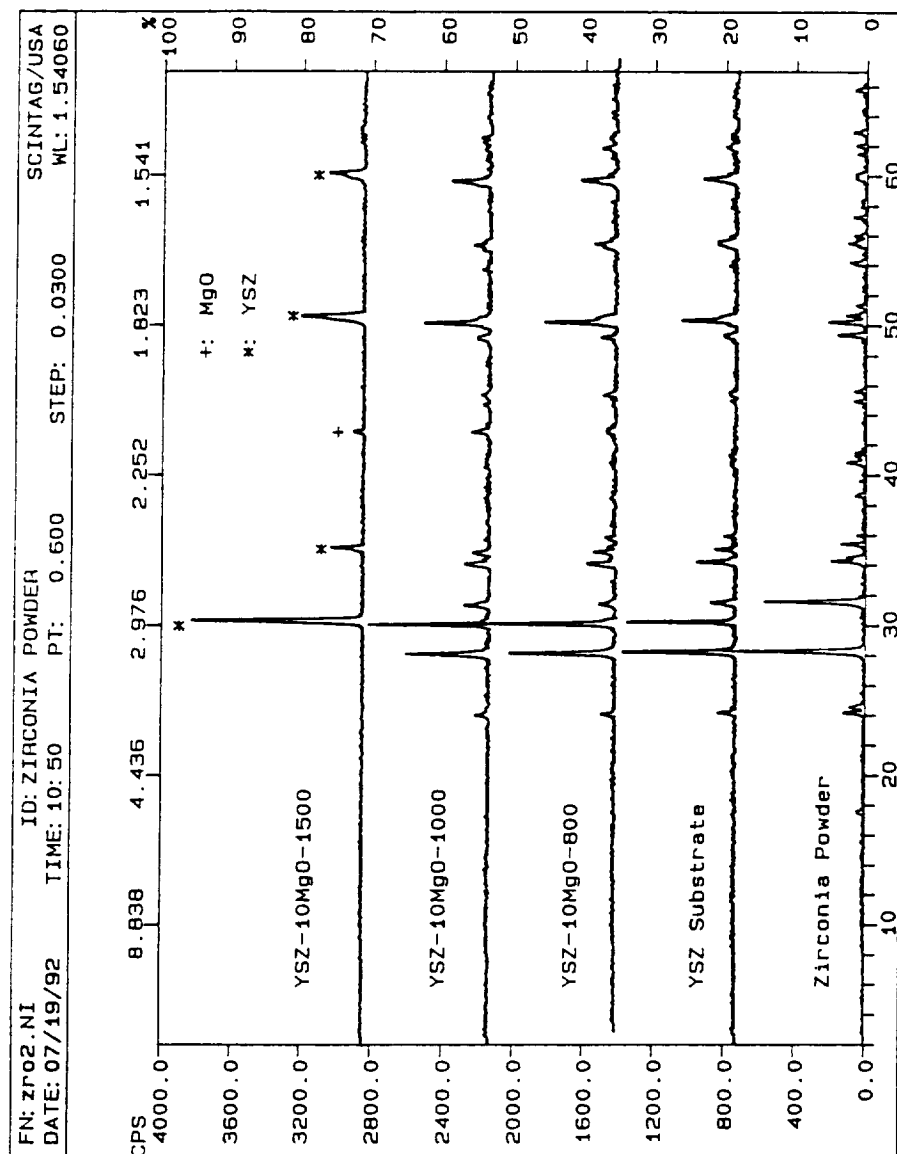
Figure 57 Xray diffraction data of a YSZ substrate, from the original zirconia powder through the annealing of the substrate to the application and annealing of the MgO buffer layer.
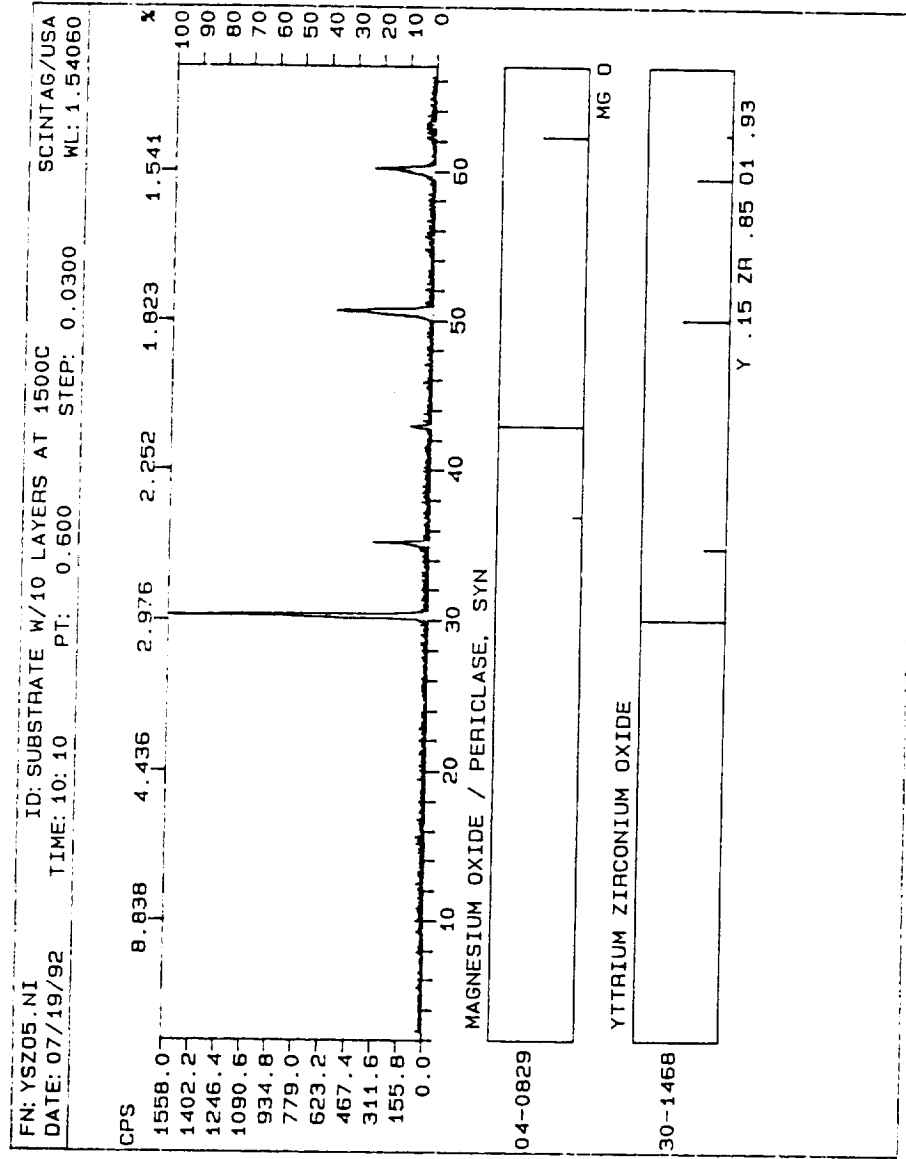
Figure 58 Xray diffraction data of a YSZ substrate with an MgO buffer layer, and the JCPDS standards XRD patterns for YSZ and MgO.

10% TSZ substrate without buffer layer
Fired at 845°C for 3 hours.

Resistance (kΩ)

Temperature (K)

a) 10 % YSZ substrates without the MgO buffer layer.

10% TSZ Substrate with 10 Layers of MgO
Fired at 845°C for 3 hours.
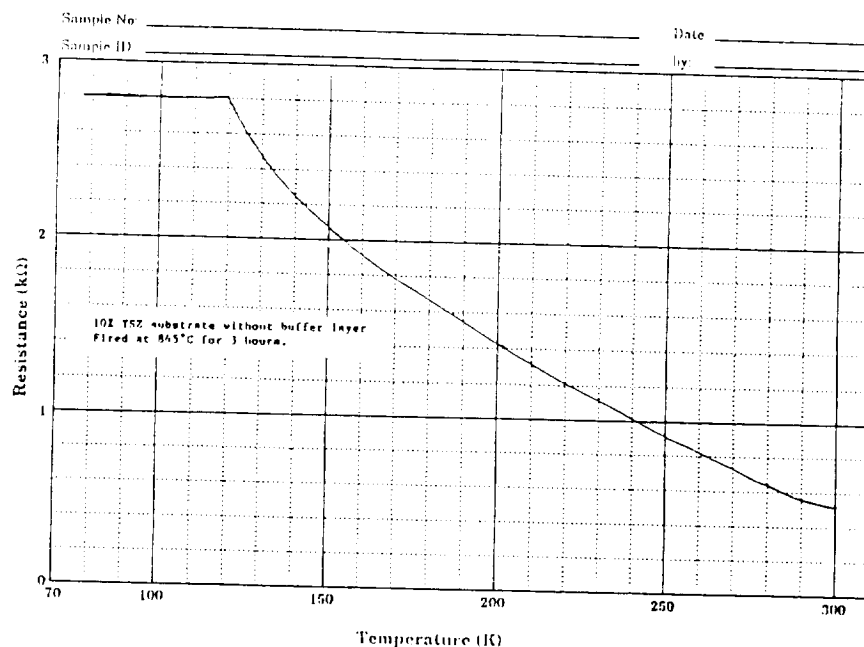
Resistance (Ω)
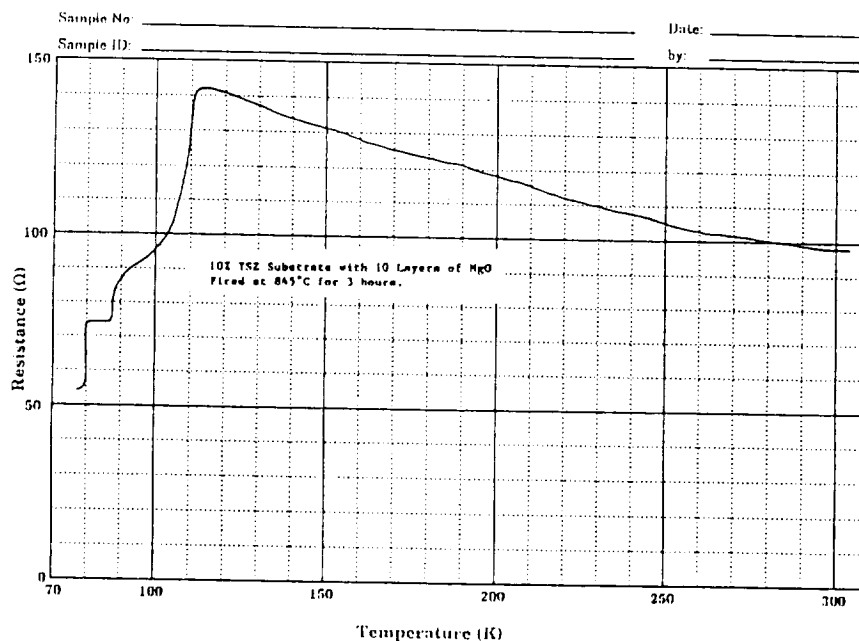
Temperature (K)

b) 10 % YSZ substrates with the MgO buffer layer.

Figure 59 Resistance versus temperature curves of BSCCO coprecipitated thick films
printed on 10 % YSZ substrates and sintered for three hours at 845 °C in air, with
and without an MgO buffer layer.
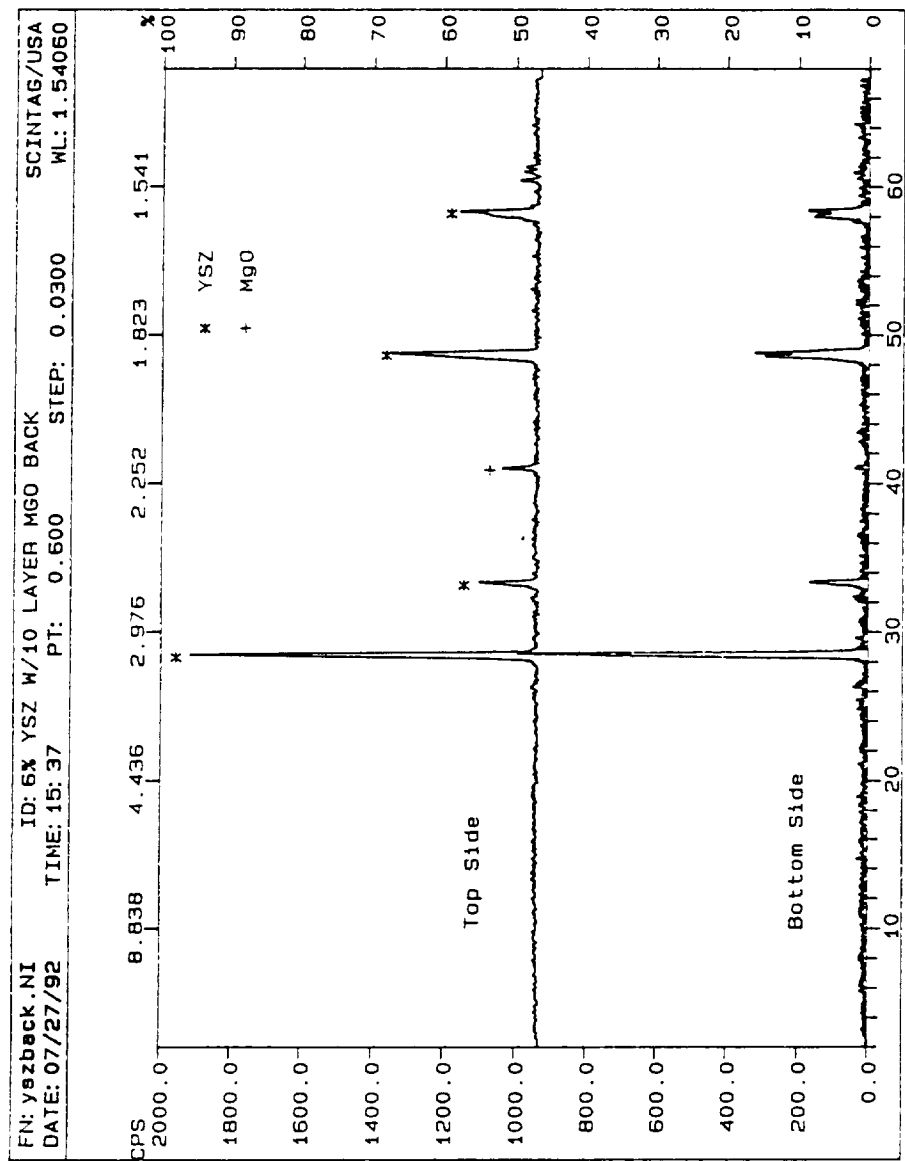
Figure 60 Xray diffraction data of the top and bottom of a YSZ substrate coated with an MgO buffer layer.
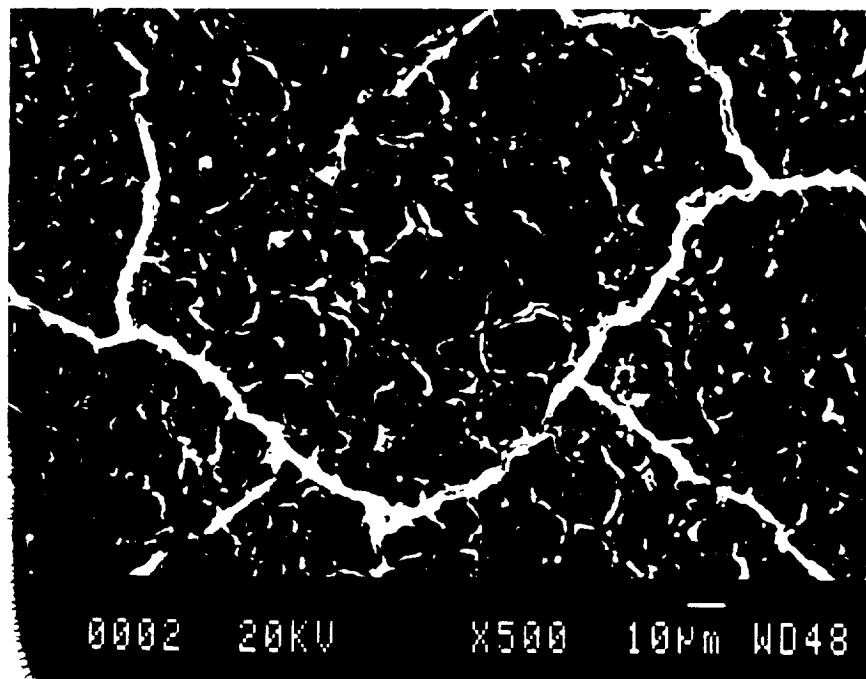
Figure 61 SEM micrograph of the MgO buffer layer showing the microcracks in the buffer layer.

750

500

Resistance (Ω)

8 % YSZ Substrate without buffer layer
Fired at 845°C for 3 hours.

250

0

70   100   150   200   250   300

Temperature (K)

a) 8 % YSZ substrates without the MgO buffer layer.

75

50

Resistance (Ω)

8 % YSZ Substrate with 10 Layers of MgO
Fired at 845°C for 3 hours.

25

0

70   100   150   200   250   300
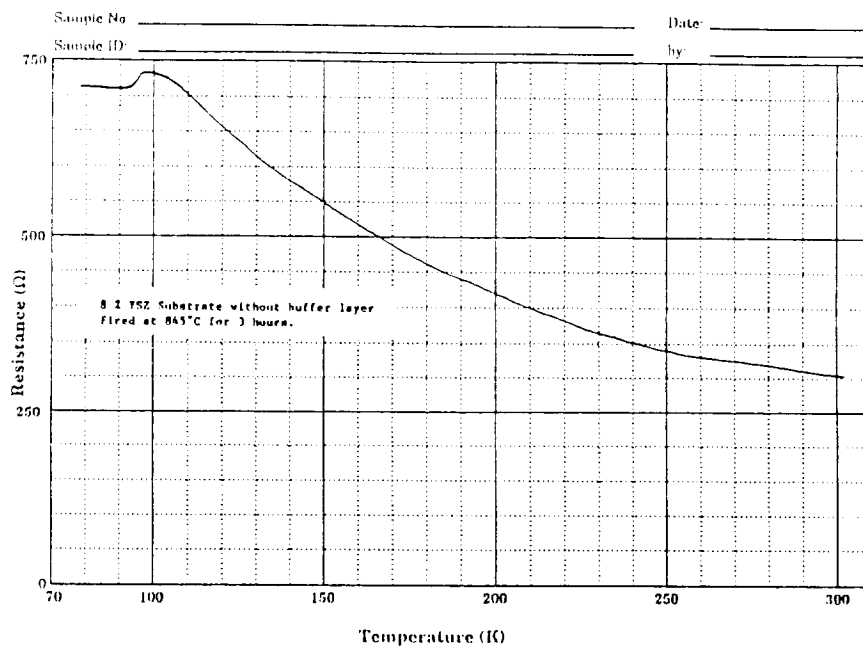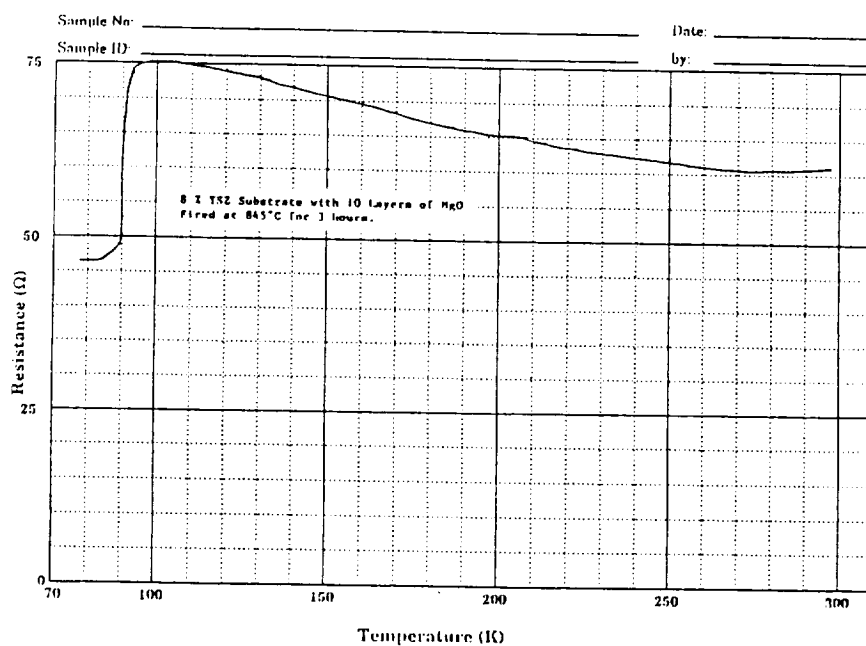
Temperature (K)

b) 8 % YSZ substrates with the MgO buffer layer.

Figure 62 Resistance versus temperature curves of BSCCO coprecipitated thick films printed on 8 % YSZ substrates and sintered for three hours at 845 °C in air, with and without an MgO buffer layer.

6 % YSZ Substrate without buffer layer
Fired at 845°C for 3 hours.

a) 6 % YSZ substrates without the MgO buffer layer.

6 % YSZ Substrate with 10 layers of MgO
Fired at 845°C for 3 hours.
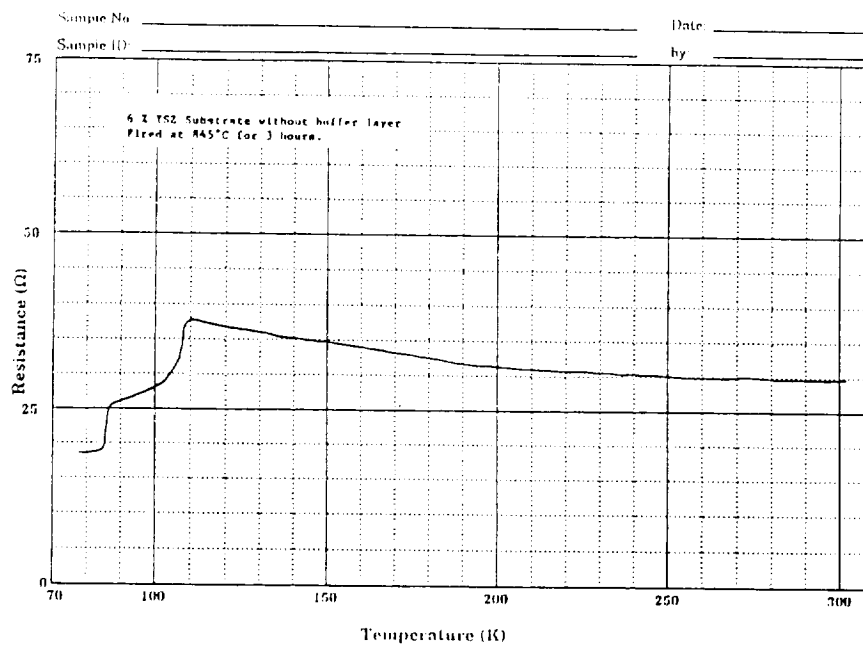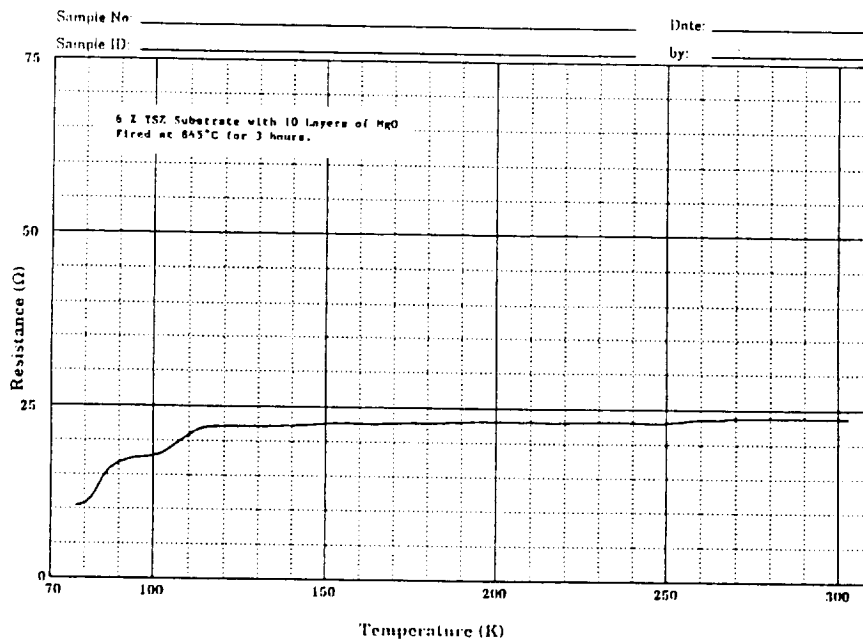
b) 6 % YSZ substrates with the MgO buffer layer.

Figure 63 Resistance versus temperature curves of BSCCO coprecipitated thick films printed on 6 % YSZ substrates and sintered for three hours at 845 °C in air, with and without an MgO buffer layer.
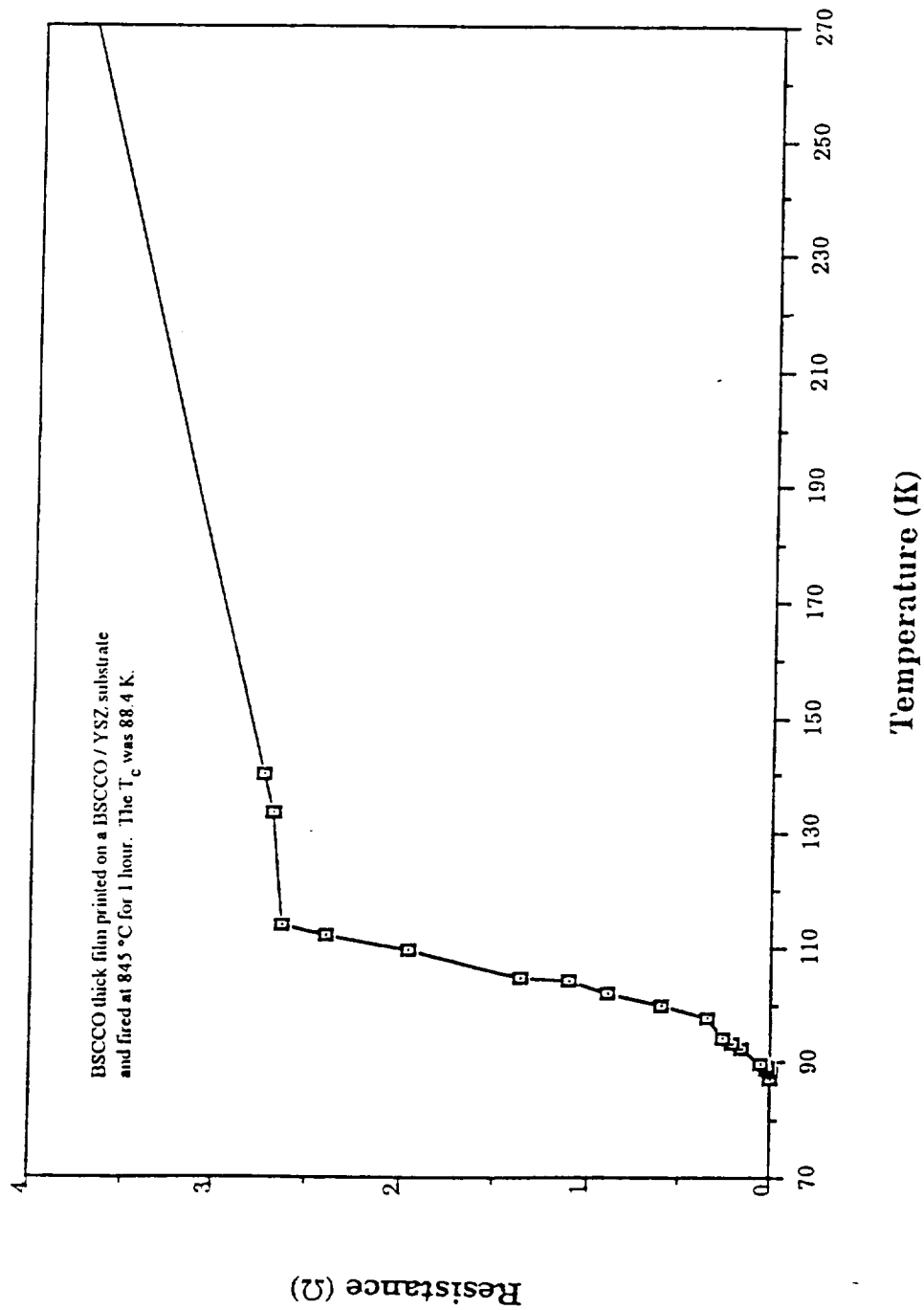
Figure 64 Resistance versus temperature curve of a BSCCO thick film printed on a BSCCO / YSZ substrate and sintered for one hour at 845 °C in air. The T_c was 88.4 K.

Sample No: _____

Sample ID: _____

Date: _____

by: _____

BSCCO / YSZ substrate fired at 880 °C for 10
minutes. The substrate shows a transition around
90 K.

Resistance (Ω)

Temperature (K)

70   100   150   200   250   300
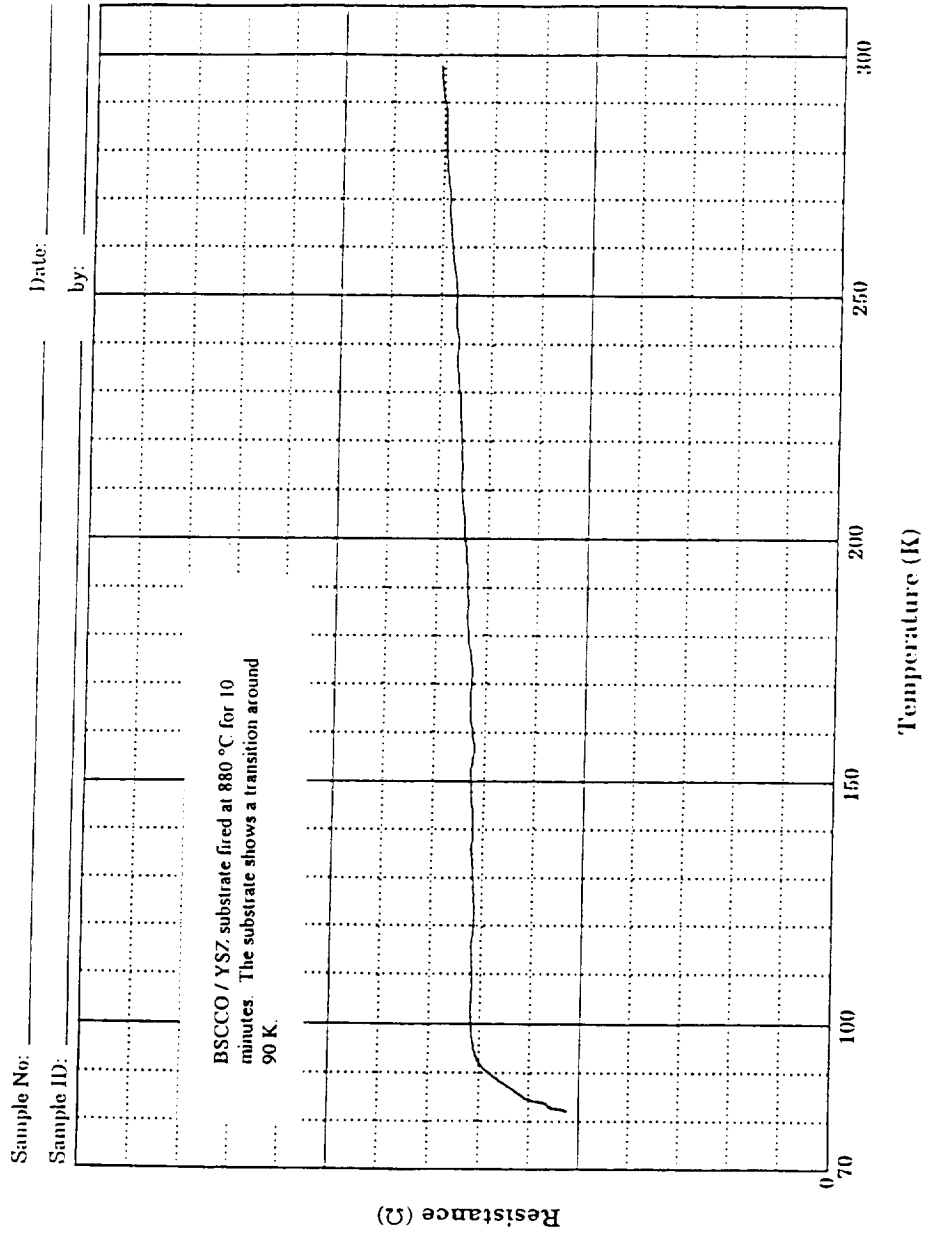
Figure 65 Resistance versus temperature curve of the BSCCO / YSZ substrate sintered at 880 °C in air for
ten minutes.
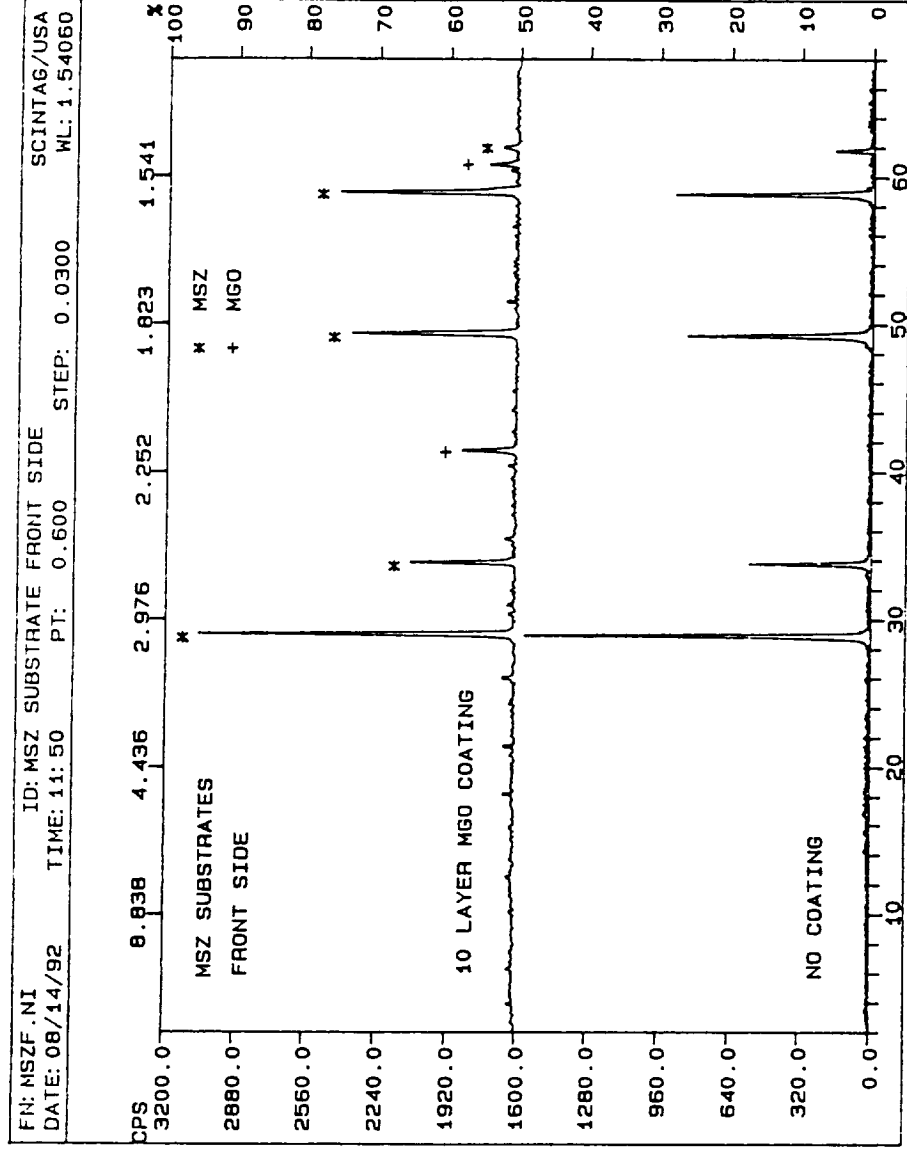
Figure 66 Xray diffraction data obtained from the MSZ substrates with and without an MgO buffer layer.
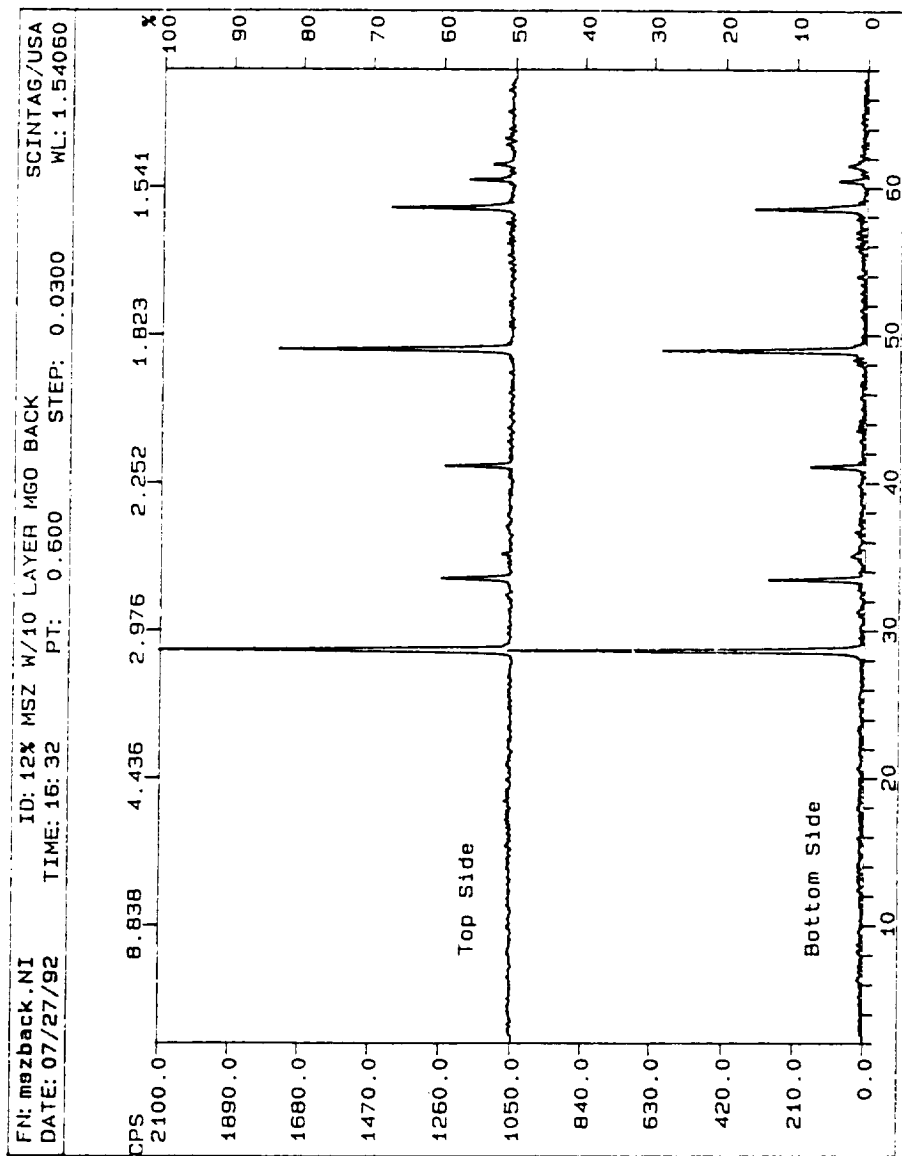
Figure 67 Xray diffraction data of the top and bottom of a MSZ substrate coated with an MgO buffer layer.
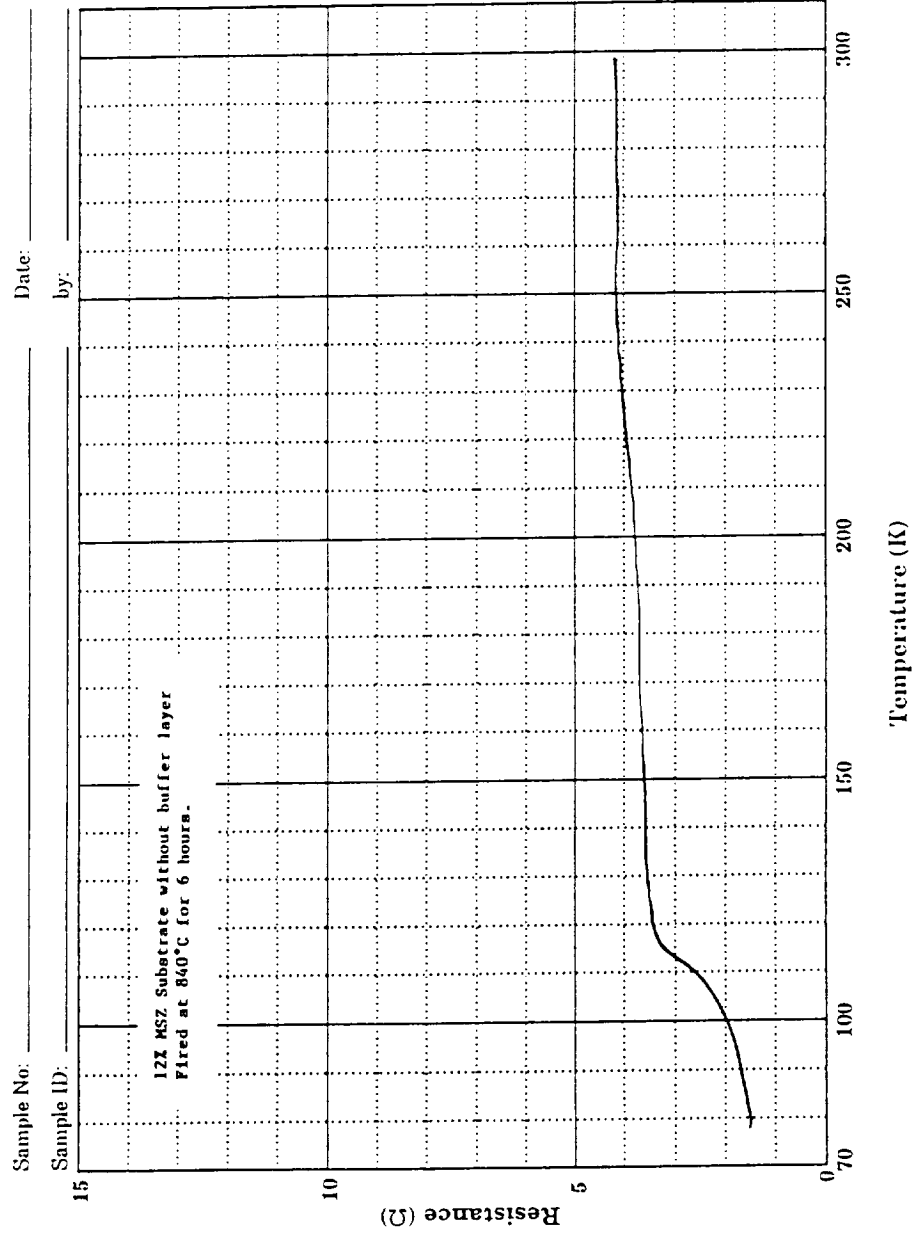
Figure 68 Resistance versus temperature curve of a BSCCO thick film printed on a 12 % MSZ substrate without a buffer layer and sintered for six hour at 845 °C in air.
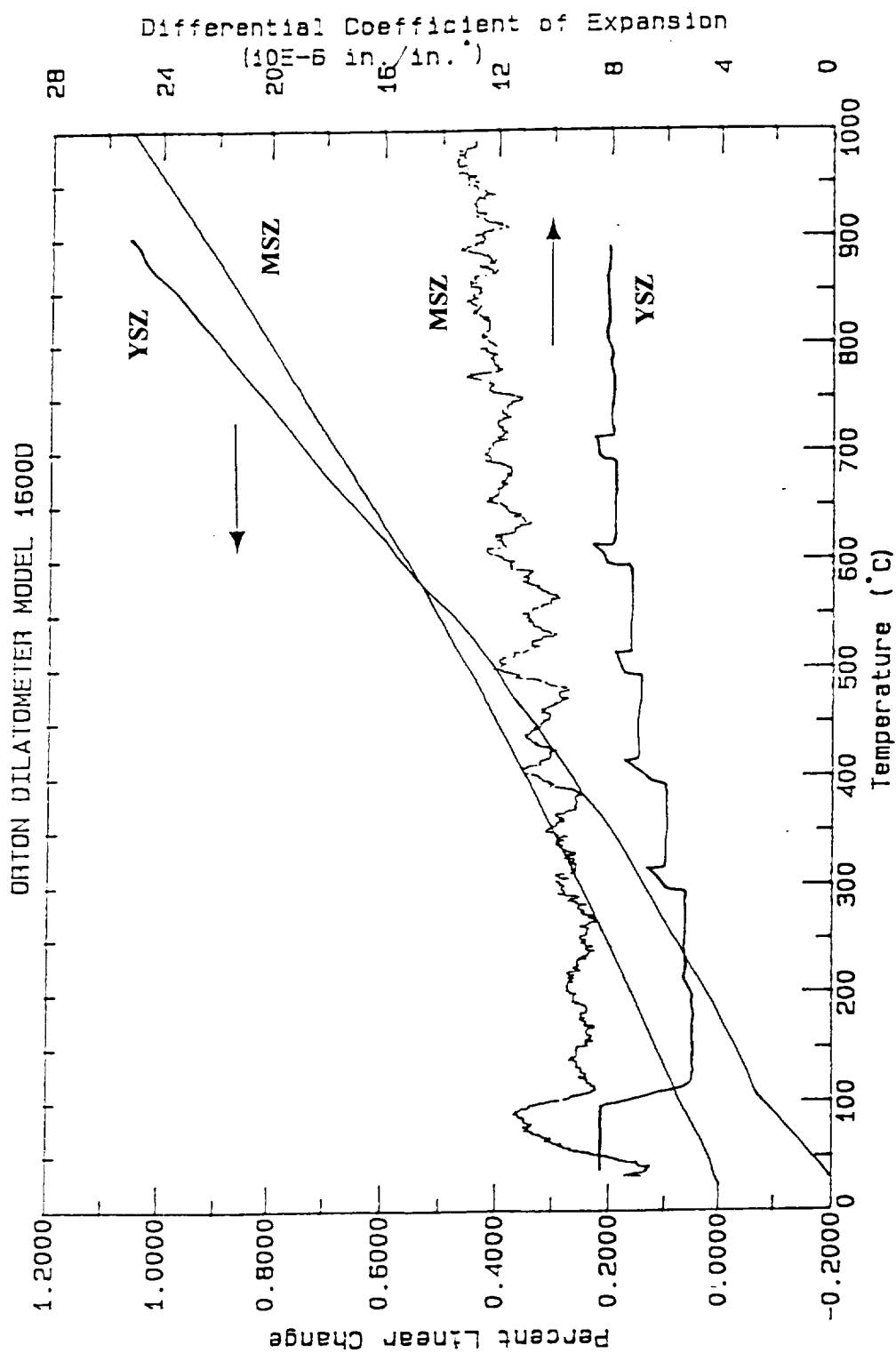
Figure 69 The thermal expansion curve of the MSZ and YSZ substrates. The TE for MSZ was 12×10^{-6} in/in °C and the TE for YSZ was 8×10^{-6} in/in °C
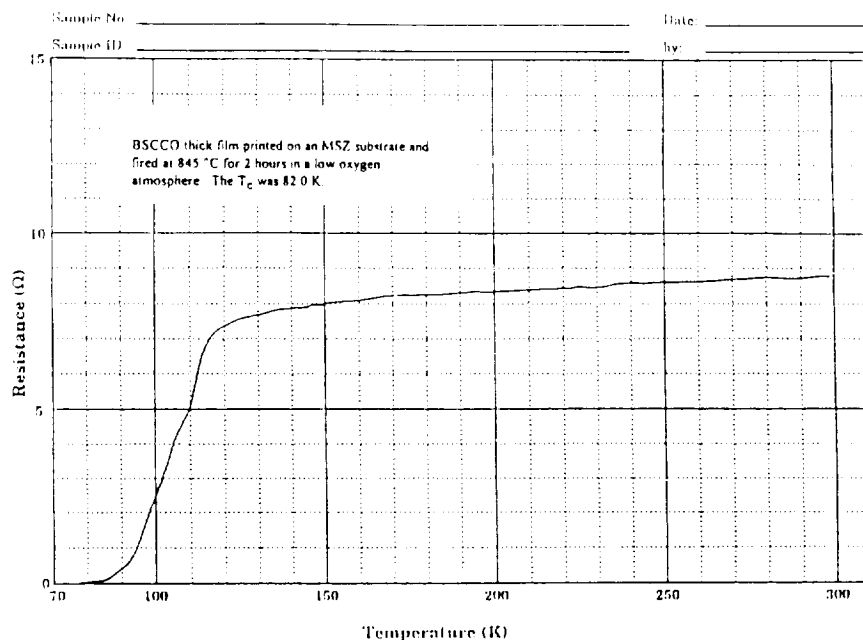
a) BSCCO thick film printed on a 12 % MSZ substrate without an MgO buffer layer.
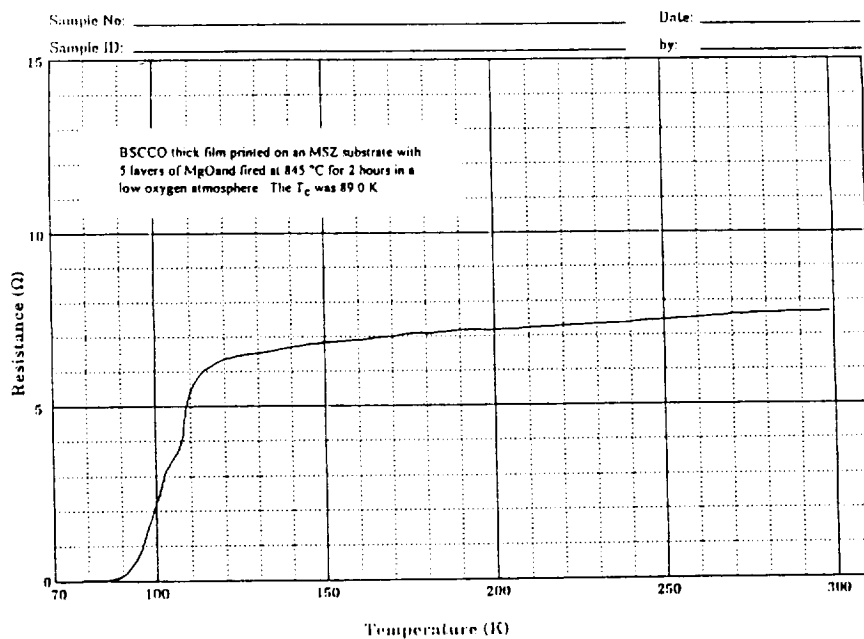
b) BSCCO thick film printed on a 12 % MSZ substrate with a five coat MgO buffer layer.

Figure 70 Resistance versus temperature curves of BSCCO coprecipitated thick films printed on 12 % MSZ substrates and sintered at 845 °C for two hours under a low oxygen atmosphere, with and without an MgO buffer layer.
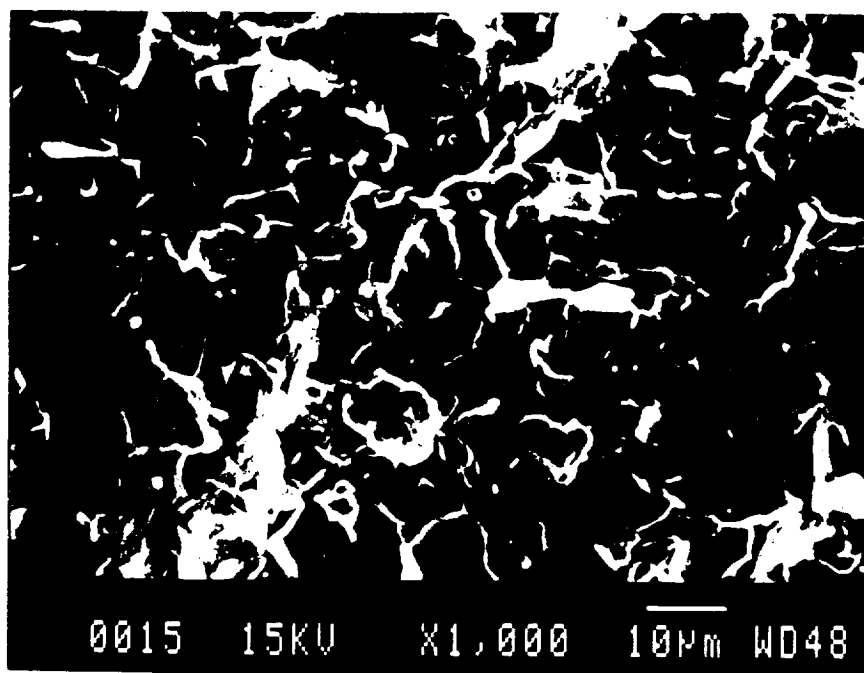
a) An example of a dense BSCCO thick film printed on a 12 % MSZ substrate. The thick film superconducted at 87 K.
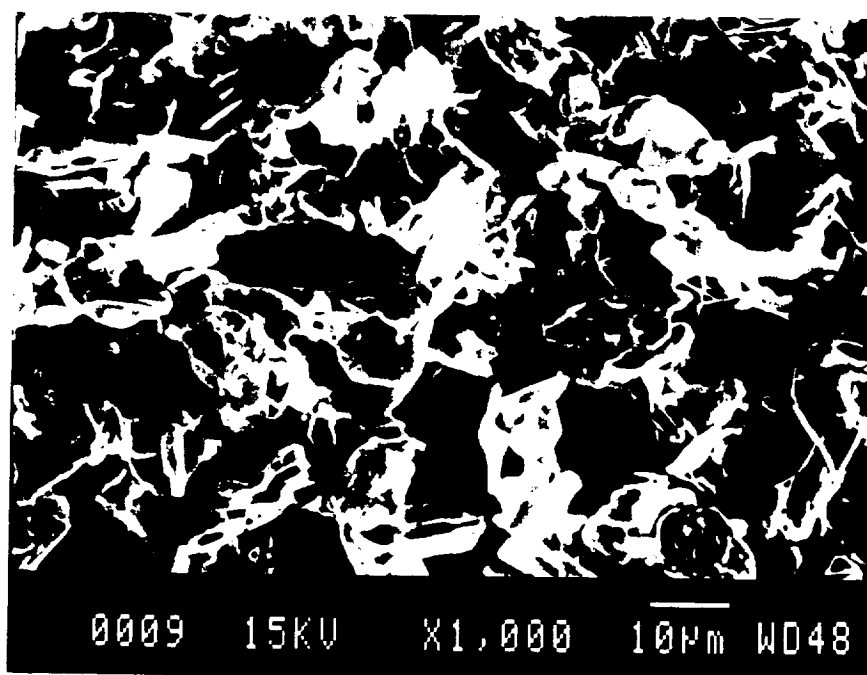
b) An example of a porous BSCCO thick film printed on a 12 % MSZ substrate. The thick film did not superconduct at liquid nitrogen temperature.

Figure 71 SEM micrographs of two BSCCO thick films on MSZ substrates.
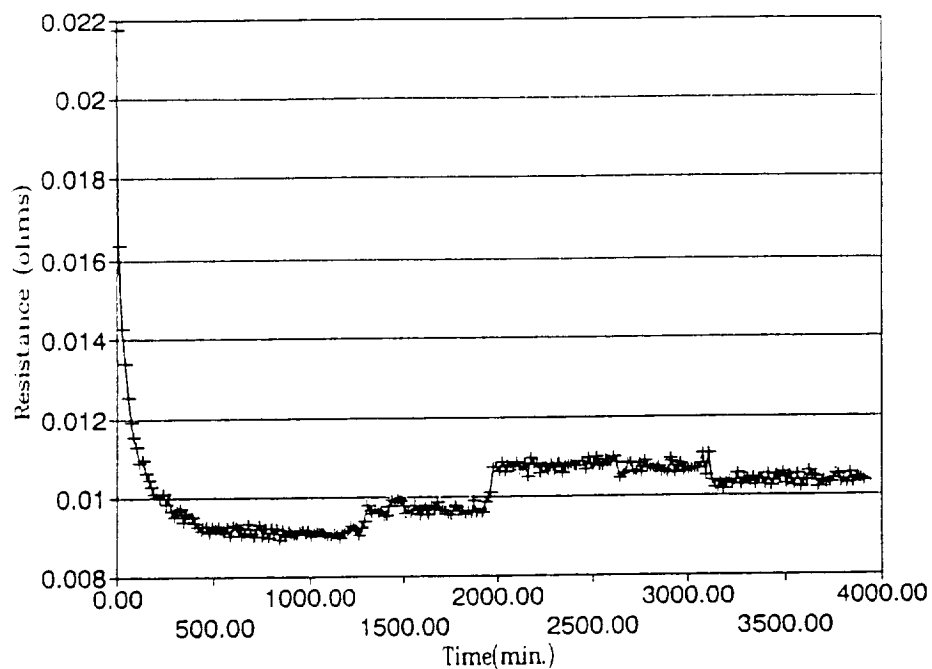
a) The entire resistivity run, from the initial dwell at 845 °C until a silver wire broke after sixty-four hours.
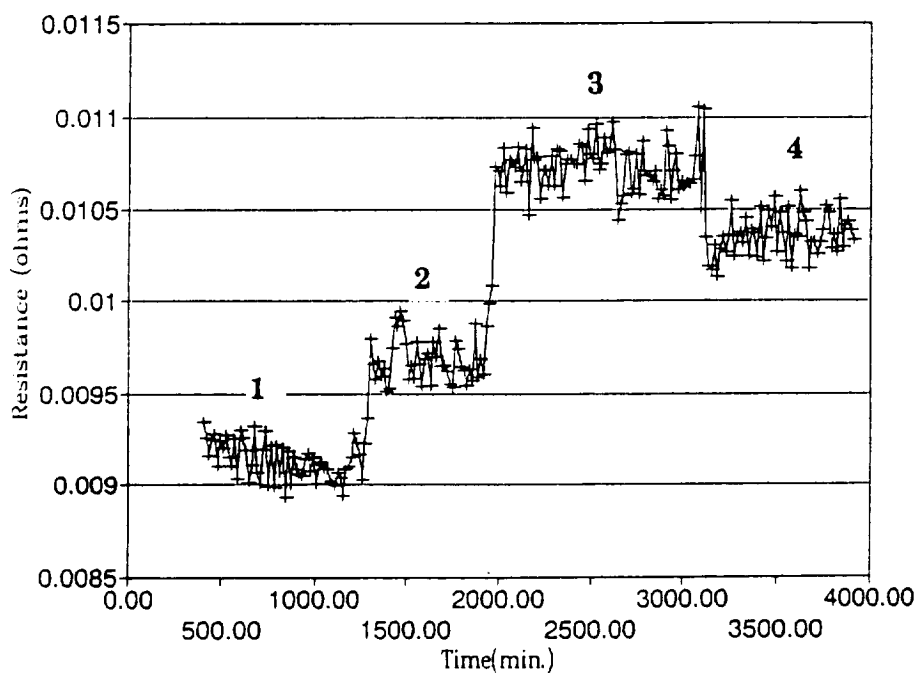
b) A close up view of the specific areas of interest.

Figure 72 In-situ resistivity development showing the resistivity data taken using the 0.25 mm silver wires and one time calcined powder.
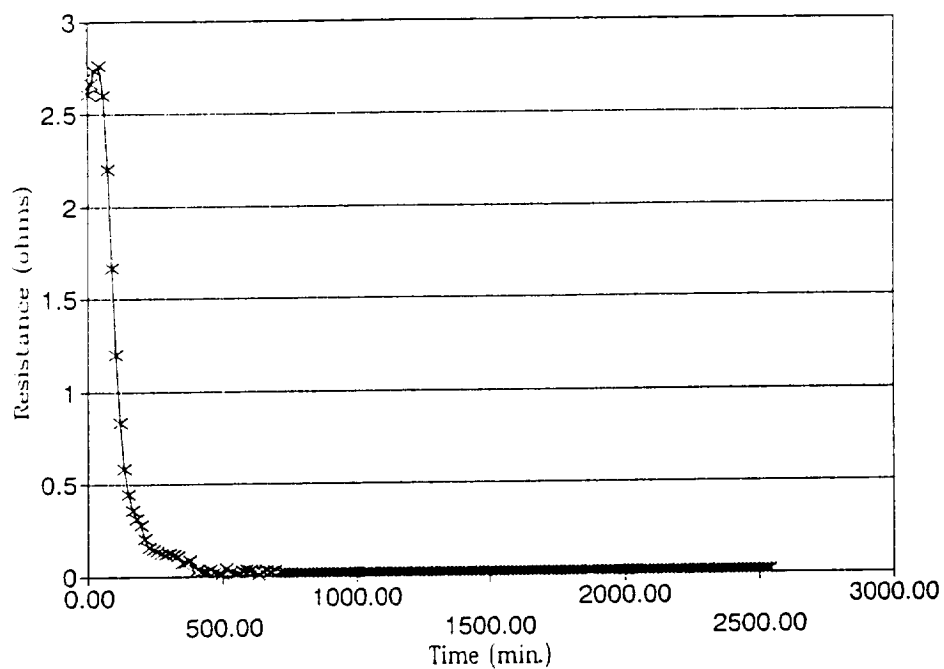
a) The entire resistivity run, from the initial dwell at 845 °C until a silver wire broke after forty-two hours.
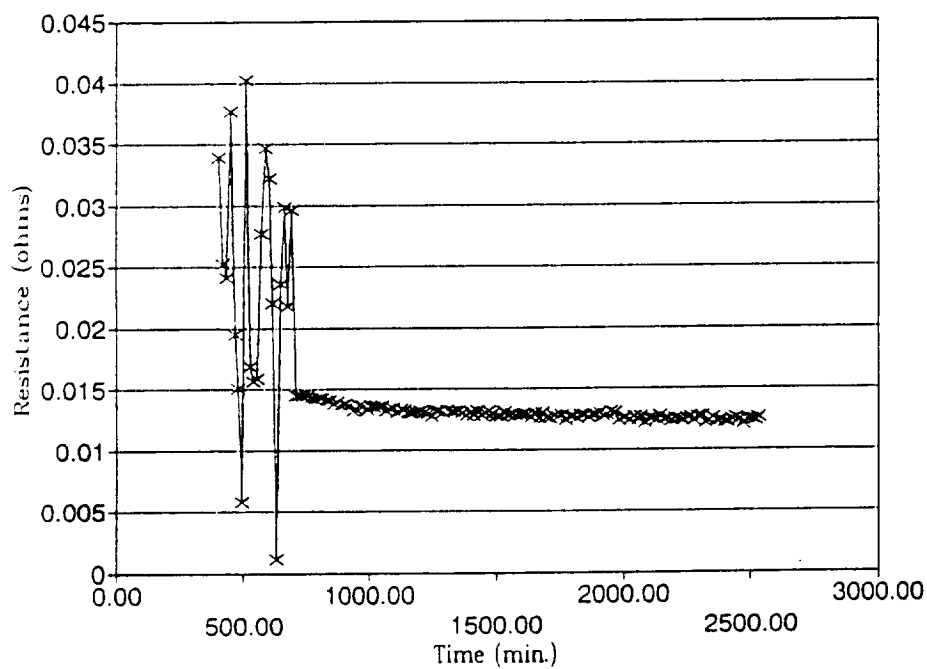
b) A close up view of the specific areas of interest.

Figure 73 In-situ resistivity development showing the resistivity data taken using the 0.25 mm silver wires and one time calcined powder.
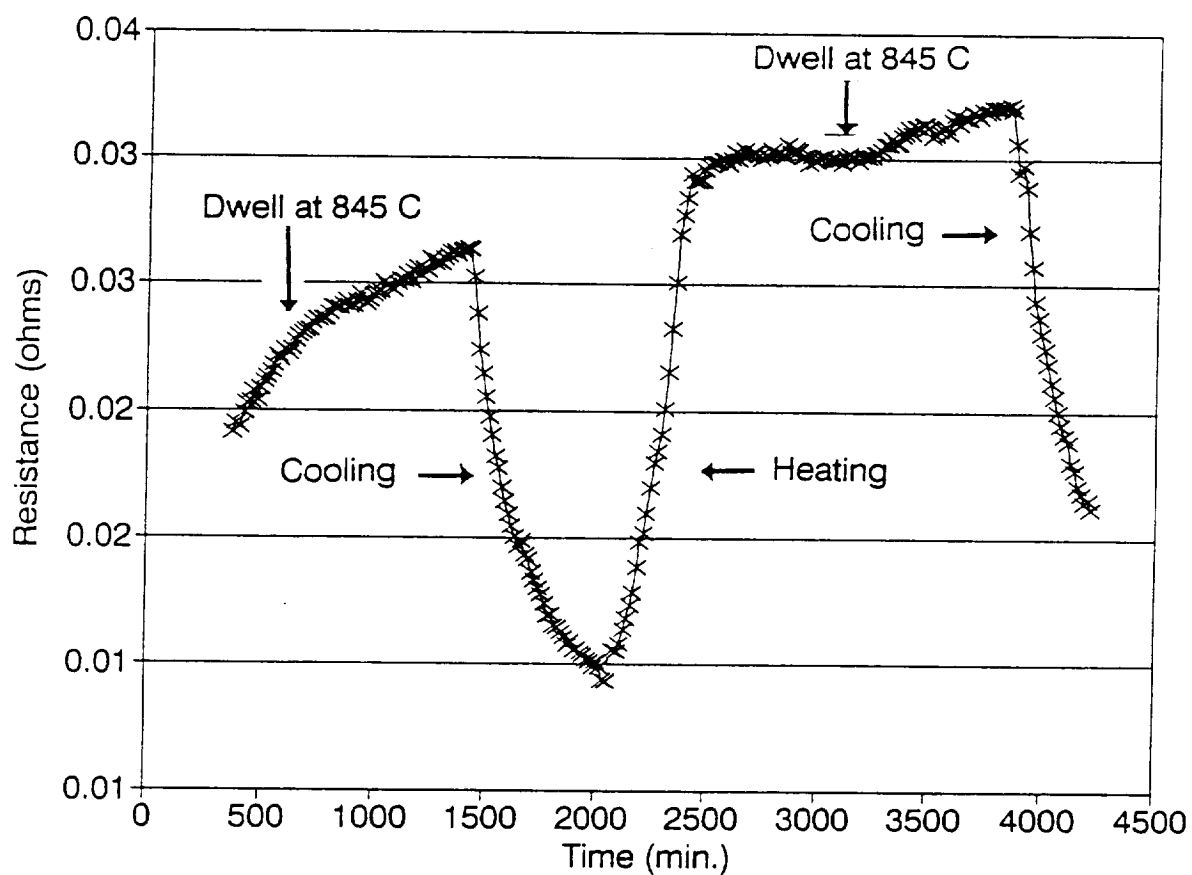
Figure 74 In-situ resistivity development showing the resistivity data taken using 1 mm silver wires and two times calcined powder. The run had two cycles, where each cycle lasted twenty-four hours.
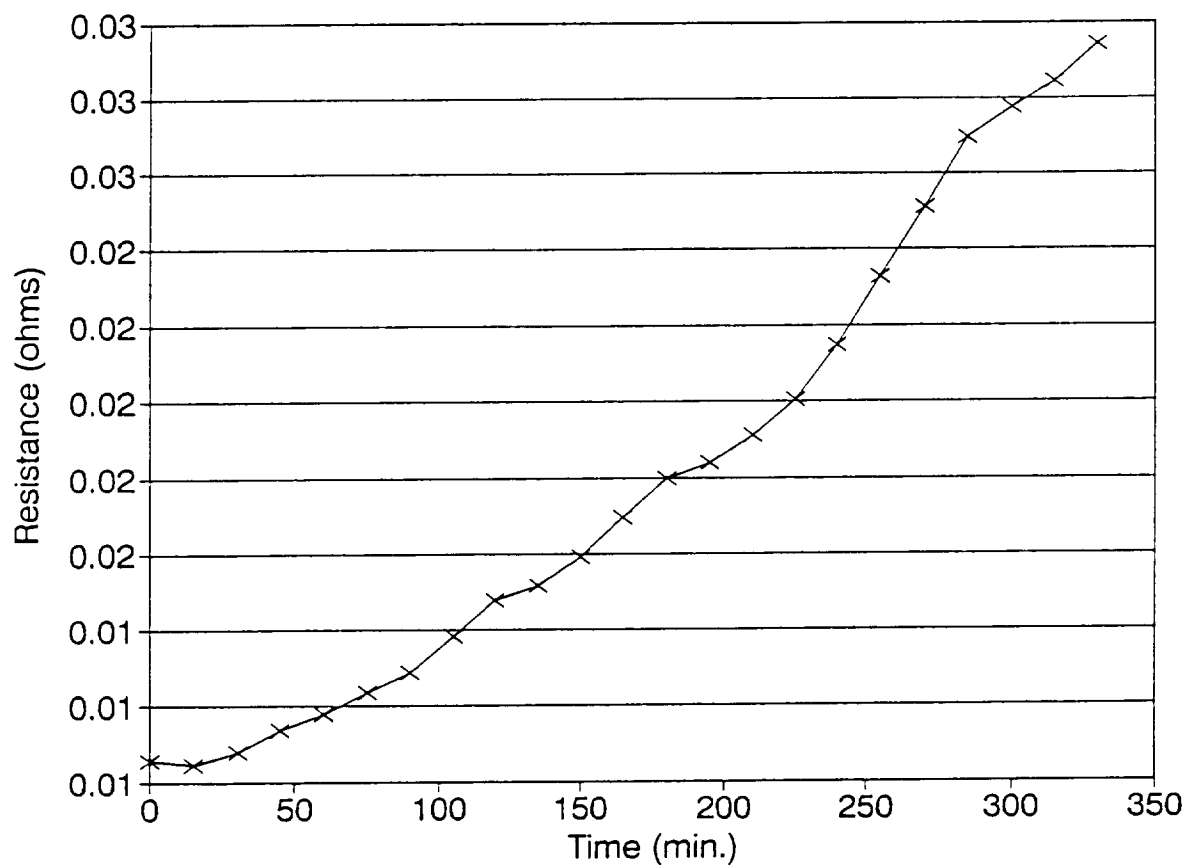
Figure 75 In-situ resistivity development showing the resistivity data taken on the heat up curve between the two cycles. 1 mm silver wires and two times calcined powder were used for this run.
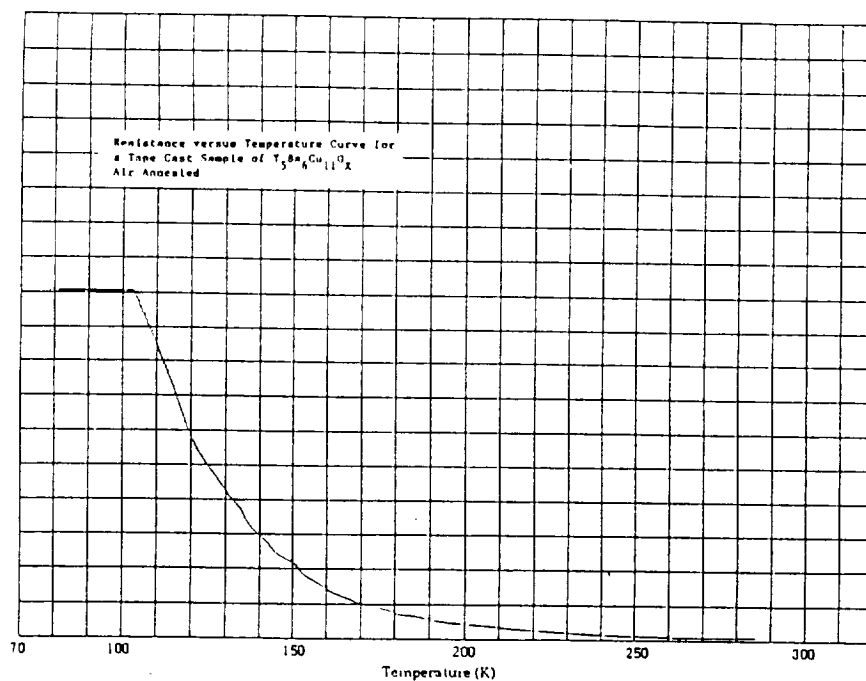
a) YBCO annealed in air.
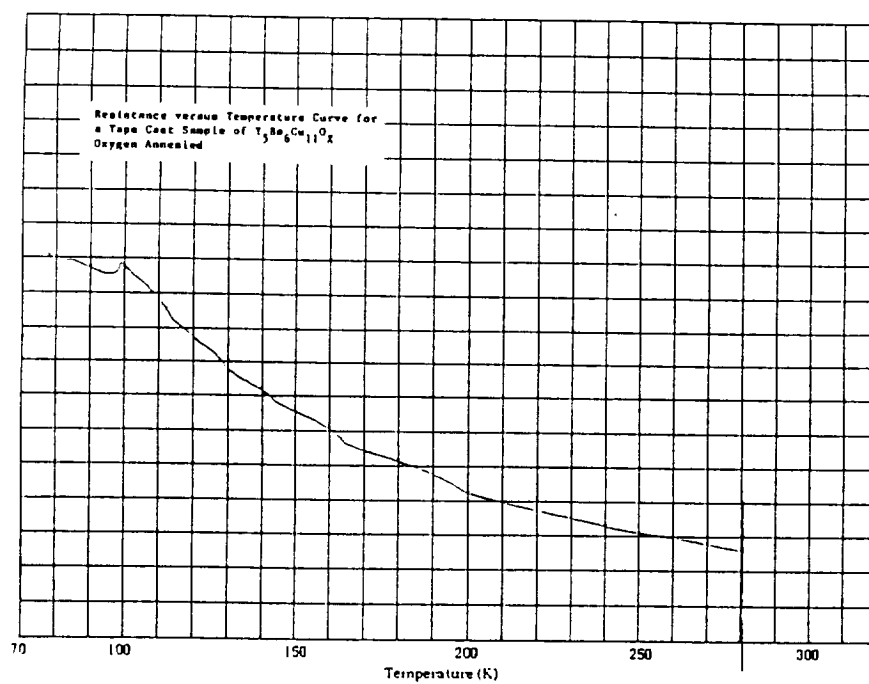
b) YBCO annealed in oxygen.

Figure 76 Resistance versus temperature curves of tapecast samples of $Y_5Ba_6Cu_{11}O_x$ annealed for twenty-four hours in air or oxygen.

DEVELOPMENT OF HIGH Tc (>110K) Bi, Tl and Y-BASED MATERIALS AS SUPERCONDUCTING CIRCUIT ELEMENTS

Final Report

Part II

Development and Characterization of Tl-Based Materials

to

National Aeronautics and Space Administration
Langley Research Center
Hampton, VA 23665-5225

Principal Investigator:

Gene Haertling

Supporting Investigator:

Phillip Gilmour

Contract No. NAG-1-1108   July, 1994

Abstract

The primary research of these investigations centered on developing thallium superconducting grounding straps for the NASA SAFIRE project. To this end conventional mixed oxide and acetate solution techniques were used to fabricate superconducting powders. Powders were tape-cast and cut into appropriate lengths then encapsulated in silver foil to contain thallium vapors. After binder burnout and firing, the tapes were encapsulated in an epoxy resin and electroded for electrical characterization. The highest transition temperature of these tapes was 112K, comparable to the thallium diffusion technique examined in many investigations.

A number of ancillary studies were performed to examine the potential of alternative processing modes for superconducting tape fabrication. Dielectrophoresis of superconducting powder was found to be a promising area of study to produce c-axis orientation of superconducting powder on a metal wire substrate. In this technique a suspension of fine grain powder in a nonconducting medium is placed in a nonuniform electric field. The high permittivity of the particles align with the field and migrate and deposit onto a metal wire.

Other studies were conducted to examine silane additions for aqueous milling of superconductors and lithium and manganese additions to thallium superconducting compounds. These studies appeared to have less potential for improving processing of thallium-based superconductors.

Introduction

Thallium-based superconductors are layered materials often described as intergrowths of perovskite and rocksalt layers. Three of the most commonly occurring thallium superconductors are shown in Figure 1. With increasing layering there is a concomitant increase in transition temperature. The $Tl_2Ba_2Ca_2Cu_3O_{10}$ structure [hereon abbreviated as the Tl-2223 phase] exhibits the highest reproducible superconducting transition temperatures to date, 120-125K.

There are several potential advantages of Tl-2223 compared to other high-temperature superconductors. Unlike $YBa_2Cu_3O_{7-\delta}$ [the 123 structure] there is no phase transition down to 1K;[2] therefore no microcracking can occur for this reason, although differential thermal expansion of different lattice directions could present a problem.[3] Complete phase formation of Tl-2223 is more easily attained than the bismuth analogue, $Bi_2Sr_2Ca_2Cu_3O_{10}$. Also, the intrinsic critical current density, greater than $1x10^8$ A/cm^2, is believed to be at least an order of magnitude higher than the 123 system.[4]

However, there are disadvantages of thallium superconductors; probably foremost among these are thallium toxicity and volatility. The highly volatile nature of thallium arises from the transition

$$Tl_2O_3 \longrightarrow Tl_2O + O_2 \quad 875°C.$$
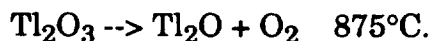
The reduction of Tl_2O_3 close to the sintering temperature creates a low melting point compound. Thallous oxide also exhibits a low boiling point which creates significant thallium loss. To ameliorate this problem, oxygen sintering is often used to shift the above reaction to the left. Thallium loss is further reduced by complete encapsulation or wrapping the material in an inert metal foil. Yet, these steps usually do not yield consistent results. Loss of thallium presents a major problem for reliable fabrication of thallium superconductors.

If one were to peruse the literature on thallium superconductor processing, a confusing and contradictory picture of how to attain the highest transition temperature and optimize the critical current density would arise. As an example, some studies use stoichiometric mixtures of thallium barium, calcium, and copper oxides to maximize the superconducting transition temperature.[5,6] Another study suggests reduced amounts of calcium will stabilize the highest transition temperatures.[8] Part of the confusing state of thallium superconductor processing stems from the similar free energies of layered structures; however, a large contribution to thallium superconductor

fabrication variability arises from the volatility of thallium and attaining correct oxygen stoichiometry and distribution.[9,10,11] The initial phase of the research centers on the development of high transition temperature, high critical current density thallium superconductor tapes for the SAFIRE project. This will possibly yield improved methods of processing of these materials. This part of the investigation may yield information not only of value for production of high quality thallium superconductor tapes, but may be applicable to improvement of alternative processing modes of thallium bismuth, and other high-temperature superconductors.

$Tl_2Ba_2Ca_2Cu_3O_{10}$ Powder Synthesis Via Oxide Precursors

Two routes were used to prepare precursor materials for sintering ceramic $Tl_2Ba_2Ca_2Cu_3O_{10}$. The first method consists of mixing the oxide compounds BaO_2, CaO, and CuO at 925°C for 24 hours to form the low melting point compound $Ba_2Ca_2Cu_3O_7$. This method was developed by Sheng and Hermann[12] to aid densification by liquid phase sintering.

The second preparation was performed by batching CaO and CuO and firing for 925°C for 24 hours. Barium peroxide was added with Tl_2O_3 prior to sintering. Barium peroxide was chosen instead of other barium compounds since it was believed that the oxygen produced in the conversion of BaO_2 to BaO at approximately 700°C could reduce the amount of thallium lost at elevated temperatures.

The general ceramic processing scheme is shown in Figure 2 while particulars of ceramic formation are as follows. Stoichiometric amounts of the initial oxides* were thoroughly mixed in a porcelain mortar and pestle. If the precursors were calcined, the powders were placed on an alumina setter and heated with the furnace to 925°C. After calcining for 8 hours, the material was allowed to cool with the furnace. The calcined material was ground and passed through a 100 mesh sieve. This process was performed three times for a total calcination time of 24 hours.

After the calcination step, Tl_2O_3 and the remaining oxide constituents were added to the calcined material in stoichiometric proportions. (To reduce

---

*The raw powders used were: Tl_2O_3/Malinckrodt, Lot 3800KCAM; BaO_2/ Eastman Kodak Co. Lot A16A; CaO/Fisher Scientific, Lot 864342; CuO/Fisher Scientific, Lot 901219; and LiO_2/Johnson Matthey Electronics, Lot K26A20.

thallium loss, thallic oxide is usually added prior to sintering and not in the calcination step.) Green pellets, 13mm diameter by 3 mm thick, were formed by pressing 1.5g of material at a pressure of $2.7 \times 10^3 Kg/cm^2$ [3.9×10^4 psi].

The green pellets were wrapped in silver foil and fast-fired in flowing oxygen. Oxygen was fed into the furnace to reduce thallium volatility. After the specified soak time, pellets were taken out of the furnace and air-quenched to room temperature.

Pellets were electroded by firing with silver paste* at 600°C for 20 minutes and cooled with the furnace. Due to the low temperature (and consequently low thallium volatility), pellets were not wrapped in silver foil.

Sintering Studies of $Tl_2Ba_2Ca_2Cu_3O_{10}$

Tables 1, 2, and 3 show the results of sintering the three different batches of precursor powders. Sintering temperatures of 870°C, 880°C, 890°C, and 910°C were studied with soak times ranging between 30 and 180 minutes. As seen the table, there appears to be a gradual increase in the superconducting critical transition temperature with increasing sintering temperature and soak times for all types of preparations studied. Apparently, the superconducting ceramics produced without prior calcination (Table 1) form a superconducting phase readily compared to batches which were calcined. The trend is clearly illustrated in Table 3; sintering the batch which contained $Ba_2Ca_2Cu_3O_7$ as a precursor for 30 minutes, did not yield a superconducting material at the lower sintering temperatures studied. Whereas the higher temperature superconducting phases seemed to gradually develop for batches which were calcined, sintering with the original metal oxides did not appreciably increase the transition temperature with time or temperature.

Figure 3 shows SEM photomicrographs of as-fired surfaces of the ceramic pellets (batched with Tl_2O_3, BaO_2, CaO, and CuO as the precursors) which were sintered for three hours at 870°C and 890°C. The surface of the 870°C fired sample shows appreciable cracking. Fissures can also be seen in the 890°C sintered sample. The microcracking appears to be a problem for all pellets sintered from the separate constituent oxides. Large scale cracking

---

*The silver paste used was formulated to fire at 600°C: Dupont conductor composition #7095, Lot 77D114.

was also obvious when examined without the aid of a microscope, yet cracking was not observed for pellets which had calcined material as a sintering precursor. This created a deleterious effect when the samples were cooled to liquid nitrogen temperature. Figure 4 illustrates the resistance as a function of temperature for a pellet sintered from the original oxide powders. The discontinuites on the curve were accompanied by an audible "snap" and indicated cracking of the sample. Cracking of the ceramic occurred in most samples prepared this way; however, few samples containing $Ba_2Ca_2Cu_3O_5$ or $Ba_2Ca_2Cu_3O_7$ showed the phenomenon when cooled.

Considerable melting of the pellet surface fired at 890°C is also apparent in Figure 3. The relatively high transition temperature of the sample, 112.3K, seems to agree with the generally acknowledged observation that slight melting must occur to create the high transition temperature phase Tl-2223.

A fracture surface of both samples is shown in Figure 5. The sample fired at 890°C shows plate-like morphology similar to the Tl-2223 phase identified by Sheng and Hermann.[12,13] The ceramic fired at the lower temperature showed similar areas but were not as prevalent.

Higher temperature superconducting phases appear to be formed at increased sintering temperatures and extended soak times as seen in Figure 6. Sintering Tl_2O_3, BaO_2, and $Ca_2Cu_3O_5$ for thirty minutes at 900°C produces a mixture of superconducting phases are present: $Tl_2Ba_2CuO_6$ (T_c=85K), $Tl_2Ba_2CaCuO_8$ (T_c=110K) and $Tl_2Ba_2Ca_2Cu_3O_{10}$ (T_c=120K). However when sintered for 180 minutes, the transition temperature of the ceramic jumps to 117.8K as illustrated in Figure 7, and the material is almost entirely Tl-2223. If this batch is sintered for 180 minutes but the temperature is decreased to 880°C, complete conversion to the Tl-2223 phase does not occur as shown in Figure 6. Instead a mixture of Tl-2212 and Tl-2223 phases suggests one should sinter close to the melting point of the material to optimize the transition temperature.

It was mentioned that pellets were fired at 910°C in this study. All samples fired at this temperature, resulted in melting the sample and silver foil. Consequently, the material was exposed to the furnace atmosphere and thallium loss resulted. The samples exhibited no superconductivity down to liquid nitrogen temperature.

$Tl_2Ba_2Ca_2Cu_3O_{10}$ Powder Synthesis Via Coprecipitation

Coprecipitation routes for superconductor synthesis has achieved much attention. Coprecipitation often yields a finer, more homogeneous powder which consequently yields improved superconducting properties.

Precursor powders were synthesized through the oxalate coprecipitation technique. Figure 8 illustrates a schematic of the oxalate coprecipitation route for thallium superconductors. A precursor made from barium, calcium, and copper nitrates was coprecipitated, calcined, and then mixed with thallium oxide before the final sintering setup. Oxalic acid was added to slightly warm methanol to facilitate the dissolution process. The number of moles of oxalic acid added was 150% of the moles of the metal ions in solution. If a molar equivalent of oxalic acid and metal ions were added, segregated regions of blue and white crystals appeared in the powder after drying; whereas, excess oxalic acid created a uniform mixture.

Calcination of coprecipitated powders were subjected to the same conditions as oxide precursors. Also, sintering was performed with the same heating schedule as the oxide precursor conditions described above.

Energy dispersive x-ray analysis coupled with scanning electron photomicrographs, shown in Figure 9, show elemental distribution of a Tl-superconductor pellet is relatively uniform within the superconducting grains (indicated by "blocky" grains); however, a small amount of copper segregation occurs outside of these grains. Also, inhomogeneities also occur, to a smaller extent, for barium and calcium. Coprecipitation was examined to determine if homogeneity can be improved in the ceramic pellets.

Resistance as a function of temperature curves for coprecipitated thallium, superconductor ceramic pellets for various soak times at 893°C are displayed in Figure 10. No pellets showed any trace of superconductivity. The results seemed surprising in light of the large number of studies which have shown coprecipitated techniques improve the final superconducting properties. Energy dispersive x-ray analysis and scanning electron micrographs of the surface of coprecipitated thallium-superconductor pellets are shown in Figure 11. The reason for nonzero resistance is evident upon examination of the figure: the surface growth is almost entirely composed of thallium. (A small region of copper is shown in the hole below the growth. Barium and calcium-rich regions were also evident underneath Tl-needle growths in regions

not pictured.) Apparently, encapsulation of pellets made via the coprecipitation route allows thallium to easily escape from the sample. A possible reason for the ease of thallium escaping is because coprecipitation often yields more homogeneous and finer grains. This may create a more reactive powder which would require a lower sintering temperature to prevent thallium from leaving.

Ceramic Tape Formation

Ceramic superconducting tapes were formed by employing the same processing steps used to make Tl-superconductors as the oxide route. After forming the superconducting phase, the powder was passed through 400 mesh, mixed with a 30 weight percent binder concentration. The slurry was placed in a slight vacuum for ten minutes and allowed to sit and defoam for 20 minutes. After defoaming the slurry, a 50 mil tape was cast with a single edge doctor-blade and allowed to dry. Tapes were cut and placed on a zirconia setter plate with the ends pinned down. Binder burnout was performed in an oxygen atmosphere with a final soak of 550°C for 90 minutes.

To contain thallium vapors during sintering, tapes were carefully wrapped in silver foil and sintered. Particulars of sintering schedules as well as binder burnout are discussed in the results section.

High-Temperature Sintering of Superconductor Tapes

There is a paucity of fabrication techniques used to create Tl-2223 or Tl-2212 tapes. Previous investigations in the literature attempt to develop thallium superconductor tapes by placing a $Ba_2Ca_2Cu_3O_7$ precursor tape and Tl_2O_3 powder (or a mixture of Tl/Ba/Ca/Cu oxides) in a hermetically sealed container. Upon heating above 720°C, thallium oxide vaporizes and diffuses into the precursor while the sealed container prevents thallium from seeping into the outside environment. Sheng and Hermann developed this method to reduce thallium volatility and toxicity in a laboratory or industrial environment. Typical transition temperatures of tapes range from 100-115K. Sheng and Hermann noted there is a large variability of the transition temperature. This could be attributed to the resulting inhomogeneity which arises from thallium diffusion into the precursor material or the sensitivity of thallium superconducting compounds to processing conditions.

A different tape fabrication approach was undertaken in this research. Instead of thallium diffusing into the precursor; it was believed a solid state reaction of thallium with other precursors during sintering may lead to greater tape homogeneity and possibly improved properties and reproducibility.

Initially Tl_2O_3, $Ba_2Ca_2Cu_3O_7$, and binder were mixed and tape cast according to the above procedure. However, this technique was abandoned since it produced exceedingly fragile tapes which were not superconducting. The SEM photomicrograph in Figure 12 depicts a "feathered" and open microstructure. When thallium is fired with barium, calcium, and copper oxides prior to mixing with binder, "feathering" did not occur and stronger tapes and better electrical properties were obtained. Apparently, thallium must be incorporated into a structure with other oxides to reduce thallium volatility. Afterwards, thallium was fired with the other oxides prior to tapecasting.

Binder burnoff rate had a considerable influence on tape uniformity, presumably because of thallium/binder interactions. Green tapes were burned off at 550°C. A TGA profile shown in Figure 13, shows a long, smooth burnoff starting at 150°C until 550°C, where virtually all binder has vaporized. If the binder burnout rate is too rapid, approximately 3°C per minute or greater, tapes were relatively strong but were distorted, bubbled, bowed, and nonuniform in color. Large density variations in the 12°C/min burn-out tapes are evident upon examination of the SEM photomicrographs displayed in Figure 14; whereas, the tape heated at 2°C/min is relatively uniform. Presumably the density variation of the rapidly burned-out tapes is due to a highly exothermic thallium/binder reaction. Portions of the tape became red-hot during the reaction even though the furnace atmosphere was at 350°C.

It was thought that reducing the amount of binder would result in less thallium loss and consequently improved tape quality. However, lowering binder concentration from 35 to 28 weight percent (the lowest binder concentration which allows the powder to be cast) produced no significant improvement of tape quality.

Tapes maintained their strength when the burnoff rate was reduced from 12°C/min to 3°C/min. However, tapes burned off at 3°C/min were still slightly distorted, bubbled, and showed color nonuniformity. Reducing the burnoff rate to 2°C/min yielded tapes which were completely free from distortion and were uniformly black, yet these tapes were more fragile than tapes burned off at 3°C/min. Apparently, higher burnoff rates do not allow

sufficient time for the organics to leave the system. Figure 15 shows a resistance versus temperature curve for a tape with a binder burnoff rate of 5°C/min and one of 3°C/min. The tape with a slower burnoff rate exhibited a transition temperature of 100K while the tape with a rapid burnoff did not superconduct.

Tapes which were fired at 840°C before sintering had a relatively coarse grain size before sintering (powder passed through 60 mesh before adding binder) did not exhibit zero resistance down to liquid nitrogen temperature (approximately 77K), as seen in Figure 16. In fact, sintering for only 30 minutes produced semiconducting behavior throughout the temperature range studied. As evident in Figure 17, tapes which had finer grain size before sintering (powder passed through 400 mesh before adding binder) displayed significantly better properties: transition temperatures rose from nonsuperconducting at liquid nitrogen temperatures to 97.3K for 120 minute soak time. Microstructure of tapes fired at 890°C for 30 minutes is shown in Figure 18. The tape of the powder which was passed through 400 mesh shows a much finer, more uniform microstructure that the tape which had powder passed through 60 mesh.

Presintering at 890°C showed a similar dependence on grain size. Figures 19 and 20 show that tapes with smaller initial grain size yielded higher transition temperatures. The smallest grain size tape with the longest soak time resulted in a transition temperature of 106.5K. It was found these tapes were composed of long rectangular grains in the microstructure, indicating Tl-2212 phase (for comparison a more acicular morphology is indicative the higher transition temperature Tl-2223 phase).

Low Sintering Temperature of Superconducting Tapes

Many studies have found it is desirable to add small amount of silver or silver oxide to the $YBa_2Cu_3O_{7-\delta}$ and Bi-Sr-Ca-Cu-O superconducting systems to drastically reduce the sintering temperature, enhance resistance to chemical degradation, and increase critical current densities.[14-20] Also, since silver can easily transport oxygen (allowing easier oxygen diffusion from the furnace atmosphere into the tape while containing thallium vapors), tapes were wrapped in thin silver foil, rather than expensive and commonly used gold foil to prevent thallium loss to the atmosphere. However, silver reacts with thallium superconductors close to the "normal" sintering temperature range of

870°-920°C and drastically reduces the superconducting transition temperature. Therefore, it was not surprising when thallium tapes wrapped in silver foil envelopes adhered to the foil. Due to this interaction, it was found that areas of the tapes were nonsuperconducting.

In order to circumvent the difficulties associated with silver-thallium reactivity, a low temperature, long soak sintering schedule was examined. While the heating schedule is uncommon, a previous study has found partial melting of the ceramic upon sintering is not needed to form appreciable amounts of the high temperature Tl-2223 phase if sintered at 740-800°C for extended times. It was believed sintering at low temperatures could enhance reproducibility (since partial melting and substantial thallium loss would not occur) while allowing the less expensive silver wrap to be used.

Figure 21 shows transition temperature curves for thallium tapes fired at 745°C for times between 12 to 48 hours. It is evident that increasing soak time increases transition temperatures. Figures 22 and 23 exhibit a similar trend for sintering temperatures of 760°C and 775°C. Also, increasing the sintering temperature increases the superconducting transition temperature. However, at 800°C, the curves of Figure 24 show that the transition temperatures decrease with increasing soak times. The relationship of longer soak time trends and an optimum sintering temperature is in accordance with the previously cited study of low temperature sintering of thallium superconductors, except the optimized temperature in this study was found to be close to 775°C instead of 760°C. The highest transition temperature found for tapes was 111K. This is comparable to transition temperatures of Tl-diffused tapes and films found in the literature.

Figure 25 shows resistance versus temperature curves for low temperature sintered tapes with binder burnoff rates of 2°C/min and 3°C/min. The tape with a slower burnoff rate exhibited a significantly lower transition temperature of 100K than the rapid binder burnoff tape, 110K. Repeated processing runs showed the slowly burned-off tapes produced consistently lower transition temperatures.

Slowly burned-off tapes were extremely fragile compared to quickly heated tapes. Density measurements of slowly ramped tapes had a low density of 3.42 g/cm^3 (determined by Archimedes method); while quickly burned-off tapes had densities of 4.33 g/cm^3. Density of tapes heated at 3°C/min probably became higher due to the red-hot heating by the exothermic

reaction during binder burnoff. Partial sample melting during the exothermic reaction could have increased strength and density. Since tapes heated at 2°C/min did not seem to give rise to an exothermic reaction and the sintering temperature is much lower than the melting point; ceramic consolidation is not effective and tapes did not acquire much strength. Another, important consideration is the quickly burned-off tapes probably had less thallium than slowly heated tapes due volatilization of the thallium during the exothermic reaction. Several studies of bulk materials have found that a greater amount of Tl-2223 can be formed when batched to deficient thallium concentrations.

Thallium Superconductor Grounding Strap Link Fabrication

Thallium superconductor tapes were encapsulated in a resin binder similar to the method of Haertling and Hsi.[20] It is known that 123, Bi-, and Tl-superconductors exhibit similar thermal expansion, approximately $7x10^{-6}K^-$ as determined by x-ray diffraction. It was anticipated that since 123 and Tl-suerconductors exhibit similar thermal expansion, fabrication of Tl-superconductor grounding straps could be accomplished by the same method of encapsulation. In addition, the low thermal expansion of the tapes relative to thermal expansion of the resin, approximately $50x10^{-6}K^-$, would create a compressive stress on the tapes resulting in enhanced structural integrity and mechanical shock resistance.

Since the tapes were fragile and easily broken, a great deal of care was taken when removing the tapes from the silver encapsulation and soldering the contacts to connecting pins. However once encapsulated, the superconducting straps seemed to show greatly improved structural integrity. An encapsulated grounding link with a transition temperature of 100K is pictured in Figure 26. This link was sintered at 775°C for 48 hours. To date, finished grounding links with lengths up to 3.5 inches have been fabricated.

Figure 27 shows two superconducting transition curves for thallium grounding straps. As expected, the transition temperatures, about 95K, were slightly lower than "bare" tapes. This was due to an artifact of the sample holder. Due to the long tape length, a large temperature gradient exists in the grounding link when the sample was cooled above the surface of liquid nitrogen. Without encapsulation, smaller length tapes yielded transition temperatures between 100 and 112K.

Ancillary Studies

Additions of Li_2O to $Tl_2Ba_2Ca_2Cu_3O_{10}$

As previously mentioned, optimization of the superconducting properties is accomplished by complete encapsulation or wrapping in an inert metal foil and sintering in an oxygen atmosphere. Because of this added processing constraint, lithium oxide additions to the superconductor were investigated. Lithium has been used in ceramic processing to induce liquid phase sintering, lower sintering temperatures, and increase the fired density of the ceramic.[23-29] The mechanism by which lithium reduces sintering temperature is generally ascribed to creating oxygen vacancies which increase anion diffusion upon sintering.[15] Since the correct oxygen distribution is critical to create a high temperature superconductor, it was thought small concentrations of lithium will reduce sintering temperatures, thereby reducing thallium volatility at sintering temperatures, while possibly improving the electrical properties of the superconductor.

A literature review of alkali metal and lithium additions to superconductors shows a series of papers by Kawai, et. al. [16,17,18] in which lithium added $Bi_2Sr_2CaCu_2O_8$ acts as a sintering aid. It was found that up to 40% of the copper could be replaced by lithium to dramatically reduce the sintering temperature to 710°C while improving phase purity and increasing the transition temperature from 80K to 91K. The increased transition temperature is particularly remarkable since gross substitutions of lithium for copper yielded a transition temperature comparable to the highest values reported for this compound.

In our investigation, 1.0, 3.3, and 6.7 mole percent substitutions of lithium for copper were added by calcining BaO_2, CaO, CuO, and LiO_2 for 24 hours at 920°C with three intermediate grindings. Thallic oxide was added to the calcined powder and mixed in a mortar and pestle. Formation of the green pellets was carried out in the same manner as described previously. The pellets were wrapped in silver foil and sintered in flowing oxygen at 900°C for 30, 60, and 90 minutes.

As evident in Figure 28, increasing amounts of lithium increases the critical transition temperature. Sintering for only one-half hour resulted in a transition temperature of 108.8K for the highest lithium concentration. A transition of 115.7K, Figure 29, occurs when sintering at the lowest lithium

concentration for one hour. Higher concentrations of lithium resulted in a melted, nonsuperconducting sample for this soak time. Also, soak times of one and one-half hour resulted in melted, nonsuperconducting samples for all lithium concentrations.

This study suggests superconducting properties can be improved with lithium additions. Furthermore, sample melting containing higher lithium concentrations and longer sintering times suggest lithium produces a strong fluxing action as expected. Since the previous studies by Kawai et. al. indicate large substitutions of lithium for copper steadily improve the superconducting properties and reduce sintering temperature (these are much greater lithium concentrations than the amounts used in this study), it is possible improved superconductors and more reliable processing (due to lower thallium volatility at lower temperature) can be developed.

Additions of MnO$_2$ to Tl$_2$Ba$_2$Ca$_2$Cu$_3$O$_{10}$

In an attempt to further improve upon the processing procedure and electrical properties of thallium superconductors manganese substitutions for copper were investigated. It was hoped that manganese would increase oxygen diffusivity while sintering, yielding improved superconductor properties.

It is well-known in the capacitor industry that small additions of manganese to perovskite-based capacitor compositions can enhance densification and dramatically increase resistivity.[30-32] A complete understanding of the mechanism by which manganese accomplishes this effect is not yet known. Since manganese ions can easily undergo redox reactions, a partial explanation may be due to enhanced anion diffusivity stemming from the ease in which manganese can change its oxidation state to accomodate oxygen/oxygen vacancy diffusion in the lattice while sintering.

Optimizing anion distribution in the perovskite sublattice is critical in attaining good electrical properties for high temperature superconductors; this similarity suggests manganese substitutions for copper could improve superconducting properties. Previous papers found manganese substitutions for copper do not degraded or only slightly degraded the transition temperature. However, manganese/copper substitutions in these studies were an order-of-magnitude higher than typical manganese/transition metal substitutions used in the capacitor industry.

Superconducting ceramic pellets containing manganese substitutions for copper were processed by the same procedure as lithium substituted superconductors. Substitutions of manganese, in the form of MnO_2, were added in concentration of 0, 0.47, 0.93, and 1.87 mole percent for copper in the Tl-2223 formulation. Figures 30 and 31 show the dependence of the superconducting transition temperature on manganese concentration and soak time. In all cases, increasing the manganese concentration decreased the transition temperature. Hence, it appears manganese produces a deleterious effect on the transition temperature under the conditions investigated.

Superconductor Films Deposited Via Dielectrophoresis

A major impetus in research of high-temperature superconductors is to develop superconducting films and wires for applications ranging from microwave resonators, magnetic technology (for motors, solenoids, and magnetic shields), and electrical conduction lines. Although a large number of investigations have examined physical properties and fabrication methods of superconducting films and wires, there are only a few methods with the potential for large scale production. A number of methods such as laser ablation and melt texturing have produced films with excellent homogeneity, transition temperatures, and critical current densities for a variety of superconducting compounds. However because these techniques are costly and somewhat difficult to apply to long-length wire fabrication, they will probably not be used in most superconductor manufacturing methods.

An extremely simple and low cost coating method which has been studied in many disciplines is electrophoresis. In this method, particles which become charged in solution deposit on the anode or cathode depending on the surface charge. Many studies have applied electrophoresis to superconducting coatings, yet strongly oriented films have not been produced by simple electrophoretic deposition.[33-35] Only if the material is doped with rare-earth ions and subjected to high magnetic fields, on the order of 8 tesla, will electrophoresis produce preferred orientation in films.

One technique which has not been investigated to date is dielectrophoretic deposition of superconducting films. In this method, a slurry of superconducting powder and a low conductivity liquid is subjected to a high, nonuniform electric field.[36] Under these conditions the superconducting grains in the slurry can develop a dipole and migrate to the region with the greatest

field intensity. If a diverging field was created around a wire electrode, e.g. a wire electrode in the center of cylindrical, counter-electrode, the suspension of the superconducting particles will migrate to and deposit on the wire electrode. The method of deposition is similar to electrophoretic deposition in that suspended particles migrate to an electrode under the presence of an electric field. Yet, more restrictive conditions of high, nonuniform electric fields allow the weak dielectric mechanism to arise.

In most systems, dielectrophoresis is a mild effect compared to electrophoresis. Yet, the utility of the dielectrophoretic technique arises from anisotropy inherent in certain particles and the consequent orientation of the particles in a strong electric field. Quite often a dielectrophoretically deposited coating exhibits a strong preferred orientation. Since the axis with the highest permittivity is along the c-axis in a superconductor crystal, it is possible that a c-axis orientation perpendicular to the axis of the wire could be created in dielectrophoretically deposited superconductor coatings. If this method were developed, it could have the potential to be a straightforward, low- cost, fabrication method of fabricating superconducting wires and conduction lines.

Before the research is presented it worthwhile to compare and contrast dielectrophoresis with its well-known counterpart, electrophoresis. As shown in Table 4 , electrophoresis can occur in a uniform or nonuniform field and could be used to create coatings on wires, plates, or substrates of virtually any configuration. However, due to the necessary condition of a diverging electric field, dielectrophoretic coatings only occur on electrode configurations which give rise to a nonuniform electric field.

In order to create chemically uniform powders, Bi-Pb-Ca-Sr-Cu-O superconducting powders were synthesized by the acetate process detailed in the bismuth-based superconductor investigation (first part) of this final report. Since aggregated or agglomerated particles usually do not create dielectrophoretic depositions due to the random orientation of the attached particles, it was necessary to disperse single crystals in a liquid. To obtain single crystals, the powder was ground in a mortar and pestle and passed through 400 mesh. Approximately 0.6 grams of the 123 superconductor powder were added to n-butanol and sonicated for 5 minutes. The suspension was left undisturbed for 10 hours. After allowing the more massive particles to settle, the suspension was decanted and dried. Scanning electron microscopy, Figure 32, found the particles which settled to the bottom were large

aggregates while those which remained in suspension had a particle size less than one micron. These fine dried particles were used to study dielectrophoretic deposition.

A number of solutions were examined under an applied electric field to assess the potential as the suspending fluid. Most of the liquids examined, i.e. toluene, trichloroethylene, acetone, alpha-terpineol, distilled/deionized water, n-butanol, and other alcohols, were too conductive to be utilized for dielectrophoresis without further purification. Also, when electrophoretic or dielectrophoretic deposition was performed with various oils, particles would not adhere to the substrate. The best candidate for dielectrophoresis applications was 1,1,2-trichlorotrifluoroethane. The liquid was highly resistive, hydrophobic, and created good particle/substrate adherence.

As previously explained, the electrode setup must produce a nonuniform field for dielectrophoretic depositions to occur. The outer electrode was a hollow copper cylinder 1.5 cm in diameter and had a length of 3 cm. The central silver wire electrode had a uniform diameter of 230 microns. To suspend the powder in the 30 ml of the cholorofluorocarbon liquid, a small drop of Triton X-100 was added to approximately 0.15 grams of fine powder followed by sonication for five minutes.

A voltage of 5,000 V was applied to the suspension producing a current of less than 1 mA. Deposition was performed for 5 minutes. After deposition, the particles remained on the wire. The wire was removed for examination with a scanning electron microscope Figure 33. Upon examination of the photomicrograph, the particle layer was approximately eight microns thick. After sintering at 845°C for 12 hours, a significant amount of particle orientation on the wire as exhibited in the SEM photomicrograph in Figure 34.

After removing the wire, another silver wire of the same diameter was inserted. Again the same voltage was applied and a deposition occurred. Then the wire was cleaned, replaced, and subjected to the same conditions but with the electrodes of opposite polarity. Again deposition occurred when opposite polarity was applied. Finally, both the cylinder counter electrode and the inner wire electrode were replaced with two 0.25 cm by 4 cm parallel sheets of silver foil. Voltages from 500 to 6,000 V were applied. With parallel plate electrodes, no deposition occurred at any voltage.

The above observations strongly suggest that the films were dielectrophoretically deposited. With the cylinder and wire configuration,

deposition occurred on the wire regardless of polarity. However, no deposition occurred in the parallel plate electrode configuration. This is to be expected since the relatively uniform field created by the parallel plates will not give rise to dielectrophoretic deposition.

Aqueous Processing of YBa2Cu3O7-δ

It is well-known that $YBa_2Cu_3O_{7-\delta}$ readily reacts with water to produce a nonsuperconducting article in a short time. However, it would be desirable to develop a method of milling 123 powders in water prior to the ceramic forming process. This would eliminate more costly, organic solvents used for milling while reducing safety hazards.

The 123 phase readily undergoes decomposition via the reaction mechanism:

$$2YBa_2Cu_3O_{7-\delta} + 3H_2O \rightarrow Y_2BaCuO_5 + 3Ba(OH)_2 + 5CuO + (0.5-x)O_2.$$
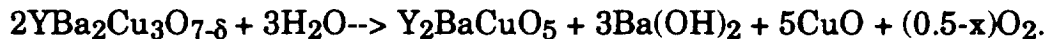
Barium hydroxide is somewhat soluble in water and increases the alkalinity of water. During this reaction, the formal valence of Cu changes from +2.3 to +2. Since high-temperature superconductors are extremely sensitive to the valence of copper, a small amount of barium leached into solution can destroy the superconductivity. If dissolved CO_2 is present in the water in the form of carbonic acid, $Ba(OH)_2$ further reacts to form $BaCO_3$ by the following reaction:

$$Ba(OH)_2 + CO_2 \rightarrow BaCO_3 + H_2O.$$
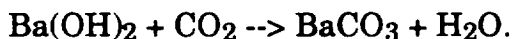
The reaction products are indicated by white crystals on the ceramic or powder surface.

To reduce these reactions in water, silane additions to water were examined. Silanes are compounds with the general formula Si_nH_{2n+2} and are analogous to alkanes. Often, these are coupled with organic functional groups. These compounds are known to readily react with many oxide surfaces to create hydrophobic layers. When placed in an aqueous system, silanes effectively compete with water molecules for surface bonding states and form bridging siloxane bonds, $-O-SiR_2$, to the oxygen on the particle surface. Because of the potential of silanes reducing water/superconductor contact while not destroying superconductivity, a preliminary examination was undertaken to examine the effectiveness of silanes for aqueous milling 123 powders. Superconducting powders were fabricated by a process outlined previously. However instead of a final milling in trichloroethylene prior to

forming, ceramic powders were milled in either 1,1,2-trichlorotrifluoroethane or water or water mixed with silanes.

Since the formation of barium hydroxide in an aqueous system increases alkalinity, the pH of the water was measured during ball-milling. Milling was performed in a nalgene bottle with zirconia media. Several batches of 75 gram 123 powder and 150 mL of water or a water/silane solution were examined for silane effects and reproducibility. Two and five weight percent (of the total solvent weight) silane concentrations were added to water in the mill. Superconducting powder was added immediately after silane additions. Also, in one 2 percent batch, silane was added to water and allowed to sit for 36 hours before the powder was added. After this time, the solution appeared slightly hazy. Then 75 grams of 123 powder were added to solution and milled.

Initial pH values of distilled water were approximately 5.5; silane additions produced no detectable effect on the initial pH. This is a typical value for water which has absorbed CO_2. Yet within a few minutes of milling, water basicity increased to 12. This is indicative of a rapid reaction of barium with water. After five minutes, pH stabilized and remained constant during the remaining milling time. Alkalinity was also seen to increase within a few minutes with silane additions, yet pH increased only to 9.0 and stabilized. Milling in two and five percent silane yielded similar and reproducible pH curves. However, when silane was allowed to age in solution before adding powder, pH values slowly climbed to 11 when milled.

After grinding, the suspension was placed in a dryer for 16 hours. A thick layer of white crystals and blue-green crystals, indicating decomposition of 123 to $Ba(OH)_2$ and Cu_2O was evident in the superconducting powder milled in water. A similar layer of crystals was noted in the solution which was allowed to sit 36 hours before grinding. Yet, milling in the water/silane solutions with powder immediately added showed only a small amount of these decomposition products.

The smaller pH change and small amount of white crystals after drying suggests silanes markedly reduce decomposition of 123 in water. Also it was evident that silane treatments produced much finer powders than milling in the organic solvent. The fine grain size could possibly be due to reduction of agglomeration by a silane layer.

The green bodies were sintered at 900°C for 5 hours and annealed at 450°C for 12 hours. After firing, pellets were cooled to liquid nitrogen

temperature and checked for the Meissner effect. Pellets made from powder milled in water or the aged silane/water mixture did not levitate a three gram Sm-Co magnet. However, grinding in organic solvent or silane/water solutions did lift the magnet off the surface. Apparently, silanes did effectively check the release of Ba^{2+} in water.

Resistance transition temperature curves were plotted for the ceramics. Superconducting transition temperatures were severely degraded for powders milled in water compared to milling in an organic (transition temperatures were only slightly above 77K compared to approximately 90K when milled in an organic). However, milling in a silane/water solution also seriously degraded the resistance transition, approximately 82K. At first, this was considered surprising since silanes appeared to limit the superconductor decomposition (suggested by lower pH values, less decomposition products evident upon drying, and the Meissner effect) yet, upon reflection, this might be expected. Silanes reduce surface reactions and protect the particle core in an aqueous system. A previous study found CO_2 reacts with 123 upon sintering to form $BaCO_3$ or the barium oxycarbonate $BaCO_{4.8}$.[9] These reaction products reside at the grain boundary without appreciable diffusion of carbon into the grain. Since silanes coat the particle surface, carbon can be expected to reside at the grain boundaries. Therefore a ceramic pellet can exhibit a strong Meissner effect while producing a poor resistive transition due to the presence of intergranular phases.

Summary

Thallium-based superconductors grounding straps have been fabricated for the NASA SAFIRE project. An outline of the optimized processing steps found in this investigation for fabricating the is described below.

•Thallium must be reacted with the $Ba_2Ca_2Cu_3O_7$ precursors before tape casting with binder. The compound $Ba_2Ca_2Cu_3O_7$ was formed when BaO_2, CaO, and CuO were mixed in stoichiometric amounts and fired at 925°C for 24 hours. Thallic oxide and $Ba_2Ca_2Cu_3O_7$ were mixed in a mortar and pestle and pelletized. The pressed pellets were encapsulated in silver foil and calcined at 880°C for one hour.

•After mixing, the superconductor composition was ground and passed through a 400 mesh sieve to produce a fine powder.

•Thirty weight percent binder mixed with the superconductor powder. The slurry was placed in a slight vacuum for ten minutes and allowed to sit and defoam for 20 minutes in a sealed container.

•A 50 mil green tape was cast by a single edge doctor-blade and allowed to dry. Tapes were cut to desired width and length.

•Binder burnout was performed in an oxygen atmosphere. The tape was heated at 2°C/min with a final soak of 550°C for 90 minutes.

•After burnout, tapes were carefully encapsulated in silver foil and fired at 775°C for a 48 hour soak.

•Sintered tapes were removed from the foil and electroded with silver electrode paste at 600°C.

•Tapes were placed on rigid plastic substrates, soldered to connecting pins, and encapsulated with epoxy resin.

The highest superconducting transition temperature of a thallium tape was found to be 100K. The low transition temperature of the tape is believed to be due to thermal gradients when cooled above the surface of liquid nitrogen. Smaller tapes which were shorter and not encapsulated (hence not subjected to large thermal gradients) yielded transition temperatures in the range of 100-112K.

Ancillary studies investigated lithium and manganese substitutions, dielectrophoretic deposition, and aqueous milling with silanes. The findings of these studies are outlined below.

•Lithium was substituted for copper in the Tl-2223 composition in the form of Li_2O. Lithium additions exhibited a fluxing action upon sintering. Also, superconducting transition temperature increased up to x=0.2 in the formula $Tl_2Ba_2Ca_2Cu_{3-x}Li_xO_{10}$. For lithium substitutions greater than 0.2 the maximum superconducting temperature decreased.

•Manganese was substituted for copper in the Tl-2223 composition in the form of MnO_2. Manganese additions decreased the superconducting temperatures for all concentrations studied.

•Dielectrophoretic depositions of BSCCO superconductors were investigated. Applying a non uniform electric field to a suspension of fine, unaggregated BSCCO particles in 1,1,2-trichlortrifluoroethane produced depositions by dielectrophoresis. Scanning electron microscopy suggested preferred particle orientation on a silver wire substrate.

•Aqueous milling of $YBa_2Cu_3O_{7-\delta}$ was studied with silane additions. Silanes appeared to protect particle surfaces from reaction with water. However while milling with silanes produced pellets with a moderately strong Meissner effect, superconducting transitions degraded. It was suggested that this may be due to carbonate formation on the grain surface due to decomposition of the silane when fired.

References

1. C. C. Torardi, M. A. Subramian, J. C. Calabrese, J. Gopalakrishnan, K. J. Morrissey, T. R. Askew, R. B. Flippen, U. Chowdry, and A. W. Sleight, "Crystal Structure of the High-Temperature Superconductor $Tl_2Ba_2Ca_2Cu_3O_{10}$," *Science* **240**, 631-634 (1988).

2. K. L. Keester, R. M. Housley, and D. B. Marshall, "Growth and Characterization of Large $YBa_2Cu_3O_{7-\delta}$ Single Crystals," *J. Cryst. Growth* **91**, 295-301 (1988).

3. J. J. Ratto, J. P. Porter, R. M. Housley, and P. E. D. Morgan, "Monitoring Sintering/Densification and Crystallization/Grain-Growth in Tl-Based High Temperature Superconductors by Electrical Conductivity Measurements, " *Japan. J. Appl. Phys.* **29**, 244-251 (1990).

4. J. R. Thompson, J. Brynestad, D. M. Kroeger, Y. C. Kim, S. T. Sekula, D. K. Christen, and E. D. Specht, "Superconductivity, Intergrain, and Intragrain Critical Current Densities of $Tl_2Ba_2Ca_2Cu_3O_{10+x}$ and $Tl_2CaBa_2Cu_2O_{8+x}$," *Phys. Rev. B* **39**, 6652-6658 (1989).

5. J. D. Smith, Q. A. Shams, M. J. Saeed, D. Marsh, F. Arammash, J. Bennett, Z. Z. Sheng, and A. M. Hermann, "Formation of Tl-Ca-Ba-Cu-O Superconducting Thick Films by Vapor Evaporation of Tl_2O_3 in Rolled $Ba_2Ca_2Cu_3O_7$," *Appl. Phys. Commun.* **9**, 129-144 (1989).

6. D. S. Ginley, E. L. Venturini, J. F. Kwak, B. J. Baughman, M. J. Carr, P. F. Hlava, J. E. Schirber, and B. Morosin, "A 120K Bulk Superconductor," *Physica C* **152**, 217-222 (1988).

7. A. W. Sleight, "Synthesis of Oxide Superconductors," *Physics Today* **44**, 24-30 (1991).

8. R. M. Iyer, G, M. Phatak, K. Gagadharan, M. D. Sastry, R. M. Kadam, P. V. P. S. S. Sastry, and J. V. Yakhmi, "Superconducting Transition Temperature of Single-Phase Tl-2223; Crucial Role of Ca-Vacancies and Tl-Content," *Physica C* **160**, 155-160 (1989).

9. B. Morosin, R. J. Baughman, D. S. Ginley, J. E. Schriber, and E. L. Venturini, "Structure Studies on Tl-Ba-Ca-Cu-O Superconductors; Effects of Cation Disorder and Oxygen Vacancies," *Physica C* **161**, 115-124 (1990).

10. M. Kikuchi, T. Kajitani, T. Suziki, S. Nakajima, K. Hiraga, N. Kobayashi, H. Iwasaki, Y. Syono, and Y. Muto, "Preparation and Chemical Composition of Superconducting Oxide $Tl_2Ba_2Ca_nCu_{n+1}Cu_3O_{10}$ with n=1, 2, and 3," *Japan. J. Appl. Phys.* **28**, L382-L1385 (1989).

11. C. Martin, A. Maignan, J. Provost, C. Michel, M. Hervieu, R. Tournier, and B. Raveau, "Thallium Cuprates: The Critical Temperature is Mainly Governed by the Oxygen Nonstoichiometry," *Physica C* **168**, 8-22 (1990).

12. Z. Z. Sheng, L. Sheng, H. M. Su, and A. M. Hermann, "Tl_2O_3 Vapor Process of Making Tl-Ba-Ca-Cu-O Superconductors," *Appl. Phys. Lett.* **53**, 2686-2688 (1988).

13. J. D. Smith, Q. A. Shams, M. J. Saeed, D. Marsh, F. Arammash, J. Bennett, Z. Z. Sheng, and A. M. Hermann, "Formation of Tl-Ca-Ba-Cu-O Superconducting Thick Films by Vapor Evaporation of Tl_2O_3 in Rolled $Ba_2Ca_2Cu_3O_7$," *Appl. Phys. Commun.* **9**, 129-144 (1989).

14. C. Laubschat and M. Domke, Interface Formation Between $MBa_2Cu_3O_{7-\delta}$ (M=Y,Sm and the Monovalent Metals Ag and Rb)," *Europhysics Lett.* **6**, 555-560 (1988).

15. A. Goyal, S. J. Burns, and P. D. Funenbusch, "Effect of Ag/AgO Additions on the Resistive Behavior of Preformed $YBa_2Cu_3O_{7-\delta}$ Compacts in the Low Temperature Sintering Regime," *Physica C* **168**, 405-416 (1990).

16. D. Pavuna, H. Berger, M. Affronte, J. Van der Maas, J. J. Cappon, M. Guillot, P. Lovejay, and J. L. Tholence, "Electronic Properties and Critical Current Densities of Superconducting $(Y_1Ba_2Cu_3O_{6.9})_{1-x}Ag_x$ Compounds," *Solid St. Commun.* **68**, 535-538 (1988).

17. M. K. Malik, V. D. Nair, A. R. Biswas, R. V. Raghvan, P. Chaddah, P. K. Mishra, G. R. Kumar, and B. A. Dasannacharya, "Texture Formation and Enhanced Critical Currents in $YBa_2Cu_3O_7$," *Applied Phys. Lett.* **52**, 1515-1527 (1988).

18. W. Eichenauer and G.. Muller, "Diffusion and Loslichkeit von Sauerstoff in Silber," *Z. Metallk.* **53**, 321-324 (1962).

19. H. Rickert and R. Steiner, "Elecktochemische Messung der Sauerstoffdiffusion in Metullen bei Hoheren Temperaturen," *Z. Physik. Chem.* **49**, 127-137 (1968).

20. J. S. Hirschorn and J. G. Berglund, "Effect of Oxygen on the Sintering Rate of Silver Compacts," *Scr. Met.* **2**, 319-322 (1968).

21. G. Haertling and D. Hsi, "Development and Evaluation of Superconducting Circuit Elements," NASA Annual Report, Contract No. NAG-1-820, October 31, 1990.

22. E. Braun, W. Schnell, H. Broicher, J. Harnischmacher, D. Wohlleben, C. Allegeier, W. Reith, J. S. Schiling, J. Bock, E. Preisler, and G. J. Vogt, "Specific Heat and Thermal Expansion of Bi and Tl High Temperature Superconductors Near T_c," *Z. Phys.* **B 84**, 333-34 (1991).

23. G. F. Chen and S. L. Fu, "Dielectric Properties of Low Firing $Pb(Mg_{1/3}Nb_{2/3})_{1-x}Ti_xO_3$-$Bi_2O$/$Li_2O$ Ceramics," *J. Mater. Science* **25** 431-433 (1990).

24. R. W. Rice, "Fabricaton of Dense MgO," NRL Report 7334, Naval Research Laboratory, Washington D. C. Nov. 16, 1971.

25. "A Pressing Way to Better Transducers," *Industrial Research* **32**, 63 (1972).

26. R. E. Newnham, "Structure-Property Relations," 66-67 (Springer Verlag, NY 1975).

27. T. Kawai, T. Horiuch, K. Mitsui, K. Ogura, S. Takagi, and S. Kawai, "Effect of Alkaline Metal Substitutions to Bi-Sr-Ca-Cu Superconductor," *Physica C* **161**, 561-566 (1989).

28. T. Horiuch, H. Kawai, K Mitsui, K. Ogura, and S. Kawai, "Li Substitution in the $Bi_2Sr_2Ca_1Cu_2O_8$ Superconductor," *Physica C* **168**, 309-314 (1990).

29. I. Matsubara, H. Taniawa, T. Ogura, J. Yamashita, and M. Kinoshita, "Flexible Superconducting Whiskers of the Li-Doped Bi-Sr-Ca-Cu Oxide," *Appl. Phys. Lett.* **56**, 2141-2143 (1990).

30. P. C. Gilmour, "The Effect of Manganese Additions on the Stoichiometry and Resistivity of a Lead-Iron-Niobate Ceramic," M.S. Thesis, The Pennsylvania State University, 1987.

31. P. Strobel, C. Paulson, and J. L. Tholence, "Superconducting Properties of Substituted $YBa_2Cu_{3(1-x)}M_{3x}O_{7-\delta}$," *Solid State. Commun.* **65**, 585-589 (1988).

32. Y. Ying-Chang, Z. Yuan-Bo, Y. Wei-Chun, Y. Ji-Lian, Z. Bui-Sheng, Z. Hui-Ming, D. Yong-Fan, J. Lan, and Y. Chun-Tang, "Substitution Effects and Neutron Diffraction Study of $YBa_2(Cu_{0.95}M_{0.05})_3O_{7-\delta}$," *Acta Phys. Sin.* **39**, 111-118 (1990).

33. R. Eggenhoffner, "Cryoelectrophoresis of Superconducting $YBa_2Cu_3O_7$ in Liquid Nitrogen," *Cryogenics* **31**, 756-759 (1991).

34. H. Nojima, M. Nagata, H. Shintaku, adn M. Koba, "Fabrication of Y-Ba-Cu-O Superconducting Films on Cu Substrates by an Electrophoretic Technique," *Japan J. Appl. Phys.* **29**, L1655-1658 (1990).

35. F. Schmidt, "Formation of Superconducting Articles by Electrodeposition, European Patent Application No. 8,930,285, Oct. 1, 1990.

36. H. A. Pohl, "Some Effects of Nonuniform Fields on Dielectrics," *J. Appl. Phys.* **29**, 1162-1188 (1958).

Table 1

Critical superconducting temperature of the nominal composition
$Tl_2Ba_2Ca_2Cu_3O_{10}$ as a function of sintering time and temperature.
Powders used for sintering: Tl_2O_3, BaO_2, CaO, CuO.

Sintering Temperature		870°C	880°C	890°C	900°C
Soak Time	30 min	97.5K	98.2K	98.3K	104.4K
	60 min	103.7K	103.1K	102.6K	102.9K
	120 min	104.4K	104.3K	104.9K	107.1K
	180 min	104.6K	103.4K	112.3K	104.3K

Table 2

Critical superconducting temperature of the nominal composition $Tl_2Ba_2Ca_2Cu_3O_{10}$ as a function of sintering time and temperature. Powders used for sintering: Tl_2O_3, BaO_2, $Ca_2Cu_3O_5$.

Sintering Temperature		870°C	880°C	890°C	900°C
Soak Time	30 min	96.8K	99.9K	99.2K	104.0K
	60 min	103.7K	106.8K	102.0K	106.2K
	120 min	102.0K	103.6K	103.5K	110.9K
	180 min	107.4K	102.9K	109.8K	117.8K

Table 3

Critical superconducting temperature of the nominal composition $Tl_2Ba_2Ca_2Cu_3O_{10}$ as a function of sintering time and temperature. Powders used for sintering: Tl_2O_3, $Ba_2Ca_2Cu_3O_7$.

Sintering Temperature		870°C	880°C	890°C	900°C
Soak Time	30 min	X	X	X	105.9K
	60 min	96.7K	96.4K	96.5K	105.2K
	120 min	96.0K	104.0K	114.8K	107.3K
	180 min	102.6K	105.2K	-------	-------

Table 4

A Comparison of Dielectrophoresis and Electrophoresis

Dielectrophoresis

Dielectrophoresis arises from the tendency of matter to become polarized and move into regions of highest field strength. Some of the characteristics of dielectrophoresis are summarized below.

1. Produces motion of the particles in which the direction if motion is independent of the direction of the field, i.e., either dc or ac voltages can be employed.

2. Should be observable most readily in relatively coarse suspensions.

3. Requires highly divergent fields. No motion should be observed in the nondivergent field between centers of parallel plates, for example.

4. Requires relatively high field strengths.

5. Would be most apparent in fluids of low viscosity.

6. Will deposit weights of the particles in direct proportion to the voltage applied in equal times of deposition.

7. Is in general a weak effect easily observable only in strong fields and with coarse particles.

Electrophoresis

Electrophoresis arises from the electrostatic attraction of charged electrodes for charged particles. The direct action of an electric field on charged particles produces a different set of phenomena when compared to dielectrophoresis.

1. Produces motion of the particles in which the direction of the motion is dependent on the direction of the field. Reversal of the field reverses the direction of travel.

2. The phenomenon is observable with particles of any molecular size.

3. Operates in either divergent or uniform fields.

4. Requires relatively low voltages.

5. Requires relatively small charges per unit volume of the particles.

Figure legend labels (right side of figure c, top to bottom): Cu, Ca, Cu, Ba, Tl, Tl, Ba, Cu, Ca, Cu, Ca, Cu, Ba, Tl, Tl, Ba, Cu, Ca, Cu

$Tl_2Ba_2CuO_6$

$Tl_2Ba_2CaCu_2O_8$

$Tl_2Ba_2Ca_2Cu_3O_{10}$

a

b

c
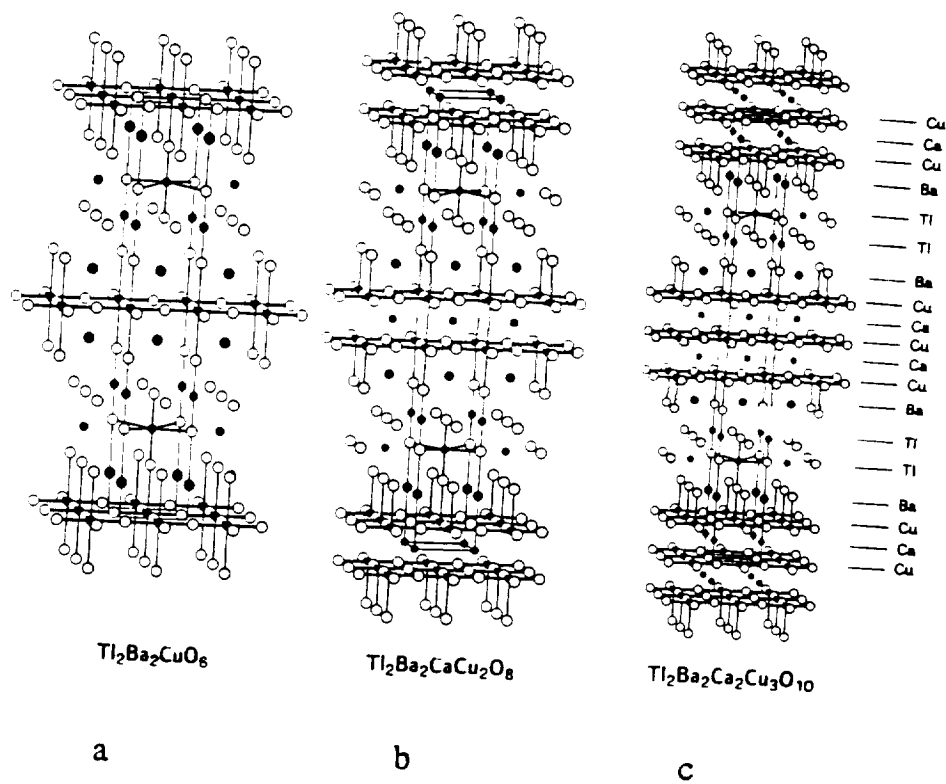
Figure 1

Commonly Appearing Superconducting Phases. Torardi, et. al.[1]

a) $Tl_2Ba_2CuO_6$ [T_c=85K]

b) $Tl_2Ba_2CaCu_2O_8$ [T_c=110K]

c) $Tl_2Ba_2Ca_2Cu_3O_{10}$ [T_c=120K]

Batch I

Mix Stoichiometric Amounts of Tl2O3, BaO2, CaO, and CuO in a Mortar and Pestle.

Batch II

Mix Stoichiometric Amounts of CaO and CuO in a Mortar and Pestle

Batch III

Mix Stoichiometric Amounts of BaO2, CaO, and CuO in a Mortar and Pestle

Calcine at 925°C for 24 hours with Two Intermediate Grindings

Mix Stoichiometric Amounts of Tl2O3 and BaO2 with Calcined Ca2Cu3O6 in a Mortar and Pestle

Mix Stoichiometric Amounts of Tl2O3 with Calcined Ba2Ca2Cu3O7

Flash-Fire Silver Wrapped Foil in Flowing Oxygen 870-910°C for 30-180 Minutes

Electrode with Silver Paste 600°C, 20 Minutes Cool with Furnace

Figure 2

Flow Sheet of Three Methods of Forming a Superconductor
Ceramic with the Nominal Composition $Tl_2Ba_2Ca_2Cu_3O_{10}$

a

b
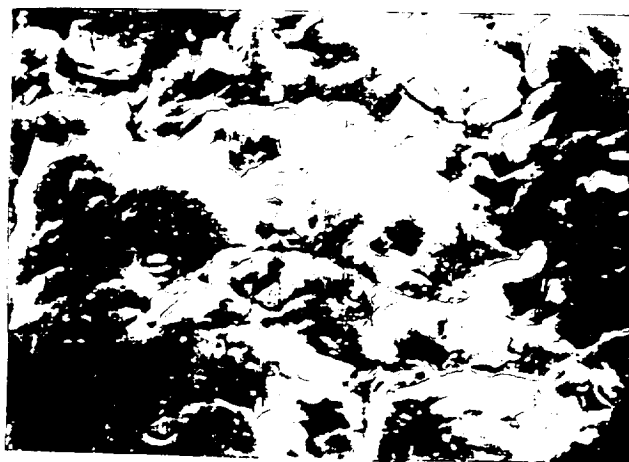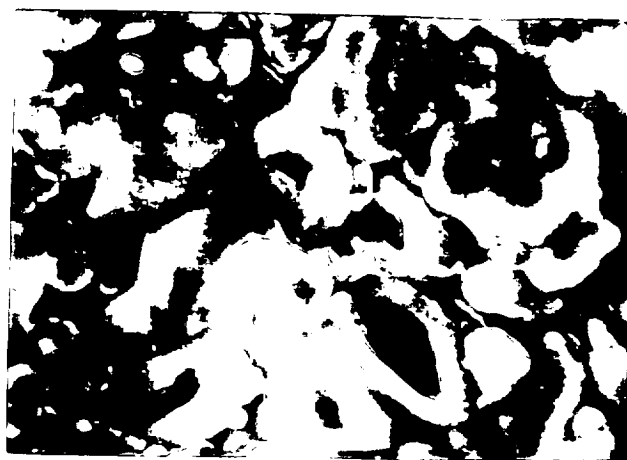
1500 MAGNIFICATION

Figure 3

SEM Photomicrographs of As-Fired Surfaces.
Pellets Batched with Tl_2O_3, BaO , CaO, and CuO
a) fired at 870°C for three hours
b) fired at 890°C for three hours.
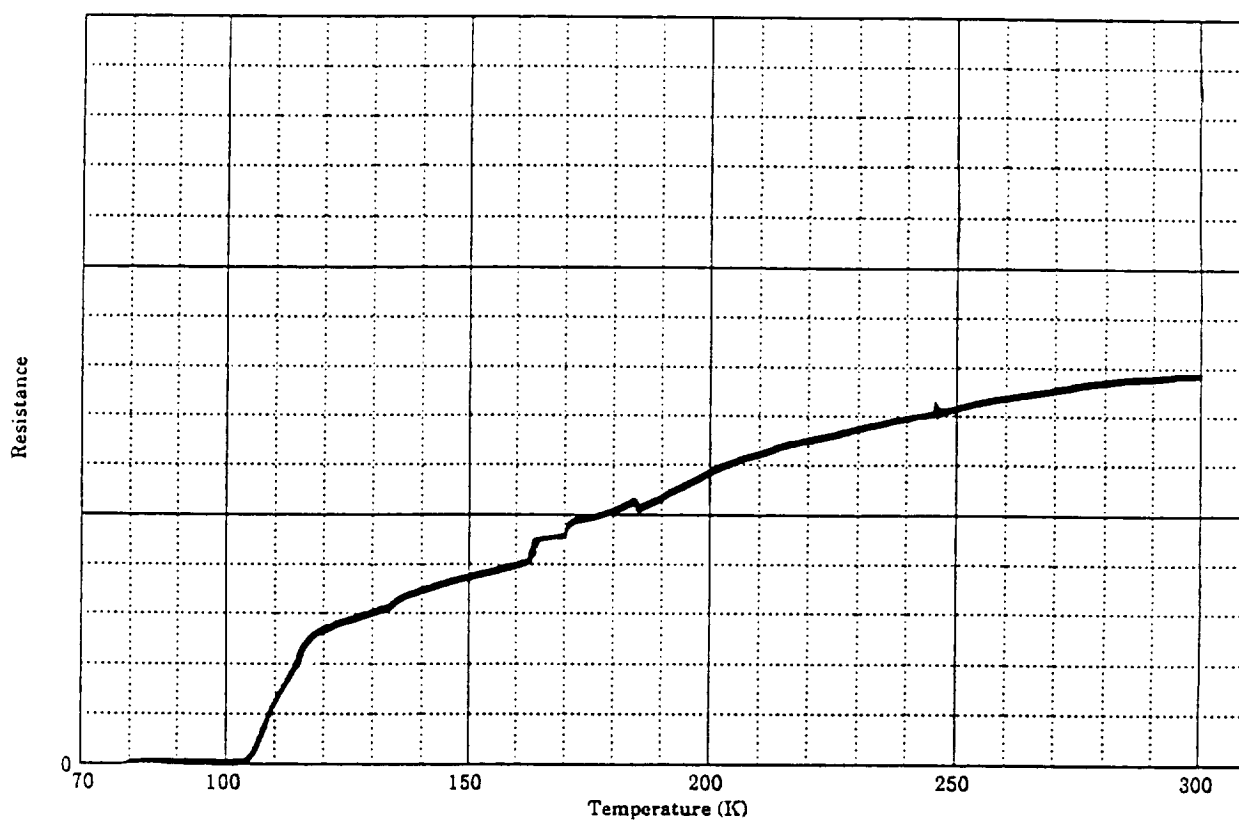
Figure 4

Resistance as a Function of Temperature for a Pellet
Batched by Tl_2O_3, BaO_2, CaO, CuO. Fired for One Hour at 880°C.
Discontinuities indicate cracking. [T_c=104.4K]

a

b
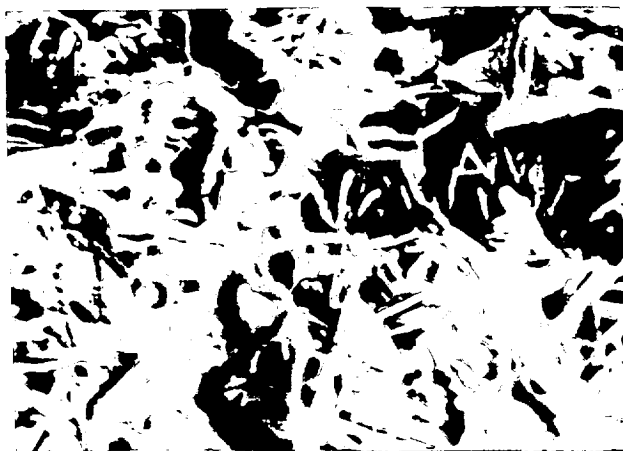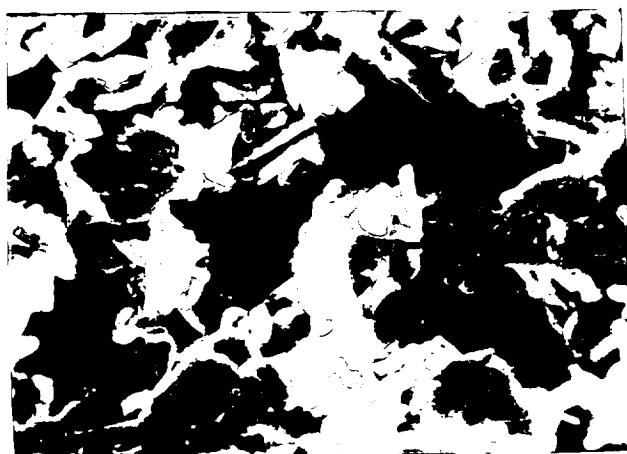
1500 MAGNIFICATION

Figure 5

SEM Photomicrographs of Fractured Surface
Ceramic Pellets Batched with Tl_2O_3, BaO_2, CaO, CuO
a) fired at 870°C for three hours
b) fired at 890°C for three hours
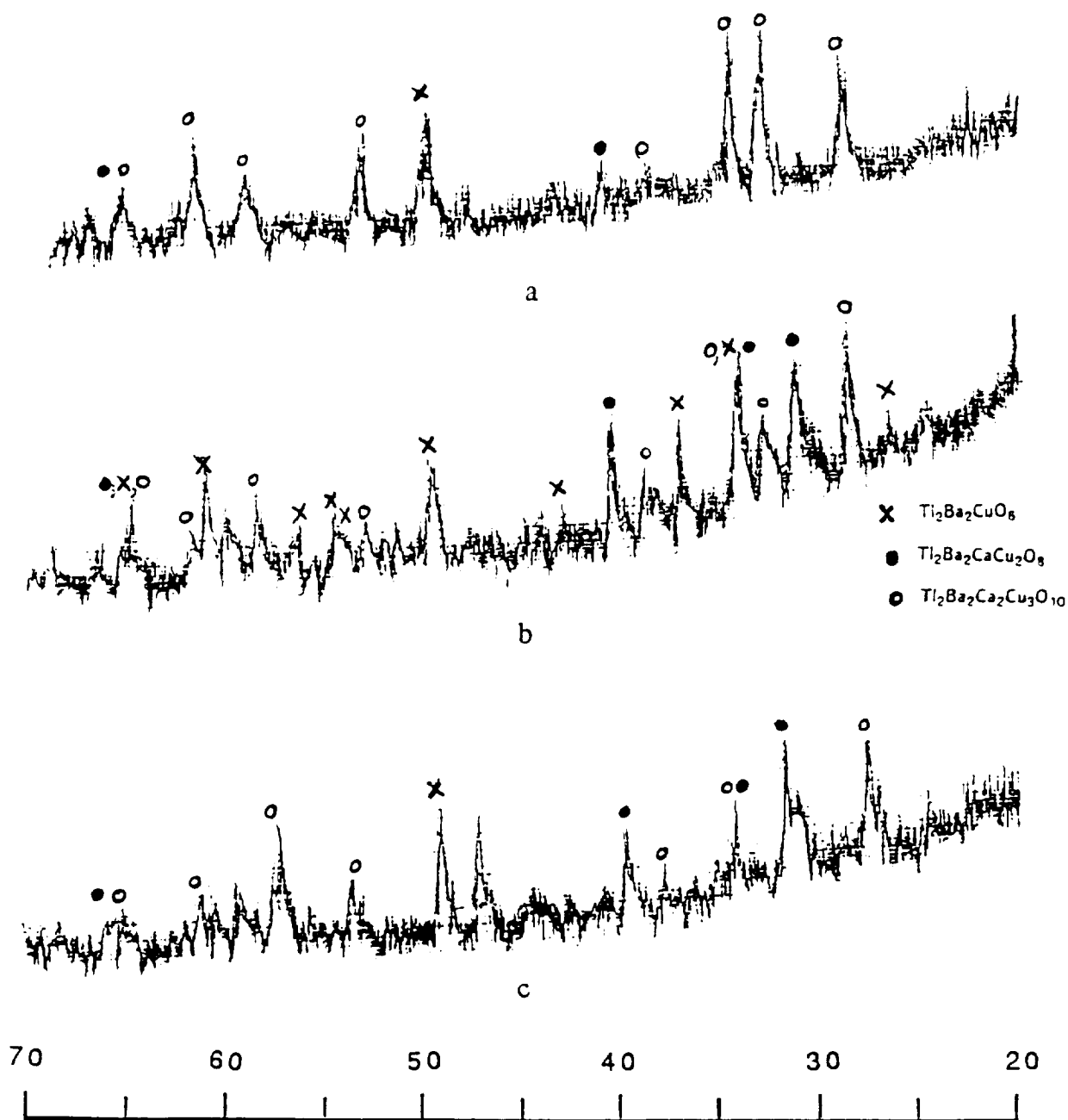
Figure 6

X-Ray Diffraction Profiles of Ceramic
Samples Batched with Tl_2O_3, BaO_2, and $Ca_2Cu_3O_5$
a) fired at 900°C for 180 minutes
b) fired at 900°C for 30 minutes
c) fired at 880°C for 180 minutes
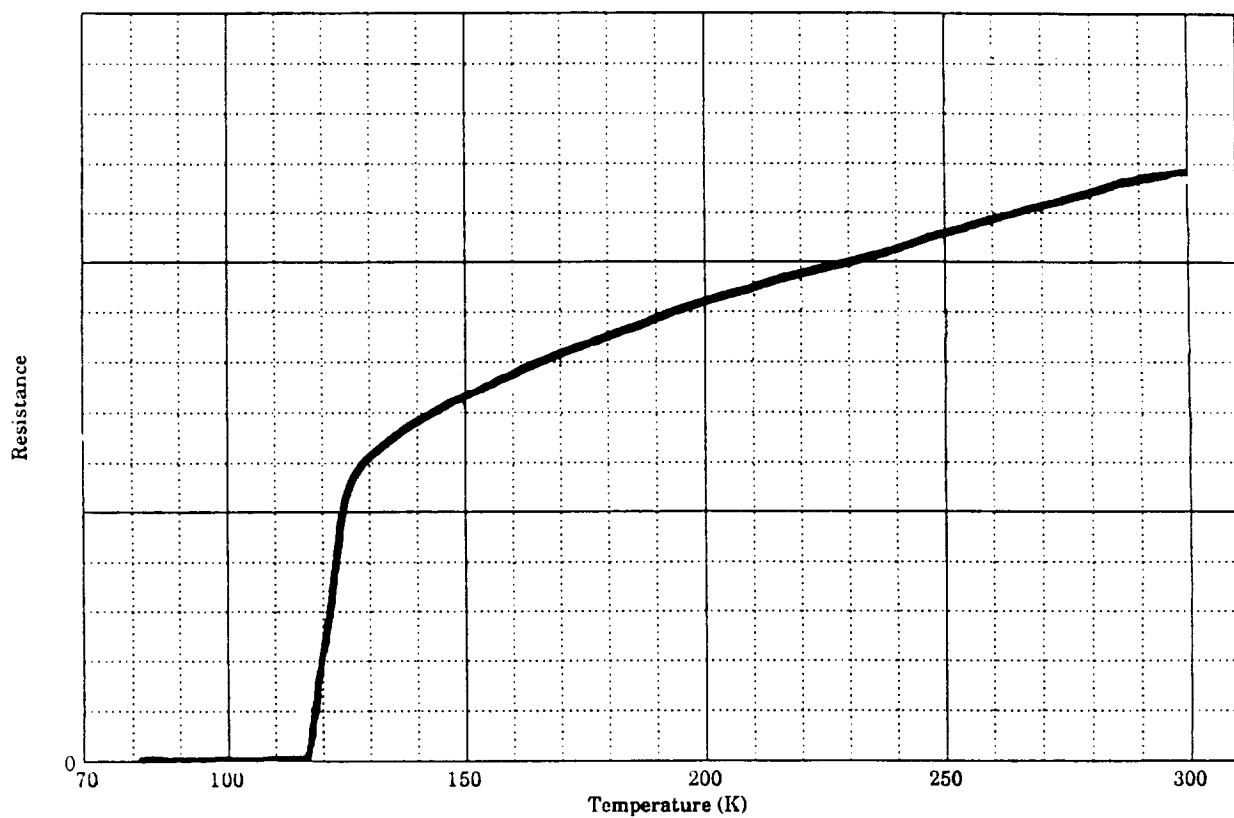
Figure 7

Resistance as a Function of Temperature for a Ceramic Sample
Batched with Tl_2O_3, BaO_2, and $Ca_2Cu_3O_5$.
Sintered at 900°C for Three Hours [T_c=117.8K].
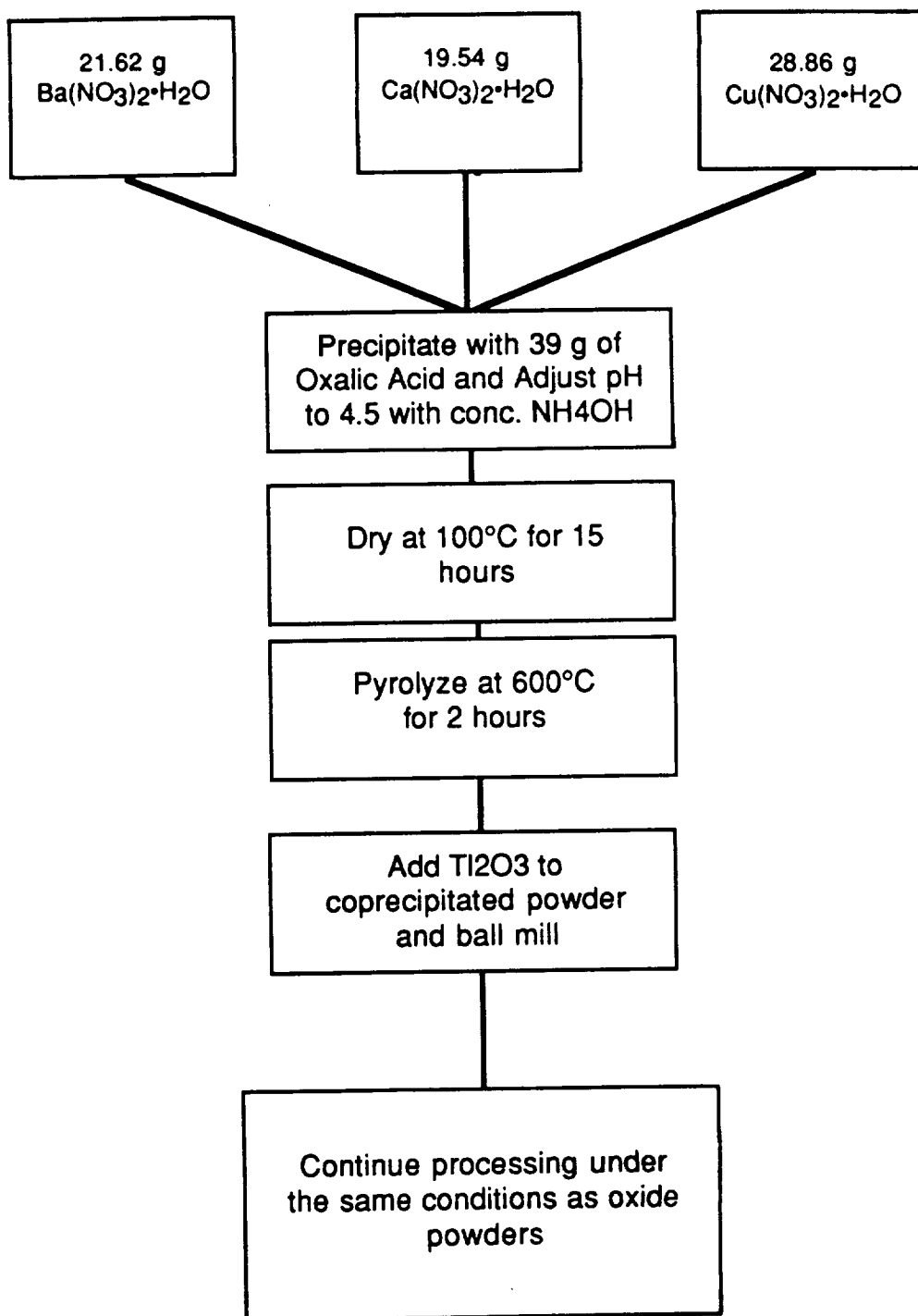
Figure 8

Schematic of the Oxalate Coprecipitation Process
Used to Make Thallium Superconductors

a

b
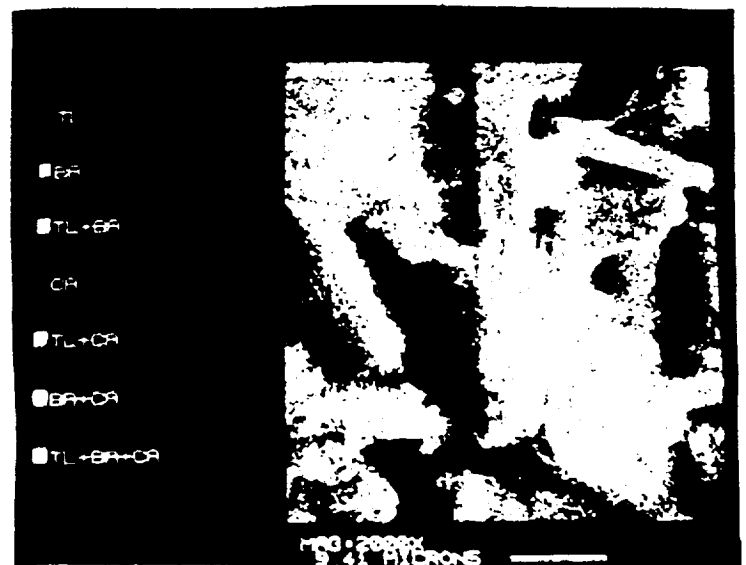
c

Figure 9

Scanning Electron Micrographs and Energy Dispersive X-Ray Analysis
Mappings of As-Fired Surface of a Thallium Superconductor Pellet
Sintered at 893°C for Two Hours--Oxide Precursors
Final Magnification after Copying--1000X
a) SEM Photomicrograph
b) SEM Photomicrograph and EDX Mappings of Tl, Ba, and Cu
c) SEM Photomicrograph and EDX Mappings of Tl, Ba, and Ca
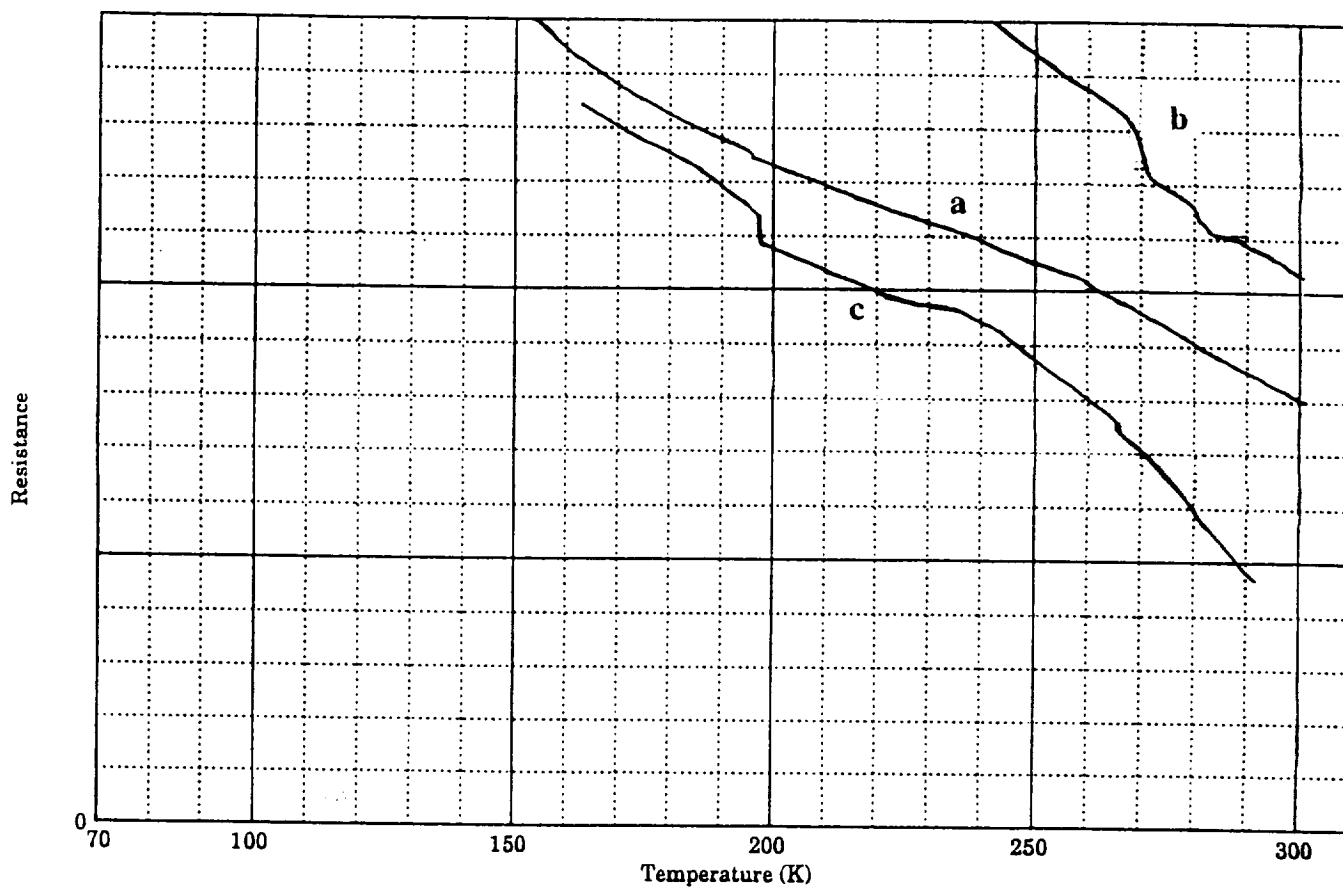
Figure 10

Resistance as a Function of Temperature for Ceramic Pellets
Made with Coprecipitated Powder
Nominal Composition of the Powder: $Tl_2Ba_2Ca_2Cu_3O_{10}$
a) 30 Minute Soak at 893°C (Nonsuperconducting at 77K)
b) 60 Minute Soak at 893°C (Nonsuperconducting at 77K)
c) 120 Minute Soak at 893°C (Nonsuperconducting at 77K)

a
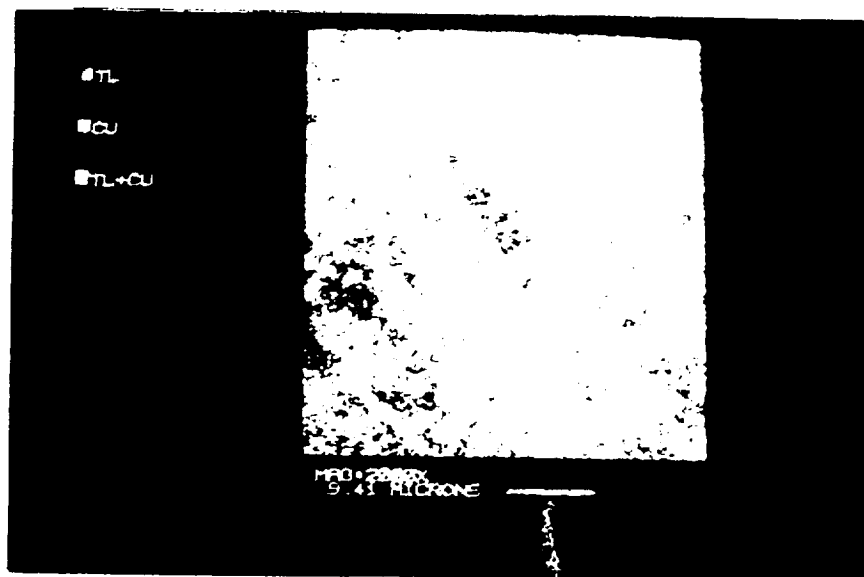
b

Figure 11

Scanning Electron Micrographs and Energy Dispersive X-Ray Analysis
Mappings of As-Fired Surface of a Thallium Superconductor Pellet
Sintered at 893°C for Two Hours--Coprecipitated Precursors
Final Magnification after Copying--1000X
a) SEM Photomicrograph
b) SEM Photomicrograph and EDX Mappings of Tl and Cu
(Ba and Ca are not present in the area shown)

Figure 12

SEM Photomicrograph of a Post-Binder Burnout Tape
Powders Mixed with Binder: Tl_2O_3 and $Ba_2Ca_2Cu_3O_7$
(sieved through 60 mesh)
Ramp: 5°C/min, 550°C Max., One Hour Soak.
400X
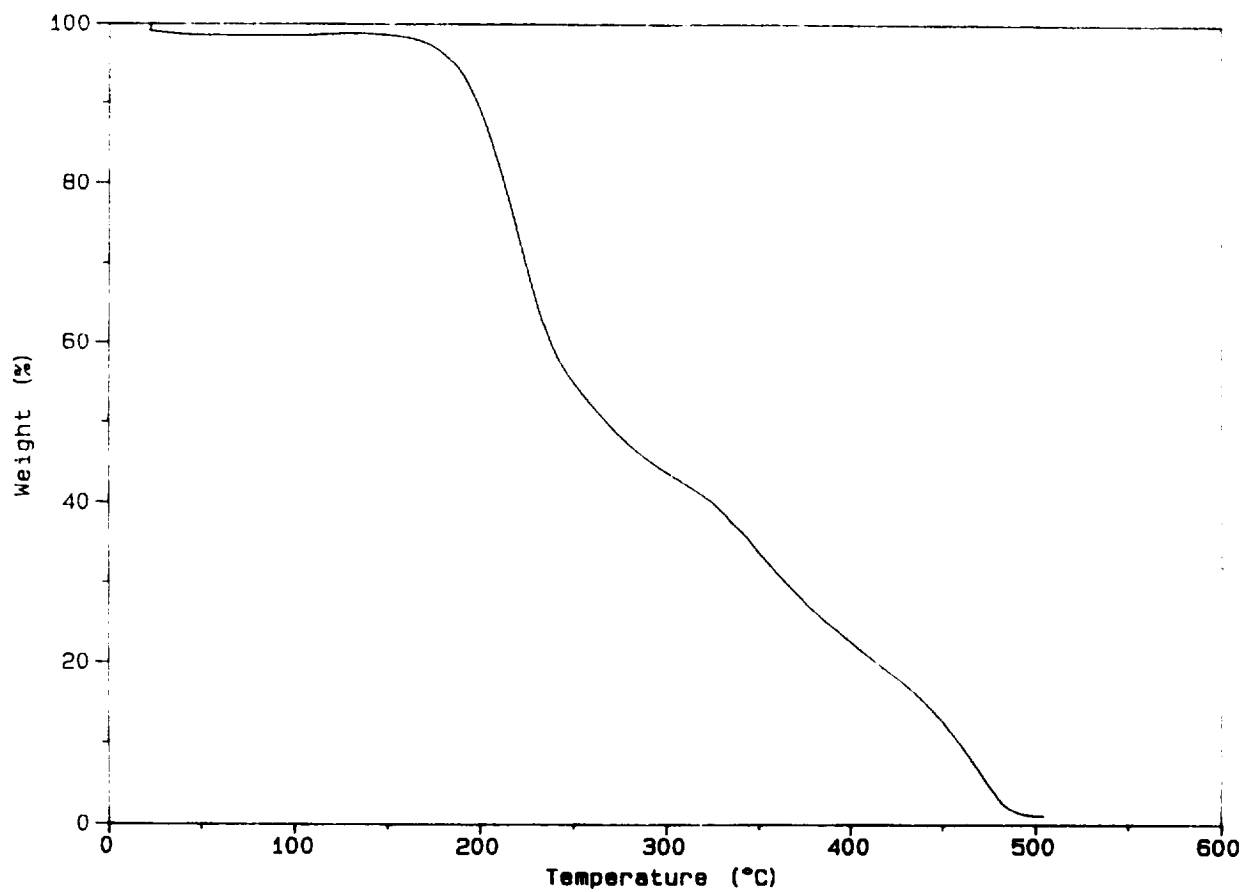
Figure 13

Thermogravimatric Analysis of Binder Used for Tape Casting.
Air Purged-Rate 1°C/min.
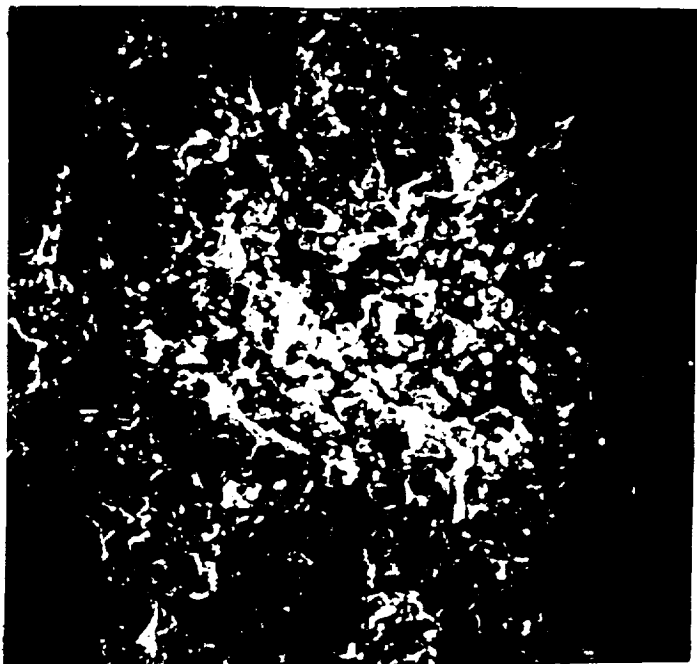
a) Ramp 2°C/min to 550°C. Soak for Two Hours.
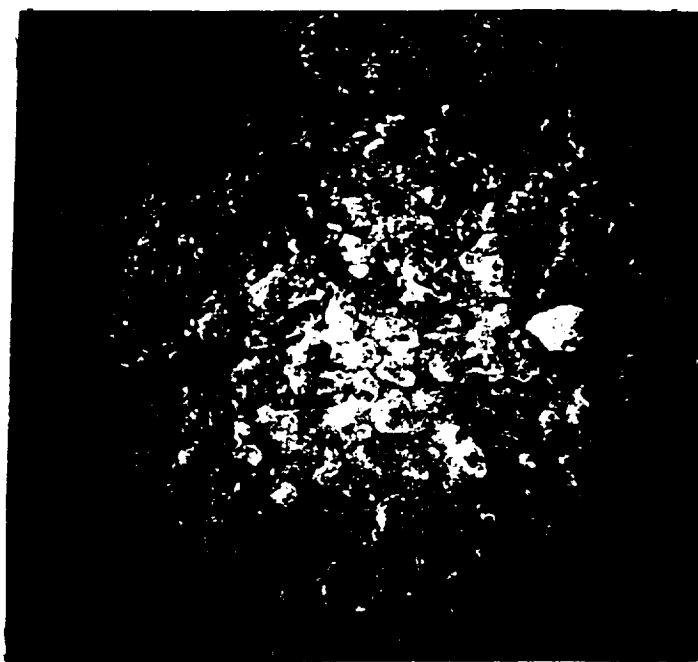
b) Ramp 12°C/min to 550°C. Soak for Two Hours.

Figure 14

SEM Photomicrographs of Post-Binder Burnout Tapes.
Nominal Composition of Precursor Powder $Tl_2Ba_2Ca_2Cu_3O_{10}$.

200X
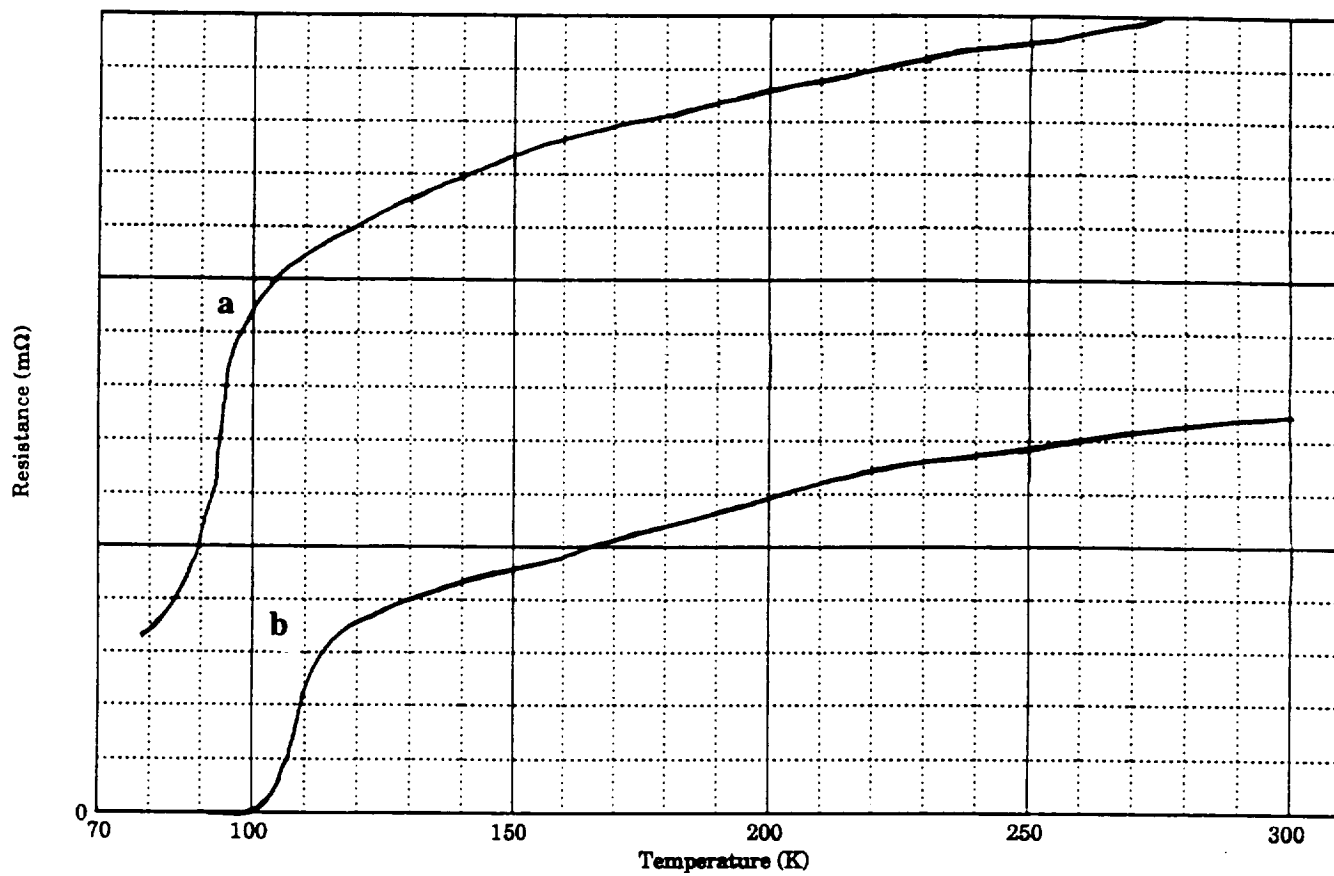
Figure 15

Resistance as a Function of Temperature for Ceramic Tapes.
Nominal Composition of the Powder: $Tl_2Ba_2Ca_2Cu_3O_{10}$

a) 5°C/min Binder Burnout Rate--893°C, 60 Minute Soak
b) 3°C/min Binder Burnout Rate--893°C, 60 Minute Soak
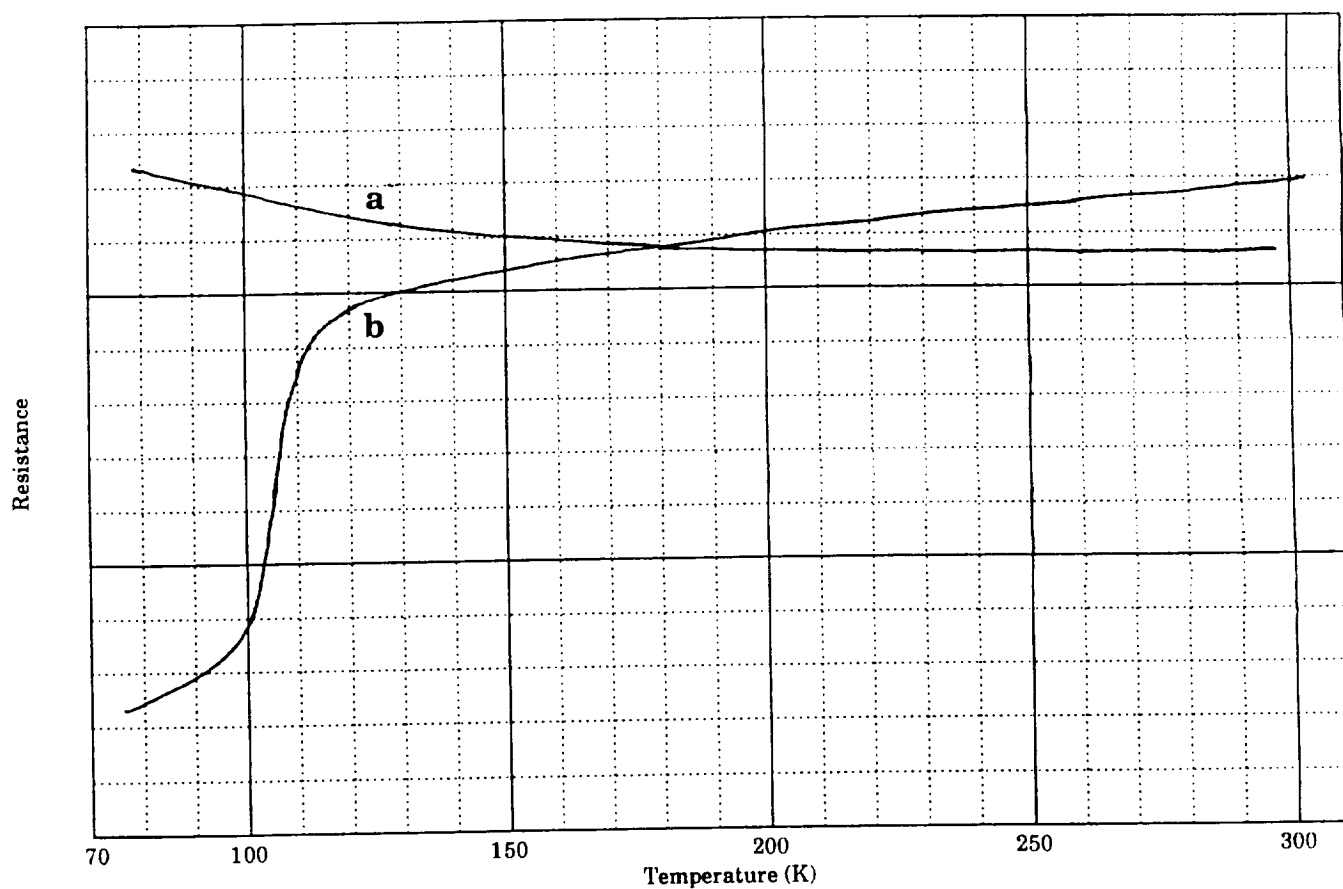
Figure 16

Superconducting Transition Curves of Ceramic Tapes.
Nominal Composition of Precursor Powder $Tl_2Ba_2Ca_2Cu_3O_{10}$.
840°C Presinter--Sieved through 60 mesh.
a) 30 Minute Soak at 890°C (Nonsuperconducting at 77.7K)
b) 60 Minute Soak at 890°C (Nonsuperconducting at 77.7K)
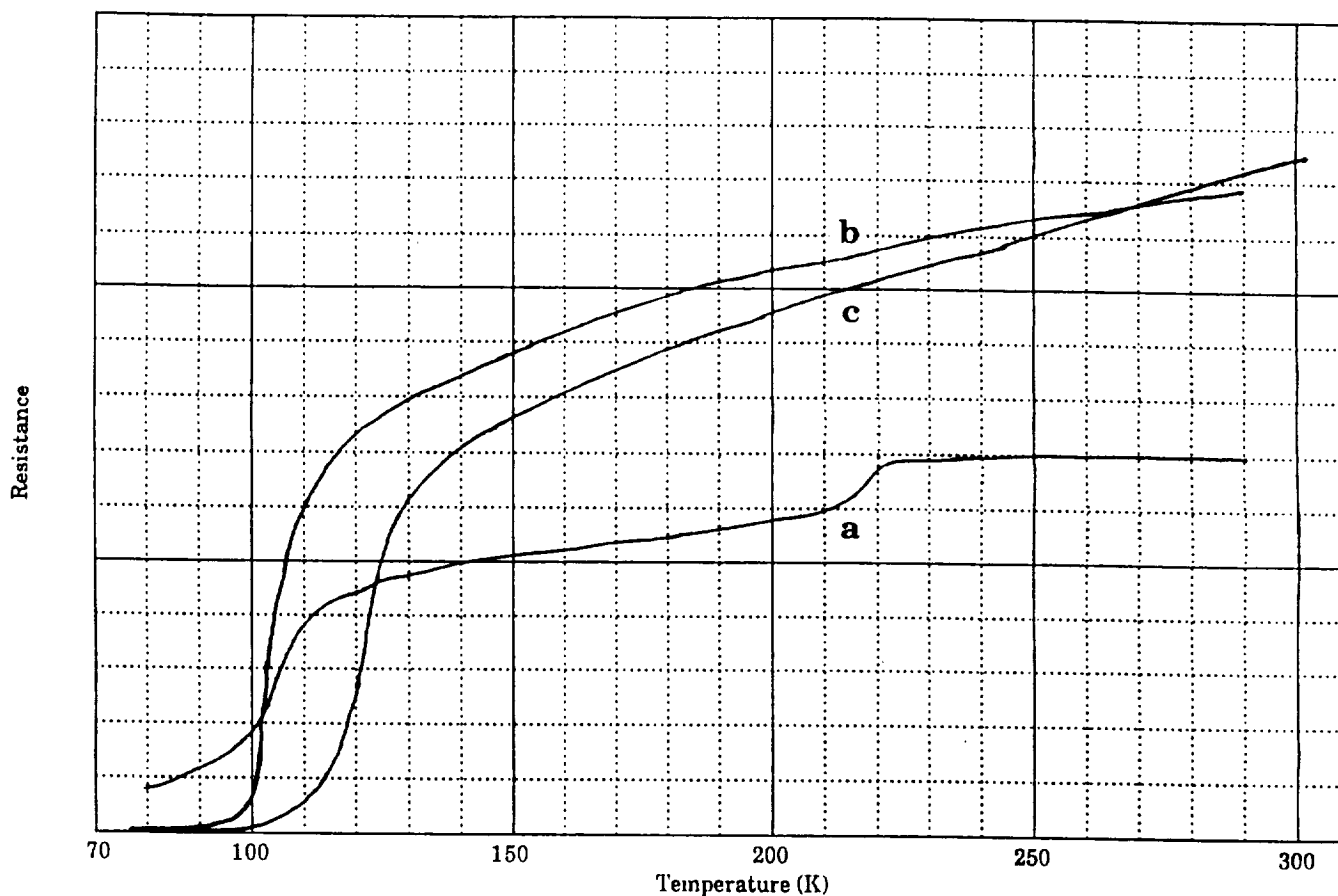
Figure 17

Superconducting Transition Curves of Ceramic Tapes.
Nominal Composition of Precursor Powder $Tl_2Ba_2Ca_2Cu_3O_{10}$.
840°C Presinter--Sieved through 400 mesh.
a) 30 Minute Soak at 890°C (Nonsuperconducting at 77.7K)
b) 60 Minute Soak at 890°C (Nonsuperconducting at 77.7K)
c) 120 Minute Soak at 890°C (T_c=97.3 at 1 mA)
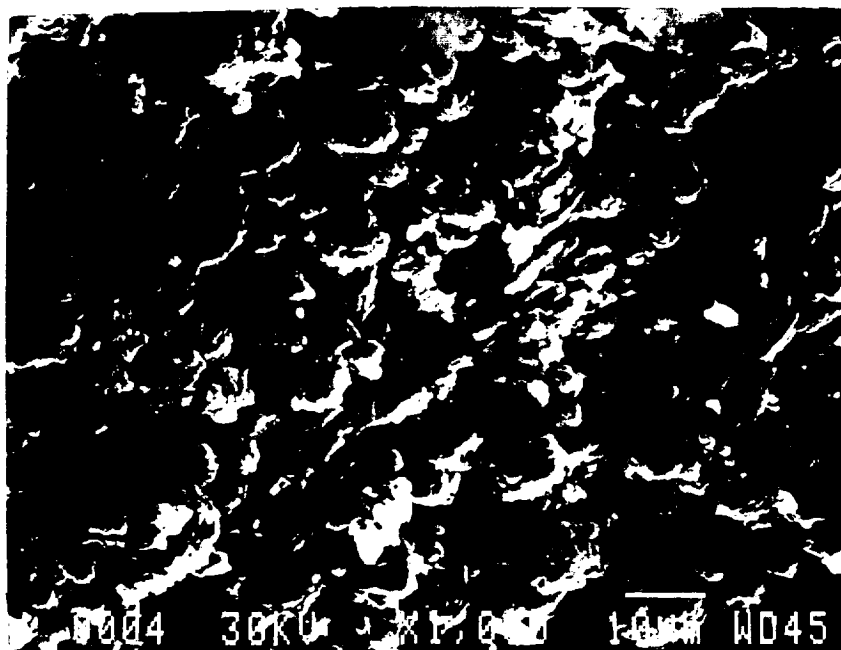
a) Precursor Powder Sieved Through 60 Mesh
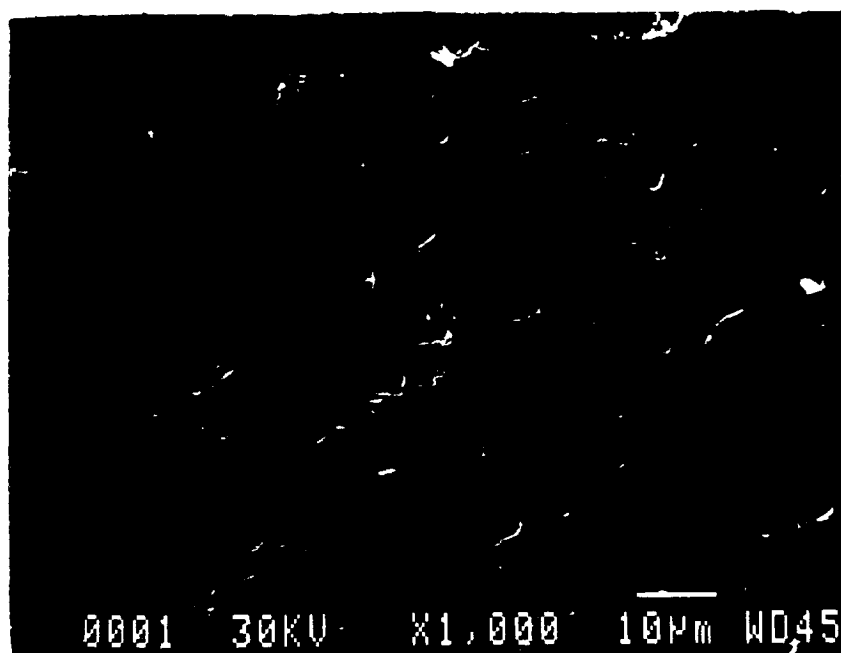
b) Precursor Powder Sieved Through 400 Mesh.

Figure 18

SEM Photomicrographs of the As-Fired Surface of Ceramic Tapes
Flash Fired at 890°C for 30 Minutes.
Nominal Composition of Precursor Powder $Tl_2Ba_2Ca_2Cu_3O_{10}$.
1000X
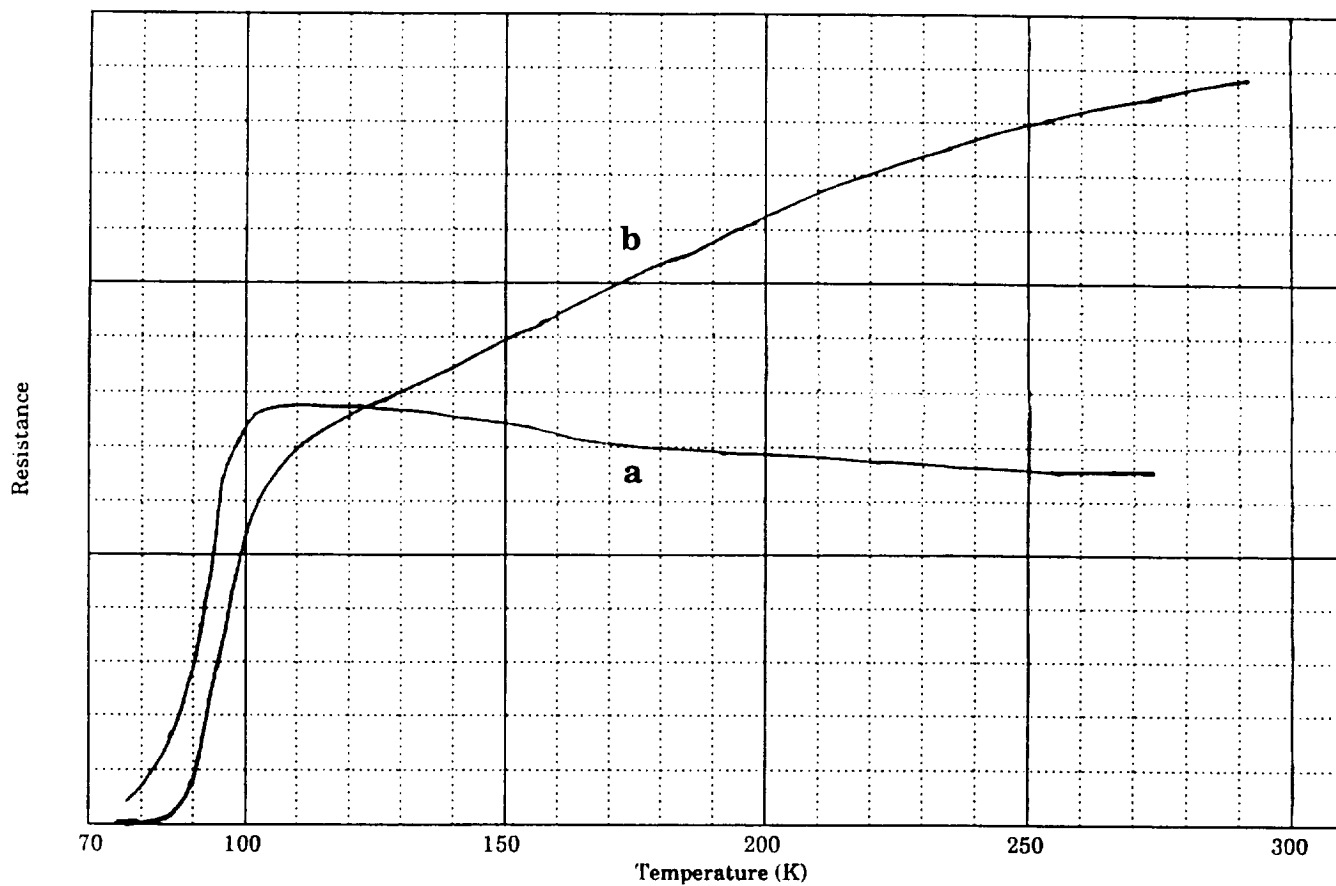
Figure 19

Superconducting Transition Curves of Ceramic Tapes.
Nominal Composition of Precursor Powder $Tl_2Ba_2Ca_2Cu_3O_{10}$.
890°C Presinter--Sieved through 60 mesh.
a) 30 Minute Soak at 890°C (Nonsuperconducting at 77.7K)
b) 60 Minute Soak at 890°C (T_c=90.7K at 100 mA)
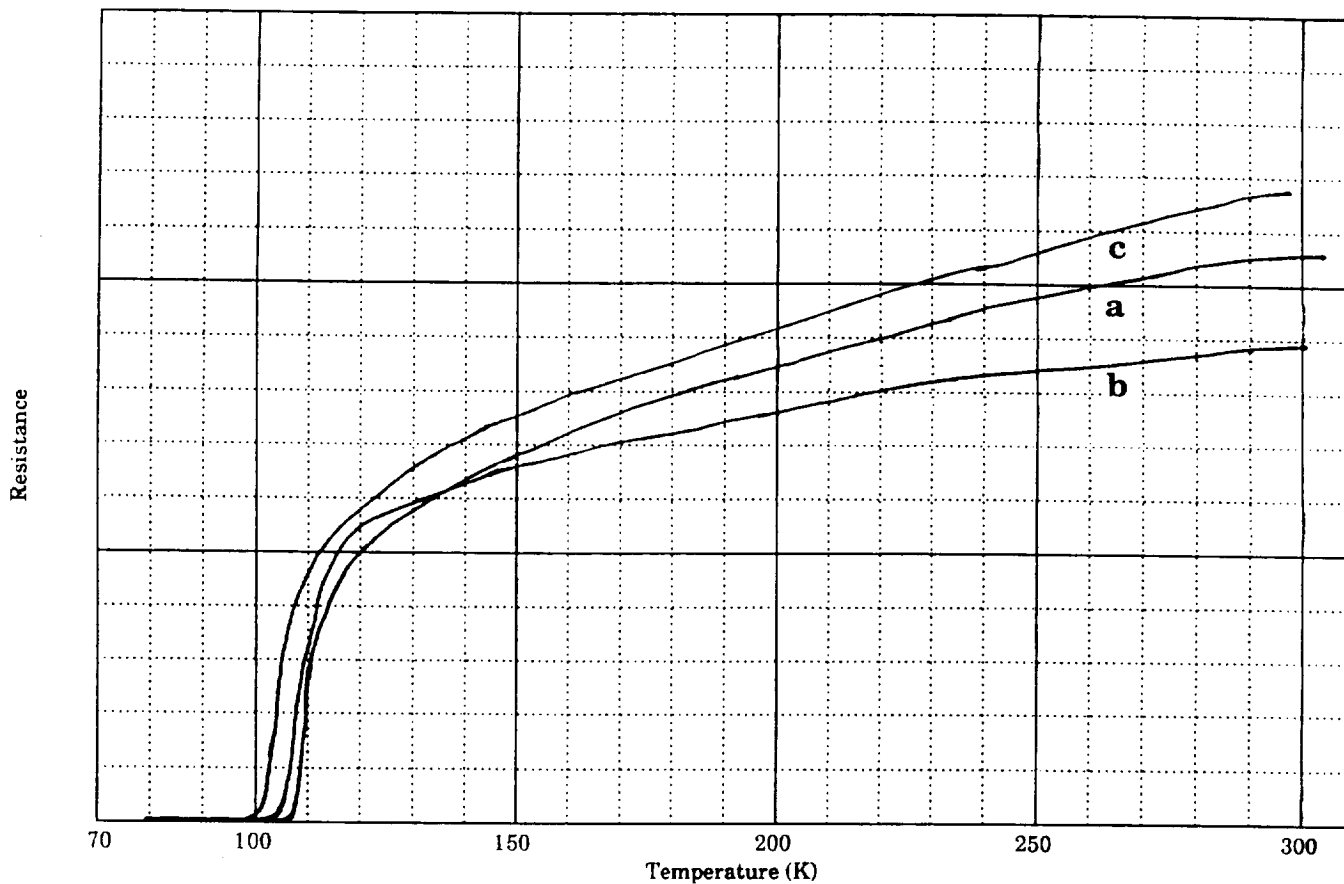
Figure 20

Superconducting Transition Curves of Ceramic Tapes.
Nominal Composition of Precursor Powder $Tl_2Ba_2Ca_2Cu_3O_{10}$.
890°C Presinter--Sieved through 400 mesh.
a) 30 Minute Soak at 890°C (T_c=96.4K at 100 mA)
b) 60 Minute Soak at 890°C (T_c=104.6K at 100 mA)
c) 120 Minute Soak at 890°C (T_c=106.5K at 100 mA)
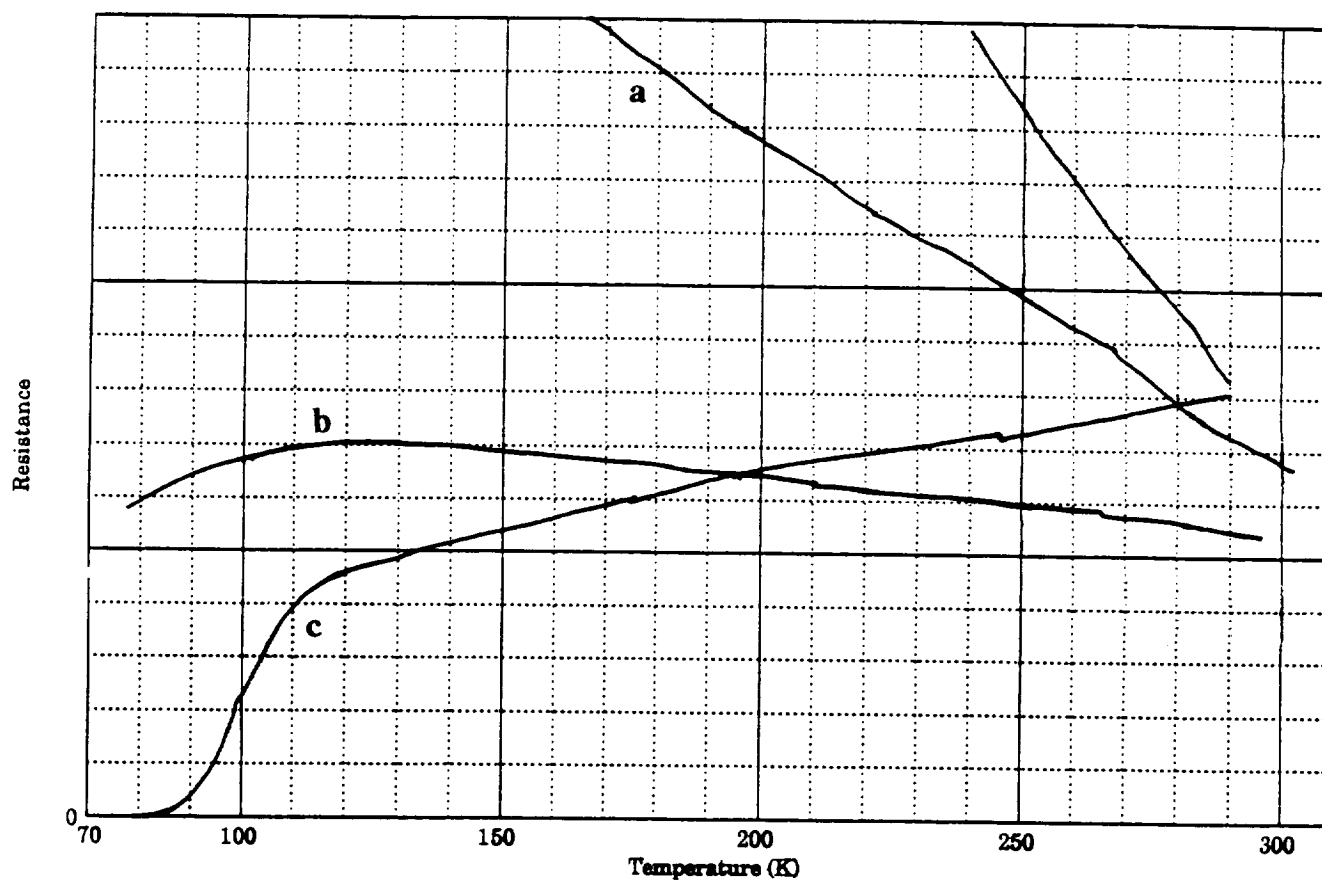
Figure 21

Superconducting Transition Temperature Curves of Ceramic Tapes.
Nominal Composition of Precursor Powder $Tl_2Ba_2Ca_2Cu_3O_{10}$.

a) 2°C/min Binder Burnout Rate--745°C, 12 Hour Soak

b) 2°C/min Binder Burnout Rate--745°C, 24 Hour Soak

c) 2°C/min Binder Burnout Rate--745°C, 48 Hour Soak
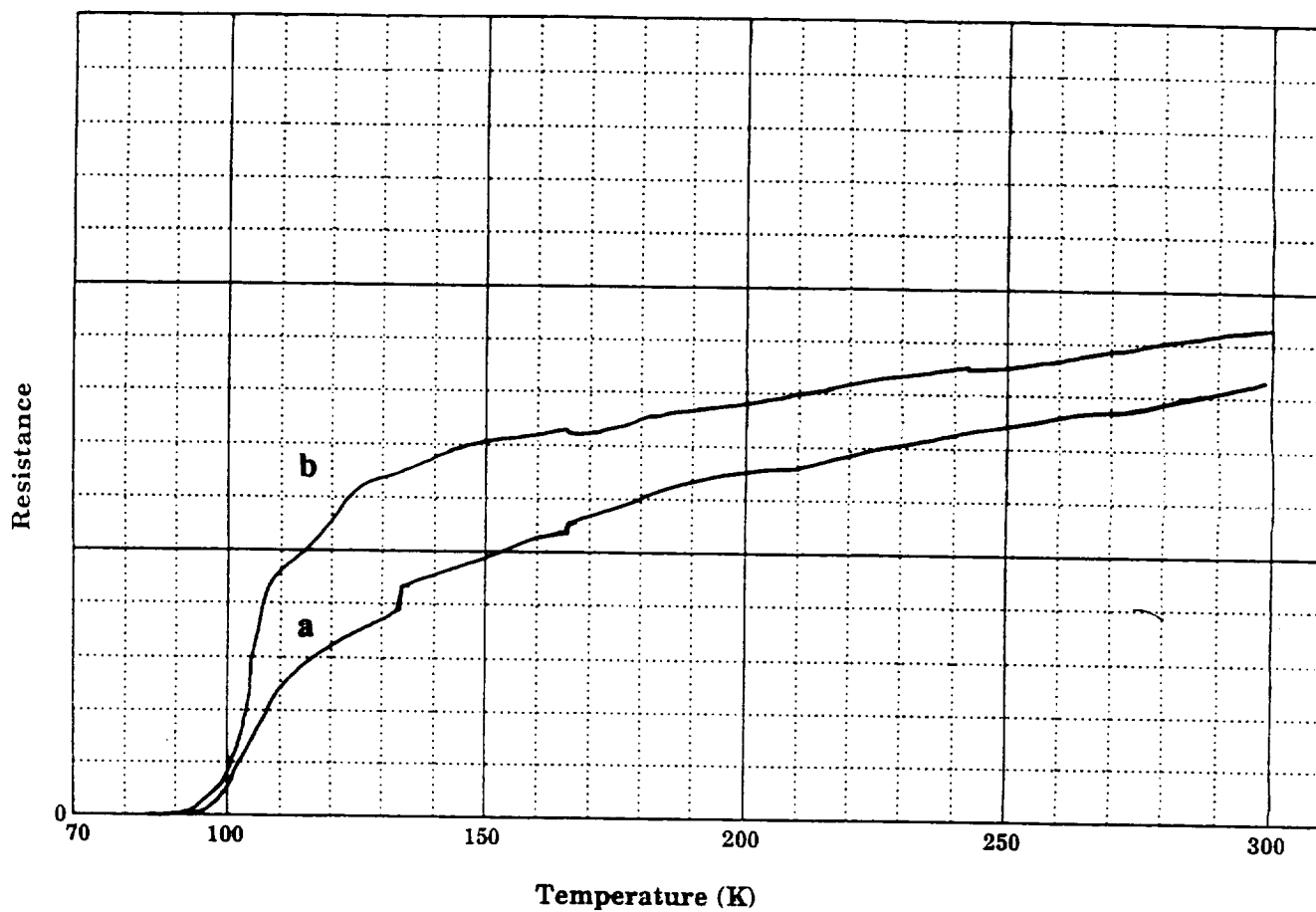
Figure 22

Superconducting Transition Temperature Curves of Ceramic Tapes.
Nominal Composition of Precursor Powder $Tl_2Ba_2Ca_2Cu_3O_{10}$.

a) 2°C/min Binder Burnout Rate--760°C, 24 Hour Soak

b) 2°C/min Binder Burnout Rate--760°C, 48 Hour Soak
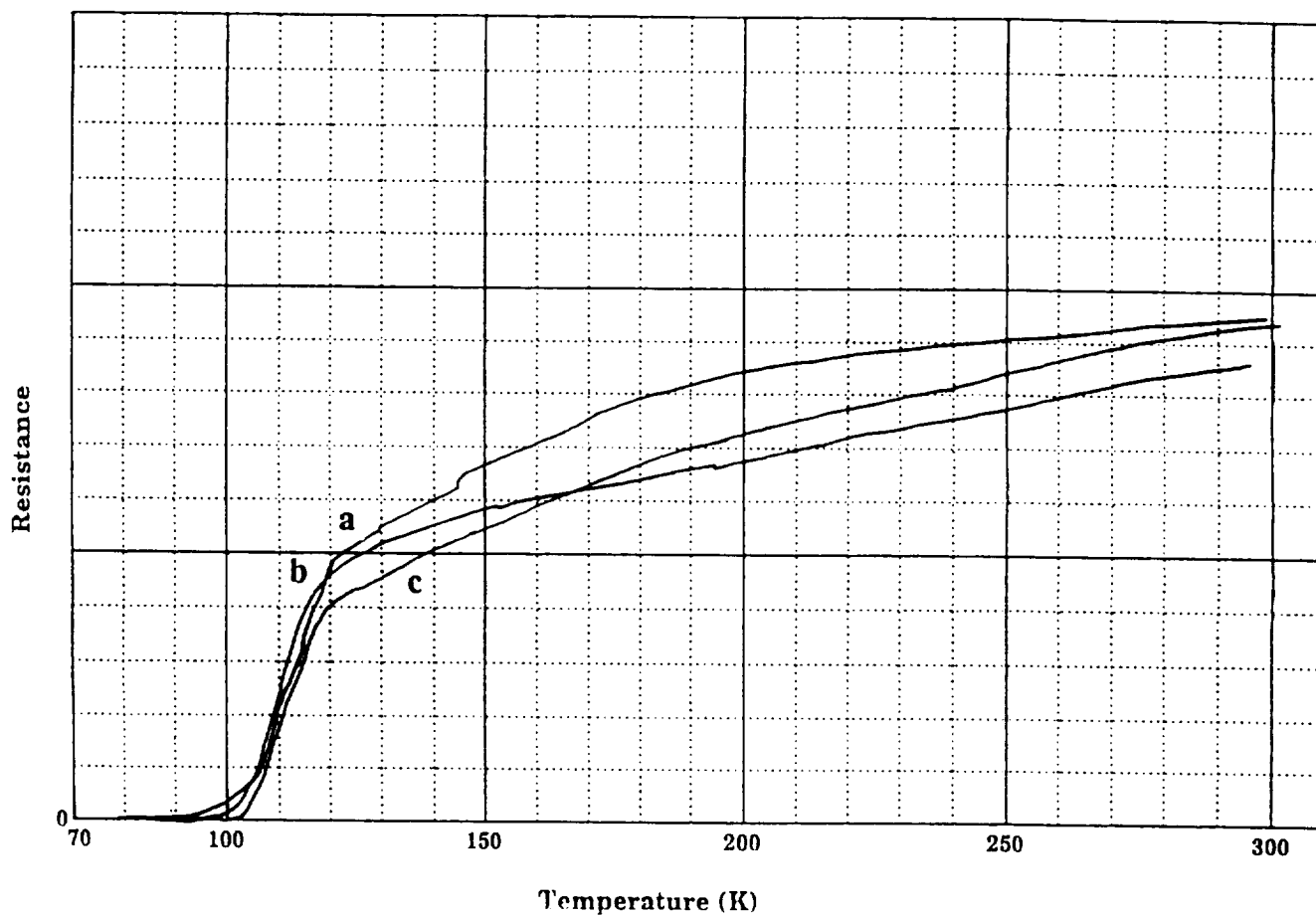
Figure 23

Superconducting Transition Temperature Curves of Ceramic Tapes.
Nominal Composition of Precursor Powder $Tl_2Ba_2Ca_2Cu_3O_{10}$.

a) 2°C/min Binder Burnout Rate--775°C, 12 Hour Soak

b) 2°C/min Binder Burnout Rate--775°C, 24 Hour Soak

c) 2°C/min Binder Burnout Rate--775°C, 48 Hour Soak
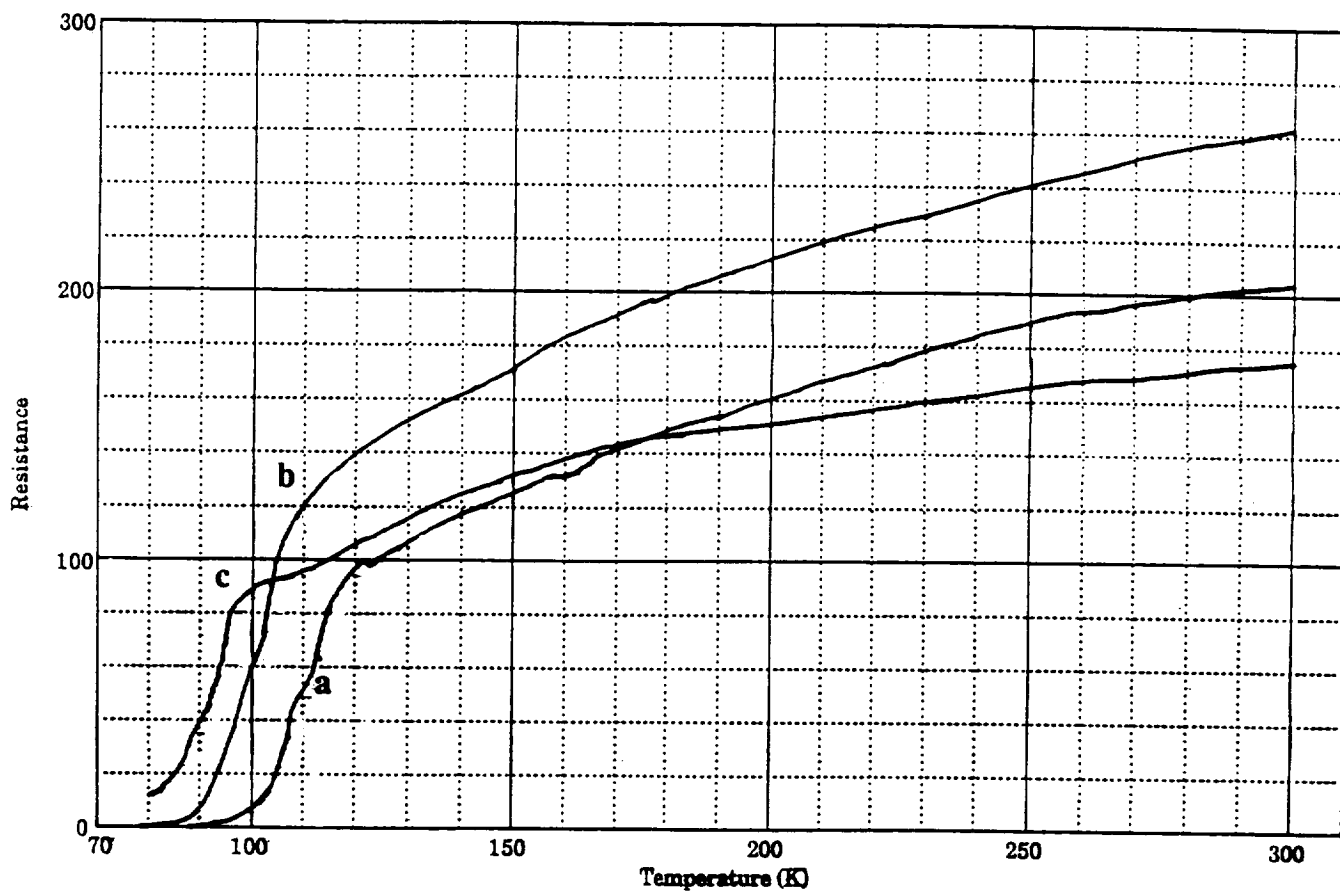
Figure 24

Superconducting Transition Temperature Curves of Ceramic Tapes.
Nominal Composition of Precursor Powder $Tl_2Ba_2Ca_2Cu_3O_{10}$.

    a) 2°C/min Binder Burnout Rate--800°C, 12 Hour Soak

    b) 2°C/min Binder Burnout Rate--800°C, 24 Hour Soak

    c) 2°C/min Binder Burnout Rate--800°C, 48 Hour Soak

Electronic Ceramics Lab., Clemson University
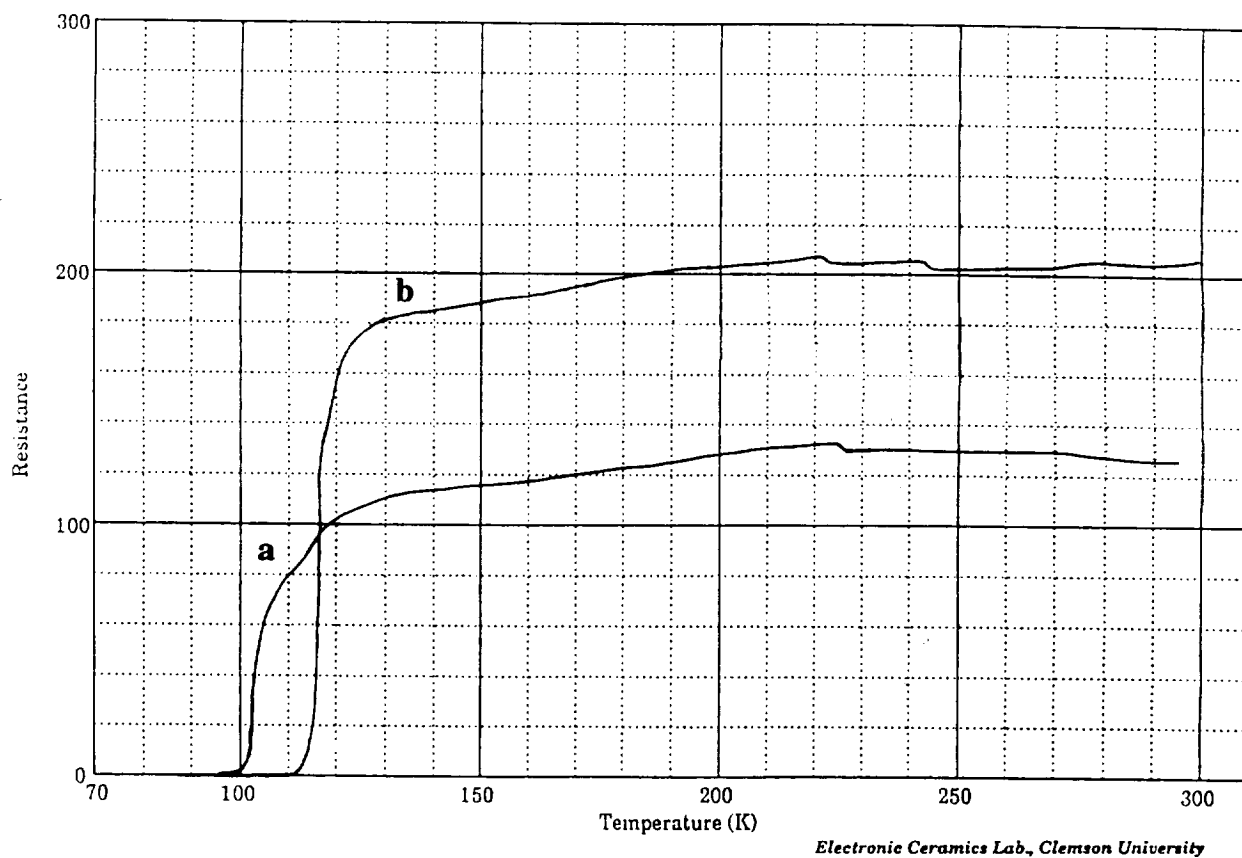
Figure 25

Superconducting Transition Temperature Curves of Ceramic Tapes.
Nominal Composition of Precursor Powder $Tl_2Ba_2Ca_2Cu_3O_{10}$.

a) 2°C/min Binder Burnout Rate--775°C, 48 Hour Soak

b) 3°C/min Binder Burnout Rate--775°C, 48 Hour Soak

100
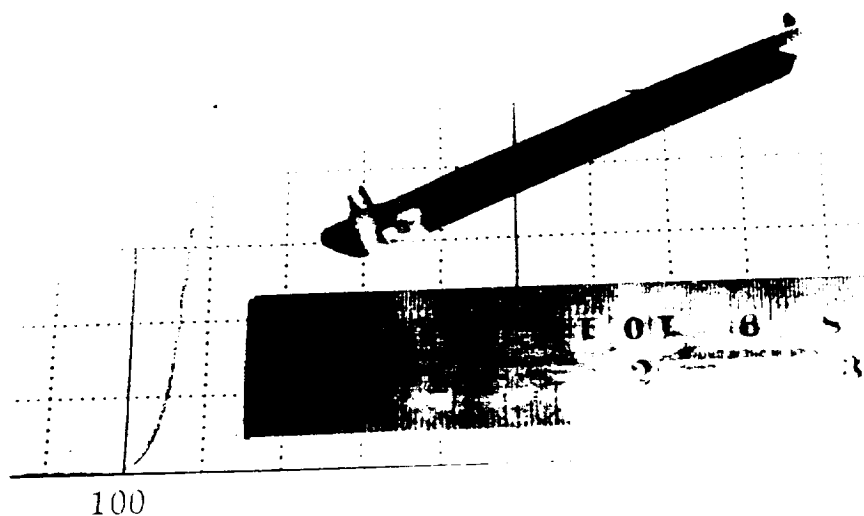
Figure 26

Photograph of Thallium Superconductor Grounding Links.
Nominal Composition of Precursor Powder $Tl_2Ba_2Ca_2Cu_3O_{10}$.
840°C Presinter--Sieved through 400 mesh.
2°C/min Binder Burnout Rate--775°C, 48 Hour Soak
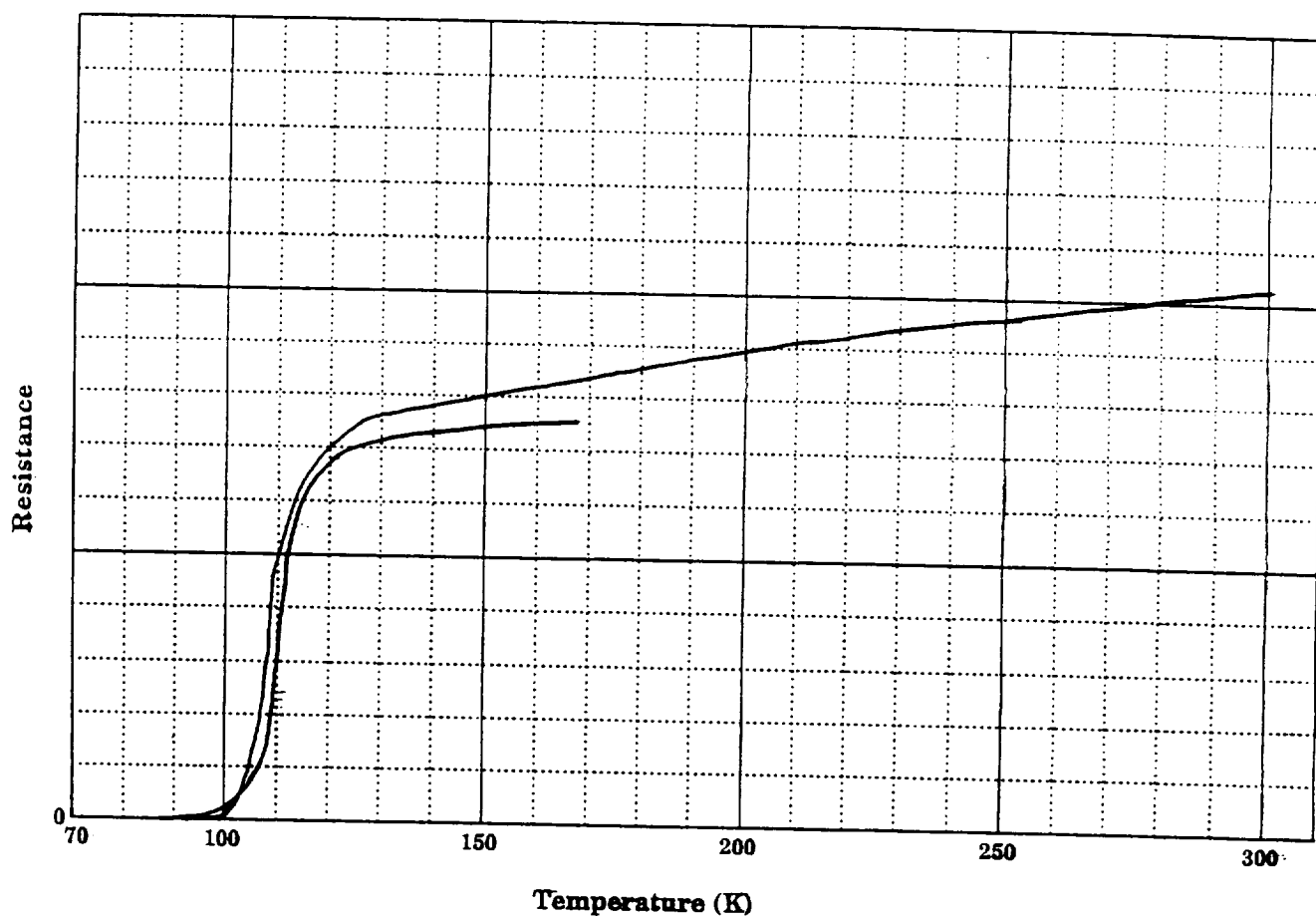
Figure 27

Superconducting Transition Temperature Curves of Grounding Links.
Nominal Composition of Precursor Powder $Tl_2Ba_2Ca_2Cu_3O_{10}$.
840°C Presinter--Sieved through 400 mesh.
2°C/min Binder Burnout Rate--775°C, 48 Hour Soak
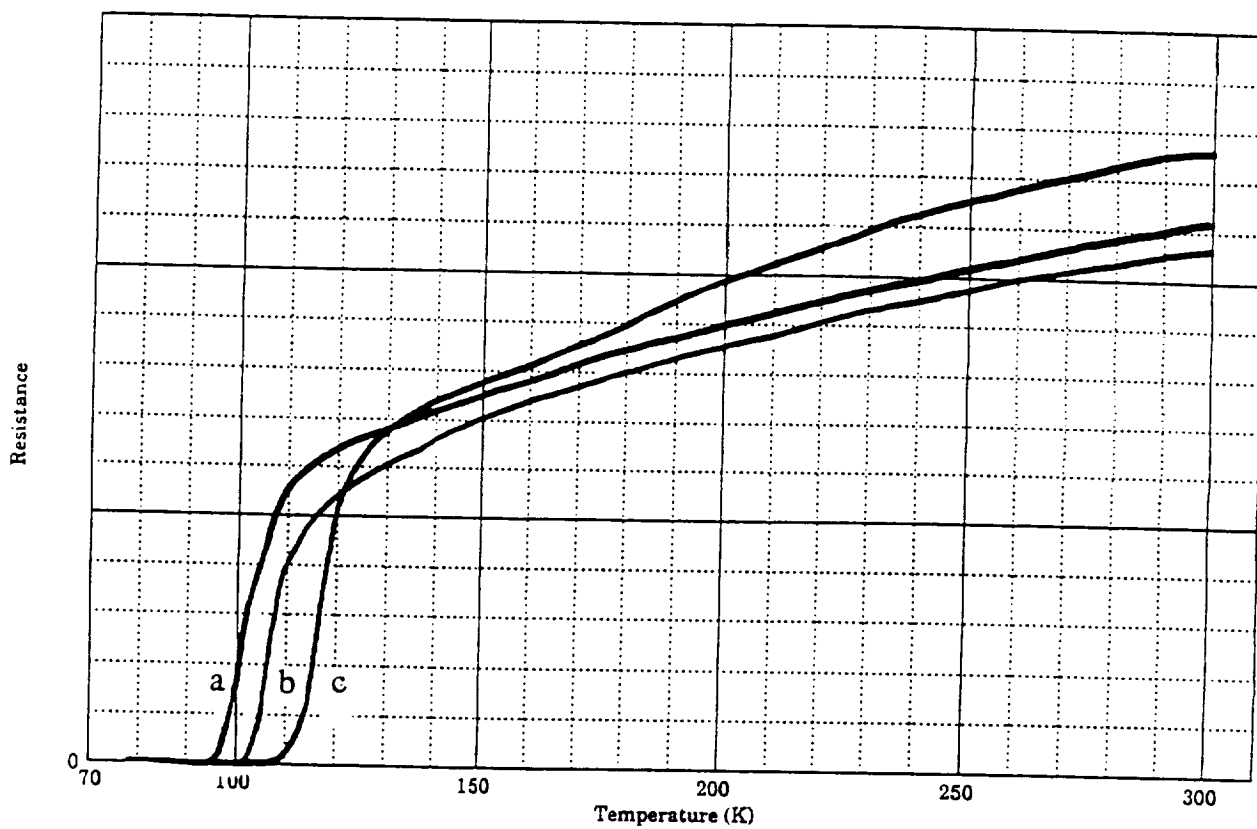
Figure 28

Resistance as a Function of Temperature for Ceramics Batched
with Tl_2O_3 and $Ba_2Ca_2Cu_{3-x}O_7/Li_x$ Fired at 900°C for 30 Minutes
a) x=0.06 [T_c=93.3K]
b) x=0.10 [T_c=101.2K]
c) x=0.20 [T_c=108.0K]
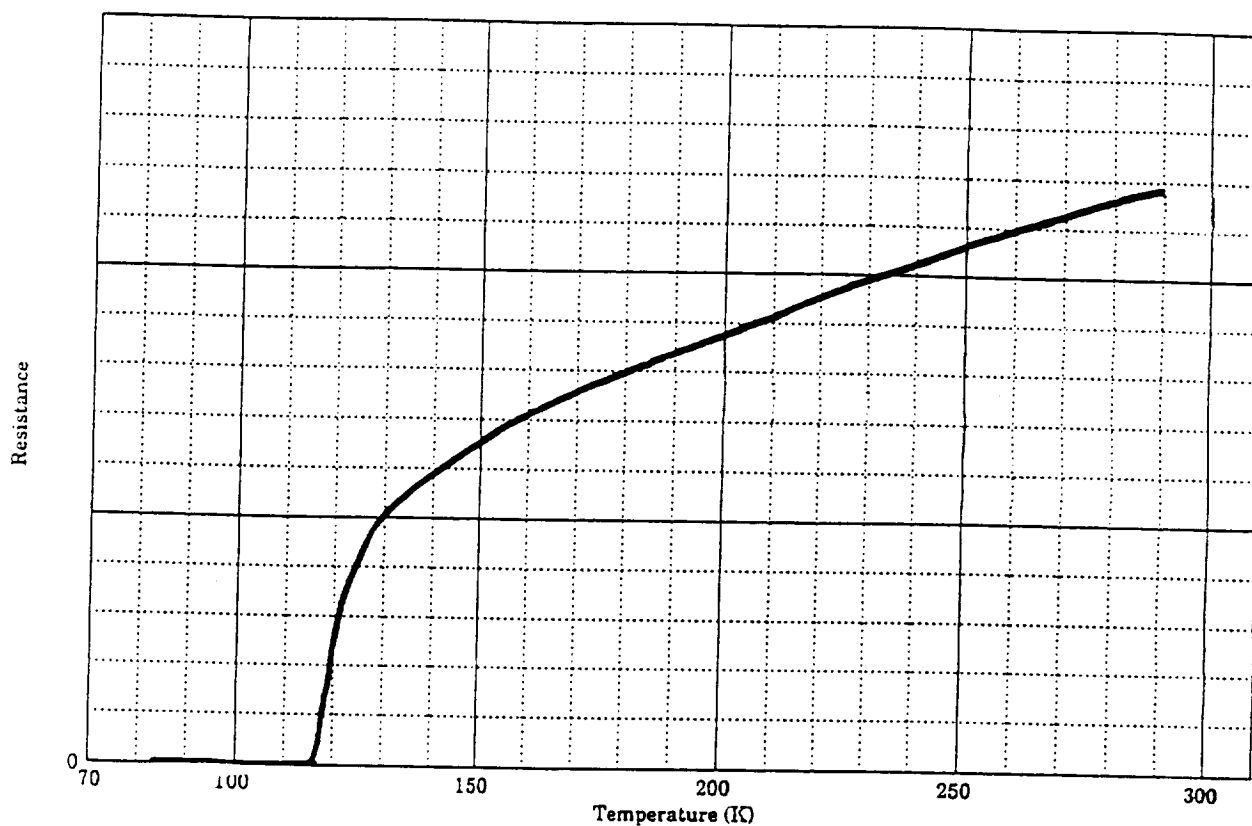
Figure 29

Resistance as a Function of Temperature for Ceramics
Batched with Tl_2O_3 and $Ba_2Ca_2Cu_{2.94}Li_{0.06}O_7$ Fired at 900°C for 60 Minutes.
[T_c=115.7K]
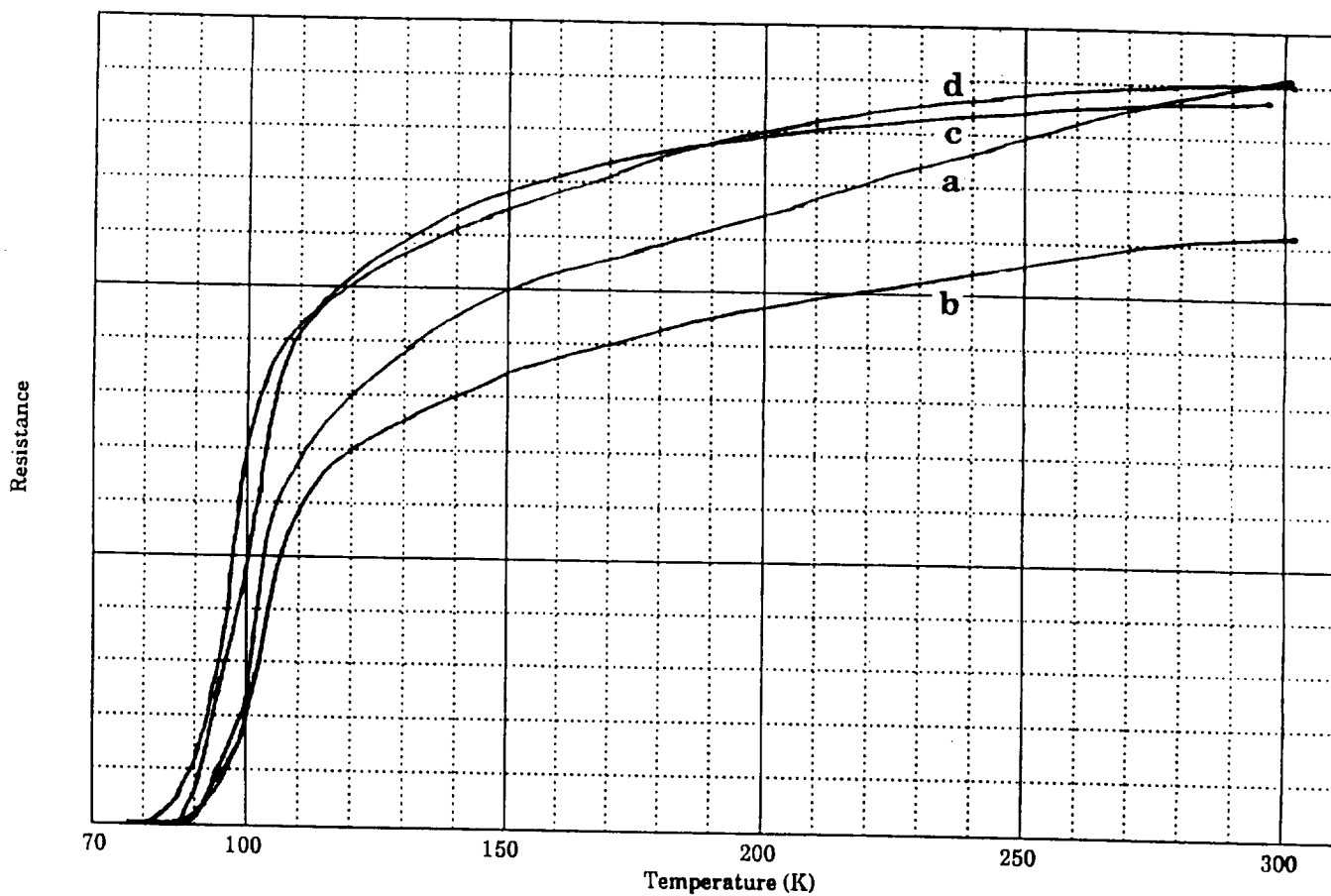
Figure 30

Superconducting Transition Curves of Ceramic Pellets with Various
Manganese Substitutions. Flash-Fired at 885°C for 30 Minutes
a) 0 mole percent Mn for Cu (T_c=88.7K)
b) 0.47 mole percent Mn for Cu (T_c=86.3K)
c) 0.93mole percent Mn for Cu (T_c=87.3K)
d) 1.87 mole percent Mn for Cu (T_c=81.6K)
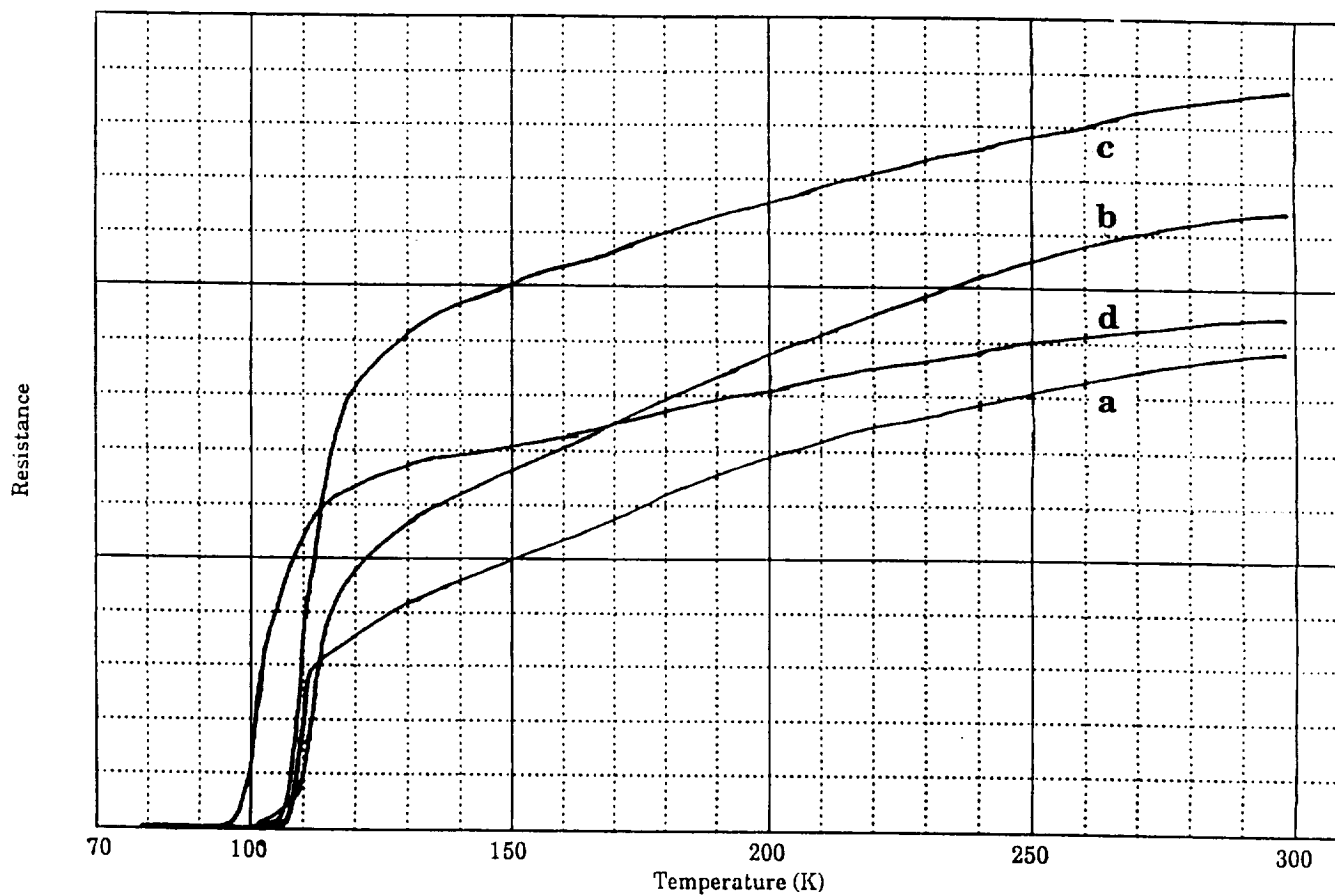
Figure 31

Superconducting Transition Curves of Ceramic Pellets with Various
Manganese Substitutions. Flash-Fired at 885°C for 120 Minutes
a) 0 mole percent Mn for Cu (T_c=108.0K)
b) 0.47 mole percent Mn for Cu (T_c=101.3K)
c) 0.93mole percent Mn for Cu (T_c=105.7K)
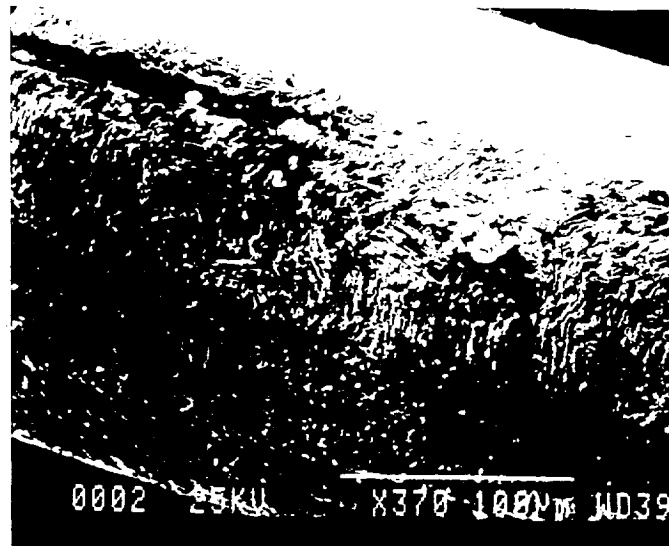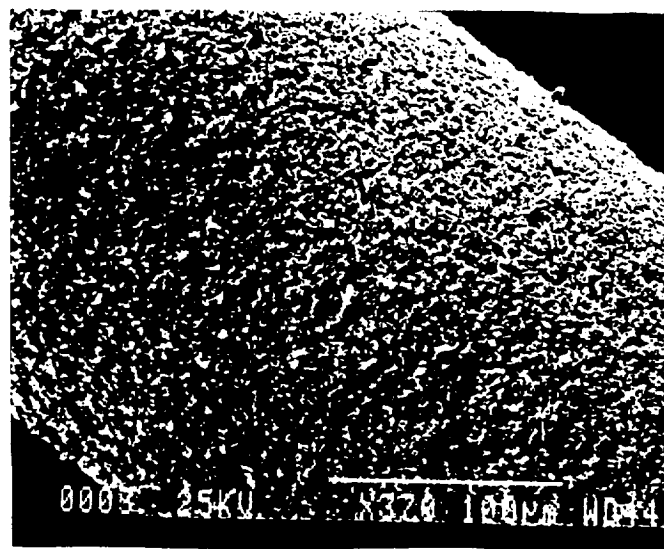d) 1.87 mole percent Mn for Cu (T_c=97.4K)
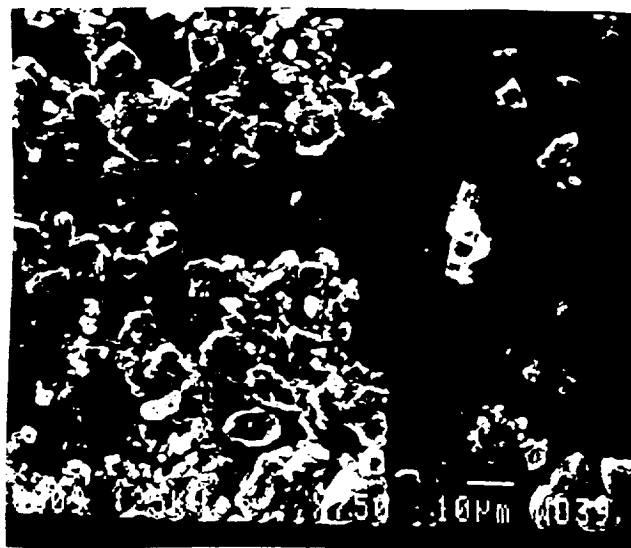
a
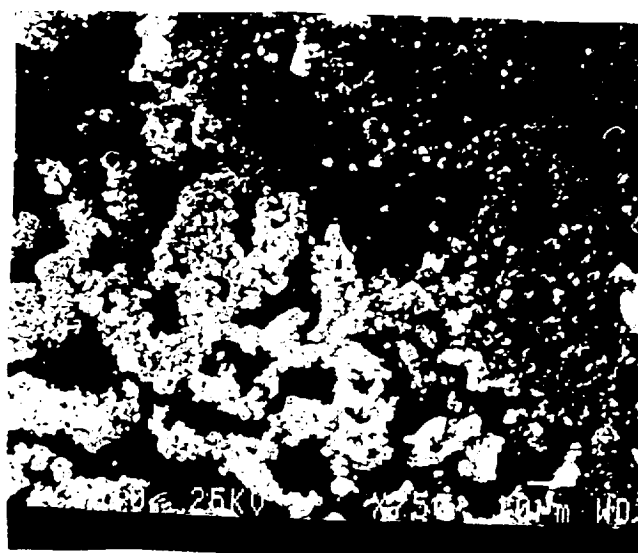
b

Figure 32

SEM Photomicrograph of Bi-Pb-Ca-Sr-Cu-O Powders
a) Particles which had settled after 10 hours in n-butanol
b) Particles which were in suspension after 10 hours in n-butanol

a

b

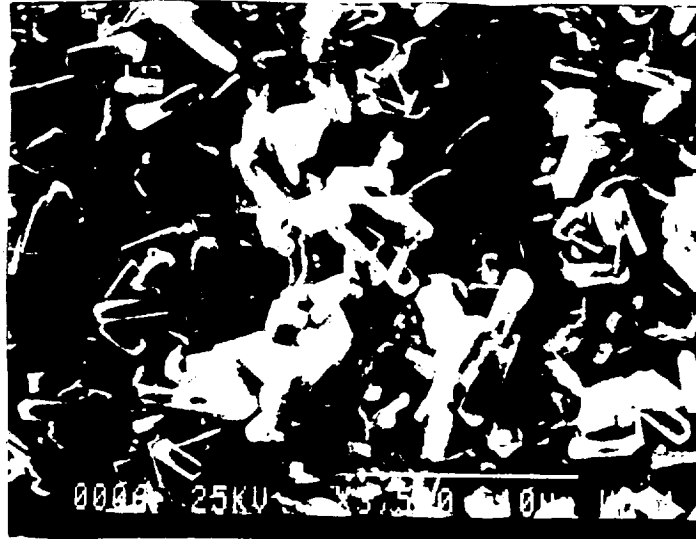**Figure 33**

SEM Photomicrographs
a) Bare Silver Wire Before Dielectrophoretic Deposition
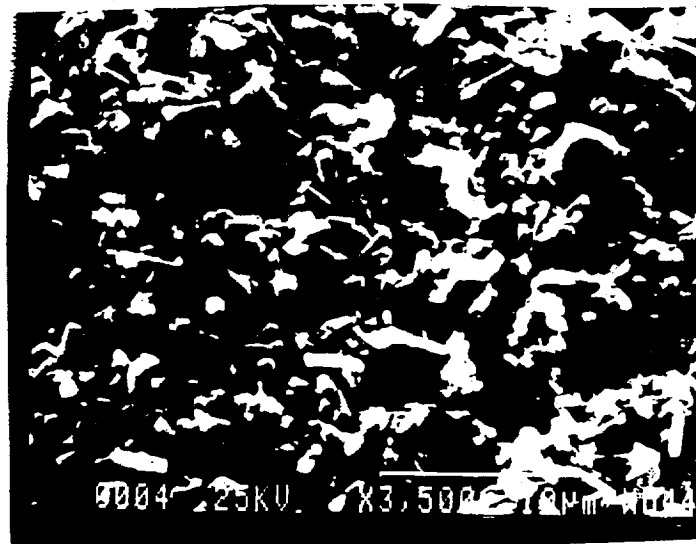b) An 8 Micron Dielectrophoretic Coating on Silver Wire.
Deposition Conditions: 1.5 cm Diameter Cylindrical Counter Electrode,
Applied Voltage was 5000V for 5 Minutes in
1,1,2-Trifluoro-Trichloroethane.

C-3

a

b

Figure 34

SEM Photomicrographs

a) Electrophoretic Deposition on Silver Foil Prior to Sintering

b) Dielectrophoretic Depostion on Silver Wire